University of Bahrain

College of Engineering



Department of Civil Engineering

Innovative Design of Green Building for Harsh Environments

Thesis submitted in partial fulfillment of the requirements for the degree of PhD in (Civil Engineering)

Submitted by:

Adel Jasim Binsanad

ID number: 19840018

Supervised by:

Mehmet Polat Saka

(Professor)

University of Bahrain

The Kingdom of Bahrain

March 2018

University of Bahrain

College of Engineering Department of Civil Engineering



Innovative Design of Green Building for Harsh Environments

Thesis submitted in partial fulfillment of the requirements for the degree of PhD
In (Civil Engineering)

Submitted by:

Adel Jasim Binsanad

ID number: 19840018

Supervised by:

Mehmet Polat Saka

(Professor)

University of Bahrain

The Kingdom of Bahrain

March 2018

University of Bahrain
Deanship of Graduate Studies
And scientific Research

جامعة البحرين
عمادة الدراسات العليا والبحث العلمي

Dissertation Deposit Form

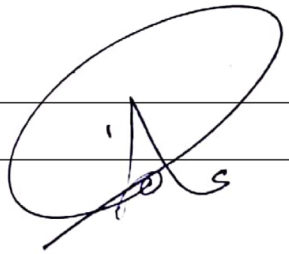
Author Name:	**Adel Jassim Binsanad**		
Email:	**asanad399@gmail.com**	Contact No:	**39939934**
College:	**Engineering**		
Department:	**Civil Engineering**		
Thesis Title:	**Innovative Design of Green Building for Harsh Environments**		
Year:	**2018**		

Author's Declaration: I agree to the following conditions:

The above thesis will be available (in the University of Bahrain library and externally) and reproduced as necessary at the discretion of the University of Bahrain. It may also be digitized by the University of Bahrain and made available via the university's repository or via other parties on the Internet.

This condition shall apply to ALL copies including electronic copies.

The above thesis has been provided on the understanding that it is copyright protected material and that no quotation from this thesis may be published without proper acknowledgement.

Signature of the Author:		Date:	28-Nov-18

Approved at the University Council 6th meeting, 2013
In accordance with Decision No. 736/2013 dated 14/3/2013
Modified by University Council Decision No. 2043/2013 dated 20/11/2013.

University of Bahrain
Deanship of Graduate Studies

Thesis Discussion Committee Decision

Student Name: ADEL JASIM BIN SANAD	Student ID: 19840018
Department: CIVIL	College: ENGINEERING
Program: PhD in Civil Engineering	
Thesis Title: INNOVATIVE DESIGN OF GREEN BUILDING FOR HARSH ENVIRONMENTS	
Supervisor Name: PROF.DR. M. P. SAKA	Student GPA:

The Discussion Committee met on 10th MAY 2018 (day and date) in Hall no. 35-109 (hall/room no.) ____. Upon discussing the student whose details are stated above in public, the discussion committee recommends the following:

كلية الهندسة
قسم الهندسة المدنية
College of Engineering
Dept. of Civil Engineering
University of Bahrain

The student awarded grade S In the thesis subject

☐ Without making any changes to the thesis
☑ After making the modifications attached with this decision

Discussion Committee Members Approval:

Name		Signature
1. Prof. M. P. SAKA	(Advisor)	
2. Prof. M. AYTEKIN	(Internal Examiner)	
3. Prof. M. Iqbal Khan	(External Examiner)	

Abstract

This thesis deals with implementing Nanotechnology and Nano innovation technics in construction to face the challenges that are confronted in the building construction industry, ranging from the performance of the materials to environmental and safety issues related to the cost, durability, and consumptions of building materials. The rationalization of the utilization of high quantities of imported cement, imported coarse aggregates and the use of marine sand in the Kingdom of Bahrain, for better quality, economic and environmental performances of the concrete industry.

One should put his figures on sustainability and durability aspects of concrete that can improve efficiency, strength, heat transfer, weight, self-consolidation, production cost and mitigate climate effects like corrosion and cracks created by Alkali-Silica Reactivity (ASR). This study provides a constructive approach "Polyforms System" to the green buildings based on the interface between solid mechanics and materials engineering, that is integrated and driven by Nanoengineered concrete and innovative insulated concrete formworks (ICF) designs. Showing how innovation increasingly combines dematerialization, eco-efficiency, advanced computational techniques and experiments methods, for developing new classes of novel products, and to characterize its structural and thermal behaviors, often considered as a substitute of conventional technologies, enabling a new design approach of green buildings.

The methodology employed in this study consists of three parts, the first part is the laboratory tests for the optimization of the Nano and EPS concrete. Nano-concrete is structural self-compacting concrete (SCC), incorporated with a nanoparticle (CNCs) that provides and enhance mechanical, chemical, thermal, self-compaction and relaxed delivery properties of the mix with a lightweight density of 1864 kg/m^3. Where as the polystyrene concrete forms the Nano formworks (Blank Block), with a lightweight density of 449 kg/m^3, that provides stronger mechanical properties, insulation and zero slumps for easy manufacturing by extrusion. For both types of these nanocomposites, vibration is not required to level off and achieve consolidation, which represents a sustainability issue because it involves a significant energy reduction needed to build concrete structures. The second part involved laboratory tests on the full-scale models of varied steel configurations of ICF slab categories consisting of (12) samples and different geometrical sections with different steel configurations of ICF wall types consisting of (4) samples, plus three samples for the Blank Block. While the third part is the evaluation of the full-scale finite element study of the structural behavior of the Blank Blocks, reinforced ICF slabs and ICF walls models carried out using ANSYS software validated against data obtained experimentally in the second part.

As a conclusion, Nano-concrete can be identified as a suitable material to replace the ordinary concrete structurally. The ICF slabs (MSJ category) and ICF walls systems passed the serviceability as well as strength tests. However, the primary function of the Blank Block, acting as formwork during construction over which essential structural slab layer of Nano-concrete shall be applied, is still vailed, provided that a prop at every 1 meter is installed. The Polyforms system conforms to LEED's main standards, as it reduces building weight by up to 50%, electricity consumption by 50%, cost by 22.73% and reduces carbon dioxide emissions by 54.03%. This study opens the doors for the civil engineering field to implement and adopt this novel methodology for similar experimental and analytical studies in exploring and developing new composite materials and adding green values to the building constructions industry.

Dedication

The author dedicates this dissertation with love, appreciation, and gratitude to his family, especially his mother and wife for her support and patience and in the memory of his father, grandmother and youngest sister.

ACKNOWLEDGMENTS

The Research's testing conducted at the University of Bahrain’s Structural Engineering Laboratories in the Department of Civil Engineering. The testing and analysis funded through the Technical Assistance Program through Bardex Building Materials Industries in conjunction with ICF Building System who provided the materials and labor to construct the walls and slabs.

Firstly, The author would like to acknowledge the advisor and thesis chair, Prof. Dr. Mehmet Polat Saka. The author is grateful for the opportunities he has given the author, and for his support and input throughout the study at UOB, as well as the knowledge, experience, direction, and suggestions that the author has obtained while working with him. The author would also like to acknowledge Dr. Alamin Mohammed Ali Elkanzi for their questions and suggestions which helped to improve the quality of this research.

Secondly, The acknowledgment must go to Architect Mr. Ehsan Abdul Qudoos for his time and effort to contribute in modeling and meshing techniques of the ICF walls and ICF slabs in ANSYS APDL and ANSYS Workbench as well as 2D and 3D graphics all the way through the project. Ehsan’s advice, feedback, and patience were very much appreciated. The acknowledgment must also go to Mr. Husain Aman, who contributed in arranging the required laboratory equipment for the project. The author would like to acknowledge Waheed Gollum, the Structural Engineering Laboratory Supervisor especially, his knowledge and assistance throughout the entire project were beneficial.

Finally, Special thanks also go to Hana Al Hayki the Civil Engineering Department Secretary for her invaluable administrative assistant. Moreover, to Bardex Industries crew for their time and effort throughout

the project in constructing and casting cylinder and prism specimens of Nano-concrete, and the setup of the full-scale ICF walls and full-scale ICF slabs testing samples.

This thesis would have been impossible without all of the above mentioned academic and applied contributors.

Thank All.

Table of Contents

Subject	Page Number
Defense Committee's Approval	A
Abstract	B
Dedication	C
Acknowledgments	D
Table of Contents	F
List of Tables	L
List of Figures	N
List of Appendices	T
List of Symbols	U
List of Abbreviations	V
Chapter One INTRODUCTION TO THE STUDY	
1.1 Introduction	2
1.2 Research Problem	4
1.2.1 Introduction to Polyforms System	9
1.2.1.1 Polyforms System Definition	9
1.2.1.2 System Elements	10
1.2.1.3 ICF Wall Element	10
1.2.1.4 ICF Ribbed Slab Element	11
1.3 Research Questions	12
1.4 Research Objectives	13
1.5 Research Significance	13
1.6 The Study's Settings	15
1.7 Expected Results	17
1.8 Research Terminology	20
Chapter 2 LITERATURE REVIEW	
2.1 Nano-concrete	25
2.1.1 Nanotechnology	26
2.1.2 Significance of Nanotechnology in The Sustainable Green	27
2.1.3 Microstructure of the Hydrated Cement Paste (C–S–H)	27

2.1.4 Nano-engineered Concrete and Formworks	29
2.1.5 A Brief History of the Cellulose	30
2.1.6 Nanocomposites Reinforced with (CNCs)	31
2.1.7 Polystyrene Concrete	33
2.1.8 Previous Experimentally Measured Properties of EPS Concrete	35
2.1.9 Expanded Polystyrene Beads (EPS)	36
2.1.10 High-Range Water Reducing Superplasticizer	36
2.1.11 Polymer	38
2.2 Insulated Concrete Walls and Slabs	39
2.2.1 Self-Consolidation in ICF Construction	60
2.3 Executive Summary	63
2.3.1 Experimental Investigation	64
2.3.2 Numerical Investigation	66
2.3.3 Beneficiary Conclusion	66
2.3.4 Researcher's Point of View	68
Chapter 3 **EXPERIMENTAL AND ANALYTICAL PROCEDURES**	
3.1Materials	73
3.1.1 Cement	73
3.1.2 Fine Aggregate	73
3.1.3 Expanded Polystyrene Beads (EPS)	73
3.1.4 Mixing Water	73
3.1.5 Fly Ash	73
3.1.6 Nano Additive	73
3.1.7 Chemical 1	73
3.1.8 Chemical 2	73
3.2 Methodology	74
3.2.1 Determination of Material Properties	75
3.2.1.1 Applications and Classifications of Lightweight Concrete	77
3.2.1.2 The Structural Properties	78
3.2.1.2.1 ICF Wall Governing Criteria	78
3.2.1.2.2 Structural Reinforced ICF Walls	78
3.2.1.2.3 Structural Plain Concrete Walls	79
3.2.1.3 ICF Slabs Governing Criteria	80

3.2.1.3.1 Geometry	81
3.2.1.3.2 Analysis	81
3.2.1.3.3 Bending Reinforcement Calculation	82
3.2.1.3.4 Ultimate Compressive Strength Calculation of Nano and Polystyrene Concrete.	84
3.2.2 Determination of Compressive Strength, Passion Ratio and Modulus of Elasticity of the Nano and Polystyrene Concrete by ASTM code Procedures	88
3.2.3 Determination of Compressive strength, Poisson Ratio and Modulus of Elasticity of the Nano and Polystyrene Concrete using ADMIT "Gauge Buster 2."	92
3.2.4 Determination of Self-Consolidation	94
3.2.4.1 Workability Requirements for SCC.	96
3.2.4.2 Self-Consolidating SCC Additives	96
3.2.4.3 Test Methods to Measure Fresh SCC Properties	97
3.2.4.4 T50 Slump-flow	98
3.2.5 The Chemical Properties	101
3.2.5.1 Alkali-Silicate Reaction (ASR)	102
3.2.5.2 Accelerated Mortar Bar Test (ASTM C 1260)	102
3.2.5.3 Double Washed Marine Sand Chemical Composition	103
3.2.5.4 Testing Procedure of Nano-concrete Specimens	104
3.2.5.5 Accelerated Mortar Bar Tests Results and Discussion	105
3.2.6 The Thermal Properties	106
3.2.7 Modulus of Rupture (Flexural Strength)	109
3.3 Optimization of Nano And Eps Concrete	110
3.3.1 Optimization of Nano-concrete	110
3.3.1.1 Compressive Strength, Poisson Ratio and Modulus of Elasticity of CSC Mixes by Gauge Buster 2	111
3.3.1.2 Compressive Strength, Poisson Ratio and Modulus of Elasticity of CS Mixes by Gauge Buster 2	112
3.3.2 Optimization of EPS Concrete	115
3.3.2.1 Trail Mix Designs	116
3.3.2.1.1 Batch one: Nano Polystyrene Concrete "Blank."	117
3.3.2.1.2 Batch Two: Fly Ash Polystyrene Concrete "PF."	117
3.3.2.1.3 Batch Three: Nano Polystyrene Concrete "BB."	118
3.3.2.1.4 Batch Four: Polystyrene Lightweight Concrete	120

3.3.2.1.5 Compressive Strength, Poisson Ratio and Modulus of Elasticity of SBNBR Mixes	122
3.3.3 Material Properties Results and Conclusion	123
3.4 Experiments on Full-scale ICF Slabs and ICF Walls	127
3.4.1 Introduction	127
3.4.2 Test Specimens	128
3.4.2.1 ICF Slabs	128
3.4.2.2 ICF Walls	135
3.4.2.3 Test Setup	133
3.4.2.4 Testing Procedure	134
3.4.3 Full-Scale Test on ICF Slabs	137
3.4.3.1 Blank Blocks (Category B)	137
3.4.3.2 ICF Ribbed Slab with Two Bars Only (Category S)	139
3.4.3.3 ICF Ribbed Slab with Two Bars and Mesh (Category MS)	141
3.4.3.4 ICF Ribbed Slab with Lattice Girder Only (Category J)	144
3.4.3.5 ICF Ribbed Slab with Lattice Girder and Mesh (Category MSJ)	147
3.4.4 Full-Scale Test on ICF Walls	151
3.4.4.1 Wall ICF-04	153
3.4.4.2 Wall ICF-06	153
3.4.4.3 Wall ICF-09	154
3.4.4.4 Wall ICF-11	155
3.5 Numerical Simulation of ICF Slabs and ICF Walls	156
3.5.1 Modeling of ICF Slabs and Walls	157
3.5.1.1 Element Types	157
3.5.1.1.1 Element Solid65	158
3.5.1.1.2 Element Solid185	158
3.5.1.1.3 Element Link180	160
3.5.1.1.4 Element Beam188	160
3.5.2 Material Properties	161
3.5.2.1 Nano-Concrete	162
3.5.2.2 Polystyrene Concrete	162
3.5.2.3 Reinforcing Steel	163
3.5.3 Modeling of ICF Slabs and Walls in ANSYS Workbench	164

3.5.3.1 Engineering Data	165
3.5.3.2 Modeling Stage	165
3.5.3.3 Element Types Assignment	167
3.5.3.4 Meshing Stage	168
3.5.3.5 Direct Generation	168
3.5.3.6 Solid Modeling	169
3.5.3.7 Meshing Technique for Embedded Modeling	169
3.5.3.8 Modeling and Meshing Technique of ICF Walls and Slabs	170
3.5.3.9 Using APDL Commands	172
3.5.3.10 Loading and Boundary Conditions	172
3.5.3.11 Solution Stage	174
3.5.4 Analytical Modeling of ICF Slabs by ANSYS	176
3.5.4.1 Blank Block (Category B)	177
3.5.4.2 ICF Ribbed Slab with Two Bars Only (Category S)	178
3.5.4.3 ICF Ribbed Slab with Two Bars and Mesh (Category MS)	179
3.5.4.4 ICF Ribbed Slab with Lattice Girder Only (Category J)	181
3.5.4.5 ICF Ribbed Slab with Lattice Girder and Mesh (Category MSJ)	182
3.5.5 Analytical Modeling of ICF Walls by ANSYS	184
3.5.5.1 Wall ICF-04	184
3.5.5.2 Wall ICF-06	184
3.5.5.3 Wall ICF-09	185
3.5.5.4 Wall ICF-11	186
Chapter 4 **RESULTS, CONCLUSIONS AND RECOMMENDATIONS**	
4.1 Results and Discussions	188
4.1.1 Blank Block and ICF Slabs	188
4.1.1.1 Blank Block (CATEGORY B)	189
4.1.1.2 ICF Ribbed Slab with Two Bars Only (Category S)	192
4.1.1.3 ICF Ribbed Slab with Two Bars and Mesh (Category MS)	196
4.1.1.4 ICF Ribbed Slab with Lattice Girder Only (Category J)	200
4.1.1.5 ICF Slab with Lattice Girder and Mesh (Category MSJ)	203
4.1.1.6 ICF Slabs Experimental and FEM Results Comparison	207

4.1.1.7 Strength Limit State of ICF Slab (Category MSJ)	211
4.1.1.8 ICF Slab MSJ of Different Spans vs. RCC Slabs	213
4.1.2 ICF Walls	219
4.1.2.1 Wall ICF-04	219
4.1.2.2 Wall ICF-06	220
4.1.2.3 Wall ICF-09	221
4.1.2.4 Wall ICF-11	223
4.1.2.5 ICF Walls Experimental and FEM results Comparison	224
4.1.3 3D ICF Building Design Example	226
4.1.4 Effect of Thermal Properties on Energy Saving	229
4.1.5 Cost Analysis	233
4.1.5.1 Cost Analysis in Various Forms	233
4.1.5.2 Cost Comparison of Conventional and Polyforms	234
4.1.5.3 Discussion on Cost Analysis	237
4.2 Conclusions	237
4.3 Future Work	241
References	243
Appendices	257

List of Tables

No.	Table Title	Page
1	Classification of density for lightweight concrete based on American Concrete Institute (ACI) 2004	77
2	Comparison between initially and finally determined models for Blank Block Slab	87
3	Test methods for workability properties if SCC	98
4	References for slump flow limits and the corresponding type of concrete	100
5	Thermal conductivity at 20 and 50°C according to DIN EN 993-14/15	109
6	Nano concrete samples compositions and compressive strengths	110
7	Derived compressive strength, modulus of elasticity and Poisson's ratio for different CSC	112
8	Derived compressive strength, modulus of elasticity and Poisson's ratio for different CS	113
9	ANOVA for CSC Samples	114
10	Batch one consists of sand, cement, polystyrene and Nano-additive	117
11	Batch two consist of cement fly ash and Nano-additive	118
12	Batch three consists of cement, polystyrene and Nano-additive	118
13	Shortlist of selected mixes of Nano-concrete	119
14	Batch four consist of cement, polystyrene, chemical 1 and chemical 2	121
15	Selected mix for PLWC	122
16	Derived compressive strength, modulus of elasticity and Poisson's ratio for different SBNBR	123
17	ANOVA for SBNBR Samples	123
18	Modulus of elasticity calculation for different mixes of Nano-concrete determined manually	125
19	Final structural material properties determined by Gauge Buster 2	125
20	Final selected recipes for use as a core in ICF walls and ribbed slabs	127
21	Details of polystyrene concrete Blank Block specimens	130
22	Details of ICF slab of category S specimens	130
23	Details of ICF slab of category MS specimens	131
24	Details of ICF slab of category J specimens	132
25	Details of ICF slab of category MSJ specimens	133
26	Details of ICF wall specimens	137
27	Load vs. deflection behavior for category B	140

28	Load vs. deflection behavior for category S	142
29	Load vs. deflection behavior for category MS	145
30	Load vs. deflection behavior for category J	145
31	Load vs. deflection behavior for category MSJ	147
32	Failure details of ICF slab elements	150
33	Failure details of ICF wall elements	156
34	Material properties of concrete	163
35	Material properties of reinforcing steel	164
36	Element types	167
37	Model generation types	168
38	Mid-span deflections of ICF slabs category B	191
39	Mid-span deflections of slabs category S	194
40	Mid-span deflections of slabs category MS	198
41	Deflection observed experimentally and analytically for category J.	201
42	Deflection observed experimentally and analytically for category MSJ	205
43	FEM stresses in the concrete and reinforcement of ICF Slabs	209
44	Comparison between different spans of ICF slabs (Category MSJ-B)	214
45	Comparison of 1.1m spans of RCC ribbed slabs and ICF slabs MSJ-A	216
46	Comparison of 2m spans of RCC ribbed slabs and ICF slabs	216
47	SJ-T deformation check	218
48	MSJ-T span comparison	218
49	ICF walls experimental and numerical strain results	225
50	Electrical consumptions for different building systems	230
51	K values of different materials used in building systems	231
52	R & U values of different types of walls	232
53	R & U values of different types of slabs	232
54	Estimated cost of job build EIFS wall	235
55	Estimated cost of industrial build ICF wall	236

List of Figures

No.	Figure Title	Page
1	Permanent insulating concrete formwork (ICF) for slabs and walls, incorporating Nano-concrete.	3
2	Effect of buildings on the environment	4
3	Three types of ICF walls	5
4	Insulated false ceiling	6
5	ICF walls and slabs	6
6	Honeycombs in flat ICF wall panels	8
7	ICF wall element	10
8	Polyforms ICF wall details	11
9	Longitudinal reinforcement of ICF slabs	11
10	ICF ribbed slabs	12
11	Effect of installed insulation materials on thermal bridges	18
12	Insulated masonry blocks	19
13	External insulation finishing system (EIFS)	20
14	Hexagonal crystals of monosulfate hydrate and needle-like crystals	28
15	Schematic diagram showing concept of incorporating CNTs/CNFs within cementitious composites by their direct growth on cement particles	31
16	Mode of action of superplasticizers (SNF)	37
17	Force interaction diagram for 4-in.-thick (100 mm) fiber reinforced concrete insulating-form wall	46
18	Force interaction diagram for 6-in.-thick (150 mm) fiber reinforced concrete insulating-form wall	47
19	Theoretical 4-point loading system	48
20	End reinforcement detailing for high ductility design.	54
21	Waffle-grid ICF with low slump concrete and no mechanical vibration	59
22	Flat-panel ICF with medium-low slump concrete and no mechanical vibration	59
23	Waffle-grid ICF with high slump concrete and no mechanical vibration	59
24	Flat-panel ICF lintel with high slump concrete (no mechanical vibration)	59
25	Flow of Research Methodology	75

26	Geometrical limitations for ribbed slabs	81
27	Cylinder and prisms samples	89
28	Compressive strength machine	89
29	Different factors influencing the strength of lightweight aggregate concrete	90
30	ADMIT “Gauge-Buster 2” data along with the Compressometer, the transducers, and software	93
31	Measurement of slump flow for the Nano-concrete	99
32	Slump flow test apparatus	100
33	Concrete wall test sample size and dimensions requested by UPM	106
34	ICF slabs and walls were ready for UPM Research Institute Laboratory	107
35	Prepared samples for thermal conductivity test	108
36	Prism testing apparatus	110
37	Stress-Strain curve for different combinations of CSC	112
38	Stress-Strain curve for different combinations of CS	113
39	Blank Block forms	115
40	Blank-3s and BB1 extrusion trial	120
41	The 1.5 long cured precast Blank Block	122
42	Stress-Strain curve for different combinations of SBNBR	122
43	Loading frame from FORM-TEST SEIDNER	134
44	Three point loading system	136
45	Four-point loading system	136
46	Chart of load vs. deflection behavior for category B	138
47	Test setup for Blank B1	138
48	Failure of Blank Block B1	138
49	Test setup for Blank Block B2	138
50	Failure of Blank B2	138
51	Test setup for Blank Block B3	139
52	Failure of Blank Block B3	139
53	Chart of load vs. deflection behavior for category S	140
54	Test setup for ICF slab S1	141
55	Failure of ICF slab S1	141
56	Test setup for ICF slab S2	141
57	Failure of ICF slab S2	141

58	Test setup for ICF slab S3	141
59	Failure of ICF slab S3	141
60	Chart of load vs. deflection behavior for category MS	143
61	Test setup for ICF slab MS1	143
62	Failure of ICF slab MS1	143
63	Test setup for ICF slab MS2	143
64	Failure of ICF slab MS2	143
65	Test setup for ICF slab MS3	145
66	Failure of ICF slab MS3	146
67	Charts of load vs. deflection behavior for category J	146
68	Test setup for ICF slab J1	146
69	Failure of ICF slab J1	146
70	Test setup for ICF slab J2	146
71	Failure of ICF slab J2	146
72	Test setup for ICF slab J3	146
73	Failure of ICF slab J3	146
74	Load vs. deflection behavior for category MSJ	148
75	Test setup for ICF slab MSJ1	148
76	Failure of ICF slab MSJ1	148
77	Test setup for ICF slab MSJ2	148
78	Failure of ICF slab MSJ2	148
79	Test setup for ICF slab MSJ3	149
80	Failure of ICF slab MSJ3	149
81	ICF walls test setup	151
82	Test setup for ICF Wall-04	153
83	Failure of ICF Wall-04	153
84	Test setup for ICF Wall-06	154
85	Failure of ICF Wall-06	154
86	Test setup for ICF Wall-09	155
87	Failure of ICF Wall-09	155
88	Test setup for ICF Wall-11	155
89	Failure of ICF Wall-11	155
90	Element Solid65 geometry	159
91	Element Solid185 homogeneous structural solid geometry	159

92	Element Link8	160
93	Element Beam188	161
94	Engineering data module	165
95	Geometry preparation	166
96	Load application on ICF slab	167
97	Meshing of ICF slab and wall	170
98	Meshing methodology for the lattice girder and Concrete	171
99	Modeling and meshing of the quarter model of ICF slab	171
100	Boundary conditions for planes of symmetry	172
101	Boundary condition for support	173
102	Boundary conditions at the loading plate	173
103	Incremental and iterative solution	174
104	Ansys workbench outline	176
105	Displacement scaling	176
106	Wireframe model of Blank Block B	177
107	Wireframe model ICF slab with two bars of category S	178
108	Quarter symmetry model of ICF slab with two bars of category S	179
109	Wireframe model ICF slab with two bars and mesh of category MS	180
110	Quarter symmetry model of ICF slab with two bars and mesh of category MS	180
111	Wireframe model ICF slab with lattice girder of category J	181
112	Quarter symmetry model of ICF slab with lattice girder of category J	182
113	Wireframe model ICF slab with lattice girder with mesh of category MSJ	183
114	Quarter symmetry model of ICF slab with lattice girder with mesh of category MSJ	183
115	Wireframe of wall model ICF-04	184
116	Wireframe of wall model ICF-06	185
117	Wireframe of wall model ICF-09	185
118	Wireframe of wall model ICF-11	186
119	Deflection contours derived from analytical model of Blank Block B	190
120	Stress contours for Blank Block B	190
121	Mid-span deflections of slab category B	191
122	Deflection contours derived from FEM of quarter symmetry model of ICF slab with two bars of category S	193

123	Stress contours for quarter symmetry model of ICF slab with two bars of category S	193
124	Mid-span deflections of slabs category S	194
125	Deflection contours derived from analytical model of quarter symmetry model of ICF slab with two bars of category MS	197
126	Stress contours for quarter symmetry model of ICF slab with two bars and mesh of category MS	197
127	Mid-span deflections of slabs category MS.	198
128	Deflection contours derived from analytical model of quarter symmetry model of ICF slab with lattice girder of category J	200
129	Stress contours for quarter symmetry model of ICF slab with lattice girder of category J	201
130	Chart of load vs. deflection of experimental and analytical values for category J	202
131	Deflection contours derived from FEM model of quarter symmetry model of ICF slab with lattice girder with mesh of category MSJ	204
132	Stress contours for quarter symmetry model of ICF slab with lattice girder with mesh of category MSJ	204
133	Chart of load vs. deflection of experimental and FEM values for category MSJ	205
134	Chart of Load vs. Deflection of experimental values for all categories.	208
135	Chart of Load vs. Deflection of FEM values for all categories.	208
136	FEM ultimate reinforcement stress of the quarter symmetry model of category S	210
137	FEM ultimate reinforcement stress of the quarter symmetry model of category J	210
138	FEM ultimate reinforcement stress of the quarter symmetry model of category J	210
139	FEM ultimate reinforcement stress of the quarter symmetry model of category MSJ	210
140	Chart of cracks in the ICF slab category MSJ at failure.	212
141	Cross-section details of MSJ-B slabs	213
142	Deflections curves of ICF slabs of category MSJ, (a) 2m span, (b) 4m span, (c) 6m span	214
143	Cross-section details of, (a) HS6-A, HS14-A, (b) MSJ-A slabs (c) shear span	215

144	Load-deflection curves of, (a) HS6-A, (b) HS14-A, (c) MSJ-A slabs	215
145	Load-deflection curve of RCC ribbed & ICF slabs, (a) HS6-A2, (b) HS14-A2 and (c) MSJ-A2	218
146	MSJ-T group cross-section	218
147	Load-deflection curve (a) MSJ-T1 (b) MSJ-T2 (c) MSJ-T3	218
148	Deflection contours (a) MSJ-T1 (b) MSJ-T2 (c) MSJ-T3	218
149	Deflection contours derived from analytical model of wall ICF-04	219
150	Stress contours of wall ICF-04	219
151	Deflection contours derived from analytical model of wall ICF-06	220
152	Stress contours for wall ICF-06	221
153	Deflection contours derived from analytical model of wall ICF-09	222
154	Stress contours for wall ICF-09	222
155	Deflection contours derived from analytical model of wall ICF-11	223
156	Stress contours for wall ICF-11	223
157	Analytical model of wall deflections	225
158	Experimental failure details of ICF slabs	226
159	Deflection contour of the ICF residential building	228
160	Stress contour of the ICF residential building	228
161	Thermal analysis of T3M house system	230
162	Thermal analysis of EIFS system	230
163	Thermal analysis of Polyforms System	230
164	Thermal deformation (mm)	232

List of Appendices

No.	Appendix
A	Sample Calculation of Modulus of Elasticity
B	Reinforcements Test Reports
C	Marine Sand and SRC Cement Test Reports
D	Thermal Conductivity Report
E	Strain Gauge Data
F	APDL Commands
G	Weight Reduction Calculations
I	House Type T3M FLOOR PLANS
J	R & U Values Calculation
K	Awards and Recognitions

List of Symbols

Symbol	Meaning
ø	Diameter
ΔL	Displacement
As	Steel reinforcement cross-sectional area
Ca (OH)	Calcium hydroxide
Ca_2	Hydroxyls ions
df	The degrees of freedom in the source
E	Modulus of elasticity
F	Force
f/c	Compressive strength
F_{cu}	Ultimate compressive strength
f_r	Uniaxial tensile cracking stress
H_2O	Water
H2SiO42	Silicon dioxide
H4SiO4	Silicic acid
K	Steel reinforcement Index
KPa	Kilo Pascal
M	Bending Moment
MPa	Mega Pascal
MS	The mean sum of squares due to the source
NaOH	Sodium hydroxide
p	Percentage of EPS
P	Load
Pa	Pascal
Q	Heat flow under steady state conditions
S1	Stress corresponding to a longitudinal strain, ε1, of 50 millionths, psi
S2	Stress corresponding to 40 % of ultimate load
SS	The sum of squares due to the source
Wc	Specific gravity
Z	Moment of inertia
ε	Strain
σ	Stress

List of Abbreviations

Code	Full Name
3D	Three dimensional
A.C.H	Air changes per Hour
ACI	American concrete institute
ASR	Alkali-silicate reaction
ASR	Alkali-silicate reaction
ASTM	American society for testing and materials
BC	Bacterial cellulose
BS	British standard
CNC	Nano-crystalline cellulose
CNF	Cellulose nanofiber
CNT	Carbon nanotube
DEF	Delayed ettringite formation
DIN	German institute for standardization
EN	European norms
EPS	Expanded poly-styrene
FE	Finite element
FEA	Finite element analysis
FEM	Finite element modeling
GCC	Gulf cooperation council
HVAC	Heating, ventilating, and air-conditioning
IBS	Industrialized building system
ICC-ES	International building code council evaluation service
ICF	Insulated concrete form
KFUP	King Fahad university of petroleum and minerals
K-value	Thermal conductivity
LEED	Leadership in energy and environmental design
LMC	latex-modified concrete
LVDT	Linear variable differential transformer
LWA	lightweight aggregates
LWPC	Light weight polystyrene concrete
MFC	Micro-fibrillated Cellulose
MLS	Modified lignosulfonates
NFC	Nano-fibrillar cellulose

NPs	Nanoparticles
PATH	Partnership for advancing technology in housing, USA
PCA	Portland cement association
psi	Pounds per square inch
PU	Poly-urethane
R-value	Thermal resistivity
SBR	Styrene-butadiene rubber
SCC	Self-compacting concrete
SGICF	Screen grid insulated concrete forms
SMF	Sulfonated melamine-formaldehyde condensate
SNF	Sulfonated naphthalene-formaldehyde condensate
SSID	Service set identifier
STC	Sound transmission class
UDL	Uniformly distributed load
U.N.	United nation
UOB	University of Bahrain
VMA	Viscosity modifying agents
WCED	World commission on environment and development
XPS	Extruded polystyrene

Chapter 1: INTRODUCTION TO THE STUDY

1.1 Introduction

1.2 Research Problem

1.2.1 Introduction to Polyforms System

1.2.1.1 Polyforms System Definition

1.2.1.2 System Elements

1.2.1.3 ICF Wall Element

1.2.1.4 ICF Ribbed Slab Element

1.3 Research Questions

1.4 Research Objectives

1.5 Research Significance

1.6 The Study's Settings

1.7 Expected Results

1.8 Research Terminology

Chapter 1: INTRODUCTION TO THE STUDY

1.1 Introduction

(Sciencedaily.com, 2012), The production of one ton of burned cement clinker of limestone and clay releases 650 to 700 kilograms of carbon dioxide, which means that concrete industry attributes 8 to 15 percent of global CO_2 production every year. Also, (Mehrabi, 2000), Building and construction works have the most extensive share of 50% in global non-renewable high resource consumption and pollution emission in today's civilization after energy production, making it one of the least sustainable industry. Since the urban population swells by around one million people every week, it is needless to mention that any innovative idea, which reduces the use of concrete in the construction industry, would be the right step in the direction of reducing CO_2 emission to the atmosphere. Thus, sustainable construction becomes very important in this respect. Sustainable construction aims at meeting present-day needs for housing by reducing the environmental and economic impacts of these constructions over their entire lifetime. This led to the design innovation of the Polyforms green construction system Figure 1 `which received international and national awards and was the primary motivation to the main objective of this study to evaluate and examine the system experimentally and analytically.

The problems concerned with the accelerating deterioration of the human-built environment and natural resources was debated in the ("Brundtland Commission"), of the United Nations, in 1987, that published the report under the title "Our Common Future," which defined the sustainable development as being the:

"Developments that meets the needs of the present generations without compromising the ability of future generations to meet their own needs".

which has been adopted by the 2030 Kingdom of Bahrain agenda for sustainable development, the objective towards green buildings standers that reduce the overall impact of the environment on human safety and health. Eventually established by LEED "Leadership in Energy and Environmental Design," which are a set of rating systems for the design and construction of green buildings, developed by the non-profit U.S. Green Building Council (USGBC) in 2003. The six standards of LEED that govern the necessary green building criteria are 1. Saving in water. 2. Saving in energy. 3. Adopting sustainable site. 4. Affordable, innovative designs for housing. 5. Reduce resource consumption by using regional materials. 6. The quality indoor environment for better health and safety of the occupants.

The innovative Polyforms Green building system is made of simple-permanent insulated concrete formworks, abbreviated by (ICF) for slabs and walls, which is filled with a defined Nano-concrete mix and steel reinforcement where required. A broad spectrum of experimental and FEM analytical investigations for the material properties and the novel full-scale structural applications of ICF walls and ICF walls conducted.



Fig. 1: Permanent insulating concrete formwork (ICF) for slabs and walls, incorporating Nano-concrete.

The building system with all its components becomes green building construction, forming together a composite monolithic three-dimensional reinforced lightweight Nano-concrete compatible cost-effective skeleton, resulting in composite construction which provides both structural capacity and thermal insulation.

1.2 Research Problem

The traditional constructions and building material factories consume 50% of all global non-renewable resources, which makes it the worst unsustainable industries in the world (ACI 2008b, 2008) as shown in Figure 2. It is quite evident from this data that the need for green construction is a necessity. Such construction is expected to cause less harm to the environment by consuming less amount of water, energy and electricity and carbon dioxide (CO_2) emissions and construction waste.

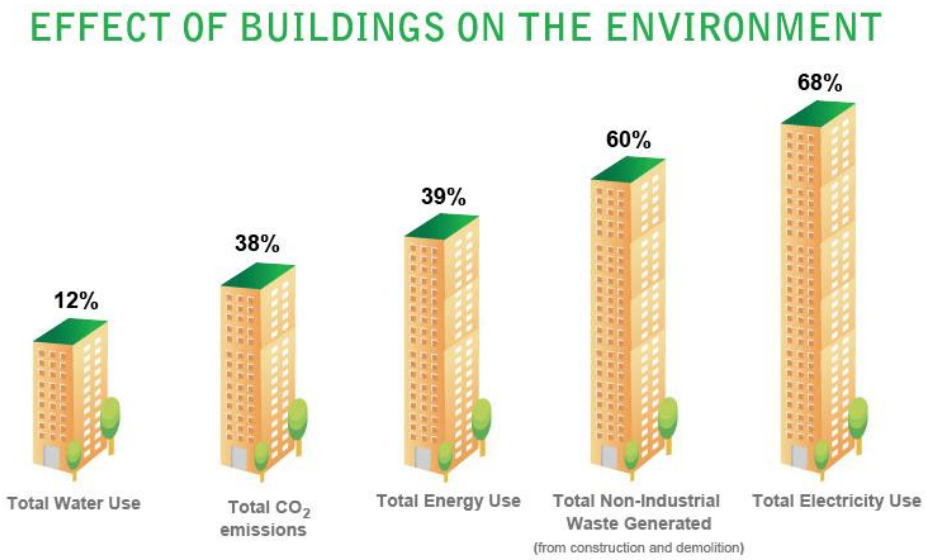


Fig. 2: Effect of buildings on the environment (Ahmed, 2013)

Insulated concrete prefabricated forms (ICFs) are green building components that mainly used in residential construction, mostly made from

three types of materials are 1.EPS beads, 2.EPS & cement, and 3. Wood chips & cement. Although there are several types of ICF walls (e.g., screen grid, waffle-grid, and flat) Figure 3.

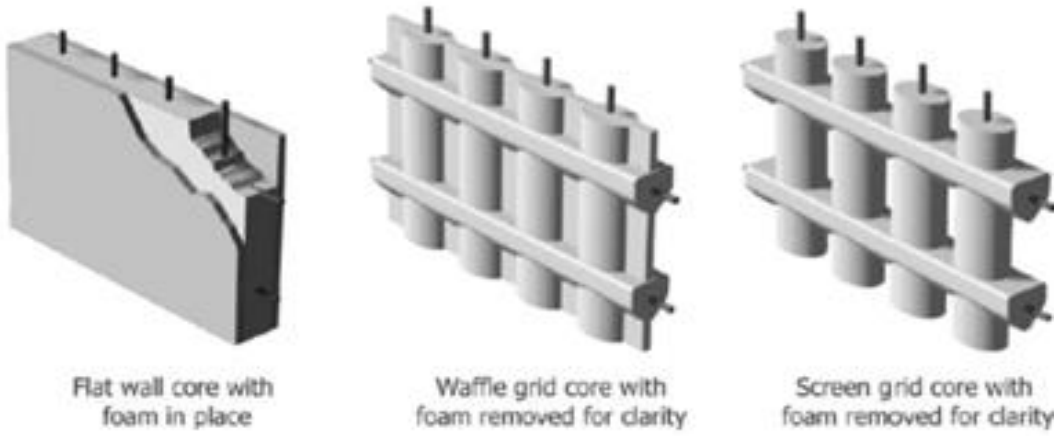


Fig. 3: Three types of ICF walls (Garth, 2014)

The only one type of Insulated Concrete Forms for slabs is purely made of polystyrene beads reinforced with some structural galvanized channels. ICFs are stay-in-place forms that have reinforced concrete cores. The presence of the ICF wall and ICF slabs forms eliminates the amount of wood for shuttering, supports and scaffoldings, comparative to a reinforced concrete system. Nevertheless, reducing the erection costs because of the speed of construction and construction waste due to the stay-in-place nature of the prefabricated forms and the energy demands over the building's service life due to the favorable insulation characteristics of the ICF forms

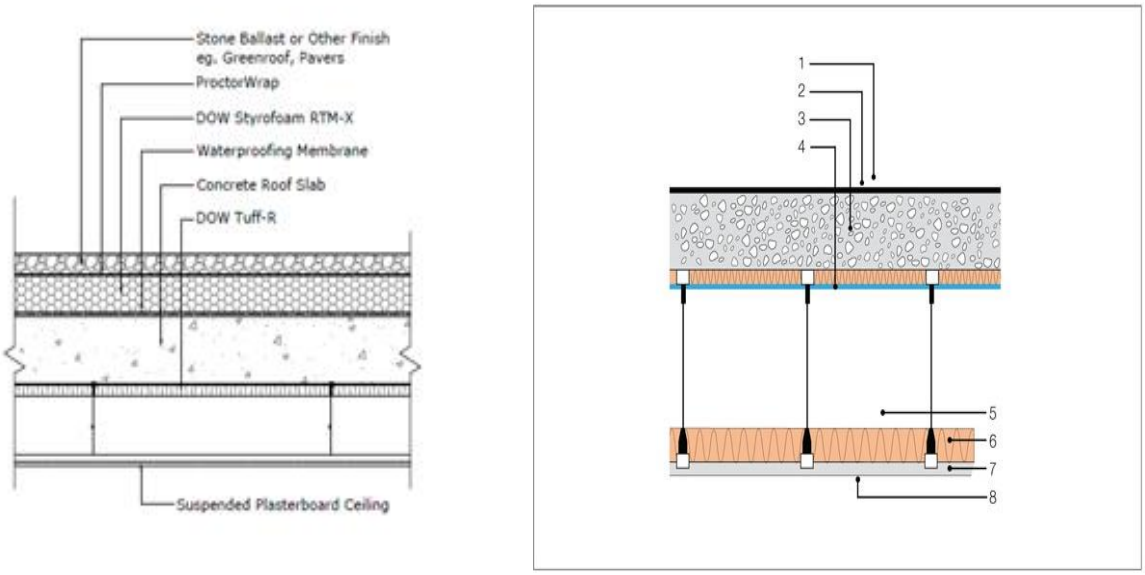


Fig. 4: Insulated false ceiling (integralbook.com, n.d.)



Fig. 5: ICF walls and slabs (donatz.info, n.d.)

The researchers on ICF walls were concentrated mainly in high hazard risk areas of seismic and hurricanes activities of the United States, Japan, and New Zealand, with some more recent contributions from Europe (Garth, 2014). Therefore, experimental research methodologies towards understanding and numerically simulating the behavior of ICF walls with different aspects such as, height to length ratio, openings and reinforcement ratios, reported manifestations and behaviors, such as; the displacements (or drift) and uplift at the base of ICF walls, ductility ratios, and failure modes in relation to lateral strength capacity. Also, the 28-days cylinder compressive strength of concrete mixes is used. The previous theoretical models considered the flat, and the waffle insulated concrete forms (ICF) walls to an insufficient extent and investigated, the screen-grid ICF walls primarily widely for being ideal to save 50% of concrete quantity despite their limitations.

This study concentrates on the introduction of the green construction Polyforms System as a substitute for the traditional construction methods that mostly provide an expectable reduction in damages caused to the environment. Therefore, an introduction of any green system for the building construction needs to be examined and approved regarding structural and thermal performances, which may reflect positively on the drawbacks mentioned above to a great extent.

As the sources for the research studies related to structural and thermal capacities which simulate the structural behavior of ICF walls using ordinary concrete or lightweight concrete, especially Nano-concrete is limited. These are being discussed in the literature review in chapter 2.

Nano-concrete does not contain any coarse aggregate. It is recently developed technology and not used neither in GCC countries nor Bahrain. For the Nano-concrete to be green, the main ingredients have to be from

local materials according to LEED standards. The need to conduct an experimental study on locally available construction materials to develop recyclable structurally reliable economical with less thermal conductivity and easy to place self-consolidated lightweight Nano-concrete, which can flow under its weight, requiring no vibration for placing and compaction, it should fill the congested areas between reinforcements to achieve particular architectural forms in ICF walls based on local materials to replace the ordinary concrete in ICF walls and ICF slabs.

ICF walls provide a more excellent economic alternative to frame walls for residential and commercial construction. They have beneficial thermal and structural properties advantages. However, honeycombing and poor consolidation of concrete around the reinforcement (leading to voids in areas of reinforcement like steel lap and joints) can harm the structural integrity and strength of the walls, even if it is compacted with different vibration methods still voids and honeycombs with noticeable reinforcement can be seen in large portions of the flat-panel ICF walls (Radovic, 2012), as shown in Figure 6.



Fig. 6: Honeycombs in flat ICF wall panels (John G. , 2003)

Also, the pressure exerted by ordinary concrete on ICF walls and ICF slabs during placing need many complicated and costly supports, scaffoldings and shuttering. Otherwise, this pressure may lead to potential blowouts in ICF walls. Also, the standard concrete does not serve this same basic idea to implement the lightweight Blank Block forms of the ICF composite slabs due to its massive weight not to mention the weight of the labors.

Firstly, the material properties such as density, modulus of elasticity, Poisson's ratios and stress-strain behaviors have to be found out for the different types of Nano-concrete mix designs. Secondly using those variables to simulate and find the structural and thermal capacities of ICF walls and ICF slabs. Finally, ICF walls and ICF slabs prototypes in their real dimensions will be ready for testing in the structures laboratory of the Civil Engineering Department. The 400kN capacity universal testing machine will test these elements to determine their real behavior under the loading.

The established and selected Nano-concrete mix designs along with the innovative designs of the ICF walls and ICF slabs should form the integrated green construction Polyforms system.

1.2.1 Introduction to Polyforms System

1.2.1.1 Polyforms System Definition

This system is an ICF Green Construction Method, designed as permanent Insulating Concrete Formwork (ICF) system. The forms of the system can be partly assembled off-site (panelized) or fully assembled on site (in-situ) to produce a permanent formwork (shuttering), which is filled with a defined concrete mix and steel reinforcement where required. The

resultant, Nano-concrete ICF walls with expanded polystyrene (EPS) panels either side used as either load-bearing or non-load-bearing insulated walls, or Nano- concrete ICF ribbed slabs with (EPS) concrete blanks, for residential or commercial buildings.

1.2.1.2 System Elements

This system consists of two elements namely wall elements and slab elements. Details of each type are mentioned in following subsections.

1.2.1.3 ICF Wall Element

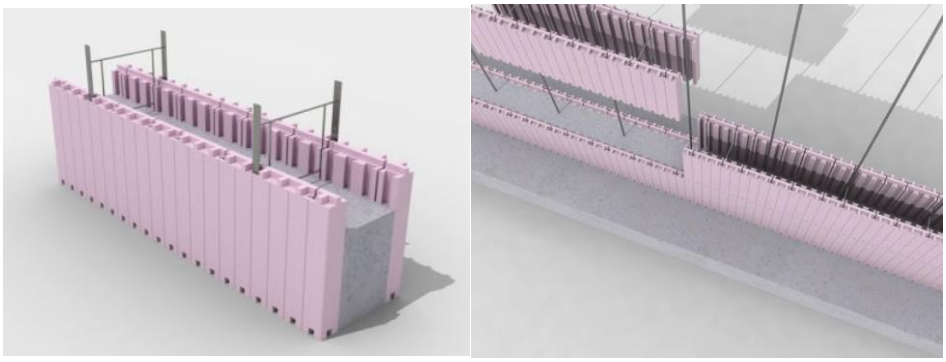


Fig. 7: ICF wall element

The EPS forms comprise of two EPS panels each having a thickness of 50mm. They are held at either 100mm or 200mm Nano-concrete core width by plastic or steel fasteners inserted in the EPS panels at variable spacing. The forms have a 300mm full height. The lengths of the forms are typically 1000mm. The EPS forms are produced in straight plan sections. Both internal and external faces of the finished walls require the addition of a protective external insulated finishing system, Figures 7 and 8.

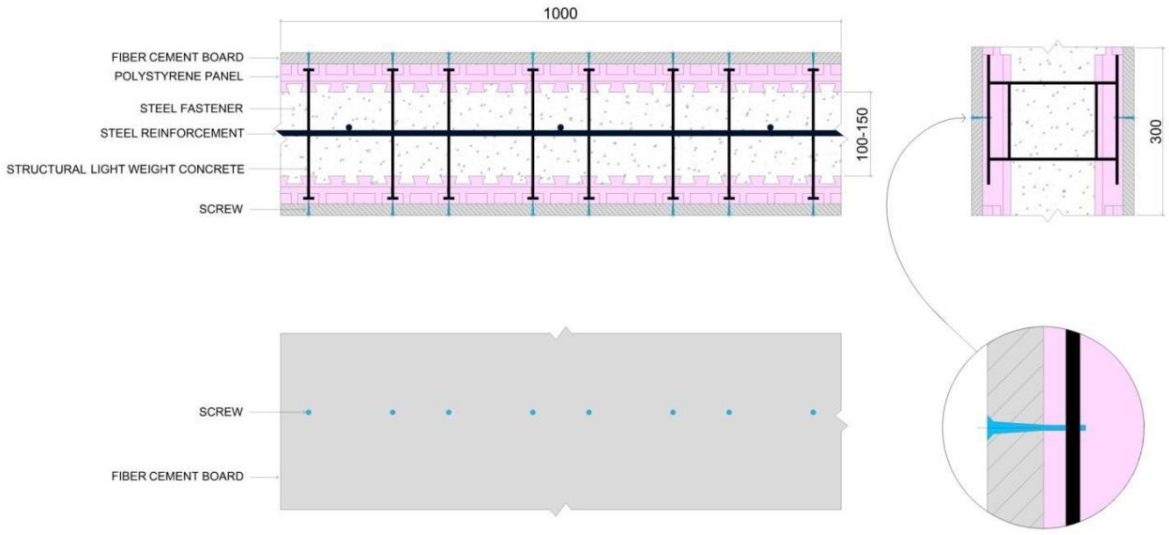


Fig. 8: Polyforms ICF wall details

1.2.1.4 ICF Ribbed Slab Element

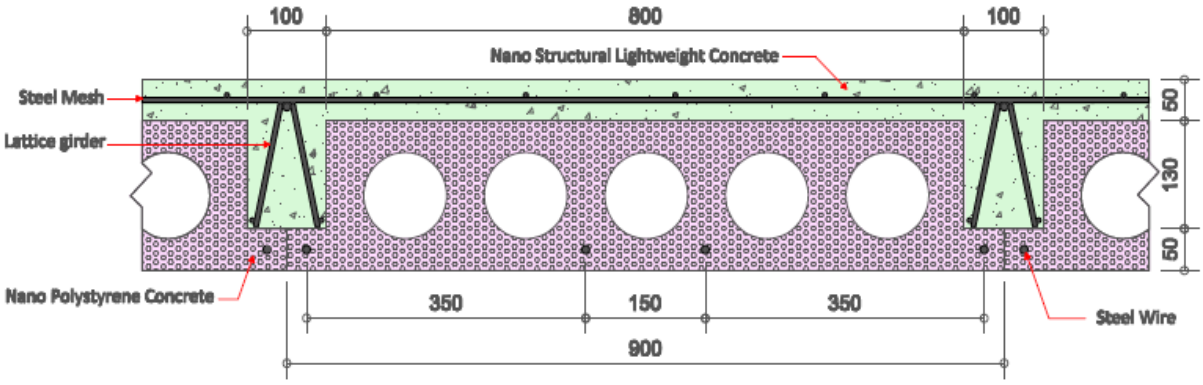


Fig. 9: Longitudinal reinforcement of ICF slabs

This study proposes the 90cm width innovative Blank Block ICF forms made of polystyrene concrete to cast simply supported or continuous Nano- concrete ICF ribbed slabs, which are more economical and faster because someone can avoid the need for extensive shuttering and Supports consumed as in ordinary ribbed slabs, Figures 9 and 10.

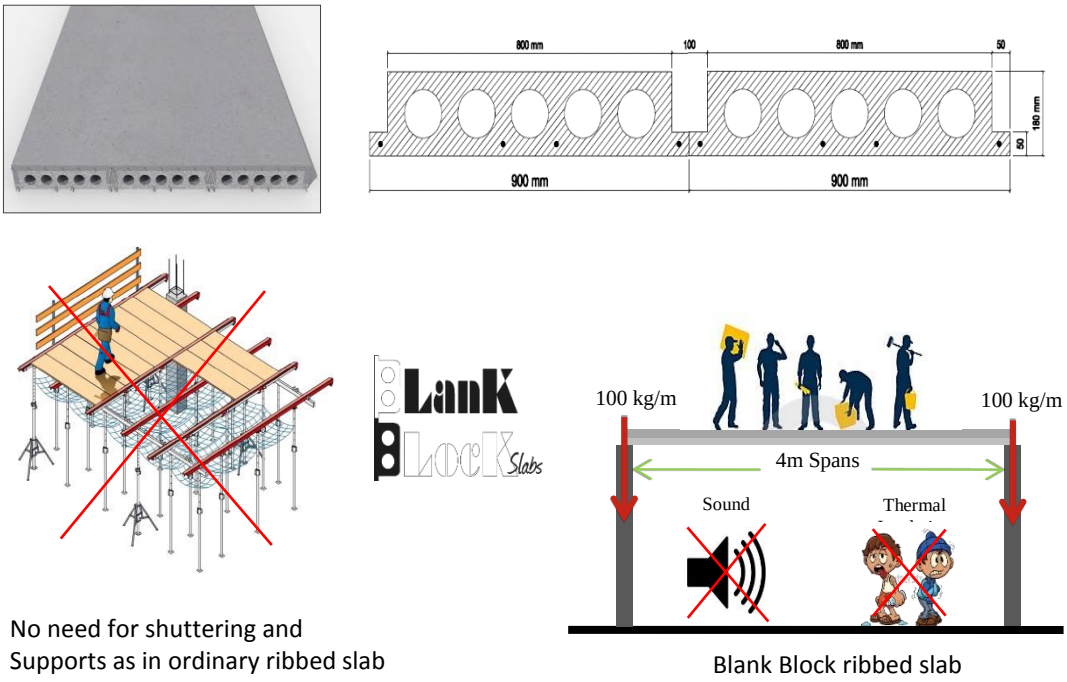


Fig. 10: ICF ribbed slabs

1.3 Research Questions

- Q1: Can an innovative Nano-concrete replace the ordinary concrete structurally?
- Q2: Can the proposed innovative polyforms system consisting of ICF slabs and ICF walls pass the strength, thermal and serviceability requirements?
- Q3: Can the pre-stressed Blank Block act as formwork during construction to carry the weights of the wet Nano-concrete and labors, tending to eliminate the underneath supports?
- Q4: How would this system contribute to the knowledge and the value of the civil engineering field?
- Q5: Would the innovative polyforms system designs contribute positively to the green buildings requirements by LEED, in terms of

construction insulation, time, cost, speed, energy and material consumption and finally safety?

1.4 Research Objectives

Outline of the principal research objectives of this thesis are:

- To develop and establish a new lightweight Self-Compacting Nano-concrete mix design,
- To develop and establish a new LWPC (Light Weight Polystyrene Concrete) for the Blank Block of the ICF slabs.
- To determine and appraise through the experimental laboratory tests the mechanical and thermal material properties of the Nano-concrete and LWPC.
- To evaluate the performance numerically and experimentally of the Blank Block, the ICF slabs systems, and the flat ICF walls separately and under vertical loads simulating the gravitational effect.
- To simulate numerically and investigate experimentally the overall behavior of the proposed accurate model under structural and thermal loads to develop an integrated green construction system to satisfy the Economics, Environment and Health & Safety criteria.

1.5 Research Significance

The most important findings expected of this research is the development of the self-consolidating Nano-concrete mix designed with the following characteristics:

- 3 MPa for tensile strength,
- Required minimum 28-days compressive strength of 17.2MPa.

This work focuses on the effect of the different design parameters on the wall and slab behavior under simulated gravitational loads. This includes different steel reinforcement arrangements, wall thicknesses, and different openings sizes.

The investigation of (LWPC) is done as Nano-concrete and the establishment of their mechanical and thermal properties for further analysis and calibration of numerical models developed for this study. When these elements are put together, they form vertical sandwich panels for walls tied by steel fasteners, and horizontal blanket panels for slabs strengthen by one of the two types of reinforcements selected according to the span of the slab. The Nano-concrete fills the gaps between the EPS panels and on the Blank Block to form the monolithic skeleton of the building, making an integrated green construction system having the following satisfying and significant main criteria:

Environmental and Economic Aspects: Walls and slabs joined such a way that the thermal insulation has preserved throughout the building. This is one of the best features of this building system in addition to thermal insulation. Because of the lightweight concrete used within the sandwich panels, which reduce the construction time tremendously, the overall weight of the building is almost 50% less than the classical building systems. This, in turn, reduces the overall dimensions of foundations required for the building.

In addition to thermal insulation, it saves air conditioning electricity by 50%, it eliminates construction tools, expensive skilled labors, set-up charges for significant cranes and equipment, significant amount of electrical conduits, Poly-Urethane (PU) foams and lightweight screed for roof, supports and wooden shuttering materials leading to considerable savings achievement in construction cost. Moreover, the system reduces

construction waste storage and does not require any import of materials. All the required materials are sustainable, recyclable, and locally available which can save lots of money throughout the lifetime of the building and provide high building reuse potential with less maintenance, providing further support to the national economy.

Health and Safety: This construction system meets the structural, fire and insulation requirements. Moreover, It provides sufficient strength to even withstand the effects of dynamic destructive seismic structural and thermal loads. Also, its resistance to moisture due to the airtight walls and slabs which does not allow moisture and air to penetrate into the building to develop corrosion which leads to structural cracks, preserving the indoor climate with a pleasant and healthy atmosphere.

1.6 The Study's Settings

This study took place at Isa Town Campus of Bahrain University at the civil engineering department from the second semester of 2012 (UOB). Initially, literature survey carried out in recent publications that cover green buildings especially ICF walls and ICF slabs. The internet is widely used in various modalities and links to Indexes & Databases for locating journal citations, finding journal articles; finding books, distance education services; library services, email service, wireless service SSID and window login labs, in addition to the supporting learning courses and academic programs. The technological facilities of the campus including a large number of computers located strategically in open laboratories and at the center of UOB library's information access browsing facilities like Atkins Library.

Experimental investigation and studies on developing mix designs and formulas of the Nano-concrete and LWPC (the core of the walls and

slabs) were done. This was done using the compression test machine with ADMET electronic compressometer. The specimens of 150 x 300 mm cylinders were used for determining the compressive strength, Poisson ratio and stress and strain relationship of the mixes. Also, prisms with sizes of 450mm x 100mm x 100mm for all mixes were cast for the determination of their uniaxial tensile cracking stress.

Further, four ICF walls were completed, six ICF slabs and three Blank Blocks were modeled and made out of the proposed innovative green system as three-dimensional finite element models. These models were analyzed under the external loads and temperature effects. Ultimately, from stress analysis, the dimensions of the elements were checked for their acceptability or not for the making the prototypes. Also for the verification of each element of the building such that design code requirements are satisfied, and the cost of the building is minimum.

Eventually, ICF walls and ICF slabs prototypes in their real dimensions were ready for testing in the structures laboratory of the Civil Engineering Department. The 400kN capacity universal testing machine has been used to test these elements to determine their real behavior under the loading. During the testing displacements as well as stresses were measured and the values obtained were compared to the ones attained from three-dimensional finite element analysis.

In addition to strength test, will perform tests in order to verify the thermal insulation of these elements. The Institute of Mineral Engineering laboratories at RWTH Aachen University in Germany conducted the thermal conductivity at 20°C and 50°C according to DIN EN for the Nano-concrete, polystyrene concrete, plaster, and polystyrene on a sample of size 230 mm x 114 mm x 64 mm.

Some of the polystyrene cylinders specimens were taken to Al Hoty laboratory for double-checking the results because of its high elastic property the compression machine at the laboratory of the Civil Engineering Department stops at specific shortening displacement. Moreover, Al Hoty laboratory used for the tensile test of the prestressed tendon. Bardex construction yard and facilities used to extrude the LWCP for the planks and casting of the ICF walls and ICF slabs prototypes.

1.7 Expected Results

This new green building system should satisfy the strength and serviceability requirements of the international design codes, and at the same time, it will provide an excellent saving in energy consumption during its construction also while the building is under occupancy. Polyforms green building system could become ideal in housing construction practice in the Gulf region.

The study has extensively reviewed the literature on structural engineering which comprises of green construction as per LEED (Leadership in Energy and Environmental Design) standards. The literature review also covers the aspects such as increasing the efficiency with which buildings and their sites use energy, water, and materials. This study has given due consideration to the literature on Insulated Concrete Form (ICF) walls patented almost 50 years ago. The literature on PATH (Partnership for Advancing Technology in Housing) of American housing sector has been reviewed, to find the new trends in the construction of housings, The systematic literature review was carried out to evaluate the flat ICF wall system for meeting the actual earthquake design resistant requirements given by the unified European code of the structural seismic design and detailing constructive provisions of reinforced concrete shear walls.

The recent trends towards sustainable green building construction have placed new emphasis on the provisions and standards of insulated walls and slabs systems that provide a highly active heat flow resistance (R-Value), especially for small, large multi-residential, commercial and institutional buildings constructed of concrete, steel, masonry and glazing systems. In these types of buildings, and particularly in the severe, harsh hot climate of the Arabian Gulf countries, thermal performance has not been treated as a last priority item. Now, however, the requirements of sustainability programs such as LEED, stipulate insulated wall and slabs (Floors/Roofs) systems that provide high levels of thermal resistance. Architects are often impressed at the difference between effective R-value of a proposed dense wall assembly and the nominal R-value of installed insulation materials Figure 11. The difference is a result of the thermal bridges associated with structural elements and connections that pass through the thermal building envelope. However, most common insulated wall and slabs systems used nonconventional residential construction possess this phenomenon.



Fig. 11: Effect of installed insulation materials on thermal bridges (Nutcher, 2015)

The available systems for insulating walls and slabs mainly involve installed complementary insulation materials to break the thermal bridges as drywall on a steel stud wall filled with batt insulation, spray polyurethane foam and expanded or extruded polystyrene boards (EPS), integrated with the masonry or concrete framed walls and slabs. Even though expended EPS is available, cheap and eco-friendly, the most commonly used material in GCC countries, it has been misused and applied in conventional residential buildings in the last decay by installing it inside the masonry blocks Figure 12. Recently rules that are more restricted implemented to use External Insulation Finishing System (EIFS) for walls and Insulated False Ceiling for slabs and roofs as shown in Figures 4 and 13.

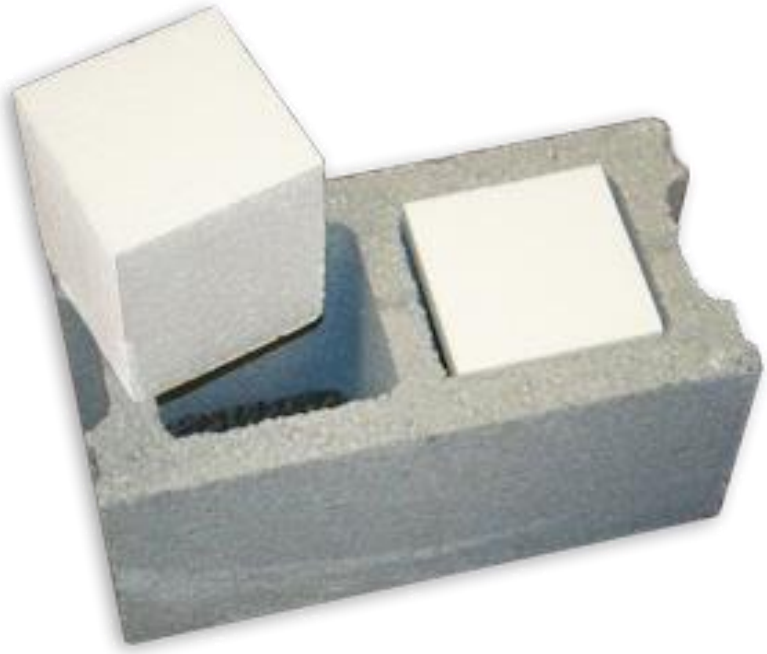


Fig. 12: Insulated masonry blocks

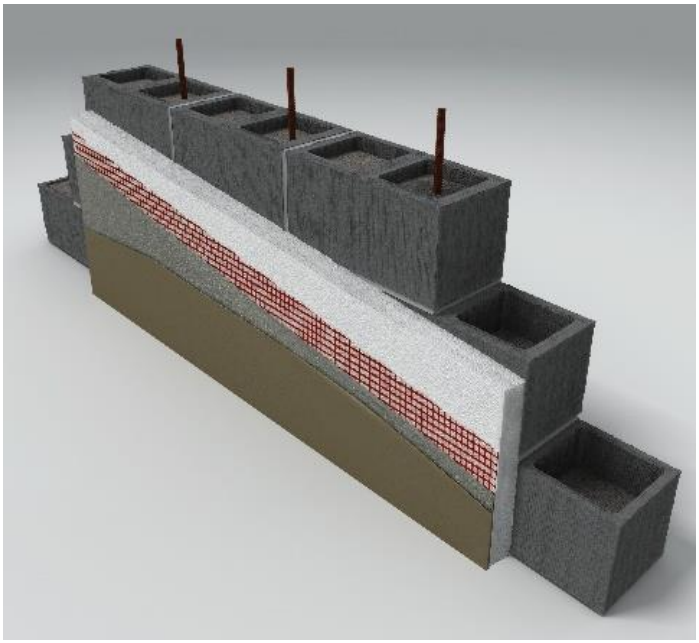


Fig. 13: External insulation finishing system (EIFS)

The above-explained insulation systems for conventional framed walls and slabs considered disadvantageous in residential constructions, in comparison to the relatively new types of wall and innovative slabs systems, such as Insulating Concrete Forms (ICF) walls and slabs Figure 5. Especially for accomplishing green construction regarding energy efficiency, speed to completion, quality, and safety, overall costs, material waste, leading to minimizing impacts on the environment and economy.

1.8 Research Terminology

Definitions of the main terms that appeared in the study:

Nanotechnology: Nanotechnology is the fine-tuning of materials at molecular and atomic scales (between 1 nm and 100 nm in size). The word Nano is a scientific prefix that stands for 10^{-9} or one-billionth; the word itself comes from the Greek word Nanos, meaning dwarf". (Patel Abhiyan, 2013). The ideas and concepts behind nanoscience and nanotechnology started with a talk entitled “There’s Plenty of Room at the Bottom” by

physicist Richard Feynman at an American Physical Society meeting at the California Institute of Technology (CalTech) on December 29, 1959.

Nano-concrete: Nano-engineering or Nanotechnology in concrete deals with the formulation of the cement-based materials (with no coarse aggregate) by introducing engineered nanoparticles (carbon nanotubes, Nano silica, and cellulose nanocrystals (CNCs)).

(Gindl W, 2004), were the first to use the CNC as reinforcement in nanocomposites in 2004, they demonstrated reinforcing cellulose acetate butyrate (photographic film) with various aspect ratios of CNCs.

(ICF): Permanent insulated concrete forms for walls, the first person accredited with combining the advantages of this modern, lightweight and insulating EPS into a concrete mold or Form in the late 1960s (helped by the coincidental expiration of the original patent for Durisol) was contractor Werner Gregori (or Gregory – as the newspaper Journal-Record reported at the time), a German born naturalized Canadian. He filed the first North American patent for a foam concrete form or "modern Plastic" ICF in March 1966 in Canada and once these patents were granted in U.S. (oct 24th 1968) and Canada, he showed his ideas to BASF in Germany, the creator of EPS, who developed his product ideas further with a view to expanding the international uses and sales of their EPS foam as an insulation product for construction.

Blank Block: Permanent Insulated concrete forms for slabs, defined by Adel Binsanad and Ehsan abdulqudoos for their invention award in Genève in 2012.

LEED: is "Leadership in Energy and Environmental Design," which are a set of rating systems for the design and construction of green buildings, developed by the non-profit U.S. Green Building Council (USGBC).

Between 1990 and 1995, the USGBC worked feverishly with the American Society of Testing and Materials in order to create a rating system for sustainability. ASTM's rigorous consensus-based process moved much too slowly for the USGBC and in 1995 it was determined that they would create their own rating system to exist under the USGBC banner. A committee was formed to study other green building programs currently in existence and after three years LEED unveiled. By 2003, LEED was refined down to its current form that is the talk of the construction and design communities.

Green Building: (also known as green construction or sustainable building) A 'green' building is a building that, in its design, construction or operation, reduces or eliminates negative impacts, and can create positive impacts, on our climate and natural environment. Green buildings preserve precious natural resources and improve our quality of life. The start of the green building movement in the U.S. can be primarily associated a with book named "Silent Spring" authored by Rachael Carson in 1962. All the international developments that took place in the milestone III had initiated a lot of debate within the environmental groups in the U.S (2003). To address sustainability, the U.S. government decided to target the construction sector, as it was one of the major consumers of the energy resources, contributors to the greenhouse gas emissions and also was a direct medium of public interaction (Bhatnagar 1999, Bondareva 2005, Dalal-Clayton et al. 1994, Kibert 2005, Landman 1999), which yielded the formation of the U.S. Green Building Council (USGBC), one of the major events occurring during this phase.

Sustainability: The problems concerned with the accelerating deterioration of the human built environment and natural resources led the ("Brundtland Commission"), of the United Nations, in 1987, that published

the report under the title “Our Common Future”, which defined the sustainable development as being the: “Developments that meets the needs of the present generations without compromising the ability of future generations to meet their own needs. “

Chapter 2: LITERATURE REVIEW

2.1 Nano-concrete

2.1.1 Nanotechnology

2.1.2 Significance of Nanotechnology in The Sustainable Green Construction Industry

2.1.3 Microstructure of the Hydrated Cement Paste (C–S–H)

2.1.4 Nano-engineered Concrete and Formworks

2.1.5 A Brief History of the Cellulose

2.1.6 Nanocomposites Reinforced with (CNCs)

2.1.7 Polystyrene Concrete

2.1.8 Previous Experimentally Measured Properties of EPS Concrete

2.1.9 Expanded Polystyrene Beads (EPS)

2.1.10 High-Range Water Reducing Superplasticizer

2.1.11 Polymer

2.2 Insulated Concrete Walls and Slabs

2.3 Executive Summary

2.3.1 Experimental Investigation

2.3.2 Numerical Investigation

2.3.3 Beneficiary Conclusion

2.3.4 Researcher’s point of view

Chapter 2: LITERATURE REVIEW

2.1 Nano Concrete

Significant improvements in the perform ance of the traditional building construction materials elapsed over the last century, starting with the famous invention of concrete in the ancient Rome were, followed by the patented method for producing Portland cement by Joseph Aspdin on 1824. Eventually, Reinforced concrete was invented in 1849 by Joseph Monier (wikipedia.org, n.d.). Safety standards and measures of living for people to a considerable extent with some small to significant changes in performance over time. Certain unresolved matters concerning economic and environmental impacts of concrete presets.

Portland cement energy-exhaustive manufacturing process accounts for nearly 5% of global CO_2 emissions and potentially $330 billion worldwide cement market, associated with the $200 billion concrete production cost, which is serious about the built environment in the U.S. and globally. (Crystal Research Associates, LLC, 2012)

Consequently, (Crystal Research Associates, LLC, 2012), green methods for producing concrete or other alternatives are being investigated. March 2012, Spain's Basque Country Conference Initiatives for Cement and Concrete Research promoted nanotechnologies in the cement and concrete industry, to organize technology transfers and jointly employed programs in the field of cement Nanoscience. Contributors, included MIT, the University of California at Berkeley, Spain's Don Ostia International Physics Center, the University of Basque Country, Lafarge, Italcementi SpA (BIT-IT), and Italy's Bozzetto Group.

Subsequently, (Gindl W, 2004), an investigation to improve the properties of concrete and cement pastes, calcium silicate hydrate (C–S–H), at the Micro- and Nanostructure levels need to be conducted for better understanding and possible benefits. It has been confirmed that nanotechnology produced material with unique improved properties that may fix and organize an intractable building construction economic and environmental impacts.

It is evident that Nano innovations touch multidisciplinary areas of building construction. Further, Nanotechnology is not about making products small or big, but it is intended to make products behave better.

2.1.1 Nanotechnology

Nanotechnology is an exciting, diverse material science techniques that take place at Nanoscale that is still developing; it is expected to create the next industrial revolution. "Nanotechnology is the study and use of structures between 1 nanometer (nm) and 100 nanometers in size. The word Nano is a scientific prefix that stands for 10^{-9} or one-billionth; the word itself comes from the Greek word Nanos, meaning dwarf". (Patel Abhiyan, 2013)

Therefore, adopting Nanotechnology would enable us to create innovative materials that provide better qualities or entirely new properties and functions, introducing a new practical scientific approach in our built environment. (Mohamed, 2015)

Nano concrete is one of the essential promising materials for sustainable building construction field. Significance innovations for the sustainable building construction industry can be exposed. "As particles become so small, the proportion of atoms on the surface increases relative to those inside, and this leads to novel properties." (Ayşin Sev, 2014)

2.1.2 Significance of Nanotechnology in The Sustainable Green Construction Industry

Sustainability expresses resistance to ecological, social and environmental impacts in the context of the built environment. The Council International du Batiment (CIB) 1994, "defined the goal of sustainable construction as creating and operating a healthy built environment based on resource efficiency and ecological design" (Ayşin Sev, 2014). The CIB 1994, established seven principles for the design and construction process of sustainable green construction:

1. Reduce resource consumption.
2. Reuse resources.
3. Use recyclable resources.
4. Protect nature.
5. Eliminate toxins.
6. Apply life-cycle costing.
7. Focus on quality.

2.1.3 Microstructure of the Hydrated Cement Paste (C–S–H)

The mechanical properties and degradation mechanisms of concrete depend on the properties of each multiple length scale layers of the (Nano to micro to macro) various ingredients. (K. E. Drexler, 1991). The amorphous layer, calcium–silicate–hydrate (C–S–H) is the ‘‘glue paste" that holds concrete aggregates together, and itself is a nanomaterial (Whatmore, 1995).

(F. Sanchez, 2010), even though (C–S–H) is well investigated at the macro-structural level. The (C–S–H) responsibility for the mechanical, chemical and thermal properties of concrete such as the compressive strength, shrinkage, creep, porosity, permeability, elasticity, thermal

conductivity and delayed ettringite formation (DEF) of concrete is not fully understood. Latest research developments of new experimental standards and techniques showed that the properties of (C–S–H) need more studies to mitigate or eliminate alkali-silicate reaction (ASR).

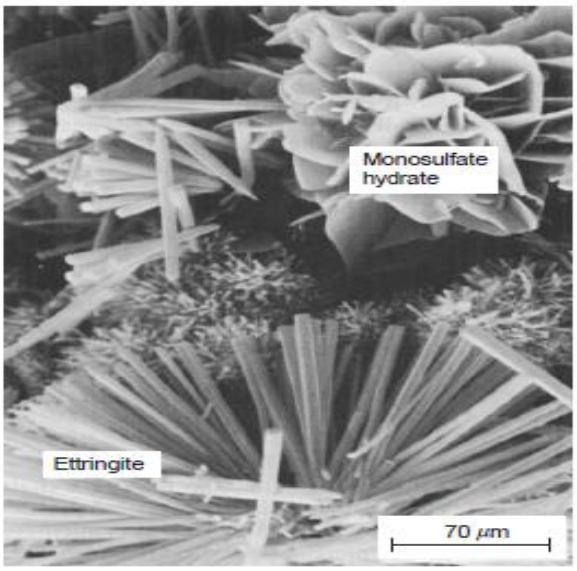


Fig. 14: Hexagonal crystals of monosulfate hydrate and needle-like crystals. (Mehta P. K., 2006)

(Mehta P. K., 2006), the low-density C-S-H gel forms an interface of the alkaline cementitious amorphous continuous inorganic high-density calcium silicate hydrate (C-S-H), the principal binding component of cement, on the non-crystalline silica aggregates. Voids and microcracks in the interfacial region between the low-density and high-density C-S-H cement past matrix prevent bridging of stress when this is the case; the bulk composite behavior is less than the behavior of the individual components of the matrix, regardless of its high individual component stiffnesses.

With a highly flocculated cement paste system, not only the size and shape of pores but also the crystalline products of hydration would be different when compared to a well-dispersed system.

(Sobolev, 2014), latest attempts tried Nano-engineered Concrete by the combination with Nanotubes, Nano-silica or Nano-fibers (Nano cellulose) for novel properties.

2.1.4 Nano-engineered Concrete and Formworks

For civil engineers, Nanoengineered concrete is the term used to describe, the enhancement of the bulk engineering properties of concrete. The National Research Council in Canada, in the area of concrete materials research, has shown the potential of improving concrete properties by modifying the structure of cement hydrates by the addition of nanoparticles and nanotubes to control the delivery of concrete (Raki, 2010).

(Raki, 2010), key goals include obtaining enhanced engineering properties of C-S-H (e.g., strength, modulus of elasticity, Poisson ratio, slump, K value, ASR mitigation and improvement of durability). Organic nanoparticles and additives showed modification that is useful for the structural and nonstructural application of nanocomposites.

Also, (F. Sanchez, 2010), SCC can offer benefits of up to 50% in labor costs, due to it being poured up to 80% faster and having reduced wear and tear on formwork. Self-Compacting Concrete (SCC) is a new type of concrete, which has generated tremendous interest since its initial development in Japan by Okamurain the late 1980s to reach durable concrete structures.

1. Degree of Fiber-Cement Bonding
2. Fiber mineralization

There are two major types of fibers: Naturally occurring fibrous minerals and synthetic Nanofibers, the natural fiber is of two kinds: 1. Cellulose vegetable Nanofibers (CNFs) and Cellulose Nanocrystals (CNC) extracted from agriculture, 2. Minerals Nanofibers Like; (Carbon

Nanotubes (CNTs), Nano Silica, Graphite, and diamond) driven from stones. 3. Eventually, the synthetic fibers which are plastics -mostly petroleum- byproducts such as;(polypropylene, rayon, nylon, polyester, Kevlar and asbestos (Bentur and Mindess, 1990),

2.1.5 A Brief History of the Cellulose

Concerns over health issues resulting from the use of asbestos fibers in the commercial production of cementitious products forced the industry to investigate and find safer reinforcing materials.

(Ning Lin, 2014), it was not until the 20th century that more intensive studies on the initial discovery of microbial cellulose, C.A. Browne studied the cellulose material obtained by fermentation of Louisiana sugar cane juice and affirmed the results by A.J. Brown. Cellulose has been shown to be a long-chain polymer with repeating units of D-glucose, a pure sugar. It occurs in the most pure form of cotton fiber. However, in wood, plant leaves, and stalks, it is found in combination with other materials, such as lignin and hemicelluloses. Although considered a plant material, some bacteria are also found to produce Cellulose.

(Tonoli, 2009), Cellulose fibers also have some disadvantages such as moisture absorption, quality variations, combustible, low dispersion, and poor compatibility with the hydrophobic polymer matrix.

(Z. S. Metaxa, 2010), Cellulose fibers are natural fibers extracted from plants. The treated cellulose fibers have comparatively excellent strength, stiffness, and a high elastic modulus compared to traditional polypropylene and polyester synthetic fibers. Also, cellulose fibers are useful in stabilizing cracks because they are closely spaced, have high length-to-diameter ratios, have small diameters, have hydrophilic surfaces, they fit well in the close-packed structure of concrete and contribute to a dense,

uniform microstructure. The incorporation of cellulose fibers into a cement matrix provides a right balance of structural and chemicals properties. The close spacing of the treated cellulose conceals cracks due to the increased intensity of its, closely spaced fibers and high length-to-diameter, fibers at the crack tips.

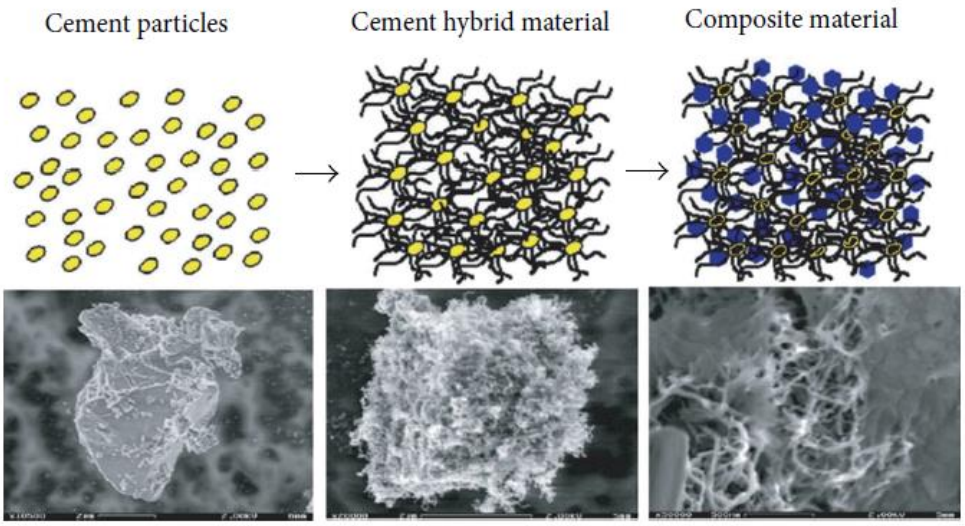


Fig. 15: Schematic diagram showing concept of incorporating CNTs/CNFs within cementitious composites by their direct growth on cement particles (Arsène M-A, 2003)

2.1.6 Nanocomposites Reinforced with (CNCs)

(Lee, 2014), non-conventional building materials have been widely investigated as an alternative possibility for cost-effective green housing in developing countries. Unfortunately, (CNFs) microfibers do deteriorate in the highly alkaline environment of the cement matrix, A reduction in strength and toughness due to the effects of porosity and permeability as they relate to the microstructure of the cement composite and the health of the cellulose fibers are attributed mainly to the attack on lignin content of natural fibers, The porosity allows the alkaline pore solution to reach the

fibers and weaken the individual fiber cells, Although, CNFs obtained by using a chemical pulping process contain negligible amounts of lignin can withstand better the alkali environment of the cement composite, research on other low-lignin fibers has found increased susceptibility, also the thermo-mechanical performance (CNFs) inferior compared to the traditional petroleum based synthetic polymers, as seen in CNFs literatures in the aforementioned section. Also, its analysis above did show that high-performance CNFs nanocomposites are more difficult to prepare due to challenges with composite fabrication methods.

(Yizheng Cao, 2013), furthermore, cellulose nanocrystals (CNC) nanomaterials, offer new possibilities for providing cementitious nanocomposites with improved mechanical, chemical and thermal performance. (Gindl W, 2004), were the first to use the CNC as reinforcement in nanocomposites, they demonstrated reinforcing cellulose acetate butyrate (photographic film) with various aspect ratios of CNCs. At CNC ratio of 32 vol. %, the tensile properties of the resulting nanocomposites improved by as much as five times compared to neat photographic film. This implies that CNCs served as excellent nano-reinforcement for polymers. CNCs high tensile strength network is possibly a key to improved nanocomposite strength and promising family nanomaterials a reinforcing phase in composite structures, they have several unique characteristics such as, they are 0.05–0.5 μm in length and 3–5 nm in width, potentially improve aging of fibers, high aspect ratio, high elastic modulus, and strength, low density, Their use as reinforcement in composite materials leads to an increase in setting time and a decrease in setting temperature.

(Obinna Onuaguluchi, 2014), proved that the addition of low volume fractions of cellulose nanocrystals (CNCs) enhanced the performance of

the cement paste (C-S-H) calcium silicate hydrate. The experiments, revealed that cellulose nanocrystals have stiffness comparable to that of steel because pf their high young's modulus value and high aspect ratio of crystals per unit of density. They have the potential to help resist material deformation in response to an applied force. The results showed an increase in the flexural strength of the cement past of approximately 30% with only 0.2% of CNCs addition, while the addition of 3% of (CNCs) and (CNFs) fibers in the cement paste mixture increased the fracture energy by more than 50% over the unreinforced material.

2.1.7 Polystyrene Concrete

Lightweight concrete (LWC) is an effective construction material in buildings, because of its lightweight, flexibility, and economic advantages. The essential characteristic of (LWC) is its low apparent specific gravity. In structural analysis, decreasing the density of concrete is a substantial factor that can reduce the self-weight, which represent a significant percentage of the total imposed load on the building. Furthermore, (LWC) reduces the cost of formwork and steel and also increases productivity. In general, it is one of the low strength lightweight concrete with good energy absorbing characteristics; it has excellent thermal and acoustic insulation properties leading mainly to non-structural applications including precast roof, precast wall panels, and lightweight infill blocks (Manolia, 2012).

(Manolia, 2012), the main aim of involving Lightweight polystyrene concrete (PC) in this study is to use it in casting the permanent forms of the ICF composite ribbed slab (Blank Block), to carry the wet concrete and labor weights. Vibration and compaction of EPS concrete during its preparation and placement causes segregation of polystyrene beads due to its low density and hydrophobic nature of the untreated beads. Therefore, bonding admixtures such as, superplasticizers and polymers, introduced to

improve the stability of the EPS concrete mixes, yielding anti-segregation EPS concrete that can be extruded and compacted under its self-weight. Mechanical (density, compressive, tensile and flexural strength), chemical, thermal and self-consolidation investigations are necessary for structural evaluations and simulations.

(Ravindrarajah, 1994), polystyrene concrete is inherently fire resistant; it can be easily cut, nailed, drilled and chased with standard woodworking tools. Given its three-dimensional cellular structure, there is a very weak or no interfacial transition zone between the aggregates and the matrix, which improves the durability aspects of the concrete matrix structure. Furthermore, it requires much less embedded energy for production and demolition compared to ordinary concrete. Also, the available produced and used Polystyrene concretes are load-bearing concrete and non-load bearing blocks; being lightweight it reduces the weight of superstructure and the size of foundations. The low-density results in the high thermal insulation of buildings and some instances reduce the thickness of roofs and walls. Many researchers tried to evaluate the ultimate mechanical and thermal properties, such as compressive strength, flexural strength, modulus of elasticity, Poisson ratio, and thermal conductivity, which are key parameters for evaluating the strength and durability of the structure and making decisions about sustainability. Their results showed that these properties are affected by the percentage of the polystyrene bead, the polystyrene bead size, and the polystyrene cement ratio.

2.1.8 Previous Experimentally Measured Properties of EPS Concrete

(Maura, 1978), concluded that the mechanical properties of EPS concrete increase with the increase of its density and these properties are controlled by the water to cement ratio. He also produced EPS concrete with densities between 220-460 kg/m3 and compressive strength between 0.7-2.3 MPa, while modulus of rapture was between 0.3-0.36 MPa. (Miled, 2003), EPS concrete can be represented by a two-phase composite material; matrix (mortar or cement paste) and inclusions (EPS beads). Since EPS aggregates have almost zero strength, EPS beads assumed as spherical shaped cavities holes of the same size. Two diameters of holes have been considered: ø=5 mm and ø=3 mm. However, the physical and chemical interactions in the interfacial transition zone that affect the bonding between EPS beads and the past matrix are not taken into consideration, which can influence the overall strength of EPS concrete lightweight concrete. The study concluded that the size effect observed experimentally on EPS concrete compressive strength is not due to the quas-brittle behavior of EPS concrete. However, it was mainly due to the randomness inclusions distribution of the EPS beads.

2.1.9 Expanded Polystyrene Beads (EPS)

(Ravindrarajah, 1994), polystyrene beads are a vinyl polymer produced from expandable polystyrene pellets (EPS), the raw material; Monomers, by free radical vinyl polymerization. The beads are inelastic and do not recover when deformed, yet they can withstand the pressure while they are embedded in the concrete matrix. When the polystyrene beads replace the coarse aggregate in concrete, the thermal properties of the mix improve, due to the polystyrene low Thermal Conductivity.

Polystyrene beads with (3-5mm) diameters used as a partial replacement of fine aggregate with an apparent density of 16.5kg/m^3.

2.1.10 High-Range Water Reducing Superplasticizer

(Zakka, 1989), superplasticizers are High-Range Water Reducing chemical admixtures capable of reducing three to four times the mixing water quantity in a given concrete mixture compared to normal water-reducing admixtures and improving the strength and workability of concrete, obtaining a better flowability as in case of self-compacting concrete. Approximately up to 1 % of superplasticizer can be added to the concrete mixture by weight of cement, with a water reduction in the range of 20 to 30 percent range can be achieved. It is probably the colloidal size of the long-chain particles of the admixture that obstructs the bleed-water flow channels in concrete; which helps eliminates segregation in concretes. The increase in compressive and flexural strength is proportionate with a reduction in the water-cement ratio.

Chemical mechanism background of the adsorption and hydration characteristics of cement and cement components is necessary for the understanding of the mode of action of superplasticizers on the mix rheology. “Superplasticizers significantly affect the rheological behavior of the cement paste. In general, the molecules of the superplasticizer align themselves around cement particles forming a watery shell as shown in Figure 16. These molecules are attracted to cement particles on one side and water molecules on the other. Thus, they create a lubricating film around the cement particles, which reduces both, the yield value and the plastic viscosity of the mix. These effects are more pronounced for higher concentrations of superplasticizer”.

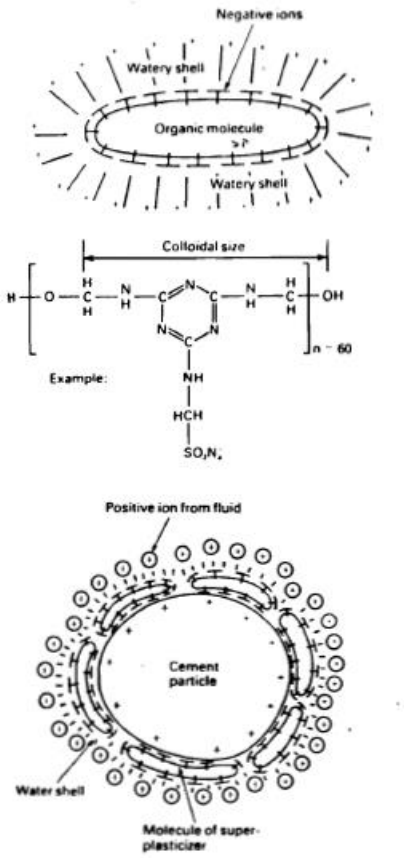


Fig. 16: Mode of action of superplasticizers (SNF) (Zakka, 1989)

When a small quantity of water is added to the cement, without the presence of the superplasticizers a well-dispersed system is not attained because, first, the water possesses high surface tension (hydrogen-bonded molecular structure), and second, the cement particles tend to cluster together or forms flocks (attractive force exists between positively and negatively charged edges, corners, and surfaces when crystalline minerals or compounds are finely ground). However, When a superplasticizers with a hydrophilic chain is added to the cement-water system, the polar chain is adsorbed alongside the cement particle; in this case the surfactant imparts a strong negative charge, which helps to lower the surface tension of the surrounding water considerably, making the cement particle hydrophilic and dramatically enhances the fluidity of the system without causing any undesirable effects on its fresh and hardened properties. As a result of layers of water dipoles

surrounding the hydrophilic cement particles, their flocculation is prevented, and a well-dispersed system is obtained. However, this high workability extends for about two hours; therefore, it is recommended to use retarding types of superplasticizers for hot weather, making it possible to add them to the concrete at the hatching plant (Zakka, 1989).

2.1.11 Polymer

(Mehta P. K., 2002), elastomeric or rubber-like polymers-based styrene-butadiene rubber copolymer (SBR) or (latex) contains about 50 percent by weight of spherical and very small (0.01 to 1 μm in diameter) Microparticles held in water suspension by surface-active agents. Since 10 to 25 percent polymer (solid basis) by weight of cement is used in typical the latex-modified concrete (LMC) formulations, the addition of latex supplies the concrete with a significant needed portion of the mixing water in concrete. Therefore, only a little more additional mixing water required; the spherical polymer molecules and the entrained air associated with the latex usually provide excellent workability. The hardening of latex takes place by drying or loss of water, forming a continuous and coherent polymer film which coats the hydrated cement products, aggregates, and even the cement matrix pores. It has excellent chemical resistance, high initial strength and high modulus of elasticity. Nevertheless, thermal and creep characteristics of the latex are not in favor for structural applications, because of polyester concrete exhibit both viscous and elastic characteristics, enabling it to fail under creep at stress levels greater than 50 percent of the ultimate strength. Creep at a stress level of 25 percent did not reduce ultimate strength capacity for a charging period of 1000 h. "The researchers recommend, therefore, that polyester concrete is considered for structures with a high ratio of live to dead load and for composite structures in which the polyester concrete may relax during long-term loading."

Latex improves the tensile and flexural strengths of mortar or concrete. Nevertheless, the strength gains are not impressive enough to justify the use of expensive latexes in making LMC products. The most impressive characteristics of latex are its ability to bond strongly with old concrete and to resist the entry of water and aggressive solutions.

2.2 Insulated Concrete Walls and Slabs (ICF)

The following studies are the ones deemed most germane and comparable to the objectives and results of the study of insulated concrete forms (ICF) walls. Their scopes illustrate the need for further study, especially for understanding different structural and thermal characteristics. This section reviews research and information available on insulated concrete form walls, engineered cementitious concrete (ECC) and standard concrete mixes, properties of self-consolidating concrete and ICF wall design procedures.

(Mehrabi, 2000). The objective of this thesis was to study the response of screen gird ICF walls subjected to lateral in-plane cyclic loading. This study aimed to compare the in-plane shear resistance of three types of significant wall systems such as ICF wall panels, wooden and steel frames with an equal thickness of 100mm (4in) and aspect ratio (height/length) of 2 used in residential buildings.

The three ICF wall specimens tested under standard monotonic-load imposed by a 60-ton-capacity lateral hydraulic ram were flat, screen-grid, and waffle-grid ICF wall panels, with an average28-day compressive strength of ordinary concrete cores of 42 MPa (6144 psi) and 35 MPa (5110 psi) for footing and ICF walls panel, respectively. The primary tools and references used for the experimental setup were the (ASTM E564, 2012)

for instrumentation requirements and the Prescriptive Method (PATH, 1998) for ICF walls.

This study proved that ICF wall systems resisted winds and earthquakes of about twice as much load as the maximum strength of wood- and steel frames, wall panels systems used in residential buildings without exhibiting any sign of damage or distress, especially when subjected to lateral in-plane loading, confirming that ICF wall systems are advantageous over other types of the residential wall systems in construction. Nevertheless, more investigations to quantify the behavior and strength of ICF walls for codes and standards serviceability matters required.

Flat ICF wall had the Maximum lateral resistance of15533 kg (34,245 lb.) over the ICF screen grid and the ICF waffle-grid with almost similar deformations. The author recommends further experimental investigations including analytical models, simulations and broad-reaching parametric studies that could yield reliable code and design standards for ICF walls panels.

(Yland, 2000), the objective of this Ph.D. thesis was to study the response of 12 screens gird ICF walls subjected to lateral in-plane cyclic loading with a set of walls. The first set was tested with monotonic flexural loading, the second set under an additional eccentric axial loading and the third set with an additional out-of-plane flexural loading; the ICF walls had two aspect height to length aspect ratios of, 1:1 and 2:1, The other wall types consisted of a single block (at component level) and had three aspect ratios: 3:1, 2.5:1, and 2:1, the results for peak forces, displacements, story drift, ductility ratios, and failure modes were reported.

The central unit used for constructing the full-scale ICF 3 M (10 ft.) grid walls was an ICF made of EPS concrete were having 254 mm (10 in) thick, 381mm (15 in) tall, and 762 mm (30 in) long with 152 mm (6-in) diameter vertical and horizontal cores spaced 381mm (15in) on center. The compressive tests performed on the EPS concrete (the material of the ICF forms) and the regular concrete used for the ICF walls, both independently and as a composite material. The EPS material by itself showed the compressive stress of 0.62 MPa (9 psi) at a strain of 0.003. Moreover, the regular concrete exhibited compressive stress of 12.4 MPa (1800 psi). Both materials as composite exhibited a 31% increase in compressive stress of 16.62 MPa (2410 psi) for specimens cured in EPS mold and tested without the EPS forms and a 102% increase in compressive stress of 25.60 MPa (3710psi) for specimens cured in EPS mold and tested with the EPS forms.

The mix design for each wall was 20.68 MPa (3000 psi), and each wall was cast in a single lift with no vibration. Each wall subjected to an axial load of 44.5 KN.The loading protocol employed took 57 total cycles before failure at the drift of 1%. The walls with higher aspect ratios performed slightly better than with lower values. The EPS concrete confined the ordinary concrete at 0.3% strain compatibility, which in turn increased resistance capacity to the lateral load and deformation.

Lastly, (Yland, 2000) noted that the maximum loads capacity resisted by a specimen subjected to cyclic loading were about 60% - 70% of a monotonically applied load on the same wall.

(McKee, 2001), this research development report investigated the effects of height-to-length aspect ratio, windows, openings and the current minimal reinforcement details experimentally, provided by the Prescriptive Method (PATH, 1998), on the lateral shear capacity and the behavior of three types of ICF walls, (flat, waffle-grid, and screen-grid) . In addition

to, evaluating the in-plane lateral shear capacity of ICF walls in residential construction to improve ICF walls design and construction rules and conditions in the Prescriptive Method (PATH, 1998) and the International Residential Code (ICC, 2000)."

The representative concrete compressive strength of an average 28-day value of 1,788 psi (12.3 MPa) found. Observations of ultimate lateral load capacity, initial stiffness, cracking energy dissipated and Load-displacement curves were plotted, The LVDTs recorded the lateral displacement of the top of the wall, the lateral displacement (or drift) and uplift at the base of the ICF walls.

The maximum lateral in-plane capacities of the three types of ICF walls with no opening and with window opening was for the favor of the flat ICF walls of 92.8 KN (20.84 kips) and 175 KN (38.57 kips) respectively. For the three ICF walls with garage opening, all had similar results of 2 kips. The flat model assumed to resist shear by its uniform core section. The screen and waffle models assumed each 4-ft segment dominated by shear and that each 2-ft segment dominated by flexure. Therefore, the ACI 318’s prescriptions for the shear capacity, was suitable for the screen and waffle models with no openings.

There are no specific code requirements to be considered when the walls are provided with openings. Therefore, the limitations should be judgmental. If the opening is near the middle of the wall, it will decrease the moment capacity of the wall only slightly; however, the shear strength may be significantly reduced. In contrast, an opening near a wall boundary may affect both the moment and shear strengths. In general, providing additional transverse boundary reinforcement can increase the strain capacity of a wall. Thus, rather than providing an arbitrary amount of confining reinforcement at the wall boundaries, confinement is selected

based on the deformation or strain demand. (Ali, 1990). It was observed from the paper that the walls exhibit stable behavior with ductility when the openings are located in the flexural compression zone. If the large openings are provided at the base has not much influence on the behavior or strength of the wall compared to walls without opening. Finally, it was concluded that the walls with openings should be designed as concrete moment frames.

(Abrams Daniel, 2002), this report studied the properties of two 150mm(6”) core ICF systems, an ICF waffle-grid wall system (Polysteel) manufactured by American Polysteel Inc. Also, a screen-grid wall system (Reddi-Form) manufactured by Reddi-Form Inc To determine their lateral capacities and in-plane flexure performance, explicitly confirming the manufacturers’ design tables and building codes and standards under static and cyclic loads and eventually rating the ICF wall types about insurance and loss for these ecological threats.

Six ICF wall panel of 2.4 M (8ft.) by 2.4M (8ft.). The wall panels constructed according to the ACI-318 Code and the International Residential Code specifications for dowel size, placement, and embedment for lateral shear and flexure wall tests. One panel of each form type reinforced as per the manufacturer’s specifications for a second story wall, while two panels of each form type reinforced as per the International Residential Code (ICC, 2000).

The design wind speed was 130 mph for determining the recommended reinforcement. All reinforcement was Grade 40. The 28-day concrete compressive strength 18.5 MPa (2686 psi), maximum aggregate size of 3/8”, and slump of 5 to 6 inches specified according to the minimum manufacturer's specifications, the Prescriptive Method (PATH, 1998) and ASTM C143/C143M (ASTM E72-95, 1995).

The methodology and procedures involved constructing twelve ICF wall specimens. Three ICF wall specimens tested with one type (wall 2) with cyclic lateral loading. Three significant displacements measured, the uplift of the leading edge, the compression at the toe of the wall and the wall using the transducers.

Three Reddi-Form ICF wall specimens tested in a horizontal position for flexure strength. The vertical actuator applied the flexural loading at the middle span of the walls. The walls were loaded until it showed flexural cracks and the failure of vertical reinforcement.

The maximum lateral monotonic static loading ranged from 16000 lb. to 19200 lb. for the twelve ICF wall specimens tested. The load-displacement graphs indicate linear behavior until footing crack initiation and dowels yielding, showing an elastic-plastic relationship with a proportional limit. The damage occurred in the concrete due to tensile and shear forces in the reinforcement specified and provided as per the International Residential Code (ICC, 2000) and the manufacturers. The capacity of ICF systems under static design loads is adequate without suffering damages, especially when they are in an actual application where connections to roofs and floors contribute to the lateral strength of the structure. For the three Reddi-Form flexure ICF wall five specimens, the walls cracked at each span is calculated maximum moment.

“Polysteel” ICF Wall 2 specimen (with, the maximum cyclic lateral loading in the horizontal actuator was 11 kips (49 KN); the toe displacement was at 0.01in. (0.26 mm). The cyclic stress pattern causes tension failure in the dowels at both ends that complicates interpretation of the experimental results, a phenomenon well documented in the literature. Therefore, approximate mathematical regression for displacement

relationships developed to relate various symbols directly or indirectly to the relative displacement of the point of lateral loading.

The ICF walls in general exceeded, their design shear, flexure, and wind load capacities. The performance of the shear wall panels was dependent on the footing connections while deflection was dependent upon the amount and location of reinforcement after the concrete had cracked and exposed the steel. The cyclic results used to identify the nature of the footing connection damage and failure. The ICF walls with manufacturer specifications were conservative but had a ductile failure. The walls built to the International Residential Code (ICC, 2000) specifications were efficient, with brittle to ductile failure behavior because of the yield of the steel reinforcement when the concrete strength exceeded.

The most important finding of this study was the minimum specification of #4 dowels at 2 ft. Spacing was not sufficient to prevent the ICF wall from overturning. The static and cyclic shear tests showed opening of the joint of the wall to the footing, cracking in the footing at the dowels and loss of load resistance at the horizontal actuator. The study recommended finite element modeling of the dowels and the interface between the footing and the ICF wall in the actual single story and two-story buildings without giving any comparison between Reddi-Form ICF wall and Polysteel ICF wall.

(Zollo, 2003), this article shows that by using the standard engineering design methods, like working stress or ultimate strength, one can design and analyze both the ICF fiber-reinforced concrete (ICF-FRC). Also, comparing that to the ICF plain structural concrete (ICF-P) wall, according to the requirements of the (ACI 318-02, 2002)Building Code (Chapters 9, 10, 11, 12, and 22). Such code-compliant designs should yield structural integrity, efficiency, and safety.

The procedure involved a comparison between the factored axial load and the ultimate magnified moment values, obtained from design procedure using the semi-empirical strength of materials (SOM) analysis. i.e., yield line method, Building Code Formulas, and procedures, and the finite element method (FEM) analysis, applied on a simple ICF-FRC rectangular exemplar house sized 24 x 50 ft. X 9 ft. (7.3 x 15 m x 2.75 m). The FRC materials and RC structural elements materials assumed to have the flexural behavior of an elastic-perfectly-plastic mode that is limited to small displacements for linear assumption validity.

The axial load capacity and the moment capacity for 4-in.-thick (100 mm) ICF-P walls and the ICF-FRC walls found as structurally inadequate per (ACI Eq. (22-5)), of (ACI Eq. (22-3)) respectively, for concrete compressive strength fc′ of 3 psi (20 MPa). For the ICF-FRC 4 in. (100 mm) Wall the wind loading conditions LC#3 and LC#4, SOM and FEM analyses shown as two points. These loading conditions each fall beyond the interaction capacity (below and to the right) when Fig 24.

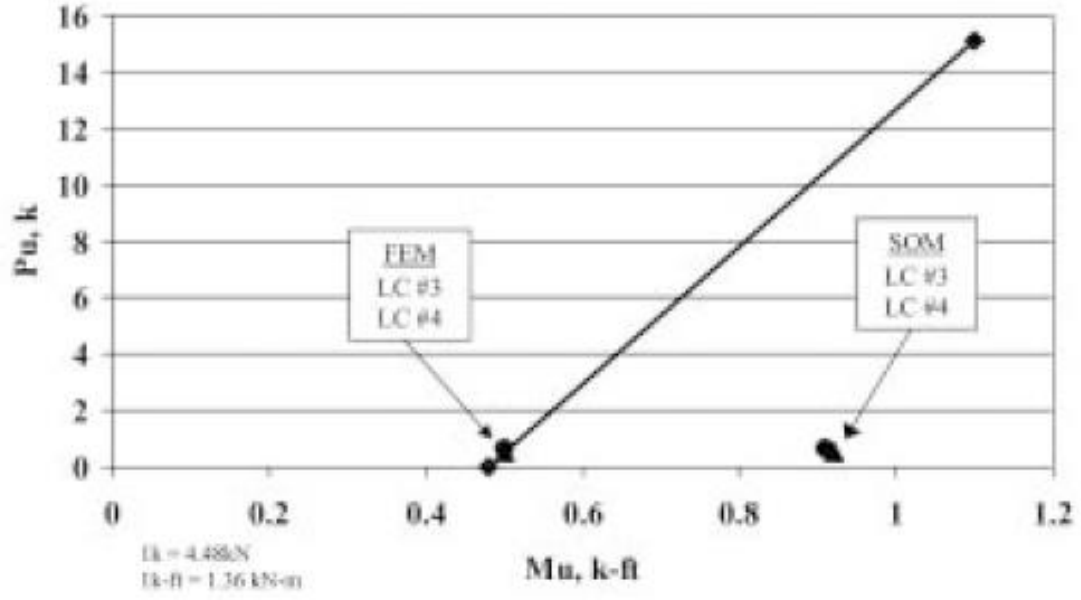


Fig. 17: Force interaction diagram for 4-in.-thick (100 mm) fiber reinforced concrete insulating-form wall

The considered factored load case LC#3, for 6in (150mm)) ICF-FRC wall as non-sway (ACI 10.12), the SOM analysis, yielded ultimate factored total axial load Pu= 0.65 k/ft. Moreover, an ultimate magnified moment M_{mu} = 0.91 k-ft. /ft. (4.1 KN-m/m) moreover, from the FEM analysis, the wind moment M_{mu} = 0.50 k-ft./ft. (2.2 KN-m/m), but for factored load case LC#4 using SOM, gives ultimate factored total axial load Pu= 0.55 k/ft. (8.0 KN-m/m) moreover, an ultimate magnified moment M_{mu} = 0.92 k-ft. /ft. (4.1 KN-m/m) compared to FEM analysis wind moment M_{mu} = 0.50 k-ft. /ft. (2.2 KN-m/m). The plotted points fall within the interaction curve to the left of the minimum vertical reinforcement line, the system satisfies the design criteria as shown by the interaction diagram and forces plotted in Fig 25.

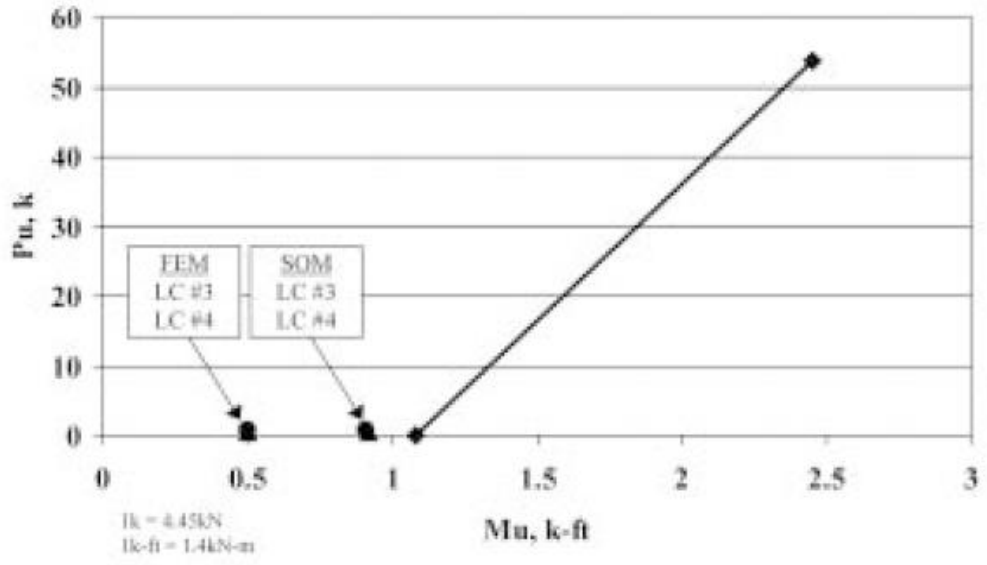


Fig. 18: Force interaction diagram for 6-in.-thick (150 mm) fiber reinforced concrete insulating-form wall

Due to the low structural axial loads, considered in ICF residential-scale structures of one- or two-story buildings that rarely controls design as per the code. Therefore, the interaction diagrams represent only the

portion of the curve bounded by points representing the yield stress (at balanced concrete compression failure and reinforcement tensile yielding) and Pure bending with zero axial loads (under-reinforced with ductile reinforcement tensile failure) and below balanced failure conditions.

(Brandon, 2009), the objective of this study report was to experimentally find the flexural strength capacity of the ICF full-scale waffle "HOBBS Wall" system especially under lateral soil pressure and compare the results to the current conventional steel-reinforced concrete wall systems designed under lateral loads.

Two ICF full-scale waffle "HOBBS Walls "each with the size of 124 inches tall by 48 inches wide tested by an equivalent four-point loading pattern in analogy to the distributed loading. The line loads were positioned (L/4) distance from the supports, thus providing a space between of (L /2), where L represents the span length. The test set-up is given as shown in Figure 19. The loading device has a 10-ton hydraulic loading ram, which centered on the full-scale waffle specimen.

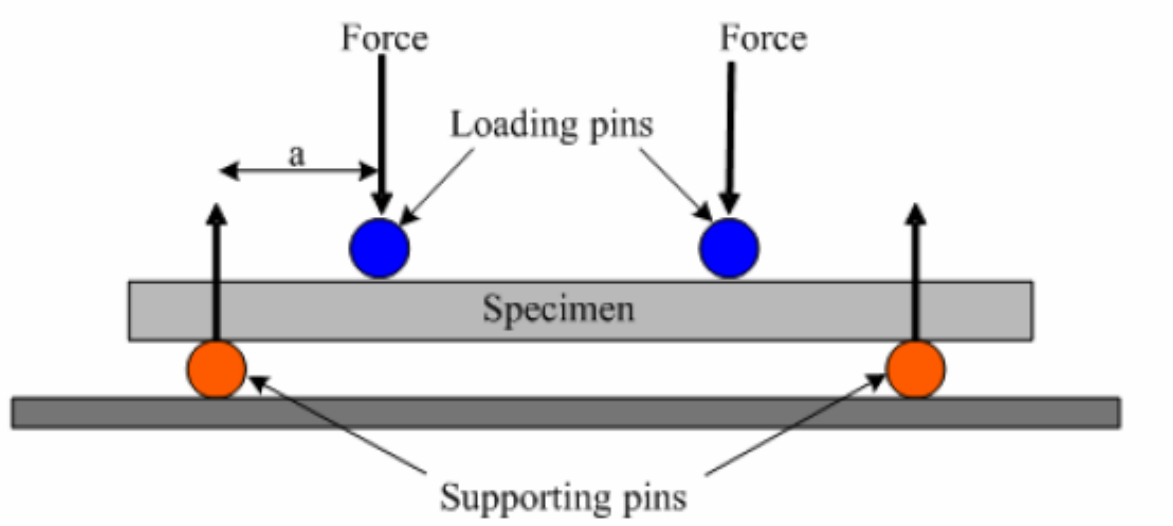


Fig. 19: Theoretical 4-point loading system

The concrete cylinders tested yielded an average strength of 16.9 MPa (2448-psi), the flexural strength of concrete yielded an average modulus of rupture of 2.57 MPa (372.2 psi). The vertical displacement of the specimens measured at mid-width and quarter points along the length of the specimen by the transducer. The ICF full-scale waffle "HOBBS Wall" specimens tested simply supported beams with one end is pinned and the other supported on rollers.

The average flexural strength capacity of the two ICF full-scale waffle "HOBBS Wall" specimens, found to be of 0.017 kN-m (12.451 k-ft.) due to applied lateral loads. Also, 0.0197 kN-m (14.56 kip-ft.) moment capacity found when considering the contribution self-weights of the testing equipment and wall specimen. At the maximum flexural capacity, the average shear force yielded 26.4 kN (5.925 kips). Therefore, the composite wall section of the "HOBBS Wall" provided additional capacity, approximately 0.0065 kN-m (4.80 k-ft.) for the four-foot wide specimen, when compared to a conventional steel-reinforced concrete wall section not incorporating the EPS foam or PVC furring assemblies of the same size.

(Werner, 2010), the primary objective of this study is to determine the lateral strength capacity and deformation (drift ratio) of – APEX and FASWALL grid ICFs Screen Grid Insulated Concrete forms (SGICFs) wall systems. With dissimilar material and geometry under cyclic loading to compare both types of ICF systems experimentally and their computer models, at the component level. For this purpose, material tests also performed on each type of ICF's formwork, both to aid the modeling process and to show the performance of each wall formwork material at target strains. The specimens' component samples tested with and without forms confinement (having the forms removed), with varying types of

reinforcement, and different types of concrete (ECC concrete versus standard PCC) to understand their impact on the performance of each ICF system.

The experimental results showed that the specimens' component with ICF's formwork resisted the lateral load by 100% and the deformation (drift) by 60% more than the specimens' component without ICF's formwork. The computer models overestimated the lateral capacity of the samples by 50-100%, and even more for other certain samples, therefore completely neglected in the thesis. The overall size of the specimen's component of the APEX made of EPS beads and cement resulted in 32in tall and 35.5in long, and that was by joining tow APEX unit blocks measured 16in x 48in. The length had to be reduced by 6.25in on each side to fit into the load frame . The prescriptive methods limit the allowable height of APEX ICF structures to no more than two 10 ft stories above grade.

FASWALL, made of wood chips and cement, unit block measures 8-in tall 24-in long, therefore four FASWALL blocks assembled which yielded a sample of 32-in tall x 24-in long and fitted to the load frame similarly as the APEX samples. Both APEX and FASWALL had varying reinforcement in the vertical cores in the specimens. FASWALL specimens had higher stiffness in the vertical cores over the horizontal cores than for the APEX specimens. APEX and FASWALL specimens demonstrated ultimate lateral loads of 48.6 kip (216 KN), 73 kip (325 KN) and ultimate shear loads of 46 kip (205 KN) and 40 kips (178 KN) respectively.

At specimen's component level, using a fiber reinforced cementitious concrete (ECC) that contains only 8mm long polyvinyl alcohol fibers and clean sand as aggregate. There is no coarse aggregate used for this mix

(ECC), which used instead of ordinary concrete (PCC), both had a compressive strength of 4000 psi to 7000 psi with strains of 0.003 and 0.002, respectively. Uncovered increased in the maximum load resistance by 24% - 68% and significantly improved the deformation (drift ratio) capacities up to 3%for both sample types.

Material property tests determined the compressive strength for EPS concrete and the woodchips concrete (the main ingredients of both ICF forms) to be 0.14 MPa (20 psi) and 0.48 MPa (70 psi) respectively and the strains of 3% for both.

The ECC did not increase the lateral capacity of the nominally reinforced specimen with form in place (F31), or the capacity of the reinforced specimen with form removed (F32R) but increased significantly the capacity to resist drifts.

(Mircea, 2010), the research aimed to evaluate the Amvic flat ICF wall system for meeting the actual earthquake design resistant requirements given by the unified European code of the structural seismic design and detailing constructive provisions of reinforced concrete shear walls, whereas ensuring its efficiency. The nominal size in of an ICF block unit is of 1.220 × 0.406 m, covering a lateral vertical area of 0.50 m^2, and the depth of the walls is 153.4 mm, 203.2 mm and 254.0 mm.

ICF flat walls with thicknesses of 153.4 mm and 203.2 mm considered in this research, corresponding to valid thicknesses of 150 mm and 200 mm respectively.

The first methodological step in the complete structural evaluation of the flat ICF wall system was the assessment of the system to meet the constructive detailing provisions for seismic design of the European structural design code. The 400 mm horizontal rebar spacing of Amvic ICF

wall system satisfies the maximum distance between horizontal rebar of (EN 1992-1-1 , 1992) with no tying in the vertical direction. The vertical shear reinforcement connected to the horizontal rebar by ties. Nevertheless, the need for minimum reinforcement due to shrinkage of concrete almost eliminated in the case of ICF walls. The end longitudinal reinforcement, to resist in-plane bending moment, is the crucial issue in detailing for seismic design. Therefore, stirrups to provide confinement of the end zones must restrain longitudinal rebar.

About the ICF system, it is more convenient to fix the longitudinal rebar by the horizontal shear reinforcement. However, this approach is suitable for gravitational design and for detailing the reinforcement above the critical region of the shear wall, but it is not an appropriate design within the critical regions. Thus, two solutions considered as given below:-

- The first one suits the situations where no confinement of the end zones needed, by placing new stirrups at 400 mm intervals, between the horizontal shear rebar.
- The second alternative, suitable for heavy duty walls presumes the introduction of the longitudinal rebar in the formwork already assembled in a spatial tied up case. The distance between the stirrups efficiently computed to avoid post-elastic buckling, and together with the stirrups diameter to provide the adequate confinement ratio.

The second methodological step was the non-linear parametric analytical and numerical evaluation based on the normalized axial force, the seismic zone and the corresponding number of stories. The results regarding the shear forces and bending moments were determined. The analyses organized in an incremental procedure following the traditional Newton-Raphson scheme, no confinement considered.

The results reveal that for 150 mm ICF flat wall with low values of the axial force can go up to 7 stories of floors and up to 9 stories for concrete walls 200 mm thick respectively. Even in the most powerful earthquake with a ground acceleration of 0.32g, the ICF flat wall structures behave in the elastic range. Shear failure risk increases with the elastic behavior. Thus, for a low number of stories, we must consider a medium ductility design, with a safety behavior factor. The first detailing solution considered by confirming shear capacity, no confinement of the end zones and the use of longitudinal end rebar with large diameters. For taller buildings, the second detailing solution adopted. Confinement of the end zones will provide more ductility and prevent the post-elastic buckling of the longitudinal rebar. It indicates a higher steel intake but provides energy dissipation and prevents brittle failure.

Given the specifics of the ICF system, which has plastic spacers that do not allow the use of sizeable transverse reinforcement placed at short distances on the vertical direction, confinement can be provided in this latter approach only in the areas placed in the vicinity of the ends. Therefore, the neutral axis of failure should be guided to lie as shown in Figure 20 using a careful analysis of the ends reinforcing ratios and confinement grades. (Stirrups at 400 mm for seven stories Stirrups at less than 400 mm cannot be provided b/c of plastic ties in our system, steel ties must be provided at 400 mm, and no seismic zones are considered.)

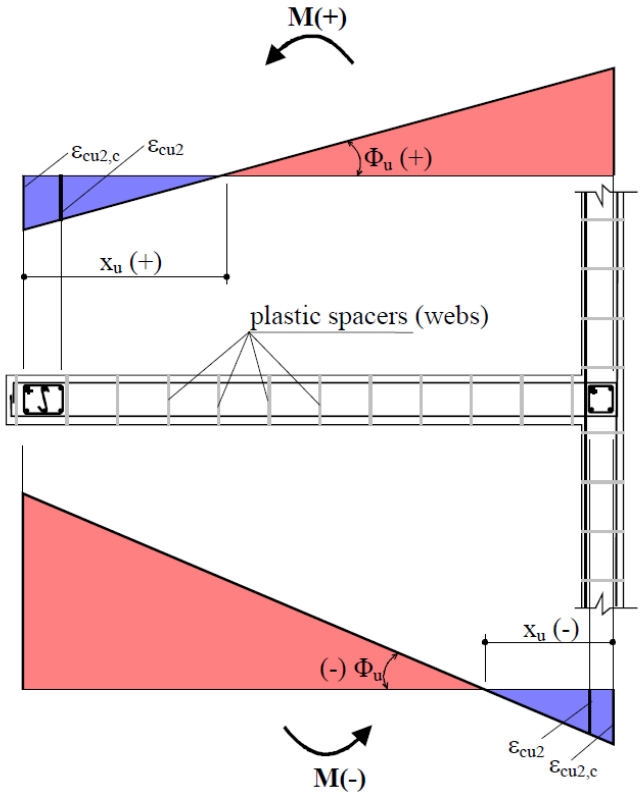


Fig. 20: End reinforcement detailing for high ductility design.

(Andreea Mircea, 2000)

The ICF flat wall systems are valuable solutions in sustainable design provided, each system should comply with performance-based design codes and standards. The research concluded, that the Amvic ICF flat wall System allows a reinforcement detailing to satisfy all structural demands, providing a reliable structural and insulation designs for green buildings.

(Peter Dusicka, 2011), the objective of this study was to determine the in-plane lateral strength capacity of 13Full-Scale screen-grid ICF specimens. All ICFG constructed by stacking of the Apex ICF forms (10 in wide, 16 in tall, and 48 in long) and the effects of two (height to length) geometrical aspect ratios (H/L = 0.89 and 2.67) investigated. Also, the walls performance and response with and without low vertical loads recorded. The displacement controlled cyclic loading protocol used for this

procedure, the test set up required vertical axial distributed compressive loads exerted by the hollow core hydraulic rams. In addition to the horizontal load from the actuator, linear displacement transducers (LDTs) fixed. Reverse cyclic loading were imposed on the wall based on the drift ratio D expressed in percent as (D = 100 Δ*H); where Δ displacement measured by LDT 1; and H = wall height from the foundation to LDT 1. The cyclic drift deformation history recorded.

This study indicated that ICFG walls strengths for low aspect ratio were more than five times greater than ICFG walls without axial load, and over four times greater than ICFG walls with axial load with the large aspect ratio which demonstrated flexural-response. Besides, considering a linear relationship between the strength and the number of vertical reinforced concrete cores of the ICFG wall is invalid by applying empirical relation to measure deformations and ductility. Although, it is affecting the general behavior of the ICFG walls because the nonlinear relationship which needs to be confirmed by the numerical analysis. It is also stated that, unlike flat ICF wall failure governed by concrete core unit, the number of reinforced concrete vertical cores of the ICFG wall instead governs the failure mode. Surprisingly, the material of the ICF forms made of polystyrene beads and cement contributed to the performance of the ICFG walls despite its very low compressive strength of 0.26 MPa (37 psi).

(Radovic, 2012), there were three interconnected objectives in this study. Firstly, numerical FEM analysis with SAP2000 conducted to determine the representative residential ICF wall model of various structural aspects to withstand the lateral loads caused by high-velocity winds to be built and tested. Secondly, experimental comparison took the place of lateral strength capacity between two flat ICF walls identical in size, reinforcement and opening but had two unique concrete mixes the

first used ordinary concrete (control mix) and the second flat ICF wall used a trail mix (experimental mix) made with recycled coarse aggregates. Also, the numerical ICF wall model validated with in-plane shear testing of full-scale ICF wall. The third Objective- construction and materials cost comparison between flat ICF residential wall system and traditional wall system took place.

Seven, linear transducer (LVDT), measured the displacement, horizontal slip, and uplift of the footing during the testing. Four PL-60 strain gauges placed on the compression sides of the wall measured the strain deformation on the concrete surface.

The compressive strength of the trail (experimental) mix yielded an 8 MPa (1,164 psi) which was below the minimum limits specified by a Prescriptive method for insulating concrete forms in residential construction for residential structural concrete of 17.2 MPa (2,500 psi). Also, the flexural strength showed the value of 16.5 MPa (2,399 psi). The compressive strength of the ordinary concrete (control mix) mix yielded a 31.5 MPa (4,565 psi). The flat ICF wall with experimental mix (SW2) shear capacity of (27.7 kips) was much less than the shear capacity of the wall with control mix (SW1) which resulted in (40.5 kips). Both flat ICF walls shear capacities were greater than the minimum shear demand of (21.1kips).

The study showed an overall saving of 13.6% via in-situ built ICF shear wall over the conventional pre-cast ICF wall.

(Garth, 2014)**,** this study studied the performance and the resisting capacity of a full-scale “Farwell” screen-grid ICF walls, same forms tested by (Werner, 2010) at components level, subjected to lateral loading series. This thesis tested the contribution of the “Farwell” wall forms and the

addition of a distributed axial load on the overall performance of the "Farwell" screen-grid ICF walls, the result was compared to the previously tested screen-grid ICF walls in terms of their the aspect ratio, performance of the walls with and without wall forms. Finally, some design comparisons and suggestions for "Farwell" screen-grid ICF walls proposed based on the results.

Seven full-scale "FASWALL" screen-grid ICF walls shown constructed with the standard FASWALL forms (8 in tall, 24 in long, and 12 in width). The aspect ratios of the ICF walls assumed to have both flexure-dominated and shear-dominated failures. For ICF walls of 48 in and 96 in long, the aspect ratios were 1.98:1 and 0.99:1, respectively, for the second set of ICF walls of 48 in and 96 in long, the aspect ratios were 1.74:1 and 0.87:1 respectively.

Regular concrete mix used for each screen grid ICF walls a 20.68 MPa (3000 psi) compressive strength at 28 days and a slump of 165.1 (6.5 in.) and assumed 17.2 MPa (2500psi) compressive strength for calculating the shear strength from (ACI 318-11, 2011).

The long walls (low aspect ratio) experienced both flexure-dominated and shear-dominated failures with a higher lateral capacity, while the short walls (high aspect ratio) showed shear-dominated failure low lateral capacity.

The ICF forms increased the peak shear by 28% and 56% and the drift capacity of by 90% and 114% for the screen grid ICF short walls and long walls, respectively. Also, this study compared mainly the lateral load capacities results to other empirical and experimental values of other comparable types of screen grid ICF walls with some attention for drift capacities.

The peak experimental loads of the Screen-grid ICF walls were compared to the ACI equation (ACI 11-3) equation for minimum required shear strength assuming no axial loads and equivalent thickness, the (ICC-ES Equation 4.1.1.7) equation for minimum required shear strength as per (ICC-ES ESR 1770, 2012) assuming equivalent thickness and FASWALL-specific load tables. Even though the study thought the three methods yielded reasonable approximations, on the contrary, it resulted in stochastic values, mostly conservative and some were underestimated and fatal, simply because the study considered an approximation for equivalent thickness and the methods above meant for constant flat wall solid sections and not for screen grid sections.

2.2.1 Self-Consolidation in ICF Construction

(John G. , 2003), the self-consolidating concrete mix with a high-range water reducer and a viscosity-modifying admixture obtain unique flow characteristics compared to the other mixes. It can flow and consolidate under its weight. At the same time, it can flow and fill spaces of almost any size and shape without segregating. As a result, SCC can safely flow longer distances than baseline concrete mixes without risk of segregation, resulting in fewer filling points. SCC with a high-range water reducer and VMA typically cost more than baseline concrete mixes. Again, these higher material costs can be offset by reduced labor efforts for good consolidation. When mechanical vibration was not utilized, there was often long voiding with the standard concrete (Mix No.1), typically were noted in areas of steel congestion, particularly below the lap regions of horizontal reinforcement. The most reliable way to minimize voids with no mechanical vibration was to use a (Mix No.4). This is illustrated in Figures 21 to 24.



Fig. 21: Waffle-grid ICF with low slump concrete and no mechanical vibration (John G. , 2003)

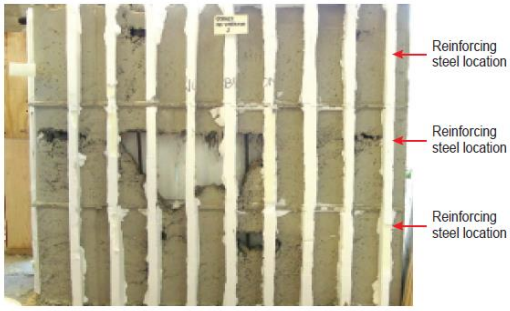


Fig. 22: Flat-panel ICF with medium-low slump concrete and no mechanical vibration (John G. , 2003)



Fig. 23: Waffle-grid ICF with high slump concrete and no mechanical vibration (John G. , 2003)

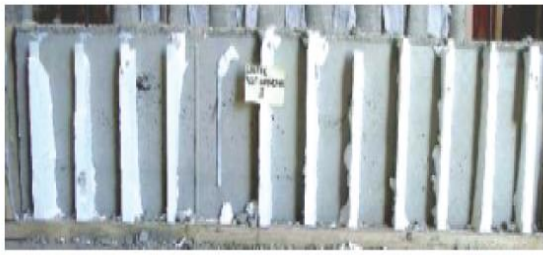


Fig. 24: Flat-panel ICF lintel with high slump concrete (no mechanical vibration) (John G. , 2003)

These findings indicate the promising role that the use of high fine content SCC concrete may have in ICF construction. However, because of this innovative development which is necessary to enhance the marketability of the SCC concrete in the ICF industry and to improve delivery mechanisms of concrete into ICF wall systems. Current sources of fines are typically readily available to the ready-mix industry in GCC countries. The fine aggregate industry's capability to bring fine materials to the concrete producers will improve the marketability of fines to the ICF construction industry (Mondal, 2007) One of the objectives of this thesis is to use Nano-concrete with CNCs nanoparticles as an alternative to SCC with a high-range water reducer and VMA in ICF systems and evaluates its self-consolidation by T_{50}Slump-flow. However, vibration and

compaction are restricted in ICF systems because it induces the possibility of blowouts due to a maximum pressure of 6.2 kPa on the unreinforced polystyrene locations of the formwork. Subsequently, the formed voids in the concrete such as honeycombing and poor consolidation around reinforcement can affect the structural integrity of the walls. The polystyrene of the ICFs is not normally removed after concrete placement, obstructing visual inspection of the concrete potential voids and improper consolidation. Additionally, as the thickness of concrete in ICF walls reduced, the potential for voids below laps of horizontal reinforcing increases significantly. This is especially the case for the 100 mm flat panel ICF corner and lintel configurations with congested reinforcement.

(Ashok, 2004), studied varieties of concrete mixes' consolidations in ICFs walls including flat-panel, waffle-grid, and screen-grid systems. Three concrete mix designs used in this study included ordinary concrete with no admixtures, modified concrete incorporating high range water reducing admixture, and self-consolidating concrete (SCC) which included a high-range water reducer and viscosity modifying agent (VMA). The objective of this study was to evaluate the effects of applicability and performance of SCC and to investigate the different consolidations of concrete mixes and its effect on reducing the quantity, size, and distribution of voids in the concrete of typical ICF walls using locally available materials, in 1200 mm and 2400 mm high lifts of ICF walls, as well as concrete flow in corner areas were investigated.

Four different types of concrete mixtures studied regarding consolidation:

1 Utilized standard concrete (baseline) mix, and no means of mechanical vibration. (Mix No.1)

2 Utilized the standard concrete (baseline) mix and different methods of

mechanical vibration. (Mix No.2)

3 Utilized (baseline) mixes high-range water reducer to increase the flowability of the concrete. The mechanical vibration was not used with the flowable concretes. (Mix No.3)

4 Utilized self-consolidating concrete (SCC) mixes with high-range water reducer and VMA. The mechanical vibration was not used with the flowable concretes. (Mix No.4)

(Bookers, 2005), the main hurdle to ICF residential construction is the excessive stalls experienced in the discharge rates allowed during placement of the ordinary concrete into the ICF wall. The CNCs improves and streamlines the place ability of an SCC in ICF systems. All of which could contribute to the advancements relate to the refinement of the structural requirements for ICF construction regarding wall thickness, concrete strength, and reinforcing requirements.

2.3 Executive Summary

To the best of my knowledge, the later listed research literature are the first studies to investigate CNCs in cement matrices of Nano-concrete and dealt only with the material properties of C-S-H. Hence making this study a premier one. For instance, previous studies were limited to the use of carbon nanotube and Nano silica sand for reinforcing cement composites because of their high aspect ratio and an associated capability to bridge Nano-cracks and increase the strength of cement. In this study the generic term ‘nanocellulose’ and ‘micro cellulose’ to describe all of the types above of CNCs and CNFs respectively adopted.

Insulating concrete form (ICF) systems are a superior alternative to slab and walls frames for residential and commercial construction. They have beneficial and higher thermal and structural properties that provide

catastrophe resistance. However, the previous studies for the ICF walls in the literature review were either numerical, exclusively dealt with flat ICF walls, or experimental with some unpromising numerical attempts, mostly dealt with screen grid ICF walls.

2.3.1 Experimental Investigation

The previous experimental studies conducted tests on specimens at the component and full-scale levels. The tests at a component level were entirely concerned with the ICF screen grid and waffle types of walls. The followings are essential observed points:

- The most of papers have concentrated in the experimental testing of ICF walls of a specific type, even though there are three types of walls – namely, flat wall, screen-grid systems and waffle type of walls. The researchers mainly investigated the lateral strength capacity against wind and seismic loads of the screen grid ICF wall systems widely.
- Investigated to limit extent the flexural strength capacity of ICF walls.
- Investigated confinement of the different prefabricated forms (EPS, EPS + cement, wood chips + cement) to screen grid ICF walls, and the compressive strength of prefabricated forms.
- The main property of ICF systems is thermal insulation which unifies the system from other modern types of construction; it was inferred from the above reviews that the thermal conductivity properties (K and R values) of the materials used in their investigations and researchers of ICF walls had not been evaluated.
- Determined the apparent reported manifestations and behaviors, such as, the displacements (or drift), uplift at the base of ICF walls, ductility ratios, and failure modes, in relation to lateral strength capacity for ICF walls of different ICF walls with openings ratios, height to length ratios

and the amount of reinforcement and the reinforcement detailing. For the three types of ICF walls, especially the screen grid ICF type.

- No testing and evaluations of the mechanical properties (Young's modulus, Poisson’s ratio and stress-strain relationship) of concrete and reinforcing steel were done as per codes and standers only quantified the effect of 28-days cylinder compressive strengths of ECC (fiber reinforced engineered cementitious concrete) concrete and standard ordinary concrete used in the ICF system on ICF walls.
- In certain papers, especially for screen grid ICF wall systems, the analytical part did not achieve their anticipated results, as they have applied only the common known mechanical properties values of the ordinary concrete and the reinforcing steel, like Young's modulus and Poisson’s ratio. Either in the approximate empirical methods or the two-dimensional FEM methods applied, that lead to complete failure of their FEM models. However, FEM modeling of a screen grid ICF is complicated and nonsense.
- The researchers did not perform the research in a proper experimental and numerical methodological way to come up with rational and convincing three-dimensional FEM simulations, results, and comparisons.

2.3.2 Numerical Investigation

Mainly two numerical research papers exclusively dealt with flat ICF walls, the followings are essential observed points:

- The research performed by (Zollo, 2003) consists of the design of ICF-FRC wall by applying the semi-empirical strength of material analysis and two-dimensional FEM methods. Using common mechanical properties of ordinary concrete and reinforced concrete to develop

design interactions diagram for flat ICF walls with confirming some codes ductility checks(RC walls) and pseudo-ductility checks (FRC walls)

- (Mircea, 2010), proposed two detailing steel reinforcements strategies for seismic design and verified that the detailing recommended satisfies all the structural shear and ductility demands, providing a reliable structural and insulation designs for green buildings. It was found that the unity of EPS forms with concrete thermal mass minimizes the temperature fluctuations by absorbing and storing heat.

2.3.3 Beneficiary Conclusion:

The experimental literature investigations provided valuable insight into the validity and capacity of the lateral strength of almost all types of the ICF walls (with or without openings) compared to any other conventional types of walls.

The choice for the screen grid ICF walls governed the afterwards research intensively, due to its advantage to save 50% of the concrete used in the flat ICF walls, but the large-scale experimental studies conducted was deficient in the experimental and numerical understanding of the screen grid wall structural characteristics variables, due to their complicated irregular internal core concrete structure. Because of this, structures using SGICFs are limited to conservative heights, not higher than two stories in residential construction as per the Prescriptive Method is allowed (PATH, 1998). Although, the confinement of the ICF forms exhibited around 30% increase in the concrete compressive strength (regardless of the concrete type) and contributed to the lateral strength and drift of ICF walls, despite its very low compressive strength of 0.26 MPa (37 psi) as stated.

(Mehrabi, 2000), recommended further experimental investigations including analytical models, simulations and broad-reaching parametric studies as follows:

- Development of finite element models for ICF wall panels.
- Calibration of analytical models using the results of the experimental study.
- Parametric studies on the behavior of ICF wall panels using the developed analytical models.

The unique methodology used in the literature above reviews was responsible for the failure to simulate numerically/empirically the generalized ICF walls structural behaviors with different aspects, even for their particular ICF wall model's conditions. Researchers concentrated only on the obvious external observation and behaviors of the structure when the ICF walls were subjected to lateral loading or cyclic loading.

The ICF walls evaluated behaviors with different aspect ratios:

- Height-to-length aspect ratio: found to possess Flexure or shear dominated deformational characteristics).
- Openings: The walls with garage or window openings were found the most brittle and should be designed as concrete moment frames.
- The minimum required reinforcement: some design efficiency has been sacrificed, particularly in the screen-grid wall type because of the variety of dimensions available in the concrete core. Therefore, the interaction diagrams cannot be unified, and experimental results cannot be generalized, to obtain a more efficient design.

However, these rules may not apply to lightly reinforced ICF walls as found in the Prescriptive Method (PATH, 1998) and (ICC, 2000) and more testing required, and methods for estimation of the strength capacity need to be improved.

2.3.4 Researcher's Point of View

It seems that the previous literature papers depleted the experimental evaluation of the lateral capacity of the ICF performance walls for low residential buildings but did not attempt to investigate the potential applications of the load-bearing capacity of the ICF walls, especially with Nano-concrete in flat ICF walls in multi-story residential buildings.

Most studies considered ICF flat walls expensive. Thus, the choice for the screen grid walls governed, even though they yielded obstacles and limitations in designs and codes, and however, flat ICF walls can come over these problems efficiently and even can be used for the constructions of multi-story residential buildings because:

- Unlike, Waffle grid ICFs forms made of wood chips and cement, Flat ICF walls forms made of EPS beads (an inert material) cannot mold and has insect resistance.
- It is ideal and suitable for numerical scientific methods to simulate the ICF wall systems due to its constant cross-sectional core.
- Unlike the Waffle and screen grid ICF, in Flat ICF walls, honeycombs can be easily avoided.
- The introduction of the lightweight Nano-concrete to flat ICF walls can replace the broad features of ordinary concrete.

All previous papers proposed and evaluated only ICF walls, even though ICF slabs are most responsible for heat transfer in buildings. Finally, the study proposes the innovative Polyforms system in developing, a new ICF green construction systems, cost-effective, site-build load bearing resisting a structural system that will be energy efficient, sustainable and easy to build, based on Insulating Concrete Forms (ICF) for flat ICF walls and ICF ribbed slabs construction.

The area of study is concerned with structural and thermal engineering; the research work is about experimental, analytical and simulation of invented Nono-concrete applied in innovative building structure designs (Insulated Nano-concrete ICF walls and composite ribbed slabs) for green construction. There is a need to confirm and improve the use of high fine Nano-concrete bearing wall design methods particularly in the context of ICF systems and residential construction practices. Thus, inefficiencies that result in conservative (uneconomical) or non-conservative (unsafe) applications may be avoided.

Since the technical information available is limited. Subsequently, this study proposes an exclusively added methodology for the determination and the evaluations of the mechanical and thermal properties of the essential elements related to the strength of materials such as, Young's modulus, Poisson’s ratio, stress-strain relationship and thermal conductivity, which are the essential functions of the overall characteristic behaviors of an individual full scale ICF building system model, including the amount of reinforcement and the reinforcement detailing towards generalized, three-dimensional, numerical and analytical FEM simulations that could yield reliable code and design standards for ICF walls.

To avoid repetitive and expensive work of investigating the lateral load capacity for ICF building systems which are prone to earthquake and hurricanes. However, since our area does not come under these types of categories, the test procedure adopted will be unique from others. The ICF building system (ICF walls and ICF slabs) evaluated experimentally and analytically only for the axial bearing capacity.

Using the properties and the recorded observations determined experimentally, the simulation of the ICF building system done using the 3D FEM Software ANSYS powerful capabilities for the research models,

or any other models of different aspect ratios like the type of imposed loading, height to length, openings and steel reinforcement ratios. Which helps in avoiding to conduct an expensive test that serves as essential references for the future generations when they practice their research.

Chapter 3: EXPERIMENTAL AND ANALYTICAL PROCEDURES

3.1 Materials

3.1.1 Cement

3.1.2 Fine aggregate

3.1.3 Expanded polystyrene beads (EPS)

3.1.4 Mixing Water

3.1.5 Fly Ash

3.1.6 Nano Additive

3.1.7 Chemical 1

3.1.8 Chemical 2

3.2 Methodology

3.2.1 Determination of Material Properties

3.2.1.1 Applications and Classifications of Lightweight Concrete

3.2.1.2 The Structural Properties

3.2.1.2.1 ICF Wall Governing Criteria

3.2.1.2.2 Structural Reinforced ICF Walls

3.2.1.2.3 Structural Plain Concrete Walls

3.2.1.3 ICF Slabs Governing Criteria

3.2.1.3.1 Geometry

3.2.1.3.2 Analysis

3.2.1.3.3 Bending Reinforcement Calculation

3.2.1.3.4 Ultimate Compressive strength Calculation of Nano and polystyrene concrete.

3.2.2 Determination of Compressive Strength, Passion Ratio and Modulus of Elasticity of the Nano and Polystyrene Concrete by ASTM code procedures

3.2.3 Determination of Compressive strength, Poisson Ratio and Modulus of elasticity of the Nano and polystyrene concrete using ADMIT "Gauge Buster 2"
3.2.4 Determination of Self-Consolidation
3.2.4.1 Workability Requirements for SCC.
3.2.4.2 Self-Consolidating SCC Additives
3.2.4.3 Test Methods to Measure Fresh SCC Properties
3.2.4.4 T50 Slump-flow
3.2.5 The Chemical Properties
3.2.5.1 Alkali-Silicate Reaction (ASR)
3.2.5.2 Accelerated Mortar Bar Test (ASTM C 1260)
3.2.5.3 Double Washed Marine Sand Chemical Composition
3.2.5.4 Testing Procedure of Nano-concrete Specimens
3.2.5.5 Accelerated Mortar Bar Tests Results and Discussion
3.2.6 The Thermal properties
3.2.7 Modulus of Rupture (Flexural Strength)
3.3 Optimization of Nano And Eps Concrete
3.3.1 Optimization of Nano-Concrete
3.3.1.1 Compressive strength, Poisson Ratio and Modulus of elasticity of CSC Mixes by Gauge Buster 2
3.3.1.2 Compressive strength, Poisson Ratio and Modulus of elasticity of CS Mixes by Gauge Buster 2
3.3.2 Optimization of EPS Concrete
3.3.2.1 Trail Mix Designs
3.3.2.1.1 Batch one: Nano Polystyrene concrete "Blank."
3.3.2.1.2 Batch Two: Fly Ash Polystyrene concrete "PF."
3.3.2.1.3 Batch Three: Nano Polystyrene concrete "BB."
3.3.2.1.4 Batch Four: Polystyrene Lightweight Concrete
3.3.2.1.5 Compressive strength, Poisson Ratio and Modulus of elasticity of SBNBR Mixes
3.3.3 Material Properties Results and Conclusion
3.4 Experiments on Full scale ICF Slabs and ICF Walls
3.4.1 Introduction

3.4.2 Test Specimens
3.4.2.1 ICF Slabs
3.4.2.2 ICF Walls
3.4.2.3 Test Setup
3.4.2.4 Testing Procedure
3.4.3 Full-Scale Test on ICF Slabs
3.4.3.1 Blank Blocks (Category B)
3.4.3.2 ICF Ribbed Slab with Two Bars Only (Category S)
3.4.3.3 ICF Ribbed Slab with Two Bars and Mesh (Category MS)
3.4.3.4 ICF Ribbed Slab with Lattice Girder Only (Category J)
3.4.3.5 ICF Ribbed Slab with Lattice Girder and Mesh (Category MSJ)
3.4.4 Full-Scale Test on ICF Walls
3.4.4.1 Wall ICF-04
3.4.4.2 Wall ICF-06
3.4.4.3 Wall ICF-09
3.4.4.4 Wall ICF-11
3.5 Numerical Simulation of ICF Slabs and ICF Walls
3.5.1 Modeling of ICF Slabs and Walls
3.5.1.1 Element Types
3.5.1.1.1 Element Solid65
3.5.1.1.2 Element Solid185
3.5.1.1.3 Element Link180
3.5.1.1.4 Element Beam188
3.5.2 Material Properties
3.5.2.1 Nano-Concrete
3.5.2.2 Polystyrene Concrete
3.5.2.3 Reinforcing Steel
3.5.3 Modelling of ICF Slabs and Walls in ANSYS Workbench
3.5.3.1 Engineering Data
3.5.3.2 Modeling Stage
3.5.3.3 Element Types Assignment

3.5.3.4 Meshing Stage
3.5.3.5 Direct Generation
3.5.3.6 Solid Modeling
3.5.3.7 Meshing Technique for Embedded Modeling
3.5.3.8 Modeling and Meshing Technique of ICF Walls and Slabs
3.5.3.9 Using APDL Commands
3.5.3.10 Loading and Boundary conditions
3.5.3.11 Solution Stage
3.5.4 Analytical Modeling of ICF Slabs by ANSYS
3.5.4.1 Blank Block (Category B)
3.5.4.2 ICF ribbed slab with two bars only (Category S)
3.5.4.3 ICF ribbed slab with two bars and mesh (Category MS)
3.5.4.4 ICF ribbed slab with lattice girder only (Category J)
3.5.4.5 ICF ribbed slab with lattice girder and mesh (Category MSJ)
3.5.5 Analytical Modeling of ICF Walls by ANSYS
3.5.5.1 Wall ICF-04
3.5.5.2 Wall ICF-06
3.5.5.3 Wall ICF-09
3.5.5.4 Wall ICF-11

Chapter 3: EXPERIMENTAL AND ANALYTICAL PROCEDURES

3.1 Materials

3.1.1 Cement: Type (1) ordinary Portland cement used, its chemical and physical properties are confirmed to the British Standard 4027:1996, strength class 42.5N.

3.1.2 Fine Aggregate: Natural marine sand used as fine aggregate and comply with BS 1199-Table 1 Type B and BS 1199-Table 1 Type B specification limits.

3.1.3 Expanded Polystyrene Beads (EPS): Polystyrene beads with diameters of (5mm) used as a partial replacement of fine aggregate with an apparent density of 16.5kg/m3.

3.1.4 Mixing Water: Ordinary tap water used in this work for all concrete mixes and curing of specimens.

3.1.5 Fly Ash: Volcanic fly ash.

3.1.6 Nano Additive: particular additive used in coating products.

3.1.7 Chemical 1: Sikament, ®-NN superplasticizer is used for the production of EPS concrete, its compositions based on Poly-naphthalene condensate. Complies with ASTM C-494 Type A & F and EN 934-2:2001. Sikament®-NN is a highly efficient dual action liquid superplasticizer for the production of free-flowing concrete or as a substantial water-reducing agent for promoting high early and ultimate strengths, suitable for use in tropical and hot climatic conditions.

3.1.8 Chemical 2: Sika Latex® (styrene-butadiene rubber copolymer) is specially designed for use in application where a significant improvement in the bonding strength to various substrates is needed,

especially adding excellent adhesion to cement mortars. Also, used to prevent segregation of polystyrene beads. Therefore, it is used in this research as a viscosity modifying agent which is needed to prevent segregation of polystyrene beads in the mixture, and with the help of the superplasticizer, it can produce a workable zero slump strong enough polystyrene concrete (extruded or molded), capable of carrying the weight of the wet Nano-concrete and the labors. Especially its application in the composite ICF slab is initially as shuttering formworks and not for long-term dead loading (Manolia, 2012).

The commercial available branded white liquid used is Sika Latex®, it is a synthetic rubber latex emulsion for adding to cement mortars, having excellent adhesion and water resistance. The product is suitable for use in tropical and hot climatic conditions. Tested by ASTM C1042, Type II, (BS 6319 part 4). The polymer (SBR) is used as a ratio by weight of cement of (10%).

3.2 Methodology

The study is based on the collection of primary data through conducting laboratory experiment and use of simulation technique by ANSYS. This study focuses on developing a novel building construction system which provides full thermal and sound insulation. The system consists of ICF walls and composite concrete ribbed ICF slabs, which is produced from Nano-concrete.

Two types of ICF slab potential reinforcements which are regular reinforcement and three-dimensional steel lattice girder, Nano structural lightweight concrete based on local resources, vertical/horizontal steel reinforcement and fiber cement board or plaster. The study expected to

result in an innovative new lightweight Self-Compacting Nano-concrete mix design and a new LWPC for the Blank Block of the ICF slabs.

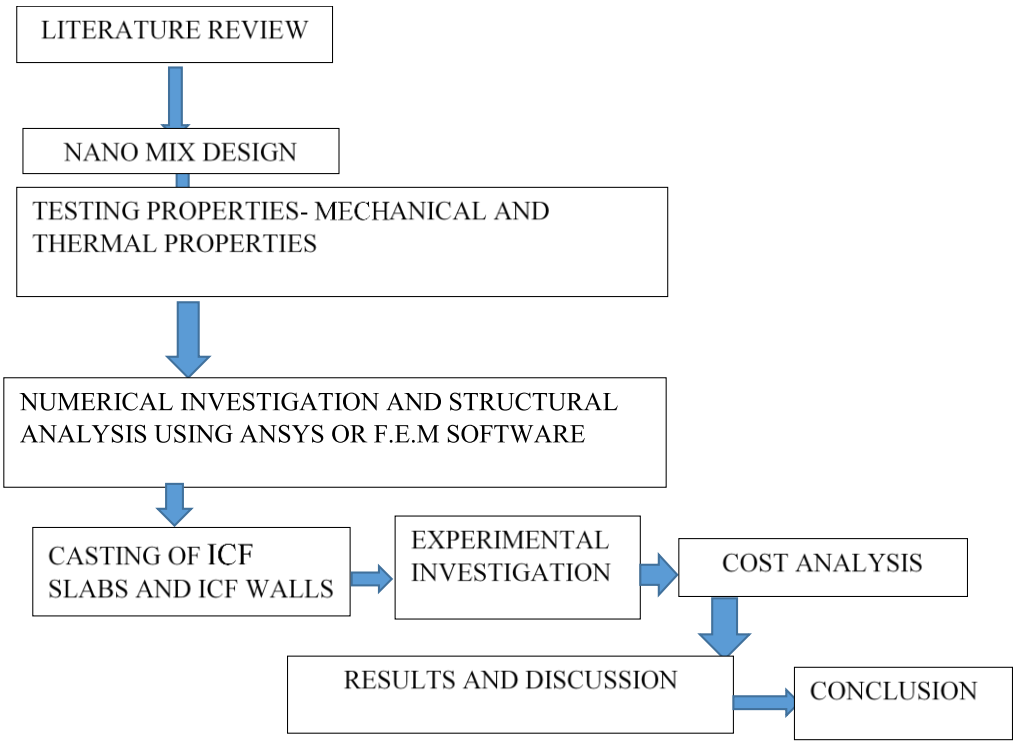


Fig. 25: Flow of research methodology

3.2.1 Determination of Material Properties

Nano and polystyrene concretes selected in this study to be used in conjugation with the ICF Polyfroms green buildings system (designs and forms), based on their aforementioned advantages and benefits over the regular concrete, such as low density, low thermal conductivity, ease of placement and pumpability, easy for extrusion, reducing the duration of construction process, decrease the cost of transportation and handling and sustainability. However, evaluating and simulating the ICF system structural capacity and integrity, thermal conductivity, resistance to aging chemicals and self-consolidating, requires the experimental determination of the mechanical, chemical and thermal properties of the Nano and polystyrene concretes. The quality and experimental results of the

properties of Nano and polystyrene concrete depend on the quality of the raw materials used, the mixture, mixing method and the compaction and preservation methods used. In general, the overall production cost of Nano and polystyrene concrete are much more economical than processing and handling of the ordinary concrete. However, to ensure the efficiency and potential of the Nano and polystyrene concretes at the desired level, there are some routine tests necessary to determine the workability (slump test) and tests which identify the proportion of the mixtures that correspond to the optimum compressive strengths, such as compressive strength test, modulus of elasticity, passion ratio, density test and flexural strength test. Bulk engineering properties like, strength, durability depends on microstructural characteristics of calcium–silicate–hydrate (C–S–H) such as, morphology of solid products, capillary pores, air voids, transition zone and technological parameters water-cement ratio, aggregate grading, compaction, curing and most important the chemical aspects such as Alkali-Silicate Reaction (ASR).

(Bin Shamsuri, 2011), Nano and polystyrene concrete can contribute to the advancement of the concrete technology to create the ready or semi-ready build concrete structure such as Industrialized Building System (IBS) and Polyforms green innovative ICF system for housing to accelerate the construction process and eventually develop housing that combines sustainability with excellent thermal insulation. These systems yet reduce the construction duration, decrease the cost of labor and increase the structural capacity and integrity. Also, its construction operations are not affected by adverse weather condition because the prefabricated component is done in a factory-controlled environment. Nevertheless, IBS is cumbersome and difficult to handle because it needs expertise in installations for construction works. It means that the process does not require ordinary workers, who cannot handle the installation and application of heavy

machineries such as cranes and carriages. Therefore, IBS is not effective if the factory is too far from the construction site, resulting in high cost for transportations and take risks for the quality of IBS damaged while transported. Consequently, one of the solutions to overcome these problems is the implementation of the Polyforms green innovative ICF system.

3.2.1.1 Applications and Classifications of Lightweight Concrete

According to ACI (2004), lightweight can be classified into six classes according to the density shown in Table 1. The concrete of LC 1.8 and LC 2.0 with a density between 1600 to 2000 kg/m3 is used as parts of the structural member in building construction.

Table (1) Classification of density for lightweight concrete based on American Concrete Institute (ACI) 2004

Density Classes	Oven-dry Density (kg/m^3)
LC 1.0	≥ 800 and ≤ 1000
LC 1.2	>1000 and ≤ 1200
LC 1.4	>1200 and ≤ 1400
LC 1.6	>1400 and ≤ 1600
LC 1.8	>1600 and ≤ 1800
LC 2.0	>1800 and ≤ 1000

For purposes of this study, Nano-concrete lightweight concrete is assumed to have a density between 1900 to 2000 kg/m3 and that lightweight polystyrene concrete to have a density of 300 to 800 kg/m3. (ACI C213, 1999).

3.2.1.2 The Structural Properties

This study reports the result of series of experiments to produce reliable, workable lightweight Nano and polystyrene concrete using the raw materials explained earlier. Fine sand used in the replacement of the coarse aggregate in the Nanoconcrete and the polystyrene beads used as part of sand replacement in the polystyrene concrete mix. Total of 225 cylinders of size 150mm diameter and 300mm high and were prepared and 18 prisms. The samples were tested to determine the strength, modulus of elasticity, passion ratio and density and self-consolidation according to international standers. Also, polystyrene and Nano-concrete can be classified as lightweight concrete for their densities of almost 800, 1900 kg/m^3 respectively, which are within the limit set by American Concrete Institute (ACI).

3.2.1.2.1 ICF Wall Governing Criteria

The design procedure of ICF walls addresses the design of flat, waffle-grid, and screen-grid ICF wall systems that are specifically in single- and multi-unit residential construction. The dimensional variances among the ICF wall types affect their structural capacity and the applicable structural analysis methods.

3.2.1.2.2 Structural Reinforced ICF Walls

(Vranka, 1998), the structural reinforced ICF flat walls are designed as compression members according to the flexible design approach (ACI 14.4). Also, the Structural reinforced ICF Flat walls may be designed by ACI 14.5 using the empirical design method if the following limiting conditions are satisfied:

- The wall cross-section has to be solid.

- The resultant of all axial loads acts within the middle one-third of the wall.
- The wall thickness should not be less than 100 mm for above-grade walls or 200 mm for basement walls.
- The wall thickness is not less than 1/25 of the supporting wall height or length of the wall, whichever is smaller.

The required minimum horizontal and vertical reinforcement ratio specified in ACI 14.3 for structural reinforced concrete walls has been relaxed under the provisions ACI 14.2.7 based on test data by (Roller, 1996), which states that "Quantity of reinforcement and limits of thickness required by 14.3 and 14.5 shall be permitted to be waived where structural analysis shows adequate strength and stability".

3.2.1.2.3 Structural Plain Concrete Walls

Structural plain concrete walls are walls that either has less than the minimum amount required or no reinforcement, which limits the use of plain concrete walls to members provided with continuous vertical support throughout the member's length. Since temperature have a negligible impact on the structural integrity of the ICF walls, it may be exempt from the obligatory contraction and isolation joints that obstruct the flexural continuity and random cracking, due to creep and shrinkage, nevertheless, some nominal level of reinforcement to control crack width may be included in the designer's decision.

Limitations on the use of plain structural concrete include the following:

- The horizontal length of the wall to be considered effective for each concentrated vertical load is not greater than the distance between loads, or width of bearing plus four times the wall thickness.

- The wall thickness is not less than 1/25 of the supporting wall height or length of the wall, whichever is smaller.
- The wall thickness is not less than 150 mm for above-grade walls or 200 mm for basement walls.
- Walls are braced against lateral translation.
- Window and door openings require not less than two 16 mm bars around the openings extending not less than 610 mm beyond the corners of the openings.

It can be proven that the constraint for two 16 mm bars around openings may be excessive for residential loading. The Standard Building Code and National Building Code have clauses modifying this requirement to one 13 mm bar provided that vertical bars span continuously from support to support and horizontal bars extend a minimum of 610 mm beyond the opening.

However, ICF wall geometry and loading conditions may be designed by ACI 22.6.5 using the empirical design method if the following additional limiting conditions are satisfied:

- The wall cross-section is solid.
- The resultant of all axial loads acts within the middle one-third of the wall thickness.

3.2.1.3 ICF Slabs Governing Criteria

Bending strength and deflection are usually the governing criteria ($(b_w/B_f) \leq 0.3$) and $M.F=20.55+ (477-Fs)/(120*(0.9+Mbd^2))) \leq 2$. The end span condition should be checked because the moments are larger in this span unless there is a cantilever or the span is shorter than the interior spans.

3.2.1.3.1 Geometry

BS 8110 gives geometrical limits for ribbed slabs Figure 26. Cover bar spacing and fire requirements determine the width of the rib. The absolute minimum is 125 mm. Typically, spacing for ribs is 600 mm, 750 mm, 900 mm and 1200 mm, with a rib, the width of 150 mm.

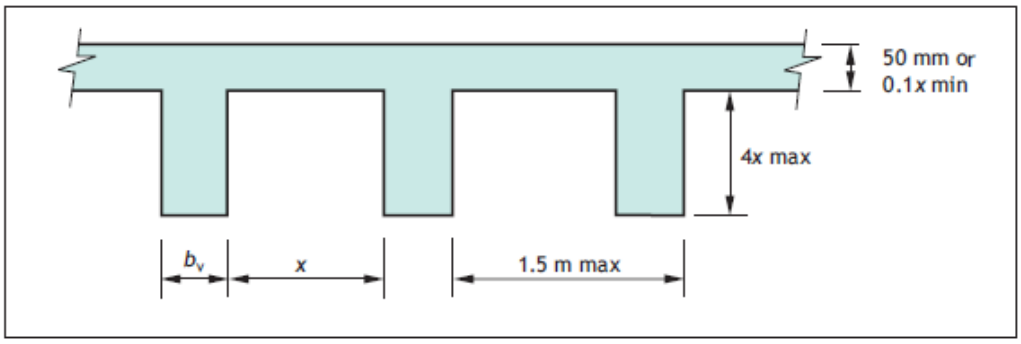


Fig. 26: Geometrical limitations for ribbed slabs (Cement and Concrete Industry, 2006)

3.2.1.3.2 Analysis

A ribbed slab should be designed as a one-way slab with the rib and topping acting as a T-beam.

(Cement and Concrete Industry, 2006), these are provided with the following conditions (note that 20% redistribution is included in the coefficients):

a) The area of the slab exceeds 30 m^2 (5 m x 6 m).
b) The ratio of characteristic imposed load to characteristic dead load does not exceed 1.25.
c) The characteristic imposed load does not exceed 5 kN/m^2 excluding partitions.
d) The spans are approximately equal (generally assumed to be 15% of the longest span, but not specified in the Code).

e) The requirements of conditions 1 and 2 will usually be met by most building designs.
f) Service load considered is the weight of labors and the fresh Nano-concrete.
g) Service load considered on the Blank Block is in KN/m.

3.2.1.3.3 Bending Reinforcement Calculation

The quantity of bending reinforcement required is calculated in the way described for beams.

A flanged beam may be treated as a rectangular beam, of full width, b, when the neutral axis is within the flange. In this case, the moment of resistance in compression of the section is:

MR = 0.45fcubhf (d – hf /2) where h_f is the thickness of the topping slab.

When the applied moment is higher than the moment of resistance of the flange (MR) the neutral axis lies in the flange, and the beam cannot be designed as a rectangular beam and reference should be made to BS 8110.

The quantity of bending reinforcement required can be determined either from charts (as given in part 3 of the Code) or from the design formula given in the Code, which are set out below:

K´ = 0.156 where redistribution of moments does not exceed 10%

K´ = 0.402 (bb – 0.4) – 0.18(bb – 0.04)2 where redistribution of moment exceeds 10%

$K = M/bd^2fcu$

If K ≤ K´, compression reinforcement is not required and the lever arm, z, can be calculated from:

z = d {0.5 + R 0.25 –K/0.9} but not greater than 0.95d i.e. if K < 0.04275

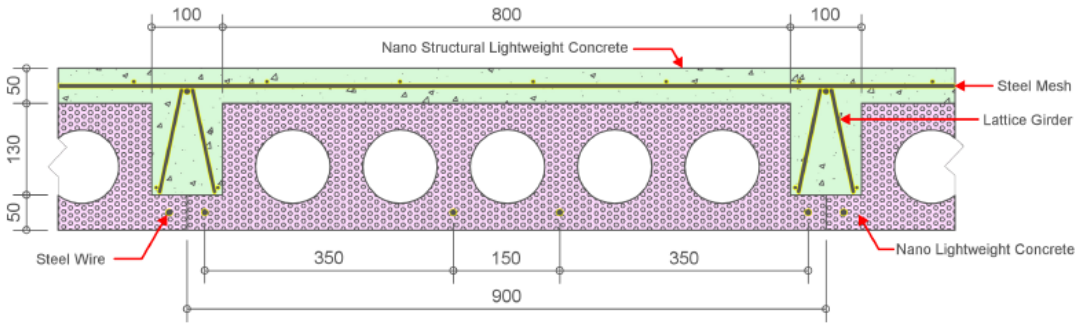
The area of reinforcement required can then be calculated using the following expression:

$As = M/0.95fyz$

For a preliminary design, compression reinforcement should be avoided.

It may be useful to write programs for a suitable calculator to carry out these calculations. The program can be written to return a value for K, which is useful for quickly assessing the efficiency of the design.

3.2.1.3.4 Ultimate Compressive Strength Calculation of Nano and Polystyrene Concrete.



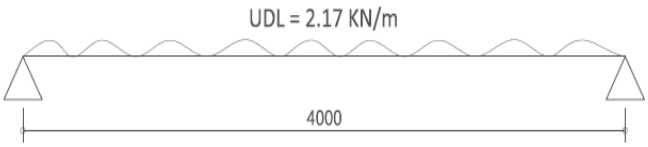
The range sizes of fine aggregates were 0-2 mm and for polystyrene beads were 1.5-5.0mm. Sulfate resisting cement was used namely. The ratios of cement: sand: polystyrene beads were used, which are 1:1.5:1.5, 1:1:2, and1:0.5:2.5. The water-cement ratio was fixed at 0.5

Density of Screed (Nano Structural Lightweight Concrete) = 1908 Kg/m^3 (19.1 KN/ m^3)

Blank Block (Nano Polystyrene Concrete) = 887 Kg/m^3 (8.87 KN/ m^3)

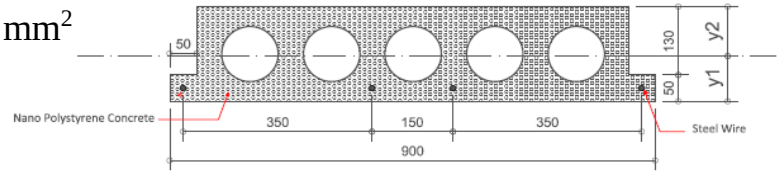
Service Load = Dead Load + Live Load = 2.04+0.75 = 2.79 KN/m

$$M\ max = \frac{2.79 \times 4^2}{8} = 5.588\ \text{KN.m}$$



$$M\ min = \frac{2.04 \times 4^2}{8} = 4.088\ \text{KN.m}$$

Cross Sectional Area = 105705 mm^2



Neutral Axis $\bar{y}$ = 86.925 mm

$Z_1 = I_X/y_1$ = 4373130.99 mm^3

$Z_2 = I_X/y_2$ = 4084173.1 mm^3

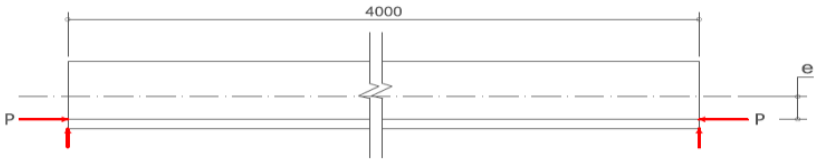
σ max $_{bottom}$ = 1.28 MPa (comp) (without pre-stressed)

σ max $_{top}$ = 1.37 MPa (comp) (without pre-stressed)

Stress At The Bottom = $\sigma_b = \frac{P}{A} - \frac{Mmax}{Z1} + \frac{Pe}{Z1} = 0$

Solving for *P*

$$P = \frac{Mmax}{(\frac{Z1}{A}+e)} = 54101.63 \text{ N}$$



Using 4 tendons of 5 mm Ø (Characteristic Strength 1760 N/mm^2)

Ultimate Load for one Tendon $P = \pi$ x 2.5^2 x 1760 =34557.52 N

For 4 tendons P = 4 x 34557.52 = 1382330.1 N > 54101.63 N

Even 3 tendons are sufficient.

Under M max = 5.588 KN/m

σ_{top} = 1.06 MPa (comp) (with pre-stressed)

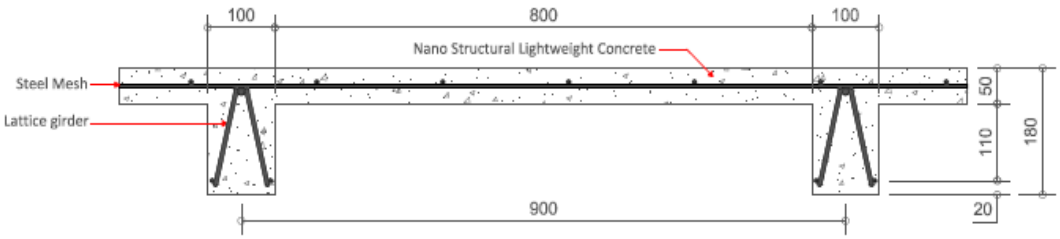
σ_{bottom} = 0 (with pre-stressed)

Under M min = 4.088 KN/m

σ_{top} 0.693 MPa (comp) (with pre-stressed)

σ_{bottom} = 0.343 MPa (comp) (with pre-stressed)

<u>Design of ribbed Slab:</u>



Considering F_{cu} =30 MPa and Fy = 250 MPa

Dead load = 1.51KN/m, Live load = 1.8 KN/m

Ultimate load = 0.9(1.4x1.51+1.6x1.8) = 4.9963 KN/m

Ultimate load on 4m span = 19.98 KN

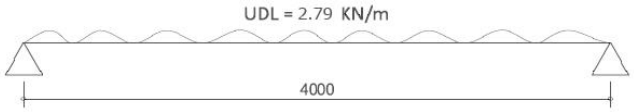
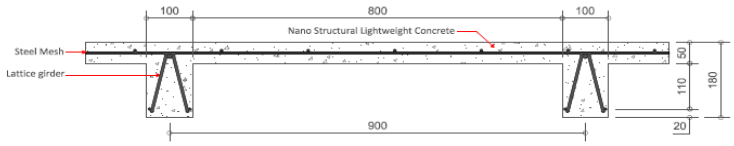
$$M = \frac{4.9963 \times 4^2}{8} = 9.9926 \text{ KNm}$$

$K = \frac{9.9926 \times 10^6}{900 \times 160^2 \times 30} = 0.0145 \rightarrow$ Fig. 7.5 $\rightarrow L_a = 0.95$

$As = \frac{9.9926 \times 10^6}{0.87 \times 250 \times 0.95 \times 160} = 276.8\ mm^2 \rightarrow$ 2 bar Ø 16 mm

The minimum compressive strength of Blank Block polystyrene concrete is 1.4 N/mm^2 as per the dimensions are given with density of 887Kg/m^3. Table 2 gives the comparison between initially and finally determined models for Blank Block Slab.

Table (2) Comparison between initially and finally determined models for Blank Block Slab

PARAMETERS \ MODEL	INITIALLY ASSUMED DESIGN PARAMETERS	THE FINAL DETERMINED PARAMETERS
Density of Nano Structural Concrete KN/ m3	19	19.1
Density of Polystyrene Concrete KN/ m3	3	8.87
Service Load	2.175	2.79
Prestressed Blank Block		
σ max $_{bottom}$ (comp) (without pre-stressed)	0.992	1.28
σ max $_{top}$ (comp) (without pre-stressed)	1.06	1.37
P N Due to Stress at The Bottom	42015.14	54101.63
Characteristic Strength N/mm2	1670	1760
Ultimate Load for one Tendon	32790	34557.52
Ultimate Load for 4 Tendon	131161	1382330.1
Even 3 tendons are sufficient.		
Under M_{max}		
σ $_{top}$ (comp) (with pre-stressed)	0.8226	1.06
σ $_{bottom}$ (with pre-stressed)	0	0
Under M_{min}		
σ $_{top}$ (comp) (with pre-stressed)	0.455	0.693
σ $_{bottom}$ (comp) (with pre-stressed)	0.343	0.343
Ribbed Slab		
$F_{cu\ (Mpa)}$	30	30
Fy (Mpa)	250	250
Dead load (KN/m)	1.3	1.51
Live load (KN/m)	1.5	1.8
Ultimate imposed load	3.798	4.9963
Ultimate Moment	7.596	9.9926
K	0.0109895	0.0145
As (mm^2)	229.76	276.8
Bar	2 bar Ø 12 mm	2 bar Ø 16 mm
		
The minimum compressive strength of Blank Block polystyrene concrete	1.2 N/mm^2	1.3 N/mm^2

3.2.2 Determination of Compressive Strength, Passion Ratio and Modulus of Elasticity of the Nano and Polystyrene Concrete by ASTM code Procedures

The inherent strength of concrete influenced by the strengths of cement paste bond, which depends mainly on the gel-space ratio which is affected by water to cement ratio and degree of hydration. The effects of cement paste on the strength of polystyrene aggregate concrete will not be any different to that of normal weight concrete because the influencing factors are independent of the strength of the aggregate. The influence of the strength of the cement paste matrix and the additives content on the strength of concrete assessed by examining the effect of the following parameters: The compressive strength, stress-strain relation, modulus of elasticity and Poisson's ratio of concrete under compression investigated by ASTM C39 and ASTM C 469. Data from these investigations will be used to simulate the real structural behavior of Polyforms ICF system in Ansys Workbench. One of the aims of this study is to produce self-compacting Nano and lightweight polystyrene concrete for the ICF concrete and formworks systems. The study primarily concentrates on the material aspects of the locally available fine aggregates and their use in high fines concrete (HFC) incorporating CNCs, regarding structural integrity and placeability. Concrete compressive strength requirements can vary from 17 Mpa for residential concrete to 28 Mpa and higher in commercial structures. (V.R.Rathi, 2014).

Concrete Mixtures Proportioning for Nano-concrete produced a total of 225 capped cylinders of size 150 x 300 mm, generally with gypsum mortar to provide uniform load distribution while testing. Various specimens produced by investigating properties of hardened concrete of one type of Nano containing varying quantities of CNCs and four different

kinds of mix batches based on EPS beads and special additives as to provide zero slumps and prevent segregation of beads. All cylindrical specimens are tested by ASTM C 39, Standard test method for compressive strength of cylindrical concrete specimens Figure 27. A test result is the average of at least three standard-cured strength specimens made from the same concrete sample and tested at the same age. Strength requirements for concrete are at the age of 28 days. Also, tested for stress-strain relation, modulus of elasticity and Poisson's ratio by ASTM C 469. The testing machine apparatus Figure 28 should be capable of imposing a load at the rate and of the rates of 2.1 KN/s and 4.2 KN/s for ASTM C 39 and ASTM C 469 tests respectively for Nano-concrete and 0.42 KN/s for both standers when applied to polystyrene concrete.



Fig. 27: Cylinder and prisms samples



Fig. 28: Compressive strength machine

With standard weight concrete, the coarse aggregates have higher strength and modulus of deformation compared with that of the mortar and, therefore, the short-term strength of normal weight concrete is a function

of the strength of the mortar. In the case of lightweight aggregates concrete, the concrete strength is limited by the strength and modulus of deformation of the lightweight aggregates, which are lower than the maximum values attainable by the mortar matrix. Figure 29 reported by (Sabaa, 1998) illustrate the factors influencing the strength of lightweight concrete.

For a constant condition, the tensile strength of the aggregate governs the limiting compressive strength of the lightweight aggregate concrete, but the upper limit strength can be increased slightly, only by any further increase in the strength of the mortar matrix. Thus, for lightweight concretes having strength below their strength limit, an increase in the compressive strength of the mortar will produce a corresponding increase in the compressive strength of the concrete. In the case of polystyrene concrete, the limiting compressive strength will be determined by the content of polystyrene beads included in the concrete and, therefore, the concrete density (Sabaa, 1998).

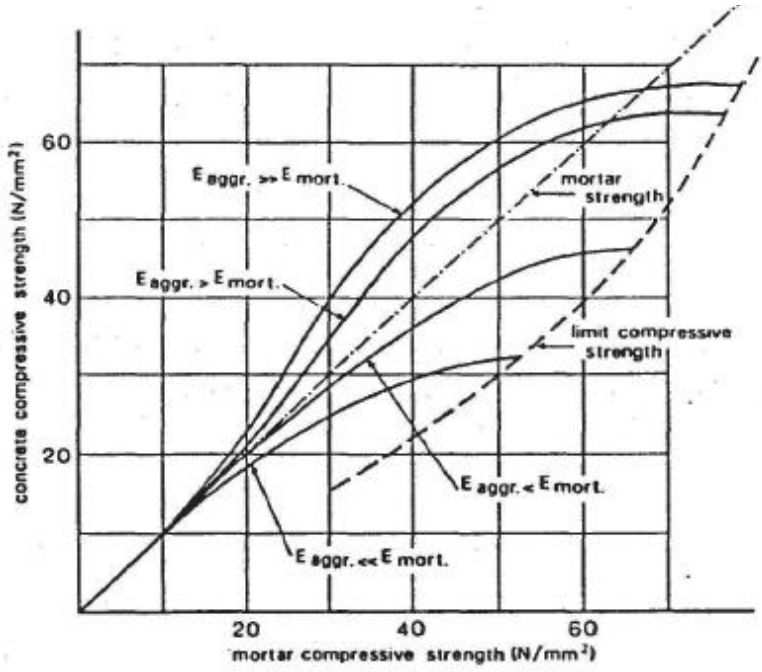


Fig. 29: Different factors influencing strength of lightweight aggregate concrete; (Sabaa, 1998)

ASTM C 39 Test Procedures:

1. During the first loading, Cylinders should be centered in the compression-testing machine and loaded to complete failure.
2. The loading rate on a hydraulic machine should be maintained in a range of 2.1 KN/s and 0.42 KN/s for Nano and polystyrene concrete, respectively, during the loading phase.
3. The concrete strength is calculated by dividing the maximum load at failure by the average cross-sectional area. At least two cylinders are tested at the same age, and the average strength is reported as the test result to the nearest 0.1 MPa.

ASTM C 469 Test Procedures:

5 Place the specimen, with the strain-measuring equipment attached, on the lower platen or bearing block of the testing machine. Carefully align the axis of the specimen with the center of thrust of the spherically seated upper bearing block. Note the reading on the strain indicators. As the spherically seated block is brought slowly to bear upon the specimen, rotate the movable portion of the block gently by hand so that uniform seating is obtained.

6 Obtain each set of readings by applying the load at a constant rate of 4.1 KN/s and 0.42 KN/s for Nano and polystyrene concrete, respectively, during the loading phase. Record, without interruption of loading, the applied load and longitudinal strain at the point (1) when the longitudinal strain is 50 millionths and (2) when the applied load is equal to 40 % of the ultimate load (see 6.5). The type of break should be recorded.

7 The longitudinal strain is defined as the total longitudinal deformation divided by the effective gauge length.

8 The Modulus of elasticity determined according to ASTM C 469-65,

$$Ec = (S2-S1) / (\varepsilon 2- \varepsilon 1)$$

$\varepsilon 1 = 50x10\text{-}6$

$\varepsilon 2 = \Delta L/2L$ L=150, L= gauge reading @ 40% of σc X Gauge factor

S1 = Load @ Guage reading g1/ cylinder area

S2 = Load @ 40% of σc

Where:

E = modulus of elasticity, psi,

S2 = stress corresponding to 40 % of ultimate load,

S1 = stress corresponding to a longitudinal strain, $\varepsilon 1$, of 50 millionths, psi, and

$\varepsilon 2$ = longitudinal strain produced by stress S2.

3.2.3 Determination of Compressive Strength, Poisson Ratio and Modulus of Elasticity of the Nano and Polystyrene Concrete using ADMIT "Gauge Buster 2"

ADMIT testing equipment is a versatile digital indicator and controller for determining the mechanical properties of concrete. The Gauge-Buster 2 (Appendix A), used to conduct the material properties for determination of modulus of elasticity, Poisson ratio, and strain-stress relationship.

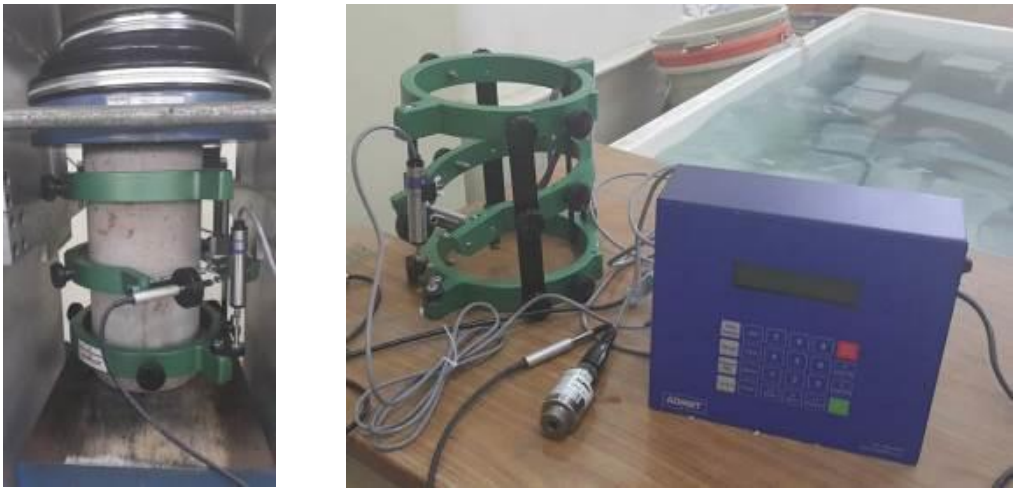


Fig. 30: ADMIT "Gauge-Buster 2" data along with the Compressometer, the transducers, and software

ASTM C469 testing provides stress to strain ratio value and a ratio of lateral to longitudinal strain for hardened cylindrical concrete at whatever age and curing conditions may be designated. ASTM C469 is a compression test whereby a load is applied with a Constant-Rate-of-Traverse (CRT) type machine until specified stress. The modulus of elasticity and Poisson's ration values will be found within the working stress range (0 to 40% of the ultimate strength). These values are used to analyze and simulate the ICF structural system and to compute the stress for observed strains. The Gauge-Buster 2 was liked and calibrated to the ELS hydraulic machine for reading the same exerted load.

ASTM C469 requires three steps:

1. Determine the ultimate strength of a companion specimen by following ASTM C39. This involves applying a compressive axial load until failure occurs. Place the specimen on the platen, so the axis of the specimen is aligned with the center of thrust of the spherically seated bearing block. Apply the load specified in the standard continuously and without shock until failure. Ensure the

specimen fails within the prescribed permissible time tolerances in the specification.

2. Attach the required strain-measuring equipment (compressometer-extensometers). Place the specimen on the lower platen. Align the axis of the specimen with the center of thrust of the spherically seated bearing block and slowly bring the block to bear the load on the specimen. This will ensure uniform seating is obtained. Apply the load at a constant rate within the range specified by the standard until it reaches 40% of the ultimate load. Return the load to zero at the same rate. The first loading is primarily used to seat the strain measuring equipment and should not be recorded.
3. (ASTM C469), recommends completing at least two subsequent loadings to ensure repeatability. If repeatable, average the results. Apply the load at a constant rate within the range specified by the standard until it reaches 40% of the ultimate load. Return the load to zero at the same rate. During loading, record applied a load, longitudinal, and transverse strain when the strain reaches 50 millionths and when the applied load is equal to 40% of the ultimate load. Ambient temperature and humidity should be maintained as constant as possible through the duration of this test.

Calculations:

- Compressive Strength
- Modulus of Elasticity
- Poisson's Ratio

3.2.4 Determination of Self-Consolidation

The development of nanotechnology delivers materials with new properties, regarding durability, sustainability, self-compacting concrete

(SCC), performance and production of cement-based materials are becoming vitally important and has generated tremendous interest for the construction industry. SCC is a highly viscous, flowable and yet stable concrete that can spread readily into place and fill the formwork, having little resistance to flow so it can be placed and compacted under its weight with no vibration and without undergoing segregation or bleeding. It is used to facilitate and ensure proper filling of restricted areas and heavily reinforced structural members. SCC was first developed to improve the durability of concrete structures in Japan in 1988 at Tokyo University (Farhad, 2015).

(Farhad, 2015), The use of SCC has gained increasing vital importance in recent years and presents an excellent alternative to conventional concrete for high-density or intricate reinforced sections and placement in narrow molds. SCC can also be pumped from the bottom of a form or dropped from the top with a recommended maximum fall height of 6 feet. The most important advantage of SCC over conventional concrete is its flowability, but other advantages of using SCC include:

- Shorter construction periods.
- Reductions in labor costs.
- Better compaction in a structure, especially in confined zones where compaction is difficult.
- Reduced noise pollution, since vibrators are not necessary.
- Higher and more homogenous concrete quality across the entire concrete cross-section, especially around the reinforcement
- Concreting deep elements in single lifts.
- Improved concrete surfaces and finishes.
- The typically higher early strength of the concrete (formwork can be removed quickly).

- Higher moisture retention may aid curing.
- SCC usage is on the rise worldwide for cast-in-place and particularly for precast concrete construction.

3.2.4.1 Workability Requirements for SCC

SCC in its fresh state must possess the following three performance characteristics to meet its below stated complex workability requirements:

1. Filling ability: The ability of SCC to flow into and fill all spaces completely within the formwork under its weight.
2. Passing ability: The ability of SCC to flow through tight openings such as between reinforcing rebar without segregation or blocking.
3. Segregation resistance: The ability of SCC to remain homogeneous during transportation and placing. (Ashok, 2004)In addition to the above workability requirements, the concrete must also possess adequate strength, durability, and bleeding resistance.

3.2.4.2 Self-Consolidating SCC Additives

For the concrete to possess adequate resistance to segregation and filling ability, the inter-particle friction of the materials must be reduced. Which can be achieved by reducing the surface tension, optimizing the packing of fine particles and minimizing the free water to avoid bleeding and by making the liquid phase more viscous to enhance suspension of particles? SCC has been produced using high powder content or using viscosity modifying agents (VMA), or a combination of the two, accomplishing higher viscosity. The addition of nanoparticles (NPs), such as silicon dioxide (SiO2), titanium dioxide (TiO2) showed a decrease in the flowability of SCC mixes, due to the effect of the large effective surface, they absorb much water, and that reduces the concrete's workability and would also increase the SCC's shear strength against

flowability and viscosity. This property of silicon dioxide or titanium dioxide NPs can be attributed to their high pozzolanic activity.

(Farhad, 2015), however, NPs like CNCs can improve the properties of concrete due to the effect of the increased surface area on reactivity and through filling the cement paste pores, improving mixing procedure, mix proportion, the heat of hydration, workability, setting time, mechanical strength and durability. The increase in raw material costs, if any, are easily offset by improvements in pouring productivity and reductions in vibrator cost and maintenance.

3.2.4.3 Test Methods to Measure Fresh SCC Properties

(Ashok, 2004), the available ASTM or AASHTO slump test standards are not accurate indications of the SCC liquefied mixes to characterize its consistency properties. For the SCC mixes tests, the current conventional workability tests methods are employed except compaction requirement during specimen preparations. Table 3 lists the workability test methods of SCC that has been employed by many researchers in the past. T_{50} Slump-flow is employed in this the study for evaluating the flowability and stability of the self -Consolidating Nano-concrete, because other tests apparatuses are not available.

Table (3) Test methods for workability properties if SCC

Test Method	Property Measured
Slump-flow	Filling ability
T50Slump-flow	Filling ability
J-Ring	Passing ability
V-funnel	Filling ability
V-funnel at T5 minutes	Segregation resistance
L-box	Passing ability
U-Box	Passing ability
Fill-box	Passing ability
GTM screen stability test	Segregation resistance
Orimet	Filling ability

3.2.4.4 T_{50} Slump-flow

The equipment consists of one slump cone and one flow table Figure 31. A concentric diameter of 500 mm is marked on the table. The slump cone is filled with concrete while pressing the slump cone to the table. Next, the slump cone is lifted vertically and time measurement started for the concrete diameter to reach 500mm (T50). However, when the concrete has stopped flowing, the diameter of the concrete pile is measured instead of the height drop.



Fig. 31: Measurement of slump flow for the Nano-concrete

(Ashok, 2004), the measurement of the concrete diameter is referred to as the slump flow (D-final), any segregation border at the concrete periphery must be measured, see Figure 32. T50 slump flow over time of 5 seconds or less is desired, and the actual spread requirement must not be less than 500 mm.

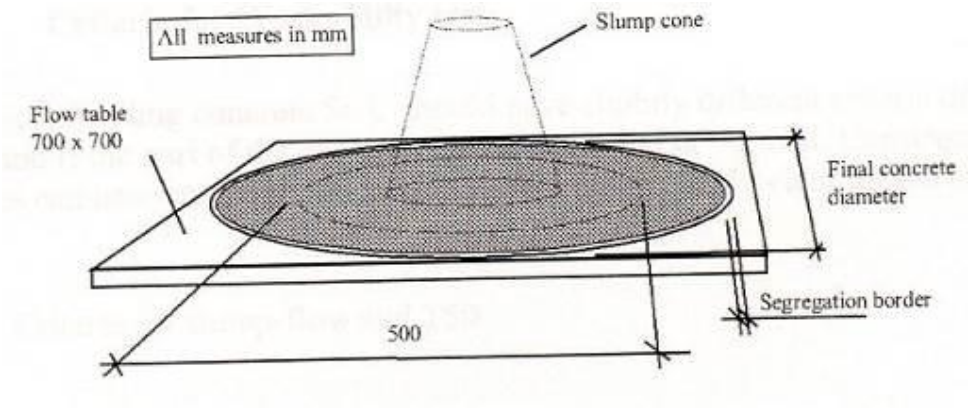


Fig. 32: Slump flow test apparatus

(John G. , 2003), the SCC (CSC-13) Nano-concrete mix T_{50} slump flow obtained was 480 mm over the time of 4 seconds giving an average compressive strength of 22 Mpa wich matches with the limits specified for high self-consolidating concrete in Table 4.

Table (4) References for slump flow limits and the corresponding type of concrete (John G. , 2003)

CONCRETE MIX		SLUMP FLOW (mm)
Slump	Type	
Low	Standard	100-150
Medium Low	Standard	150-200
Medium-High	Superplasticizer	200-250
High	Self-consolidating	410-560

3.2.5 The Chemical Properties

The deterioration of concrete is one of the most complicated phenomena in the material science and engineering mechanics of concrete durability.

(Brown, 2010), degradation of concrete is caused explicitly by delayed ettringite formation (DEF); a phenomenon of the most complex holistic model which has attracted considerable attention around the globe the last decade. Three causes promote DEF-induced deteriorations; 1. alkali-silicate reaction (ASR), 2. steam curing at high at high temperatures above 65°C and 3. Localized high stress in pre-stressed structures. The best way of mitigating the DEF-induced damage-risk is either to avoid cement with large clinker Sulfate which is responsible for the late sulfate release or to adopt lower and more homogeneous stress distribution, anyhow, stress singularity can be easily handled structurally. However, with the advent of the discipline of concrete science and engineering mechanics of material, the attention and curiosity moved from the chemistry of the cement hydration process and specific microstructure to a more productive approach based on material science and technology (Material laboratory testing). In this thesis, the DEF-induced damage-occurrence due to steam curing at high temperatures overlooked. Because high cement sulfate content and high temperatures are beyond our applications, instead, the integration of CNCs into the mainstream NanKoncrete mix operation for added values and benefits of the alkaline stability of the fine silica aggregates and cracking resistance studied the concrete microstructure through Nanotechnology applications to stop or reduce ASR. The ASTM C1260 testing method determines how far CNCs is affecting the development of the ASR in the NanKoncrete used in this research.

3.2.5.1 Alkali-Silicate Reaction (ASR):

ASR is a simple chemical acid-base reaction between calcium hydroxide, also known as Portlandite, or (Ca (OH)2), and silicic acid (H4SiO4, or Si(OH)4). For the sake of simplicity, this reaction can be chemically formulated as following:

$$Ca(OH)_2 + H_4SiO_4 \rightarrow Ca^{2+} + H_2SiO_4^{2-} + 2H_2O \rightarrow CaH_2SiO_4 \cdot 2H$$

Ca (OH) 2 = calcium hydroxide (Portlandite)

H4SiO4 = silicic acid

Ca2+ = hydroxyls ions

H2SiO42− = Silicon dioxide "60%low-density C-S-H gel" un-hydrated bulky alkali Silicate swellable gel + calcium hydroxide."

2 H2O = Water

CaH2SiO4 · 2 H = "40% high-density C-S-H Amorphous Calcium Silicate Hydrate."

Ettringite = needle-shaped crystals

(Collepardi, 2003), the discontinuous micrKracks due to first expansion and microcracking caused by the ASR act as the originator of ettringite in the cement matrix itself, but after sometimes more ASR reactions may happen, due to re-watering of fine silica aggregates existing in the C-S-H gel, thus subsequent further expansion would be caused by deposition of DEF. Therefore, ASR is the primary cause of deterioration in the form of cracks.

3.2.5.2 Accelerated Mortar Bar Test (ASTM C 1260)

(Brown, 2010), marine double washed sand is one of the main element of the NanKoncrete composition, which contains active silica and silicate minerals that is potentially dangerous for alkali-silica reaction (ASR)

commencement. Therefore, Nanoconcrete has to be tested for ASR, tow mixtures of the Nanoconcretes prepared, one with and another without CNCs. The accelerated mortar bar tests ASTM C 1260 which involve casting of three specimens for each type of mix, having sizes 25 mm x 25 mm x 285 mm (1 in. x 1 in. x 11.25 in.) with the Nanoconcrete bars containing the fine silica aggregates in question. After releasing the bars from the mold, the Nanoconcrete bars cured for one day in the water at 80°C followed by immersion in 1N NaOH Sodium hydroxide solution at 800 Co for 14 days. The test produces results within approximately 16 days from the time of casting. The test determines the expansions of the specimen, and a check then made with the ASR-expansion minimum allowable limits, mortar bar expansions of less than 0.10 % at 14days after immersion in 1 N NaOH solution are indicative of the innocuous behavior of nonreactive silica fine aggregates.

Three main necessary components to initiate and sustain ASR in concrete:

1. A critical amount of reactive silica mineral phases in the aggregate particles.
2. A high concentration of alkali hydroxides (Na+, K+–OH) in the concrete pore fluid.
3. Sufficient moisture (Hasdemir).

3.2.5.3 Double-Washed Marine Sand Chemical Composition

Mineralogical examinations and chemical analyses were first conducted to determine the mineralogical and chemical composition of the double washed marine sands. Additionally, sands containing active silica and silicate minerals found to be potentially dangerous for alkali-silica reaction (ASR) unless the expansions test data and observations are within the minimum allowable limits.

Excessive expansion of concrete due to ASR will not occur if any one of the following circumstances exists:

1. The aggregate is insufficiently reactive.
2. The pH of the pore fluid is not too high.
3. The amount of reaction product formed is not sufficiently large or not sufficiently capacious so that its expansion can cause damage.
4. Mixing potentially reactive aggregate with less or non-reactive aggregate to lower the amount of potentially reactive minerals to percentages less than threshold values.
5. There is not enough available water to cause the reaction to progress to develop the expansive product and to be available for inhibitions by the product to cause it to swell and disrupt the concrete.
6. Mixing with cement that contained a Sulfate resisting ability to counter potential reactivity.

The kinds of aggregate components known to be involved in ASR to a sufficient degree to create a problem in concrete are numerous. By the definition of ASR, all of these are composed of, or contain, significant percentages of SiO2. (Hasdemir). The mineralogical investigations and the chemical analysis, of the cement and marine sand used in the Nano-concrete, executed at Alhoty Analytical Services Laboratories, Bahrain. The results listed in (Appendix C), which show significant percentages of SiO2, 59.6%, and 20.61% respectively, even with a Sulfate resisting cement (Portland cement Type V).

3.2.5.4 Testing Procedure of Nano-concrete Specimens

A) The specimens examined were cast into three mortar bar samples.

B) The bars are moist cured for 24h.

C) The bars are submerged in water and heated to 80°C for 24h.

D) The initial lengths of the bars recorded.

E) The bars are submerged at 80°C 1.0 N NaOH Sodium hydroxide alkali solution for 14 days.

F) The final lengths of the bars recorded.

G) The average of the length changes of the bars is obtained and correlated to the reactivity limits.

3.2.5.5 Accelerated Mortar Bar Tests Results and Discussion

The use of a low-level load of CNCs in reducing expansion of mortar bars due to alkali-silica reaction (ASR) investigated and examined through the accelerated mortar bar tests, ASTM C 1260. Although the mixtures contained a high percentage of the deleterious reactive materials (SiO2), the mixtures with CNCs powder showed less reactivity than the one without CNCs powder. The CNCs powder under investigation was able to bring expansions to 0.10% from 0.20% just off the threshold limit of deleterious expansion specified by ASTM C1260, proving their potential to mitigate ASR in Nano-concrete.

Nevertheless, The only characteristic of the marine sand for resisting an ASR expansion was its fineness, expressed as the percent retained in the No. 325 sieve. Expansions between 0.10% and 0.20% at 16 days include both aggregates that are known to be innocuous and deleterious. Percent expansion at 14 days should be under 0.10%. The expansion is less than 0.10% related to nonreactive aggregates and expansion between 0.10% and 0.40% related with aggregates having the potential for significant slow ASR. Although, according to test results, samples with CNCs powder showed expansions of 0.10% (Appendix D). (Davies G, 1987) moreover,

(Hooton RD, 1992) also indicated that expansions of less than 0.10% at 16 days after casting are indicative of satisfactory behavior in most cases.

In conclusion, the expansions due to ASR completely suppressed when sufficient CNCs powder added to the Nano-concrete formulation.

3.2.6 The Thermal Properties

Initially, full-scale tests were planned to be done at the Research Institute facilities of the King Fahd University of Petroleum and Minerals (UPM), KSA. Figure 33 shows a wall sample with dimensions 61 cm x 61 cm x 20 cm. The blocks are to be cut and joined using cement mortar. All test samples should be prepared similarly and should be dry. Q is the Heat flow under steady-state conditions and d = thickness, up to 200 mm only. The surfaces of the samples should be flat and parallel.

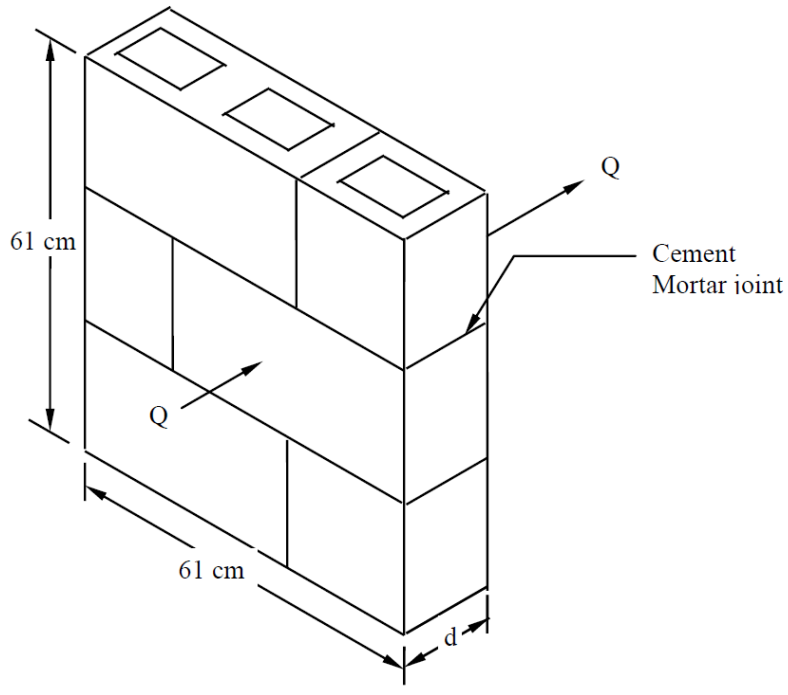


Fig. 33: Concrete wall test sample size and dimensions requested by UPM

Indeed, the samples for the ICF slabs and walls were ready Figure 34, but the laboratory service quotation was BD 850/- per sample which was summing up to BD 3400/-, in addition to, the results we were to get was the Thermal conductivity (K value) for the whole sample and not for the ingredients of it, which attributed us to Cancel the plan.

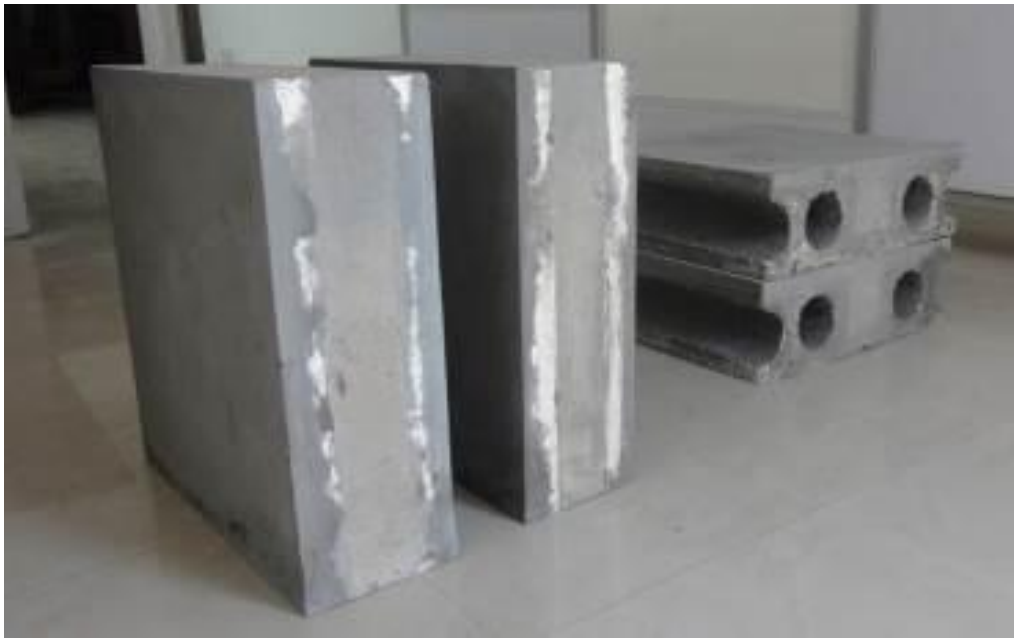


Fig. 34: ICF slabs and walls were ready for UPM Research Institute Laboratory

Eventually, the thermal conductivity (K value) test of the essential materials samples used in the ICF slabs and walls of the Polyforms system, were prepared, cast and packed at the University of Bahrain and then sent to RWTH Aachen University, Institute of Mineral Engineering, Department of Ceramics and Refractory Materials for testing, Figure 35 shows Sample No. 7957 to No.7961 for Nano and Polystyrene concretes, Polystyrene and Plaster.



Fig. 35: Prepared samples for thermal conductivity test

The thermal conductivity tests performed RWTH Aachen University, using the hot wire method according to DIN EN 993-14/15 at 20 and 50°C. The samples of the size dried at 50°C immediately before testing. For each sample, three specimens measured 230 mm x 114 mm x 64 mm required and tested. The thermal conductivity measured at 20°C and 55°C temperatures. The mean values of thermal conductivity (K value) and bulk density of each sample given in Table 5, See (Appendix D) for full report details.

Table (5) Thermal conductivity at 20 and 50°C according to DIN EN 993-14/15

Sample No.	Type	Temperature [°C]	Thermal conductivity Mean value / standard deviation [W/mK]	Bulk density Mean value / standard deviation [kg/m³] Before test	After test
7957	SBNBR 2	22	0,31 / < 0,01	887 / 63	875 / 64
		50	0,34 / 0,01		
7958	CSC1-11	20	1,33 / 0,03	1908 / 71	1880 / 85
		50	1,37 / 0,07		
7959	CSC1-12	20	1,29 / 0,05	1919 / 17	1905 / 21
		50	1,23 / 0,02		
7960	Plaster	20	1,05 / 0,02	1864 / 23	1850 / 28
		50	1,08 / 0,05		
7961	P24	20	0,032 / 0,001	22 / 1	22 / 1
		50	-		

It is apparent that the thermal conductivity values of the Nano and Polystyrene concretes of approximately 1.3 (W/mK) is much less than the thermal conductivity of ordinary concrete of 2 to 2.5 (W/mK).

3.2.7 Modulus of Rupture (Flexural Strength)

The traverse strength of hardened concrete determined according to BS 1881: Part 118: 1983, Uniaxial tensile cracking stress fr determination (fr) = 3FL/2bt2 where F= Force KN, L=450mm, b=100mm and t=100mm.

This test was carried out according to BS 1881: Part 118: 1983, by using (450x100x100) mm prism specimens. The prisms were subjected to two point load and tested at 28days of water curing. The average of three specimens was adopted for each mix. The flexural strength is calculated according to the following equation.

$$(fr) = 3FL/2bt2 \qquad (2)$$

Where:
fr = Uniaxial tensile cracking stress (Mpa).
F = maximum load (N).
L = distance between the supports (450 mm).
b = the width of the specimen (100 mm).
t = the depth of the specimen (100 mm).



Fig. 36: Prism testing apparatus

3.3 Optimization of Nano and Eps Concrete

3.3.1 Optimization of Nano-Concrete

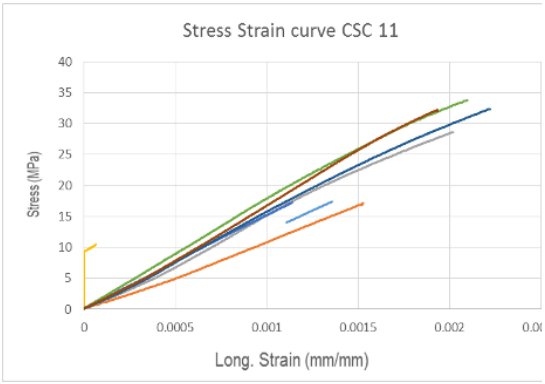
Self-compacted high fine Nano-concrete mixes with different sand, cement and Nano CNCs ratios for use as a structural core in ICF slabs and walls, see Table 6.

Table (6) Nano-concrete samples compositions and compressive strengths

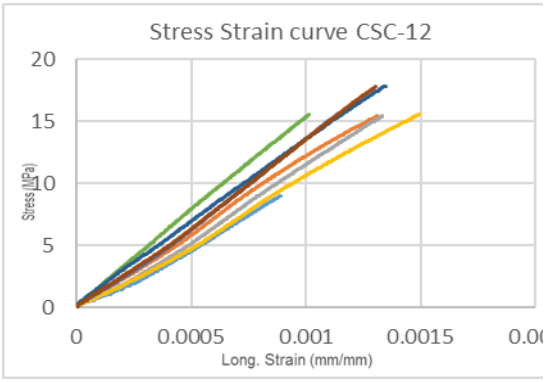
Specimens	Cement (KG)	Sand (KG)	CNCs (g)	Water (L)	28-days Fcu (Mpa)
CSC1-11	9	9	6.42	4.30	29
CSC1-12	6	12	6.42	3.60	22
CSC1-13	4.5	13.5	6.42	3.20	14

The results show varying 28-days compressive strength from 14 Mpa to 29 Mpa of the various mix designs. According to ASTM C143 and complying with the Prescriptive Method (PATH, 1998), the minimum allowable 28-days compressive strength is (17.2 MPa) for ICF walls. Since these initial strength results of only three sample cylinders of each mix, including the critical need for other parameters like position ratios. However, further sample ranges and trials were done using ADMIT "Gauge Buster 2" digital equipment discussed in section 3.1.1.1 for final selections of the structural core in ICF slabs and walls.

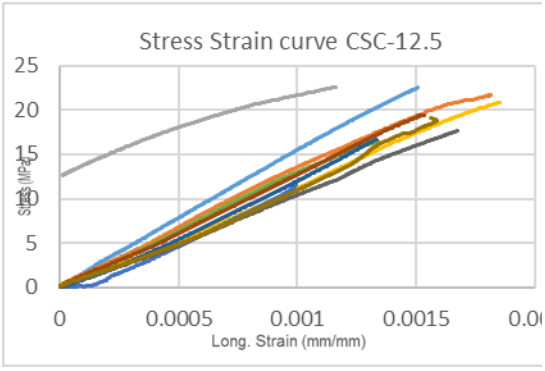
3.1.1.1 Compressive Strength, Poisson Ratio and Modulus of Elasticity of CSC Mixes by Gauge Buster 2



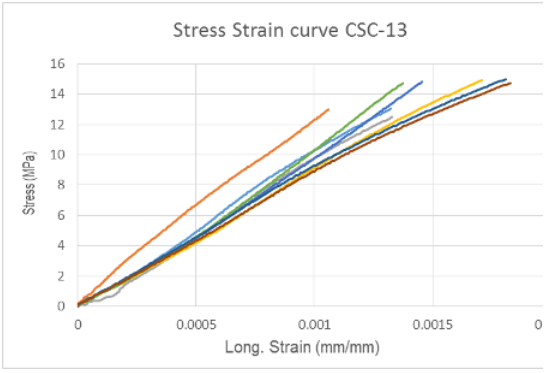
(a)



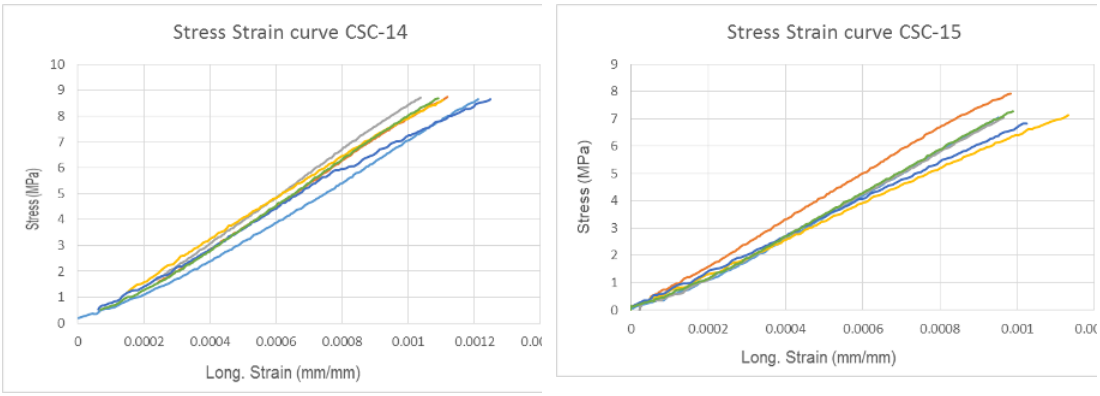
(b)



(c)



(d)



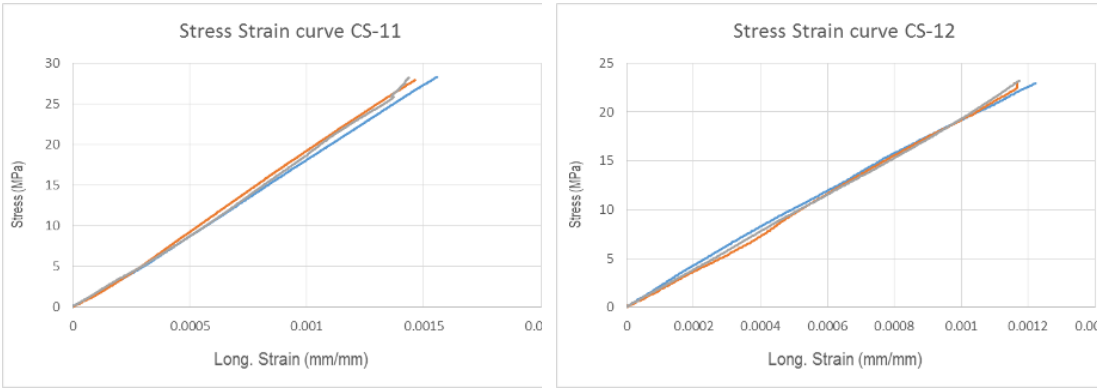
(e) (f)

Fig. 37: Stress-Strain curve for different combinations of CSC

Table (7) Derived compressive strength, modulus of elasticity and Poisson's ratio for different CSC

	CSC-11	CSC-12	CSC-12.5	CSC-13	CSC-14	CSC-15
Compressive Strength (MPa)	40.672	25.600	24.123	22.064	10.992	10.065
Modulus of Elasticity (MPa)	15628.711	13033.446	12488.217	9990.763	8141.523	7600.461
Poisson Ratio (Metric)	0.234	0.184	0.230	0.198	0.162	0.122

3.1.1.2 Compressive Strength, Poisson Ratio and Modulus of Elasticity of CS Mixes by Gauge Buster 2



(a) (b)

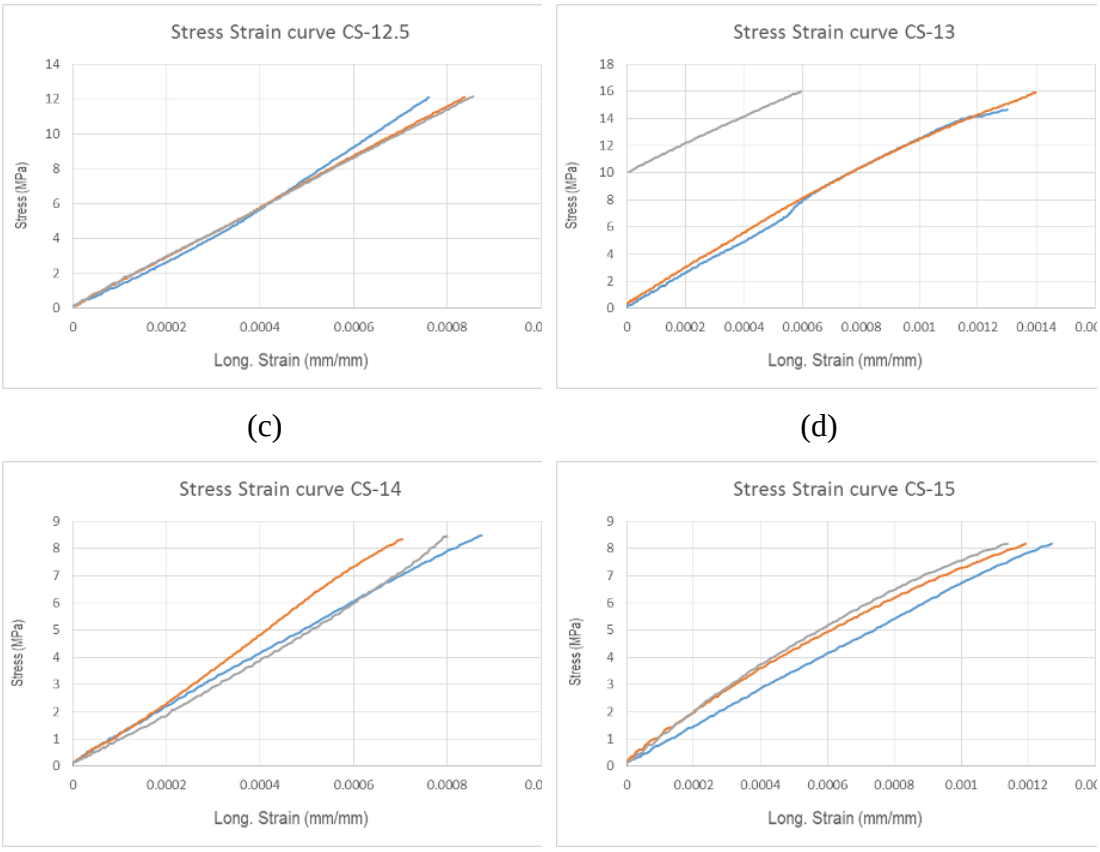


Fig. 38: Stress-Strain curve for different combinations of CS

Table (8) Derived compressive strength, modulus of elasticity and Poisson's ratio for different CS

	CS-11	CS-12	CS-12.5	CS-13	CS-14	CS-15
Compressive Strength (MPa)	39.56	28.34	23.92766	18.09	12.2	10.49
Modulus of Elasticity (MPa)	19131.300	19373.535	15427.961	11532.264	10759.087	6909.997
Poisson Ratio (Metric)	0.206	0.235	0.145	0.221	0.219	0.230

Table (9) ANOVA for CSC Samples

SUMMARY				
Groups	*Count*	*Sum*	*Average*	*Variance*
CSC-11 (MPa)	12	479.1769127	39.9314094	26.43648347
CSC-12 (MPa)	12	297.9922588	24.83268823	12.88454264
CSC-12.5 (MPa)	12	297.5627558	24.79689632	22.12446477
CSC-13 (MPa)	12	275.8437267	22.98697722	47.60293346
CSC-14 (MPa)	12	131.9072227	10.99226856	1.072198606
CSC-15 (MPa)	12	120.781589	10.06513242	2.019973817

ANOVA						
Source of Variation	*SS*	*df*	*MS*	*F-statistic*	*P-value*	*F crit*
Between Groups	7218.455972	5	1443.691194	77.24363358	3.14259E-26	2.353809
Within Groups	1233.546564	66	18.69009946			
Total	8452.002536	71				

The investigations were done to find the best CSC mix for use as the structural core of the ICF slabs and ICF walls. 17 Samples (CS group) without Nano additive and 125 Samples (CSC group) with Nano additive. P-value as per ANOVA result shown in Table 9, is greater than one which indicates that other mixes are also compatible, but sample CSC13 was selected as the candidate for the core concrete with, f_{cu} 22.1 Mpa, E 10000 Mpa, Poisson Ratio of 0.198 and maximum strain of 0.0014 Table 8, because of its pumpablity nature and coast effectiveness.

3.3.2 Optimization of EPS Concrete

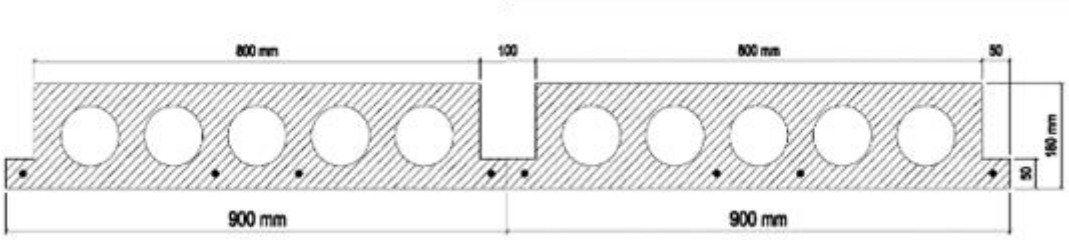


Fig. 39: Blank Block forms

Polystyrene Lightweight concrete (PLWC) the material behaves like a semi-solid and made by the use of polycarboxylates, a material similar to plastic developed using nanotechnology, is one of the essential materials in the construction industry because of its practical and economic advantages. The essential characteristic of PLWC is its porosity, which results in low apparent specific gravity. In concrete construction, self-weight represents a vast portion of the load on the structure, and there are considerable advantages in reducing the density of concrete. Furthermore, the criteria of the mixes for PLWC, required for the Blank Block forms Figure 39 is different from that of the Nano-concrete mixes that are used for the ICF Walls and the ribbed slabs. Despite its thermal and sound insulation, it should be ultra-light and Strong enough to carry its self and the labor while casting the ribbed slab; thus, avoiding wood shuttering and supports, the Blank Block forms innovative design provides larger simply supported and continuous spans, all of which contributes to safe and economical green construction.

(Whatmore, 1995), many productions of lightweight concrete (LWC) had been designed by the use of lightweight aggregates (LWA) such as fly ash, slag, and lightweight expanded clay aggregate (Leica) in which most of the process of manufacturing LWC is very costly, and complicated machinery or expensive LWC used. This resulted in a search for a

substitute of inexpensive LWA like the polystyrene beads due to its lightweight properties with a density between (16-27) kg/m3, excellent acoustic, and humidity insulation characteristic and excellent thermal insulator leading mainly to the non-structural application.

The primary aim of this investigation is to use polystyrene beads to produce ultra-light and strong Blank Block forms to carry its self and the labor during casting the ribbed slab, by a particular type of concrete mixture characterized by high resistance to segregation that can be cast and leveled without mechanical compaction and vibration. Therefore, it is crucial to study the mechanical properties (density, compressive, water to cement ratio, the polystyrene cement ratio, tensile and flexural strength) of PLWC.

3.3.2.1 Trial Mix designs

Four different trail batch Table 10,11,12 and 14 of Polystyrene lightweight concrete mix designs investigated to be used as a core in the Blank Block forms. The initially estimated density of 300 Kg/m^3 and ultimate estimated compressive strength of 1.2 Mpa. The first three batches designed and tested with not many promising results. For The (PLWC) to satisfy the criteria for flowability and zero slumps the four batches introduced by using Chemical 1. However, with adding it in the PLWC mixes, the polystyrene beads began to float and accumulate at the top surface during mixing, which resulted in adding another chemical admixture that prevents the beads from segregation. The purpose of using (Chemical 2), a viscosity-modifying agent, introduced, is to improve the bonding strength of the various materials and prevents the beads from floating. The emulsion (Chemical 2) used after mixing it with water by volume proportion. After many trails with (w/c) ratios utilized in this research (0.325- .550), with different dosage of (Chemical 1) to satisfy the

properties of PLWC. The details of the four batches used throughout this research as follows:

3.3.2.1.1 Batch one: Nano Polystyrene Concrete "Blank Block"

The first batch Table 10 obtained by the proportions by weights of (cement, sand, polystyrene and Nano Additive). Then prepared different PLWC mixes from the control mix by a partial replacement of sand with polystyrene beads. Therefore, they differ from each other by the content of polystyrene beads. The polystyrene measured by volume because the beads are very light in weight and density compared with other materials.

Table (10) Batch one consists of sand, cement, polystyrene and Nano additive

Nano Polystyrene concrete Trial MIXES										
Mix Code	Mix	Cement Kg	Sand Kg	Poly Kg	Nano Additive g	Water L	7 Days Comp.Strength N/mm^2	14 Days Comp.Strength N/mm2	28 Days Comp.Strength N/mm2	Density Kg/m^3
P-16s	Cement+Sand+Poly+Chem.1	8.0	12.0	0.713	7.14	6.5	0.230	0.301	0.433	387.300
Blank-1s		8.0	12.0	0.400	7.14	6	1.161	1.130	1.429	609.600
Blank-5s		8.0	12.0	0.450	7.14	5.7	0.409	0.510	0.624	564.000
Blank-2s		8.0	12.0	0.509	7.14	6	0.410	0.324	0.440	424.900
Blank-6s		8.0	12.0	0.550	7.14	5.25	4.092	4.230	4.961	
Blank-3s		8.0	12.0	0.600	7.14	5	1.645	1.910	1.926	708.000

3.3.2.1.2 Batch Two: Fly Ash Polystyrene Concrete "PF."

The second batch Table 11 obtained by the proportions by weights of (Cement, Fly Ash, and polystyrene). Then prepared different PLWC mixes from the control mix by a partial replacement of polystyrene beads with Fly Ash. Therefore, they differ from each other by the content of Fly Ash. The polystyrene measured by volume because the beads are very light in weight and density compared with other materials.

Table (11) Batch two consist of cement fly ash and Nano-additive

Fly Ash Trial MIXES Max Beads Size 5mm										
Mix Code	Mix	Cement Kg/m3	Poly Kg	Cement Kg	FA Kg	Water L	7 Days Comp. Strength N/mm^2	14 Days Comp. Strength N/mm2	28 Days Comp. Strength N/mm2	Density Kg/m^3
PF-1	Cement+FA+Poly	490.5	0.63	11.70	7.80		2.476	2.517	2..287	472.3
PF-2		450.0	0.63	10.73	7.16		1.827	1.752	1.851	461.6
PF-3		400.0	0.63	9.54	6.36		1.249	1.04	1.263	411.9
PF-4		350.0	0.63	8.35	5.57		0.757	0.776	0.678	362.6
PF-5		300.0	0.63	7.16	4.77		0.558	0.654	0.582	303.6
PF-6		250.0	0.63	5.96	3.98		0.182	0.189	0.205	248
PF-7		200.0	0.63	4.77	3.18		0.23	0.189	0.69	207.4

3.3.2.1.3 Batch Three: Nano Polystyrene Concrete "BB."

The third batch Table 12 obtained by the proportions by weights of (cement, polystyrene and Nano Additive). Then prepared different PLWC mixes from the control mix by a partial replacement of cement with polystyrene beads. Therefore, they differ from each other by the content of cement. The polystyrene measured by volume because the beads are very light in weight and density compared with other materials.

Table (12) Batch three consists of cement, polystyrene and Nano-additive

BB Trial MIXES										
Mix Code	Mix	Cement Kg/m3	Cement Kg	Poly Kg	Nano Additive g	Water L	7 Days Comp. Strength N/mm^2	14 Days Comp. Strength N/mm2	28 Days Comp. Strength N/mm2	Density Kg/m^3
BB1	Cement+Poly+Chem.1	490.5	19.5	0.630	6.96	7.0	1.186	1.649	2.986	582.9
BB2		300.0	11.9	0.630	4.24	5.0	0.446	0.983	0.875	552
BB3		250.0	9.9	0.630	3.53	3.5	0.274	0.301	0.341	536.8
BB4		200.0	8.0	0.630	2.86	3.0	0.156	0.172	0.193	379.8

The shortlisted mixes Table 13 from the first three batches, selected based on their required compressive strength and lower density.

Unfortunately, all the attempts failed utterly to extrude the Blank Block forms Figure 40 because it is hard to keep such mixes as dry as possible with zero slumps (semi-dry). The other ingredients which require much water, (Nano additive which retains water and marine sand which live in water and the fly ash) lose of adherent due to the very low water/cement ratio which falls far below its limit, disabling the hydration reaction from taking place.

Table (13) Shortlist of selected mixes of Nano-concrete

Blank Block Trail MIXES						
Mix Code	Cement Kg	Sand Kg	Poly Kg	Nano Additive g	Water L	Ave. N/mm2
Blank-3s	8	12	0.6	7.14	5	1.926
BB Basic MIXES						
Mix Code	Cement Kg	Sand Kg	Poly Kg	Nano Additive g	Water L	Ave. N/mm2
BB1	19.5	-	0.63	6.96	7	2.98



Fig. 40: Blank-3s and BB1 extrusion trial

3.3.2.1.4 Batch Four: Polystyrene Lightweight Concrete

This batch of PLWC mix has to be designed with one more added criteria for the machine to extrude it and that is to be semi-dry with zero slumps. Therefore, other additives are introduced, which can react with cement in a dry environment. So, the fourth batch obtained by the proportions by weights of (cement, polystyrene, Chemical-1, and Chemical-2). Then prepared different PLWC mixes from the control mix by a partial replacement of polystyrene beads with cement. Therefore, they differ from each other by the content of polystyrene beads. The polystyrene measured by volume because the beads are very light in weight and density compared with other materials Table 14.

Table (14) Batch four consist of cement, polystyrene, Chemical 1 and Chemical 2

Code	Cement Kg	EPS Kg	Chemical 1	Chemical 2	Water L	Average Strength
SBNBR-1	20.00	0.60	0.70	0.36	4.30	1.27
SBNBR-2	20.00	0.50	0.70	0.36	4.00	2.79
SBNBR-3	20.00	0.45	0.70	0.36	4.00	3.83
SBNBR-4	20.00	0.40	0.70	0.36	4.00	4.29
SBNBR-5	20.00	0.35	0.70	0.36	3.50	2.35
SBNBR-6	20.00	0.30	0.70	0.36	3.40	4.10
SBNBR-7	20.00	0.55	0.70	0.36	4.50	1.75

Finally, The selected trial mix (SBNSR-2) Table 15, unfortunately, worked unsuccessfully and was not extruded and produced correctly. However, producing the required precast Blank Block forms with a compressive strength of (2.79 Mpa), exceeding the final determined ultimate compressive strength was possible with molds, and with lowest possible density for of (499 Kg/M^3). Also, Figure 40 shows the first attempt to extrude precast Blank Block form, with an (SBNSR-2) mixture which produced with partial failure. Furthermore, by adjusting the water/cement ratio of the mixture the precast, Blank Block forms were prepared in a better form. Figure 41 shows the 1.5 long cured precast Blank Block form made of Polystyrene Lightweight concrete (PLWC) carrying five people. Unfortunately, the extruder machine was unable to produce a full scale of at least 2m Blank Block for a full-scale ICF composite slab testing.

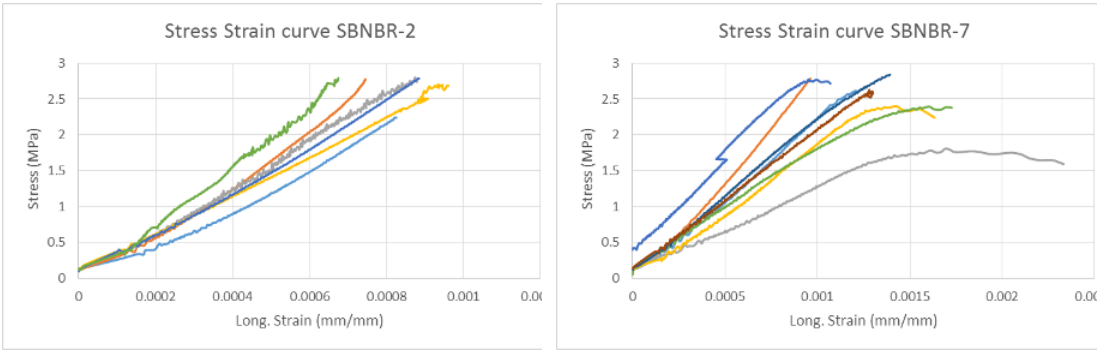
Table (15) Selected mix for PLWC

Chemical -1 and Chemical-2 Mixes						
Code	Cement Kg	EPS Kg	Chemical -1 L	Chemical-2 L	Water L	Ave. N/mm2
SBNBR-2	20.00	0.50	0.70	0.36	3.70	2.79



Fig. 41: The 1.5 long cured precast Blank Block

3.3.2.1.5 Compressive strength, Poisson Ratio and Modulus of elasticity of SBNBR Mixes by Gauge Buster 2



(a) (b)

Fig. 42: Stress-Strain curve for different combinations of SBNBR

Table (16) Derived compressive strength, modulus of elasticity and Poisson's ratio for different SBNBR

	SBNBR-2	SBNBR-7
Compressive Strength (MPa)	3.650	3.017
Modulus of Elasticity (MPa)	3463.252	2379.779
Poisson Ratio (Metric)	0.189	0.204

Table (17) ANOVA for SBNBR Sample

Groups	*Count*	*Sum*	*Average*	*Variance*
SBNBR-2 Mpa	7	24.49127	3.498753	0.96404
SBNBR-7 Mpa	7	23.67059	3.381513	0.317384

ANOVA

Source of Variation	*SS*	*df*	*MS*	*F-statistic*	*P-value*	*F crit*
Between Groups	0.048109	1	0.048109	0.075087	0.788729	4.747225
Within Groups	7.688548	12	0.640712			
Total	7.736657	13				

Based on the ANOVA results the SBNBR-2 was selected

Similar tests were done for EPS concrete. 57 samples for SBNBR-2 and 14 samples for SBNBR-7. This Includes the samples taken from the full-scale Blank Block casting. The P-value as per ANOVA result is shown in Table 17, is less than one. Thus SBNBR-2 sample is promising, therefore, SBNBR-2 was selected as the candidate for the Blank Block with f_{cu} 3.65 Mpa, E 3463 Mpa, Poisson Ratio of 0.189 and maximum strain of 0.0009 Table 16.

3.3.3 Material Properties Results and Conclusion

The resulting reading for the compressive strengths and modulus of elasticity with the digital Gauge buster are more accurate and can be adopted. However, using the ASTM manual method is almost impossible for measuring lateral and transverse displacements of polystyrene concrete

because reading very tiny displacements are impossible. For finite element analysis, the CSC-13 mix design (F_{cu}= 22 Mpa) is embraced because they comply with ASTM C143 and with the Prescriptive Method (PATH, 1998), of the minimum allowable 28-days compressive strength (17.2 MPa) for ICF walls and would be more economical.

The material properties parameters; Compressive strength, flexural strength, modulus of elasticity, Poisson Ratios, K-value and densities of the Nano and polystyrene concrete trial specimens are listed in Table 18 and 19.

The result obtained using the digital Gauge buster gave better and accurate readings.

Table (18) Modulus of elasticity calculation for different mixes of Nano concrete determined

	CSC1-12		CSC1-11		CSC1-13		BB-1		Blank-3s		CSC1-13 R		SBNBR 2		SBNBR 7	
compressive strength	22	22	29	29	14	14	2.98	2.98	1.926	1.926	14	14	2.79	2.79	1.75	1.75
cylinder area	17670	17670	17670	17670	17670	17670	17670	17670	17670	17670	17670	17670	17670	17670	17670	17670
Cylinder Diameter	150	150	150	150	150	150	150	150	150	150	150	150	150	150	150	150
Gauge Value	0.002	0.002	0.002	0.002	0.002	0.002	0.002	0.002	0.002	0.002	0.002	0.002	0.002	0.002	0.002	0.002
Gauge Reading	70	78	88	103	53	63	190	201	27	45	70	76	68	20	41	50
Load 1	14.2	17.2	16.7	15.7	14.2	13.1	4.8	3.2	5.1	2.1	9.9	9.1	8.2	8.9	8.1	8.7
Strain 1	5.00E-05	5.00E-05	5.00E-05	5.00E-05	5.00E-05	5.00E-05	5.00E-05	5.00E-05	5.00E-05	5.00E-05	5.00E-05	5.00E-05	5.00E-05	5.00E-05	5.00E-05	5.00E-05
Strain 2	0.00046667	0.00052	0.00058667	0.00068667	0.00035333	0.00042	0.00127	0.00134	0.00018	0.0003	0.00047	0.00051	0.00045	0.00013	0.00027	0.00033
S1	0.80362196	0.97340125	0.9451047	0.8885116	0.80362196	0.74137	0.27165	0.1811	0.28862	0.11885	0.56027	0.515	0.46406	0.50368	0.4584	0.49236
S2	8.8	8.8	11.6	11.6	5.6	5.6	1.192	1.192	0.7704	0.7704	5.6	5.6	1.116	1.116	0.7	0.7
Modulus of easticity	1.92E+04	1.67E+04	1.99E+04	1.68E+04	1.58E+04	1.31E+04	7.56E+02	7.84E+02	3.71E+03	2.61E+03	1.21E+04	1.11E+04	1.62E+03	7.35E+03	1.08E+03	7.33E+02
Av. Modulus of easticity	17921.8225		18339.0848		14471.8345		770.05		3156.09		11615.2		4482.11		907.31	

Table (19) Final structural material properties determined by Gauge Buster 2 manually

Specimens / properties	CS-11	CSC1-11*	CSC-11	CS-12	CSC1-12*	CSC-12	CS-13	CSC1-13*	CSC-13	CS-14	CSC-14	CS-15	CSC-15	SBNBR2*	SBNBR2	SBNBR7*	SBNBR7
Compressive Strength (Mpa)	42.8	29	40.67	30.1	22	25.6	20.4	14	22.1	14	10	10.75	10.1	2.79	3.65	1.75	3.017
Modulus of Elasticity (Mpa)	19131.3	18339.08	15628.7	19373.5	17921.8	13034	11532	14471.83	9990.8	10759	8141.5	6910	7600	4482	3463.3	907	2379.8
Poisson's Ratio	0.206	0	0.234	0.235	0	0.184	0.221	0	0.198	0.219	0.162	0.23	0.122	0	0.189	0	0.204
Flexural Strength (Mpa)	0	0	2.36	0	0	1.69	2.03	0	1.52	0	0	0	0	0	1.69	0	1.35
K-Value [W/mK]	1.35	1.35	1.35	1.35	1.26	1.26	1.35	1.065	1.065	0		0		0.325		0	
Density [Kg/m^3]	1908			1919			1864			0		0		449			

* : Results are calculated manually.

The table shows the results of two mixes; CS and CSC (with CNC), the addition of CNCs to the CSC mixtures increased some and reduced some of the structural properties of the CSC specimens between 16-25%, except for the compressive strength of sample CSC-13 which recorded value of 22.1 Mpa, which is greater than 18.1 Mpa of sample CS-13, Generally, most of the structural values are close, but the measured flow rate of CSC mixes are within the required limits. CSC-13 adopted and used for the structural core of the ICF slabs and walls, since it contributes to the least density, less cement content, good k-value, better flexural strength and 28-days compressive strength (22.1 Mpa) is greater than the minimum required 28-days compressive strength of (17.2 MPa) complying with (ASTM C143/C143M-15a, 2000) and the *Prescriptive Method* (PATH, 1998).

Finally, SBNBR-2 polystyrene lightweight concrete will be used for the Blank Block precast formwork of the ICF slab, it has a compressive strength of (fcu =3.65Mpa), complying with the final determined ultimate compressive strength of 1.4 Mpa.

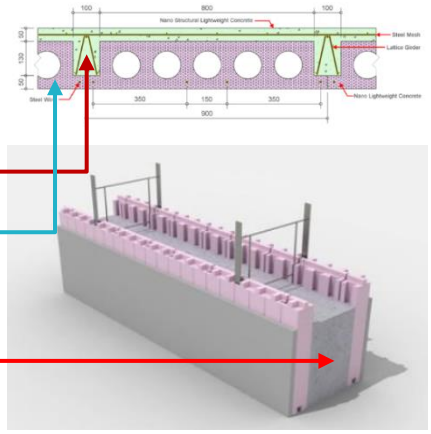
Also, it contributes to the least density, have good k-value, better flexural strength and can be extruded readily.

Finally:

- (CSC13) mix design used in the structural core of the ICF slabs and walls.
- (SBNBR-2) mix design used in the Blank Block precast formwork of the ICF slab.

Table (20) Final selected recipes for use as a core in ICF walls and ribbed slabs

Code	Density Kg/m^3	K- Value [W/mK]	E N/mm^2	Ave. N/mm^2
CSC1-13	1864	1.065	9990.8	22.1
SBNBR-2	449	0.325	3463.3	3.65



3.4 Experiments on Full-Scale ICF Slabs and ICF Walls

3.4.1 Introduction

Insulated concrete forms (ICFs) are green building components that are primarily used in residential construction. Although there are several types of ICFs (e.g., screen grid, waffle-grid, and flat), the principles behind each remain the same. ICFs are stay-in-place forms that have reinforced concrete cores. The presence of the ICF wall forms reduces the amount of concrete, relative to a purely reinforced concrete system, required to complete a job. Buildings constructed with ICFs can be very energy efficient due to the high R-value and thermal mass of the blocks. Here, R-value is the thermal resistance to heat flow through a unit area of homogeneous material when there is a unit temperature difference between two surfaces. It is equivalent to the inverse of the thermal conductance (MEW, 2006), and thermal mass is the property of the mass of a building, which enables it to store heat, providing "inertia" against temperature fluctuations in building design.

Finally, Nano mix design polystyrene lightweight concrete is used for the Blank Block slab. A new mix is designed and prepared which is tested to get the required (17.2 MPa). Nano-concrete is produced by using combination of different materials (i.e., cement, sand, and Nano additives), Polystyrene lightweight concrete is produced by investigating four different mix batches based on EPS beads and special additives as to prevent the segregation of beads, also properties of Nano and polystyrene lightweight concrete (density, compressive strength, and tensile strength) is investigated.

Furthermore, in this study, nonlinear FEM structural modeling of the lightweight concrete Blank Block slab along with for ICF walls (Polyforms) is carried out to obtain the structural and thermal behavior of these elements.

3.4.2 Test Specimens

The dimensions of the specimens are decided to take into consideration the capacity of civil engineering laboratory machines and the practicality of casting, transporting and unloading the specimens on the loading-frame.

3.4.2.1 ICF Slabs

Initially, the span of ICF blocks is intended to made 4metres. However due to the difficulties of transportation and placement on the universal testing machine, later it is decided that the length of each ICF slab should be 2m to have eased in handling these specimens in structures laboratory. Geometric dimensions and other properties of each specimen are given in Table 21 to 25.

The polystyrene concrete elements which shall be used as formwork and an insulating layer for the floor with the overlying of Nano-concrete is

considered as a separate type of element. Usually, three typically same samples are tested in all the experimental evaluations to verify the similar behavior, and finally, the average behavior is considered for further investigation. Here, in this study also three similar elements are tested in each category of the slab. Three Blank Blocks of category B are tested for two-point loading system as per the details are given in Table 21. These blank blocks are made from polystyrene concrete with hollow cores in the middle as per the cross-section is shown in Table 21. No reinforcement is used in the casting of these elements. These are designed such a way that they can carry construction load; hence, they can be used as formwork during construction activities.

Four different categories by keeping variation in overlying reinforcement and reinforcement spacing with polystyrene concrete namely category S, MS, J, and MSJ have been incorporated in the present study.

In the first category S, two 10 mm reinforcing bars are kept in the rib beam. The details of the S-slab are given in Table 22. The second category of type MS is provided with two 10 mm reinforcing bars and 5 mm wire mesh as mentioned in Table 23. For the major load application of rib, the beam is having lattice girder placed inside as per the details are shown in Table 24. This third category is named as J. In the fourth category of slabs which is named as MSJ, rib beam is provided with lattice girder and 5 mm wire mesh is provided at the top as per details mentioned in Table 25.

Formerly, 6-specimen configuration with different thicknesses of the Nano-concrete is discarded and replaced with three configurations of steel reinforcement for the ICF slab. This is because; initial calculations showed that the 50 mm slab thickness is sufficient for residential buildings imposed

surface loading as mentioned in Chapter 3. Hence, for economical purposes, other thicknesses initially considered omitted.

Table (21) Details of polystyrene concrete Blank Block specimens

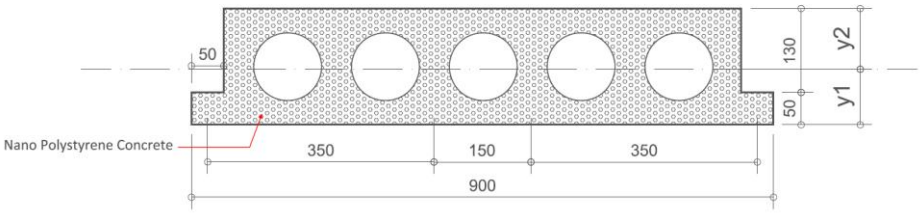
GROUP	B		
SPECIMEN	B1	B2	B3
B-Slab Configuration			
Overall width (m)	0.9	0.9	0.9
Span (m)	2	2	2
Thickness (mm)	180	180	180
No. of Samples	1	1	1

Table (22) Details of ICF slab of category S specimens

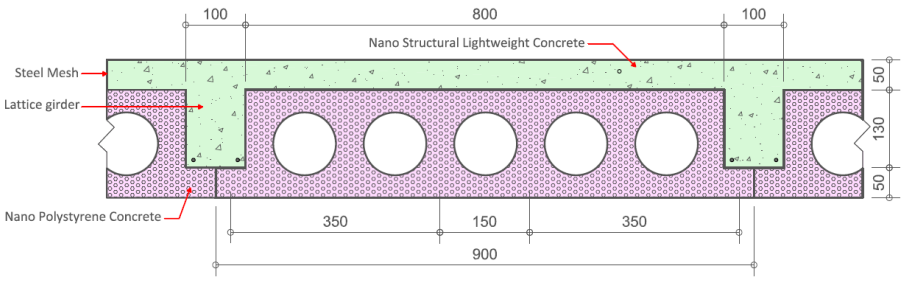
CATEGORY	S		
SPECIMEN	S1	S2	S3
S-Slab Configuration			
Overall width (m)	1.8	1.8	1.8
Span (m)	2	2	2
Thickness (mm)	230	230	230
No. of Samples	1	1	1

Table (23) Details of ICF slab of category MS specimens

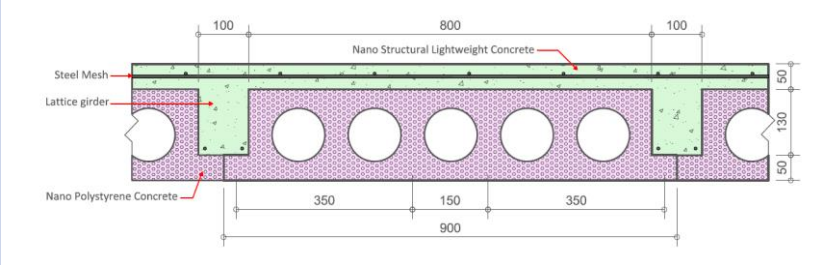
CATEGORY	MS		
SPECIMEN	MS1	MS2	MS3
MS-Slab Configuration			
Overall width (m)	1.8	1.8	1.8
Span (m)	2	2	2
Mesh Reinforcement	#5mm@ 200mm c/c	#5mm@ 200mm c/c	#5mm@ 200mm c/c
Thickness (mm)	230	230	230
No. of Samples	1	1	1

Table (24) Details of ICF slab of category J specimens

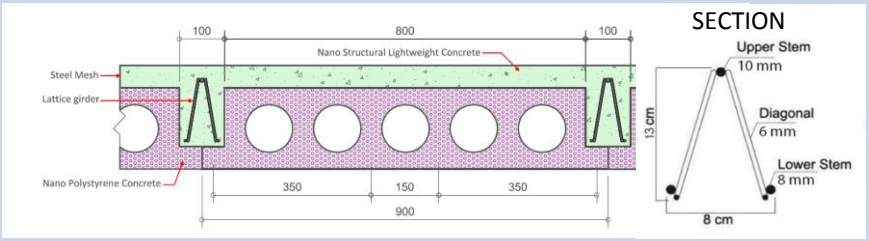
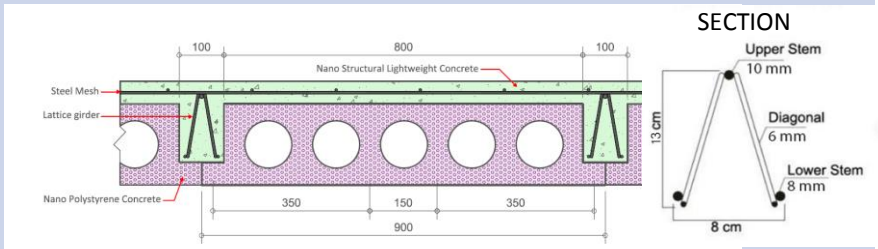
CATEGORY	J		
SPECIMEN	J1	J2	J3
J-Slab Configuration			
Overall width (m)	1.8	1.8	1.8
Span (m)	2	2	2
Lattice Girder	See Section	See Section	See Section
Thickness (mm)	230	230	230
No. of Samples	1	1	1

Table (25) Details of ICF slab of category MSJ specimens

CATEGORY	B		
SPECIMEN	MSJ1	MSJ2	MSJ3
MSJ-Slab Configuration			
Overall width (m)	1.8	1.8	1.8
Span (m)	2	2	2
Lattice Girder	See Section	See Section	See Section
Mesh Reinforcement	#5mm@ 200mm c/c	#5mm@ 200mm c/c	#5mm@ 200mm c/c
Thickness (mm)	230	230	230
No. of Samples	1	1	1

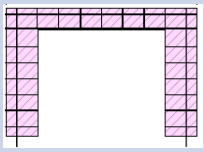
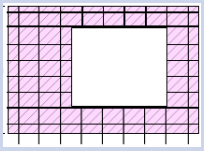
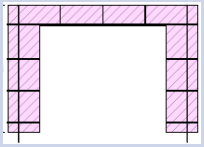
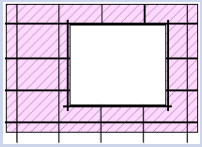
3.4.2.2 ICF Walls

The selection of ICF walls configurations are minimized from 12 to only four specimens, and the dimensions of the original selection have been reduced to half which results in 1/8 of the original volume. Moreover, that is due to the incapability of entering the specimens in the laboratory and the difficulty in transporting them to the university.

In the experimentation, only two types of openings are selected in the wall elements, first of a door type and second of a window type. Two different thicknesses particularly 75 mm and 50 mm are considered in this study. Four type of wall elements is prepared by keeping both the types of openings each thickness of the wall. Dimensional details of all four wall are given in Table 26. The solid walls are discarded because they are

expected to exceed the capacity of the loading-frame according to the results attained from ANSYS simulation.

Table (26) Details of ICF wall specimens

SPECIMEN	ICF04	ICF06	ICF09	ICF11
Wall Configuration				
Overall Size	1.8mX1.2m	1.8mX1.2m	1.8mX1.2m	1.8mX1.2m
Openings	1.2mX1.05m	0.9mX0.9m	1.2mX1.05m	0.9mX0.9m
Horizontal Reinforcement	#10 mm @ 150 mm c/c	#10 mm @ 150 mm c/c	#10 mm @ 300 mm c/c	#10 mm @ 300 mm c/c
Vertical Reinforcement	#10 mm @ 200 mm c/c	#10 mm @ 200 mm c/c	#10 mm @ 400 mm c/c	#10 mm @ 400 mm c/c
Wall Thickness (mm)	75	75	50	50
No. of Samples	1	1	1	1

3.4.2.3 Test Setup

The aim of the experimental study is to determine the ultimate load-bearing capacity of these specimens. The experiments are conducted in the structural laboratory of Civil Engineering, University of Bahrain. The Universal testing machine shown in Figure 43 with the brand name of "FORM-TEST SEIDNER" is used for this purpose. The apparatus is connected with two hydraulic jacks each of them having an individual capacity of 200 kN. The testing machine is capable of accommodating

various elements like slab, beams, pipes, and columns. These experiments are carried out during the months June 2016 to August 2016. The testing of four different types of slabs, namely ICF04, ICF06, ICF09, and ICF11 have been done. To observe the failure behavior, two strain gauges are applied. These are connected to the data logger to observe the strain values throughout the test.

Blank Block, ICF slab category S (ribbed slab with two bars only), ICF slab category MS (ribbed slab with two bars and mesh), ICF slab category J (ribbed slab with lattice girder only), and ICF slab category MSJ (ribbed slab with lattice girder and mesh) having dimensions mentioned in Table 21 to 25 for deflection are tested. Upon completion of testing, the data is analyzed and then compared to the results obtained from ANSYS simulation tool.



Fig. 43 Loading Frame from FORM-TEST SEIDNER

3.4.2.4 Testing Procedure

Tests on the ICF slabs specimens carried out after curing 28 days. The slabs are tested under pure bending. Sample loading arrangement is shown in

Figure 43, and the loading diagrams is shown in Figures 44 and 45. The elements are cast at Bardex Industries, Bahrain and were transported to the Structural Engineering Lab of the University of Bahrain. The elements were brought in place, positioned in the loading frame for four-point load system. Under monotonic loading, a specimen is pushed or pulled in only one direction with a steadily increasing load until failure occurs or the test stopped. ICF slab specimens tested in a horizontal position until failure. The monotonic universal testing assembly, with the vertical actuator, applied the lateral monotonic static loading which incorporated the use of hold-downs, were performed according to ASTM E564, to the slabs by the which have two hydraulic jacks with a capacity of 200 kN each. The resulting loads applied to the Blank Block and ICF slabs over the beam through one and two points loads located at each of the vertical hydraulic actuators as shown in Figures 44 and 45 respectively. The vertical loads continuously recorded manually and electronically.

The arrangement of the displacement transducer is carried out as shown in Figure 51 to record the mid-span deflection of these slabs during the loading. The transducer is connected to the data logger where the data are collected twice per second. The slabs are supported on two end edges as shown in Figure 49 such that the orientation of the rib beam remained parallel to the loading span.

Two 50 mm diameter solid steel rod are placed over the slab to produce the two-point load effect on the slab. Steel girders are used to transfer the load from loading jack to the solid rods for the equal distribution of load on each rod as shown in Figures 44 and 45.

Items of interest are observations of cracking during displacement history, ultimate load capacity, load distribution, initial stiffness, and energy

dissipated. Load-displacement curves are plotted for each wall specimens to understand their behavior.

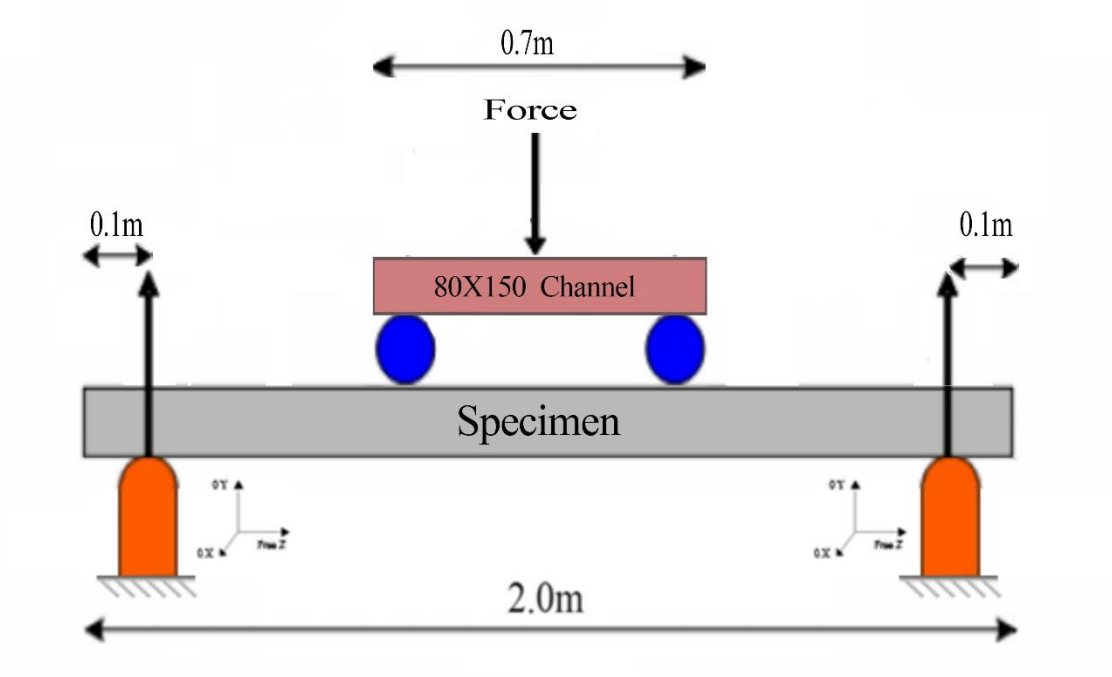


Fig. 44: Three-point loading system

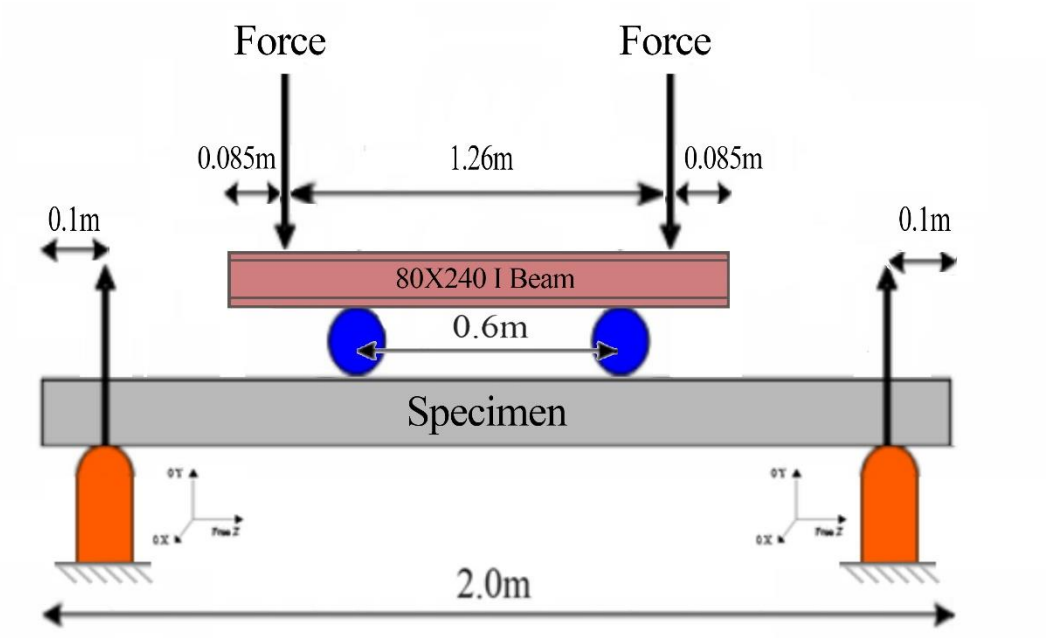


Fig. 45: Four-point loading system

3.4.3 Full-Scale Test on ICF Slabs

Following subsections gives the details of the results and behavior observed in the experimentation done on all the categories of ICF slabs.

3.4.3.1 Blank Blocks (Category B)

All the three elements of category B namely B1, B2 and B3 are tested in four point load system. The test data Load vs. Deflection for the category B are shown in Table 27. Figure 46 shows the chart of the load vs. deflection behavior along with their average value. Figures 47 to 52 are showing the pictures of the test setup and failed elements B1, B2, and B3.

Table (27) Load vs. deflection behavior for category B

Load (KN)	Deflection (mm)			
	B1	B2	B3	Average
1	0.17959	0.23973	0.11944	0.179586
2	0.42857	0.41553	0.44161	0.428567
3	0.63128	0.62329	0.63928	0.631284
4	0.93158	0.92779	0.93536	0.931576
5	1.03504	1.01527	1.05481	1.035038
6	1.32818	1.23145	1.42491	1.328179
7	1.87198	1.56791	2.17606	1.871984

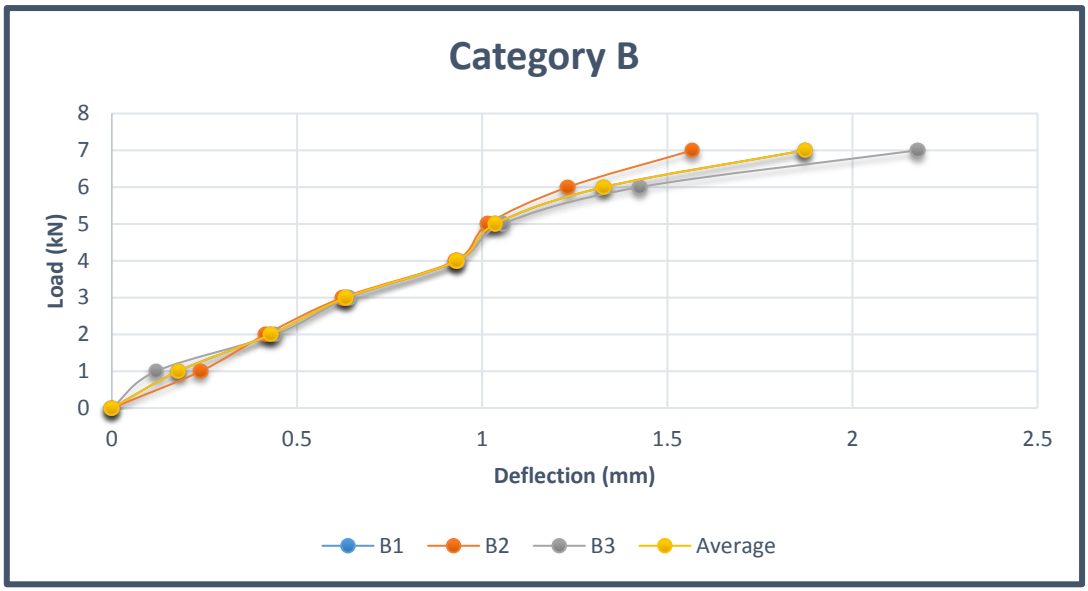


Fig. 46: Chart of load vs. deflection behavior for category B



Fig. 47: Test setup for Blank Block B1



Fig. 48: Failure of Blank Block B1



Fig. 49: Test setup for Blank Block B2

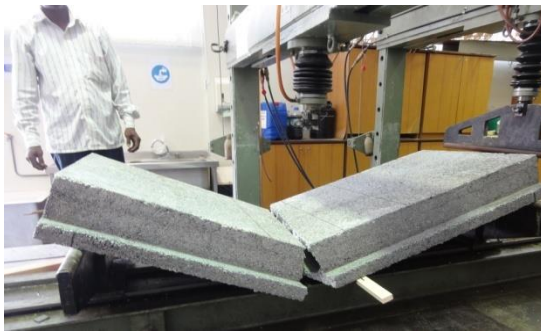


Fig. 50: Failure of Blank Block B2

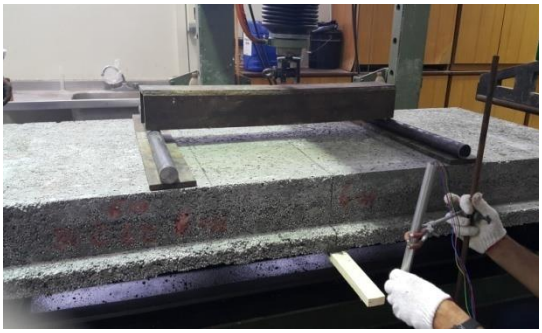


Fig. 51: Test setup for Blank Block B3

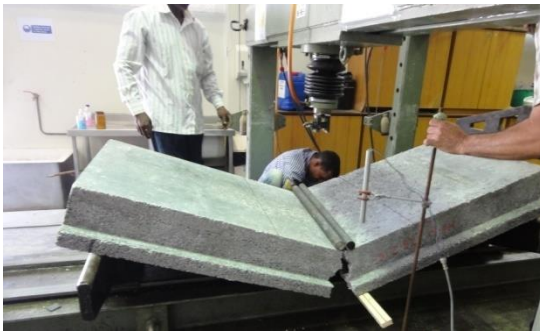


Fig. 52: Failure of Blank Block B3

3.4.3.2 ICF Ribbed Slab with Two Bars Only (Category S)

In this category S, two bars of 10 mm diameter is provided in the rib beam to provide interaction between adjacent polystyrene slab panels. The test data Load vs. Deflection for the category S are shown in Table 28. Figure 53 shows the chart of the load vs. deflection behavior along with their average value. Figures 54 to 59 are showing the pictures of the test setup and failed elements S1, S2, and S3. Here, first cracks are observed at 42 kN, 41 kN, and 42 kN whereas ultimate load remained 48 kN, 48 kN and 47 kN for the elements S1, S2 and S3 respectively. The sharp curve is observed at these levels of the first crack in Figure 55 also. Extensive elongation is observed after the first crack due to steel slipping before ultimate failure.

Table (28) Load vs. deflection behavior for category S

Load (KN)	Deflection (mm)			
	S1	S2	S3	Average
6	0.37179	0.121967	0.360013	0.28459
12	0.62077	0.322161	1.039662	0.660864
18	0.92443	0.719185	1.213784	0.952465
24	1.51828	1.02957	1.521646	1.356499
30	2.02886	1.41734	2.496538	1.980911
36	2.67739	1.936332	3.732192	2.78197
42	4.19146	2.864962	4.443806	3.833409
48	11.5145	11.48674	11.32	11.4404

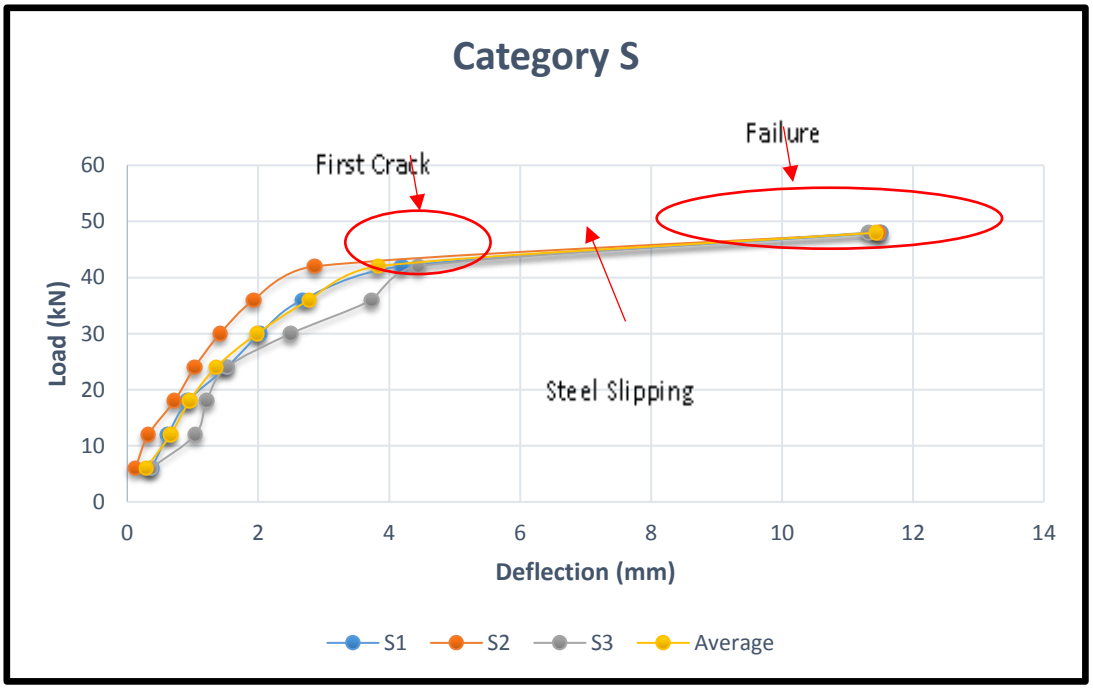


Fig. 53: Chart of load vs. deflection behavior for category S



Fig. 54: Test Setup for ICF slab S1

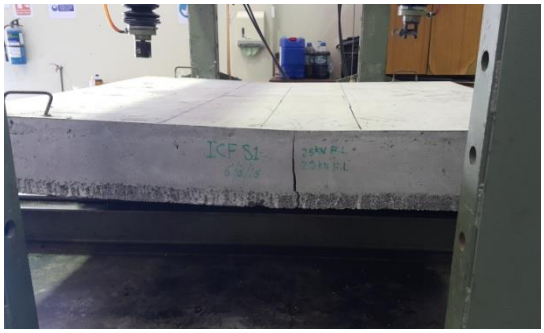


Fig. 55: Failure of ICF slab S1



Fig. 56: Test Setup for ICF slab S2

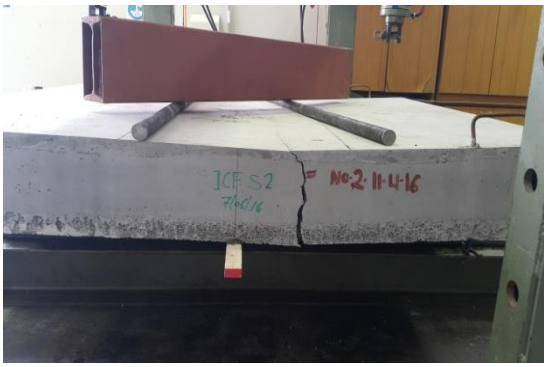


Fig. 57: Failure of ICF slab S2



Fig. 58: Test setup for ICF slab S3



Fig. 59: Failure of ICF slab S3

3.4.3.3 ICF Ribbed Slab with Two Bars and Mesh (Category MS)

In this category MS, two bars of 10 mm diameter is provided in the rib beam along with the 5 mm diameter size square mesh at the top with the spacing of 200mm c/c both ways. The results obtained during the testing between Load and Deflection for the category MS are shown in

Table 29. Figure 60 shows the chart of the load vs. deflection behavior along with their average value. Figures 61 to 66 the pictures of the test setup and failed elements MS1, MS2, and MS3. Here, first cracks are observed at 48 kN in all the three elements whereas ultimate load remained 54 kN, 53 kN and 54 kN for the elements MS1, MS2 and MS3 respectively. The sharp curve is observed at these levels of the first crack in Figure 64 also. Extensive elongation is observed after the first crack due to steel slipping before ultimate failure.

Table (29) Load vs. deflection behavior for category MS

Load (KN)	Deflection (mm)			
	MS1	MS2	MS3	Average
6	0.1	0.220382	0.212812	0.177731
12	0.2	0.325526	0.365901	0.297142
18	0.5	0.418894	0.541702	0.486865
24	0.6	0.826852	1.045552	0.824135
30	1	2.207182	1.435004	1.547395
36	1.7	3.778454	2.335036	2.604497
42	2.7	4.967	3.145908	3.604303
48	5		7.188486	6.094243
54			9.558008	9.558008
60			16.59002	16.59002

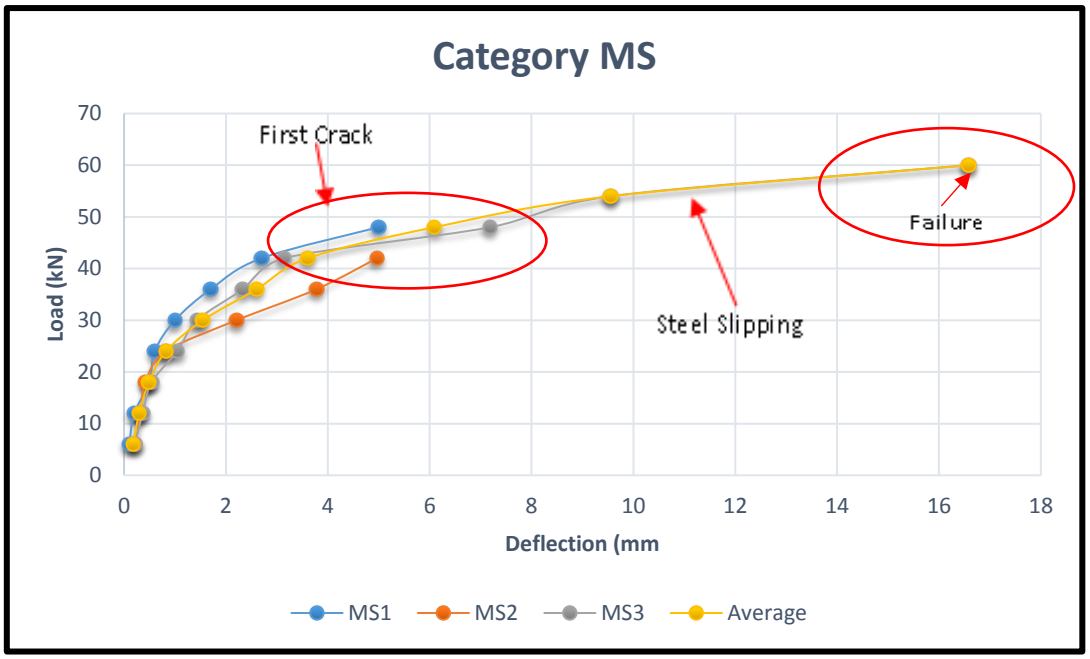


Fig. 60: Chart of load vs. deflection behavior for category MS

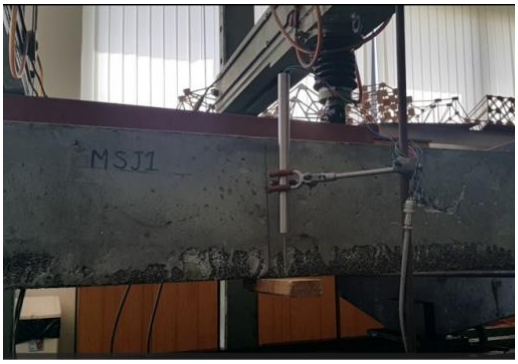


Fig. 61: Test setup for ICF slab MS1



Fig. 62: Failure of ICF slab MS1



Fig. 63: Test setup for ICF slab MS2

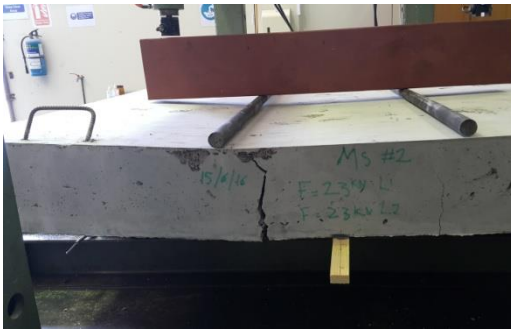


Fig. 64: Failure of ICF slab MS2



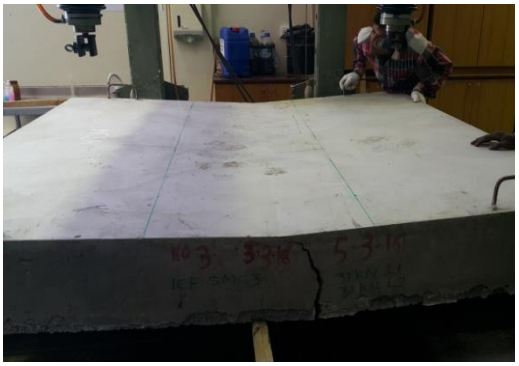


Fig. 65: Test setup for ICF slab MS3 **Fig. 66: Failure of ICF slab MS3**

3.4.3.4 ICF Ribbed Slab with Lattice Girder Only (Category J)

In this category J, one lattice girder as given in Table 24 is provided for the improved behavior of the slab panel. The test data Load vs. Deflection for the category J are shown in Table 30. Figure 67 shows the chart of the load vs. deflection behavior along with their average value. Figures 68 to 73 are showing the pictures of the test setup and failed elements J1, J2, and J3. Here, first cracks are observed at 47 kN, 46 kN, and 48 kN whereas ultimate load remained 52 kN, 54 kN and 52 kN for the elements J1, J2 and J3 respectively. The sharp curve is observed at these levels of the first crack in Figure 69 also. Extensive elongation is observed after the first crack due to steel slipping before ultimate failure.

Table (30) Load vs. deflection behavior for category J

Load (KN)	Deflection (mm)			
	J1	J2	J3	Average
6	0.6275	0.406276	0.324685	0.45282
12	0.91349	0.719185	0.75199	0.794889
18	1.27939	0.808347	1.112844	1.066861
24	1.76726	1.012748	1.326498	1.368835
30	2.20887	1.250792	1.721836	1.727165
36	2.93646	1.64277	2.264382	2.281204
42	5.00401	2.3813	2.939826	3.441713
48	7.79916	9.879326	9.657264	9.111917
54	17.4379	27.8413	15.33252	20.20392

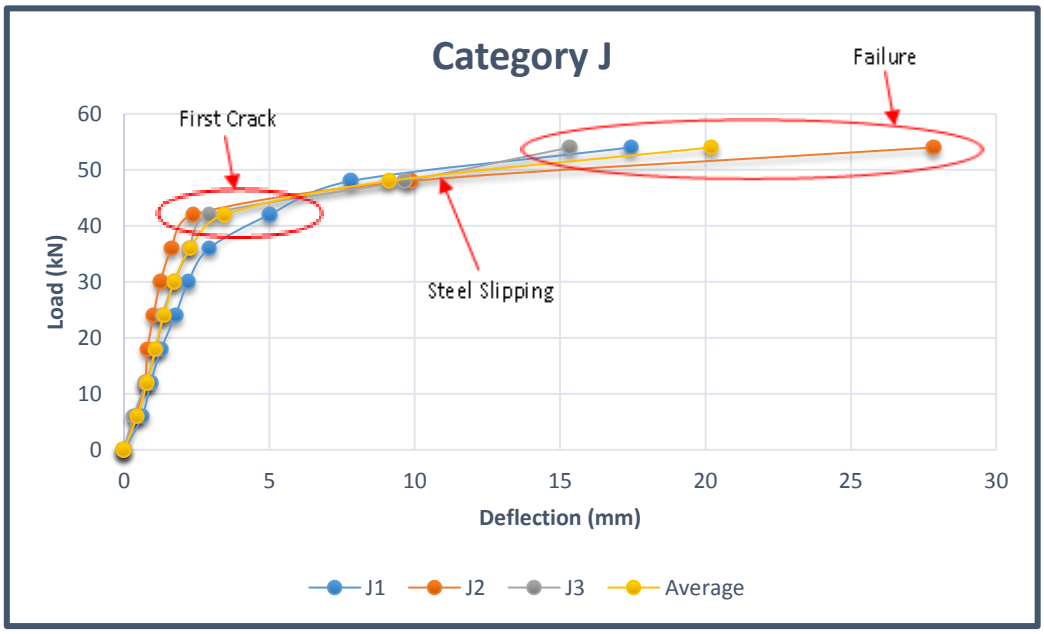


Fig. 67: Charts of load vs. deflection behavior for category J



Fig. 68: Test Setup for ICF slab J1

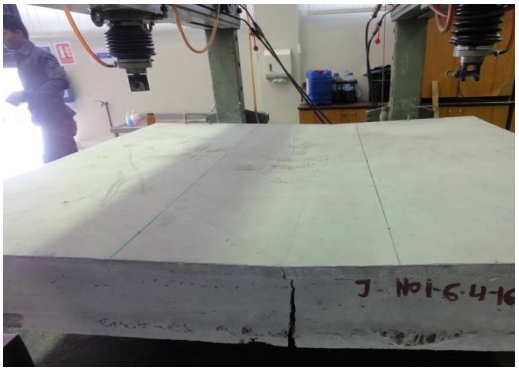


Fig. 69: Failure of ICF slab J1



Fig. 70: Test Setup for ICF slab J2

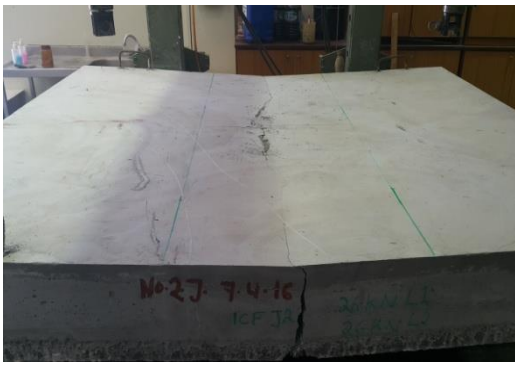


Fig. 71: Failure of ICF slab J2



Fig. 72: Test Setup for ICF slab J3



Fig. 73: Failure of ICF slab J3

3.4.3.5 ICF Ribbed Slab with Lattice Girder and Mesh (Category MSJ)

In this category MSJ, lattice girder is provided in the rib beam along with the 5 mm diameter size square mesh at the top with the spacing of 200mm c/c both ways. The details of the slab panel are given in Table 25. The test data Load vs. Deflection for the category MSJ are shown in Table 31. Figure 74 shows the chart of the load vs. deflection behavior along with their average value. Figures 75 to 80 are showing the pictures of the test setup and failed elements MSJ1, MSJ2, and MSJ3. Single action due to lattice girder is observed up to 35 kN, and combined action of lattice girder and mesh is observed then after. Overall this combination has shown uniform behavior up to end.

Table (31) Load vs. deflection behavior for category MSJ

Load (kN)	Deflection (mm)			
	MSJ1	MSJ2	MSJ3	Average
6	0.11566	0.008412	0.222905	0.115658
12	0.55011	0.736849	0.363377	0.550113
18	1.14691	1.619218	0.674604	1.146911
24	1.25037	1.755482	0.745261	1.250371
30	1.49515	2.08101	0.909285	1.495148
36	1.78955	2.323262	1.255838	1.78955
42	3.03151	2.742996	3.320024	3.03151
48	3.577	3.222452	3.931544	3.576998
54	4.08253	3.532838	4.632222	4.08253
60	4.81223	4.266322	5.358136	4.812229
66	5.58062	4.877842	6.283404	5.580623
72	6.49285	5.90741	7.078294	6.492852
78	7.80211	7.753736	7.850474	7.802105
84	9.72834	10.04335	9.41333	9.728341
90	12.6514	13.10432	12.1984	12.65136

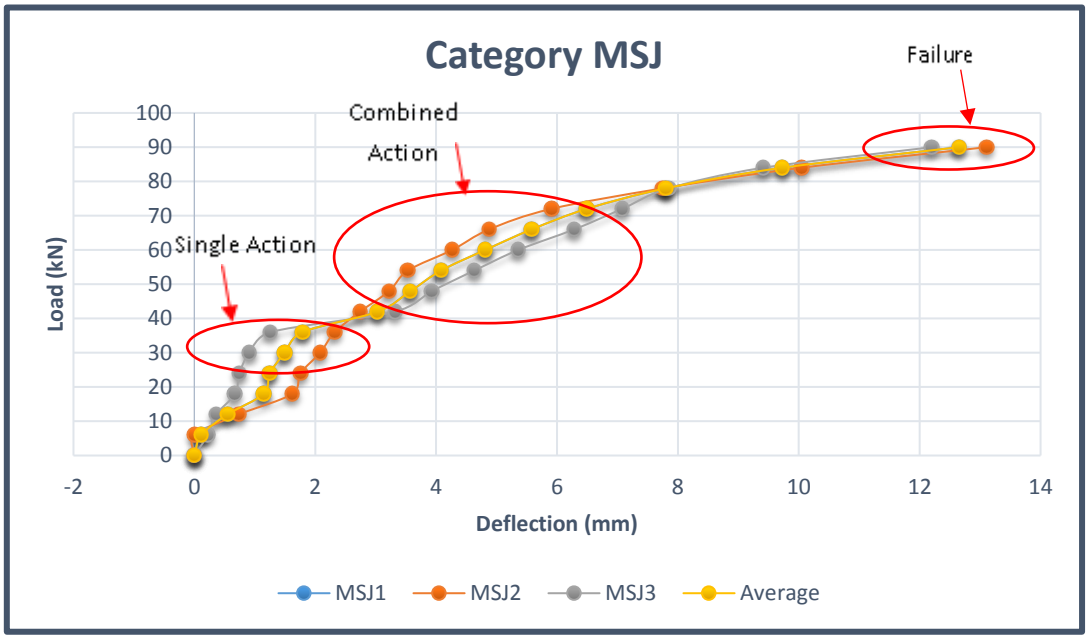


Fig. 74: Load vs. deflection behavior for category MSJ



Fig. 75: Test setup for ICF slab

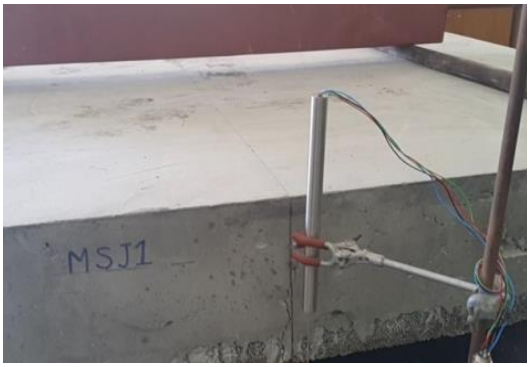


Fig. 76: Failure of ICF slab MSJ1



Fig. 77: Test setup for ICF slab MSJ2



Fig. 78: Failure of ICF slab MSJ2



Fig. 79: Test setup for ICF slab MSJ3



Fig. 80: Failure of ICF slab MSJ3

Observations made for all the fifteen slabs including Blank Block elements are compiled in Table 32. The table includes first crack load, ultimate load, maximum deflection observed and type of failure. The basic objective of the study is to identify the capacity of different categories of slabs with different reinforcement details so that they can be applied as per the specific need.

Initially, Blank Blocks are tested, and they are designed such that they would act as formwork where they should be capable of carrying the weights of the labor and the fresh concrete (service load on Blank Block) during construction. Testing of blank elements have been done and type of failure observed is a sudden failure as there is no reinforcement inside. The capacity of the elements remained as per the presumptions; Initially designed and calculated in chapter 3 for the service load on the Blank Block found as 2.79 kN/m, which less than the ultimate capacity of the Blank Block by 20%, which was found to be (3.5 kN/m) by experimental and numerical analysis.

Other than those four varieties namely S, MS, J, and MSJ are adopted with different reinforcement configurations. The behavior of each category remained as per the expectations. Capacity and deflection observed in category S are less compared to other slab types, and the slabs have entirely

failed after generation of the first crack and reaching ultimate conditions. Whereas, in other cases like MS, J and MSJ capacities are more compared to category S. These categories have shown good behavior in post cracking stage also. The elements are in a self-supported conditions even after reaching the ultimate failure condition. The category MSJ remained the best option with highest-capacity compared to other options.

Table (32) Failure details of ICF slab elements

ICF Slabs Specimen	Reinforcement Configuration	Mesh Provided	First Crack Load (kN)	Ultimate Load (kN)	Maximum Deflection (mm)	Type of Failure
B1	2#10	No	6.00	6.00	1.87	Sudden Brittle
B2			7.00	7.00	1.56	
B3			7.00	7.00	2.17	
S1	2#10	No	42.00	48.00	11.51	Failed after crack development
S2			41.00	48.00	11.48	
S3			42.00	47.00	17.70	
MS1	2#10	Yes	48.00	54.00	16.59	Self-supported after failure
MS2			48.00	53.00	26.52	
MS3			48.00	54.00	16.59	
J1	Lattice Girder	No	47.00	52.00	17.43	Self-supported after failure
J2			46.00	54.00	27.84	
J3			48.00	52.00	15.33	
MSJ1	Lattice Girder	Yes	78.00	88.00	12.65	Self-supported after failure
MSJ2			86.00	90.00	13.10	
MSJ3			82.00	90.00	12.19	

3.4.4 Full-Scale Test on ICF Walls

Slabs and walls are the basic structural elements and cover most of the surface area of a load bearing structure. The walls without any opening are not included in this study as they would be safer in strength. Therefore, walls only with an opening are considered in the experimental study.

The axial monotonic vertical loading applied to the wall performed according to ASTM E564, by the universal testing assembly which has two hydraulic jacks with capacity 200kN each. The resulting load applied to the wall through the beam girder. The axial loads continuously recorded manually. The load applied to the beam girder through 2 point loads located at each of the vertical hydraulic actuators. The distance from the center of the wall to the point of loading was 0.63meters Figure 81. In the laboratory, the transfer of the axial load to the wall was designed to be similar to field conditions, a steel beam girder used with a cross-section size of 7.5 cm x 15 cm. and 1.8 M in length to ensure direct transfer of the axial load to the walls.

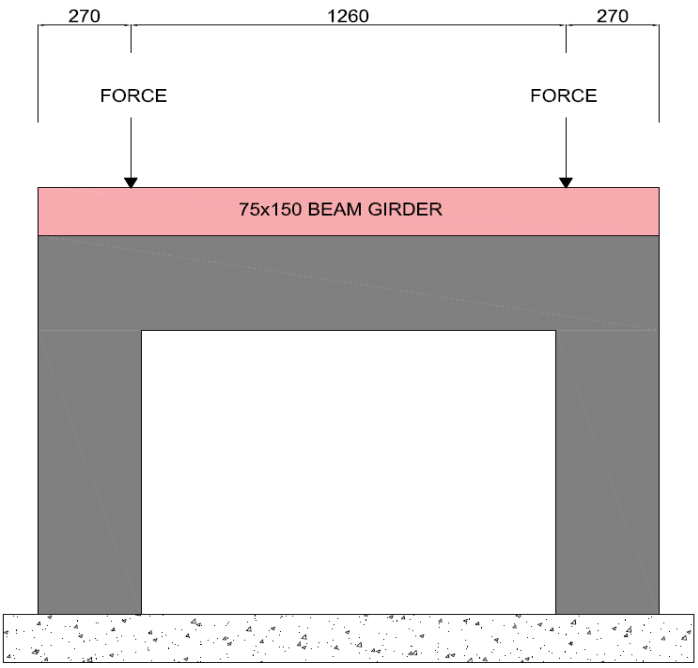


Fig. 81: ICF walls test setup

Four walls of different types have been cast in the Bardex Industries, Bahrain. Then, they brought to the structures laboratory of Department of Civil Engineering, University of Bahrain. Two strain gauges are applied at each of the internal corners to observe the strain (stress) at the corners. PFL-30-11-3LT types of strain gauges used explicitly on concrete applications are purchased from Tokyo Sokky Kenkyujo, Japan. These strain gauges are applied on the Nano-concrete surface of the wall and connected to the data logger.

The design of structural reinforced concrete walls is ruled by the Prescriptive Method (F. Sanchez, 2010) and ACI 318 Chapter 14, "Walls."ICF wall geometry and loading conditions often do not satisfy the restrictions of the empirical design method specified in ACI 14.5; therefore, the design procedure below provides a more flexible approach by which walls designed as compression members by ACI 14.4. Although not discussed in detail here, walls may be designed by ACI 14.5. Using the empirical design method if the following limiting conditions are satisfied:

- The wall cross-section is solid.
- The resultant of all axial loads acts within the middle one-third of the wall thickness.
- The wall thickness is not less than 4 inches (102 mm) for above-grade walls or 7.5 inches (191 mm) for basement walls.
- The wall thickness is not less than 1/25 of the supporting wall height or length of the wall, whichever is smaller.
- The minimum yield strength of reinforcing steel shall be Grade 40 (300 MPa) except for seismic design categories D1 & D2 the minimum yield strength of reinforcing steel shall be Grade 60 (400 MPa).

(Vranka, 1998), the required minimum horizontal and vertical reinforcement ratio specified in ACI 14.3 for structural reinforced concrete walls have been relaxed in the following design approach based on testdata4 under the provisions of ACI 14.2.7, which states “Quantity of reinforcement and limits of thickness required by 14.3 and 14.5 shall be permitted to be waived where structural analysis shows adequate strength and stability.”

However, a minimum equivalent rectangular section with the dimensions listed in Table 26 is used to generate minimum reinforcement tables in the Prescriptive Method for use with as many ICF products as reasonably possible without adversely impacting design economy or practicality. Details of the test observations are mentioned in the subsequent sections.

3.4.4.1 Wall ICF-04

The ICF-04 type of wall is 75 mm thick of size 1.8 m x 1.2 m overall. The size of the opening provided is 1.2 m x 1.05 m. The spacing of 10 mm diameter steel bar is 150 mm c/c in the horizontal direction and 200 mm c/c in the vertical direction. The load with constant rate is applied to the wall. Data observed through strain gauge is attached to Table A1 of (Appendix E). The test setup of ICF-04 is shown in Figure 82 and picture of the failed element is shown in Figure 83.



Fig. 82: Test setup for ICF Wall-04



Fig. 83: Failure of ICF Wall-04

3.4.4.2 Wall ICF-06

The ICF-06 type of wall is 75 mm thick of size 1.8 m x 1.2 m overall. The size of the opening provided is 0.9 m x 0.9 m. The spacing of 10 mm diameter steel rod is 150 mm c/c in the horizontal direction and 200 mm c/c in the vertical direction. The load with constant rate is applied to the wall. Data observed through strain gauge is attached to Table A2 of (Appendix E). The test setup of ICF-06 is shown in Figure 84 and picture of the failed element is shown in Figure 85.



Fig. 84: Test setup for ICF Wall-06

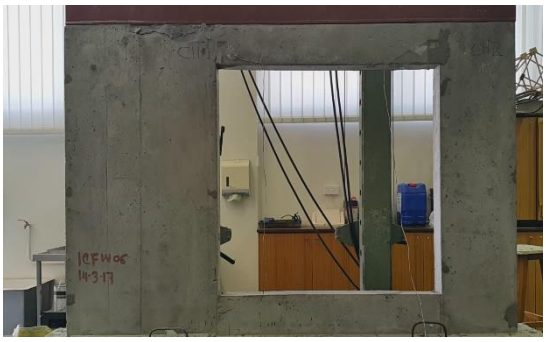


Fig. 85: Failure of ICF Wall-06

3.4.4.3 Wall ICF-09

The ICF-09 type of wall is 50 mm thick of size 1.8 m x 1.2 m overall. The size of the opening provided is 1.2 m x 1.05 m. The spacing of 10 mm diameter steel rod is 300 mm c/c in the horizontal direction and 400 mm c/c in the vertical direction. The load with constant rate is applied to the wall. Data observed through strain gauge is attached to Table A3 of (Appendix E). The test setup of ICF-09 is shown in Figure 86 and picture of the failed element is shown in Figure 87.





Fig. 86: Test setup for ICF Wall-09 **Fig. 87: Failure of ICF Wall-09**

3.4.4.4 Wall ICF-11

The ICF-11 type of wall is 50 mm thick of size 1.8 m x 1.2 m overall. The size of the opening provided is 0.9 m x 0.9 m. The spacing of 10 mm diameter steel rod is 300 mm c/c in the horizontal direction and 400 mm c/c in the vertical direction. The load with constant rate is applied to the wall. Data observed through strain gauge is attached to Table A4 of (Appendix E). The test setup of ICF-11 is shown in Figure 88 and picture of the failed element is shown in Figure 89.





Fig. 88: Test setup for ICF Wall-11 **Fig. 89: Failure of ICF Wall-11**

As mentioned in Table 33, machine capacity is limited compared to the capacities of the wall type ICF-06 and ICF-11. As the opening size is less in this category and bearing area of the wall is minor deformation is observed in this category; however, nothing had happened to the wall elements. To determine the capacities of these elements further

investigation of such elements is required to be tested in the higher capacity loading frame. Whereas, in ICF-04 horizontal and vertical crack have been observed and in ICF-09 due to the weakest element from thickness point of view and reinforcement point of view had failed completely.

Table (33) Failure details of ICF wall elements

ICF Wall Specimen	Load 1 kN	Max. Strain 1	Load 2 kN	Max. Strain 2	Type of Failure
ICF 04	312	0.000173	316	0	Horizontal and Vertical Cracks Observed (did not exceed the maximum stain of Nano-concrete, but the wall was very slender)
ICF 06	256.4	0.000532	335.4	0	Intact-Universal testing frame capacity reached
ICF 09	310	0.00542	318.4	0	Failed (exceeded the maximum strain of Nano-concrete of 0.0014)
ICF 11	382.6	0	382.6	0	Intact-Universal testing frame capacity reached

3.5 Numerical Simulation of ICF Slabs and ICF Walls

Finite element modeling is indeed a necessary approach which helps in predicting the behavior of any complex composite sections. ICF slabs and walls are composite elements having various layers of different materials like polystyrene concrete, Nano-concrete and steel reinforcement in it. In this chapter results derived from the finite element simulations. ANSYS version 18 is used to carry out the analysis of both slabs and walls and results obtained are presented in this chapter. In this chapter a total of nine finite element models are explicitly developed one Blank Block of polystyrene concrete, four types of ICF composite slabs and four types of ICF wall, having four different types of configurations. The primary study

parameter is to compare and validate the FEM analytical and the experimental results. Specimens' dimensions aforementioned.

3.5.1 Modeling of ICF Slabs and Walls

3.5.1.1 Element Types

Element library of the finite element software "ANSYS" provides various types of elements. Selection of the element is very crucial, as the material may be isotropic, orthotropic or anisotropic; and its behavior may be linear, bilinear or non-linear. Four element types considered in the modeling of slabs and walls are discussed in the following subsections.

(Gheitasi, 2014), usually, for the specific case of concrete, one may use the element called Solid65, which can capture cracking/crushing, plastic deformations, and creep features of concrete material. Unfortunately, element Solid65 is not suitable for this type of analysis. Also it predicts the initiation of the cracks, not the cohesive behavior of the solid elements when they lose their resistance. Solid185 is the best general-purpose modeling for material nonlinearity problem of 3D homogeneous solid geometry structures in ANSYS Workbench. In our cases, Solid185 used for modeling the EPS concrete in which ANSYS APDL implement generic failure surfaces for granular materials such as Dracker-Prager or Mohr-Coulomb to add up material and geometric non-linearity in numerical analysis.

The reinforcement steel bars are line elements structures that are "long" compared to their cross-section. These elements are the simplest to geometric models but are complex in post-processing usage and easier with Power Graphics. Usually, direct definition of nodes and elements are used to define the truss (spar) elements as a subset of beam-type elements which can't carry moments. These are commonly called "two-force members,"

carrying the axial load only. Unfortunately, Link180 cannot be directly used for solid modeling and automatic meshing in Ansys workbench graphic interface except through command scripts, and the element Link180 appears as a rectangular shape for the steel bars. Moreover, it is not the best representation of our model; it was used as the ICF walls reinforcement. To choose the suitable element types, the load carrying capacity as criteria whether it is two-force members (axial load only) or bending/shear members should prevail. Beam188 element would be more appropriate for modeling and handling bending and can accept a generalized cross section for input. Therefore it was used for ICF slabs reinforcement. It is suitable for analyzing slender to moderately stubby/thick beam structures. The element is based on Timoshenko beam theory which includes shear-deformation effects and rotational bending effects, making it suitable for describing the behavior of thick beams, sandwich composite beams.

3.4.1.1.1 Element Solid65

The Solid65 concrete brick element is used for 3D modeling of the Nano-concrete with or without reinforcing bars (rebar) (Wolanski, 2004). This element has eight nodes with three degrees of freedom at each node translations in the global x, y and z directions. The element is capable of handling plastic deformation, cracking in three orthogonal directions and crushing. It also can model the reinforcement as equivalent smeared within the element with the proper orientation. The element geometry of solid65 is shown in Figure 90.

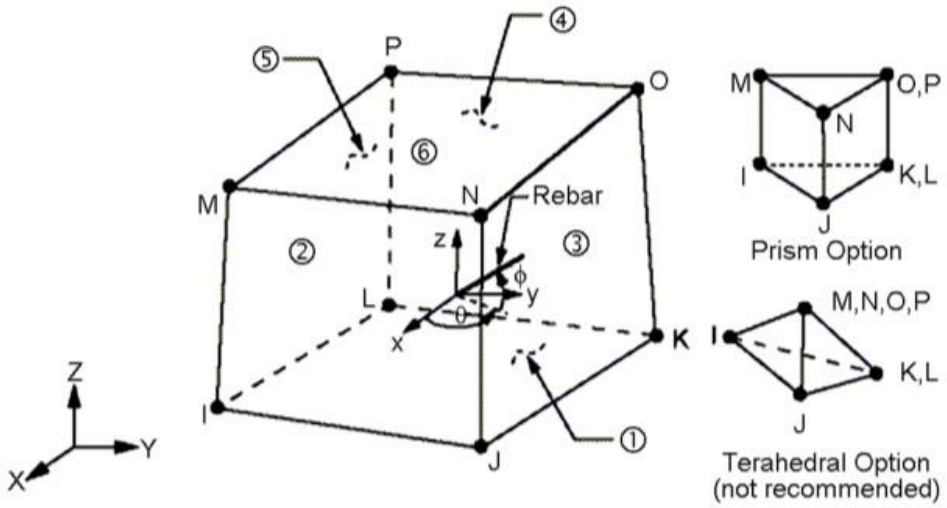


Fig. 90: Element Solid65 geometry

3.5.1.1.2 Element Solid185

The element SOLID185 is defined by eight nodes having three degrees of freedom at each node: translations in the nodal x, y, and z directions Figure 91. The element has plasticity, creep, swelling, stress stiffening, large deflection, and large strain capabilities.

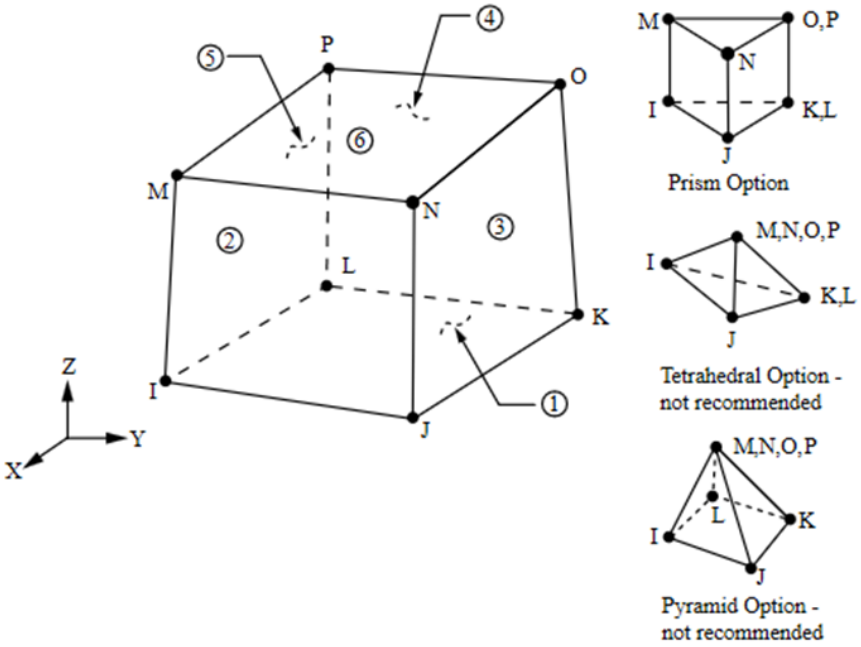


Fig. 91: Element Solid185 homogeneous structural solid geometry

3.5.1.1.3 Element Link180

Link180 Figure 92 is a 3D spar element; the elements do not handle bending, so the cross-sectional shape should not matter; only the section area. This element can be used to model trusses, sagging cables, links, springs, reinforcement, etc. The 3D spar element is a uniaxial tension-compression element with three degrees of freedom at each node translation in the nodal x, y and z directions. As in a pin-jointed structure, no bending of the element considered. Plasticity, creep, swelling, stress stiffening, and large deflection capabilities can be considered with this element.

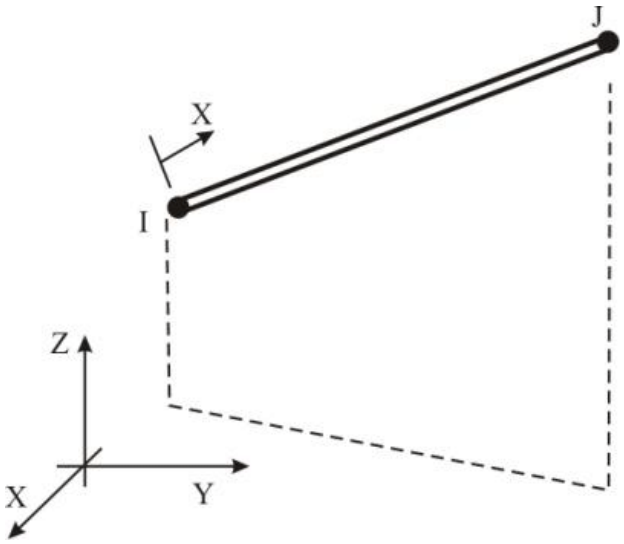


Fig. 92: Element Link8

3.5.1.1.4 Element Beam188

The Beam188 Figure 93 element is a linear, quadratic, or cubic two-node beam element in 3-D. Beam188 has six or seven degrees of freedom at each node. These include translations in the x, y, and z directions and rotations about the x, y, and z directions. The seventh degree of freedom (warping magnitude of cross-sections) is optional. This element is well-suited for linear, large rotation, and large strain nonlinear applications.

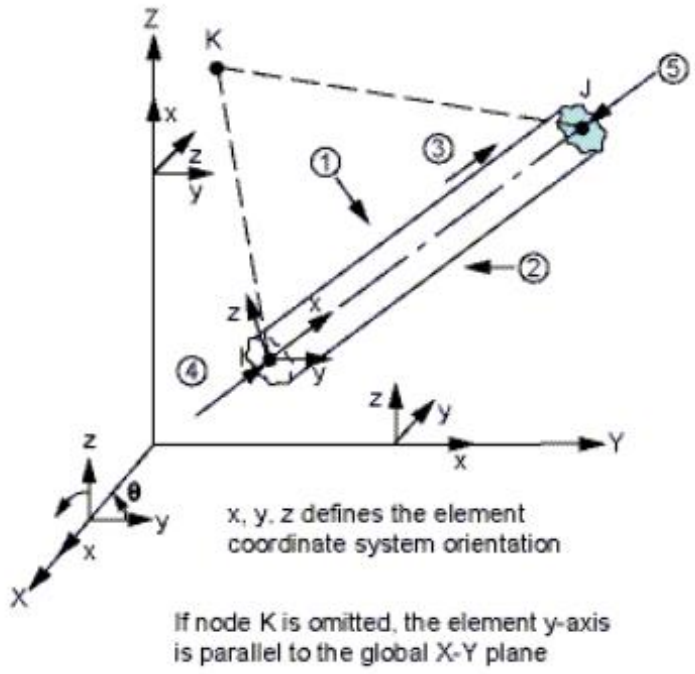


Fig. 93: Element Beam188

The main advantage of Beam188:

- The Beam 188 element can create "user defined" section geometry and allow rendering the real shape of the section on the beam model which permits the user to plot results (such as stresses) on the 3D shape of the element, not only on the direct axis of the beam.
- Support linear as well as nonlinear analysis, includes plasticity, large deformation, and nonlinear collapse.
- It can include multiple materials to simulate layered materials, composites, reinforced sections.
- Easy to use, both in preprocessing and post-processing phases

3.5.2 Material Properties

Three different types of materials are used in producing the slabs and walls which are Nano-concrete, polystyrene concrete and reinforcing steel

for the ICF slabs, and Nano-concrete, polystyrene panels and reinforcing steel for the ICF walls. Properties of all the materials are derived experimentally as explained in chapter 3. These actual properties are used in the modeling carried out in ANSYS. Material properties of all the materials used are discussed in following subsections.

3.5.2.1 Nano-Concrete

Nano-concrete is used in the top layer of the composite ICF slab. This is going to be the main part which bears the majority of the load in the composite element. The properties derived from the experimentations are listed in Table 34. These same properties are also used to in ANSYS modeling.

3.5.2.2 Polystyrene Concrete

Polystyrene concrete is used to cast Blank Blocks. These Blocks act as formwork during constructions. Cylindrical voids provided in these Blocks are useful as conduits for different types of pipelines or cabling within the floor. Such type of formwork needs certain strength as they are to carry the entire construction load. The properties derived from the experimentations are mentioned in Table 34. These same properties are also used to in ANSYS modeling also.

Table (34) Material properties of concrete

Element Type	Description		
Solid 65	Density	EPS Concrete (3MPa)	Nano Concrete (23.57MPa)
	Kg/mm3	4.49e-7	1.864e-6
	Linear Isotropic	EPS Concrete (3MPa)	Nano Concrete (23.57MPa)
	Ex (MPa)	3463	11532
	PRXY	0.189	0.198
	concrete	EPS Concrete (3MPa)	Nano Concrete (23.57MPa)
	Open Shear Transfer Coef.	0.01	0.01
	Close Shear Transfer Coef.	1	1
	Uniaxial Cracking Stress	1.69	1.52
	Uniaxial Crushing Stress	-1	23.57
	Biaxial Crushing Stress	0	0
	Hydrostatic Pressure	0	0
	Hydro Biaxial Crush Stress	0	0
	Hydro Uniaxial Crush Stress	0	0
	Tensile Crack Fractor	0	0
Solid 185	Density	EPS Concrete (3MPa)	
	Kg/mm3	4.49e-7	
	Linear Isotropic	EPS Concrete (3MPa)	
	Ex (MPa)	3463	
	PROXY	0.189	

3.5.2.3 Reinforcing Steel

Reinforcement in a concrete structure is of prime importance. There are five categories of the slabs namely B, S, MS, J and MSJ and four categories walls namely ICF-04, ICF-06, ICF-09 and ICF-11 that are considered in this study, where different reinforcing bars are used. Total four sizes of reinforcements are used in this study. The properties derived from the experimentations are mentioned in Table 35. These same properties are also used to in ANSYS modeling.

Table (35) Material properties of reinforcing steel

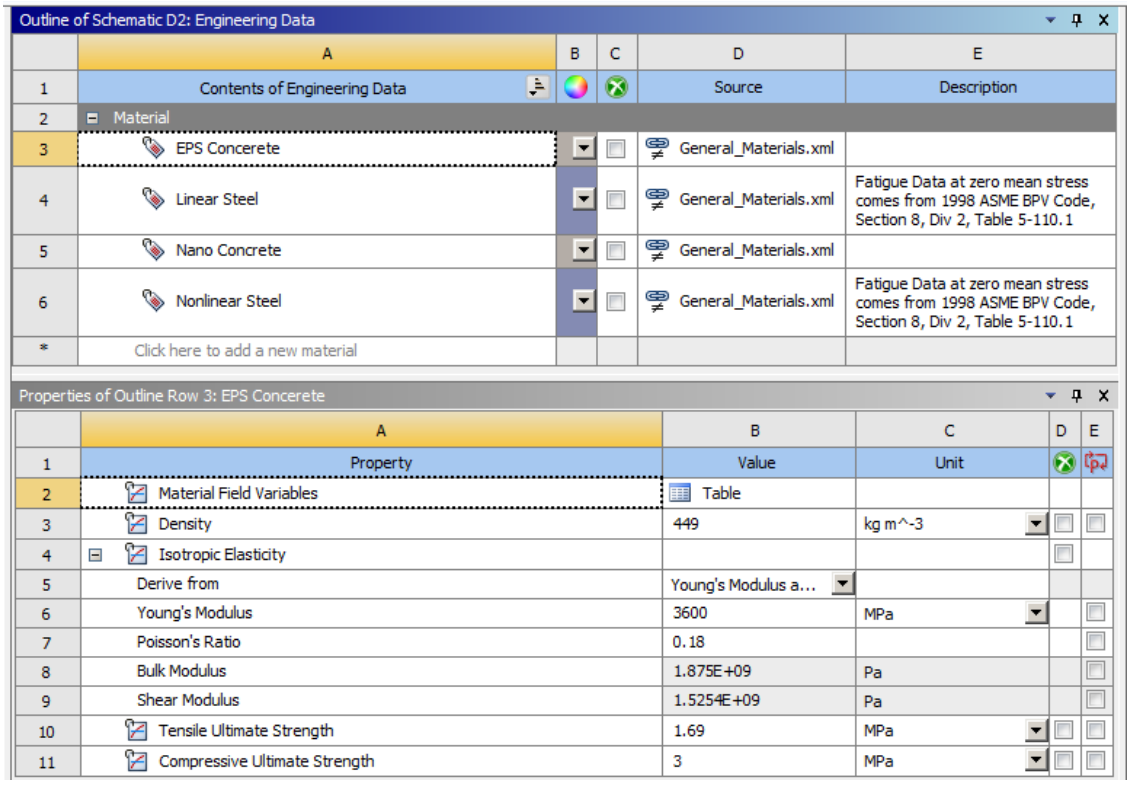
Element Type	Description	
Link 180 (ICF walls)	Cross-sectional Areas	ICF Wall
	Area 1(mm²) (Horizontal & Vertical	78.54
	Area 2 (mm²) (Foundation)	113.04
	Density	
	Kg/mm3	7.85e-6
	Linear Isotropic	
	Ex (MPa)	2e+5
	PROXY	0.3
	Bilinear Isotropic	
	Yield Strength (MPa)	240
	Tangent Modulus (MPa)	1400
Beam 188 (ICF slabs)	Cross-sectional Areas	ICF Slab
	Area 1(mm²) (Steel Mesh)	15.904
	Area 2 (mm²) (Lattice Girder diagonal)	28.274
	Area 3 (mm²)(Lattice Girder Lower	50.265
	Area 4 (mm²)(Lattice Girder Upper	78.54
	Density	
	Kg/mm3	7.85e-6
	Linear Isotropic	
	Ex (MPa)	2e+5
	PROXY	0.3
	Bilinear Isotropic	
	Yield Strength (MPa)	240
	Tangent Modulus (MPa)	1400
Solid 185 (Steel supports)	Density	
	7.85e-6	
	Linear Isotropic	
	Ex (MPa)	2e+5
	PROXY	0.3

3.5.3 Modeling of ICF Slabs and Walls in ANSYS Workbench

ANSYS Workbench is the advanced version of ANSYS APDL. This is more user-friendly with more features compared to the previous version. There are various stages involved in the total finite element solutions. Stepwise model generation and its solution are broadly divided into the following modules.

3.5.3.1 Engineering Data

This module allows selecting various materials whose standard properties are already stored in the ANSYS library. Depending upon the problem definition materials can be selected here; even, if the material is not there or one would like to change the properties of the material then new material also can be generated in this module. These selected materials are to be assigned to the respective elements in the geometry module once the model is generated. Typical view of the engineering data section is shown in Figure 94.



Outline of Schematic D2: Engineering Data

	A	B	C	D	E
1	Contents of Engineering Data			Source	Description
2	Material				
3	EPS Concerete			General_Materials.xml	
4	Linear Steel			General_Materials.xml	Fatigue Data at zero mean stress comes from 1998 ASME BPV Code, Section 8, Div 2, Table 5-110.1
5	Nano Concrete			General_Materials.xml	
6	Nonlinear Steel			General_Materials.xml	Fatigue Data at zero mean stress comes from 1998 ASME BPV Code, Section 8, Div 2, Table 5-110.1
*	Click here to add a new material				

Properties of Outline Row 3: EPS Concerete

	A	B	C	D	E
1	Property	Value	Unit		
2	Material Field Variables	Table			
3	Density	449	kg m^-3		
4	Isotropic Elasticity				
5	Derive from	Young's Modulus a...			
6	Young's Modulus	3600	MPa		
7	Poisson's Ratio	0.18			
8	Bulk Modulus	1.875E+09	Pa		
9	Shear Modulus	1.5254E+09	Pa		
10	Tensile Ultimate Strength	1.69	MPa		
11	Compressive Ultimate Strength	3	MPa		

Fig. 94: Engineering data module

3.5.3.2 Modeling Stage

The geometry is modeled using the Ansys Design Modeler. This is a very user-friendly module to generate any geometry having a complex shape. It also allows the geometry to import from other drafting software.

The prepared geometry of the ICF slab is shown in Figure 95, and load application on the slab is shown in Figure 96.

Since the ICF slabs are symmetrical in geometry, and loading in both longitudinal and transverse directions, the ICF slabs were modeled as quarter models to significantly reduce the expensive computational time resulting from the complexity of ICF slab geometry, without affecting the results as shown in Figure 99.

(Sanis, 1983), In this study, a small-scale model of The ICF walls was developed to evaluate the load-bearing performance. The ICF walls and their reinforcement were scaled down to half of the original size due to the capacity limitation of the loading frame and due to the size of the full-scale model, as laboratory was inadequate to accommodate the full-scale test. To be in similarity with the prototype (full scale) and small-scale model, they should have proportional dimensions, for example, if the scaling factor for elastic modulus is 1 and the scaling factor is 2, the force of prototype has to be four times that of the half small-scale model. Therefore, on checking similarities, the value of half small-scale model test results should be multiplied by four in force, by two in displacement.

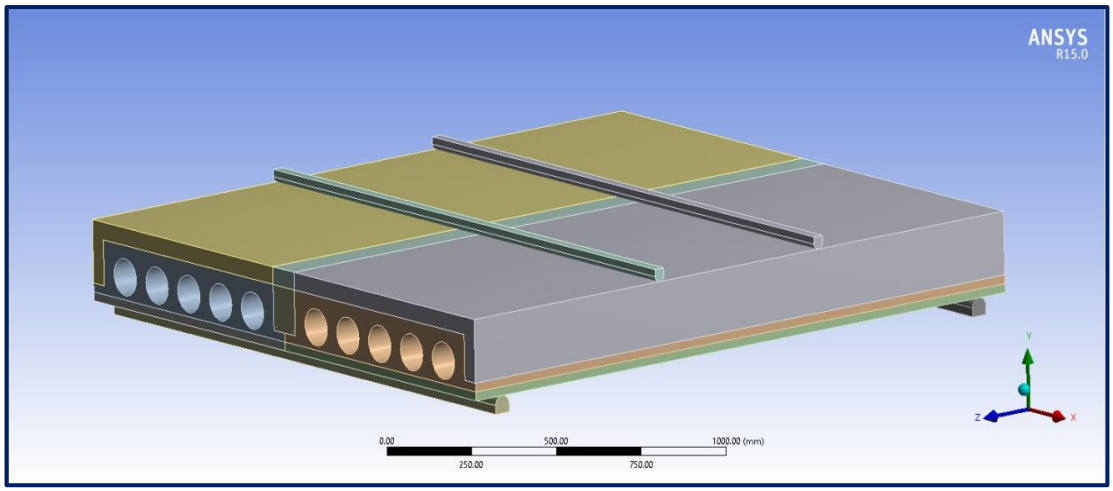


Fig. 95: Geometry preparation

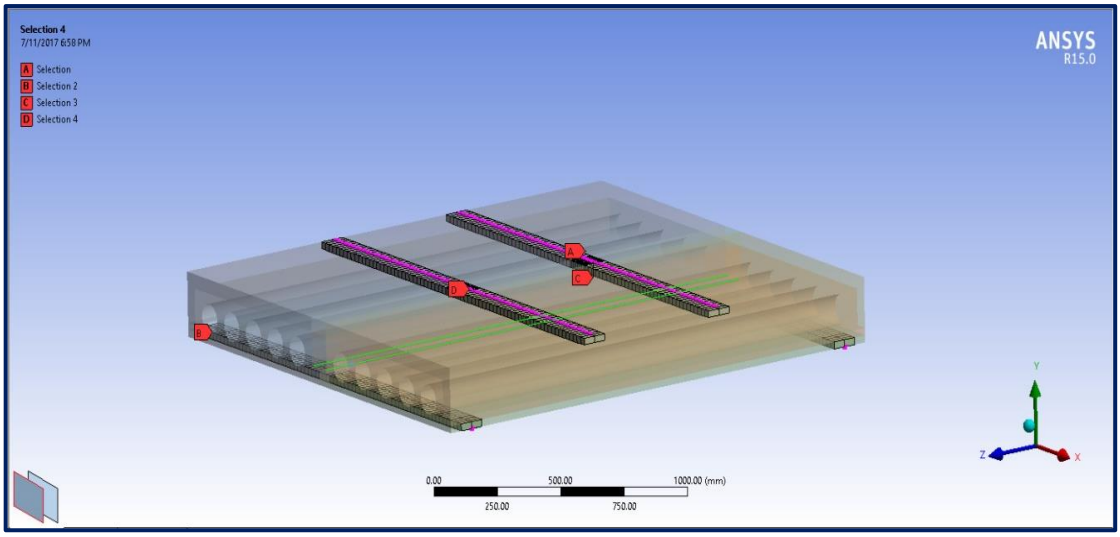


Fig. 96: Load application on ICF slab

3.5.3.3 Element Types Assignment

Table 36 shows different element types assignment to the ICF slab and wall parts. For ICF slabs S and MS categories, solid 185 was used for modeling the Blank Block, because of the great instability and geometrical nonlinearity under the loading, therefor Ansys did not give correct results comparing to experimental when the model was run using solid 65.

Unlike ICF slabs J and MSJ categories did not experience the same instability and geometrical nonlinearity because the lattice girder prevented the influence of the shear stresses on the models' instability.

Table (36) Element Types

FEM Model	Nano Concrete	EPS Concrete	Reinforcement
Blank Block	-	Solid 65	-
ICF Slab S	Solid 65	Solid 185	Beam 188
ICF Slab MS	Solid 65	Solid 185	Beam 188
ICF Slab J	Solid 65	Solid 65	Beam 188
ICF Slab MSJ	Solid 65	Solid 65	Beam 188
All ICF Walls	Solid 65	-	Link 180

3.5.3.4 Meshing Stage

There exist different methods to mesh the geometry of a structure. They can be classified into two categories: direct generation of mesh and solid modeling. Commercial FE codes allow the direct definition of finite element entities (nodes, elements, and boundary conditions on nodes and elements) or the definition of geometric entities (points, lines, surfaces, or volumes) which are meshed later to obtain the nodes and elements.

Table (37) Model generation types

Generation Type	Considerations
Direct Generation	Convenient for simple models. Direct control of nodes and elements. Program skills are needed. Allows the translation of the model between different commercial codes or definition using standard codes.
Solid Modeling	Convenient for large models. Requires larger computational resources. It is easy to modify the geometry. No direct control over the mesh entities.

3.5.3.5 Direct Generation

The process of creating elements out of nothing, without starting from any geometric entity is called direct generation or direct mesh. In this process, the user imposes explicitly the location of the nodes and the size of the elements. In this process, the user has total control of the node location and element size. This approach is used for simple geometries.

Direct generation consists of defining first the node distribution in the geometry. The position of each node is defined according to a

coordinate system. Some commercial codes allow using different types of coordinate systems (Cartesian, cylindrical, spherical, and others).

Once the nodes have been generated, the elements can be defined. The element is defined using the connectivity with its nodes. The set of elements defined should define the whole geometry.

3.5.3.6 Solid Modeling

The mesh may also be created starting from geometric entities (which can be created in the pre-processor or imported from other CAD software), and the software creates the mesh. The user, however, may impose some restrictions or conditions on the meshing process. Some of these restrictions are:

- Imposing some divisions in edges or lines of the primitive geometry.
- Giving some values for the element size, regarding edge length.
- Starting the mesh from lower order geometric entities and extrude or sweep the created elements to fill higher order geometries. For instance, to mesh a regular volume some of the areas may mesh.

3.5.3.7 Meshing Technique for Embedded Modeling

Straightforward embedded model using solid modeling implemented in this study. The reinforcement in the embedded model uses beam elements (Beam188) that are connected to concrete mesh nodes by merging the separate nodes that have the same location. Therefore, the concrete and the reinforcement mesh share the same nodes and concrete occupies the same regions as the reinforcement. The drawbacks to this technique in Ansys workbench is that the order of merging before meshings can not be controlled, therefore cause the nodes to become “orphaned”; that is, the nodes lose their association with the solid model. The orphaned nodes can cause certain operations (such as boundary condition transfers, surface load transfers, and

so on) to fail. Moreover, the concrete mesh is restricted by the location of the reinforcement, and the volume of the mild-steel reinforcement is not deduced from the concrete volume causing a small percentage of error in the final results. The typical mesh of ICF slab and the wall is shown in Figure 97.

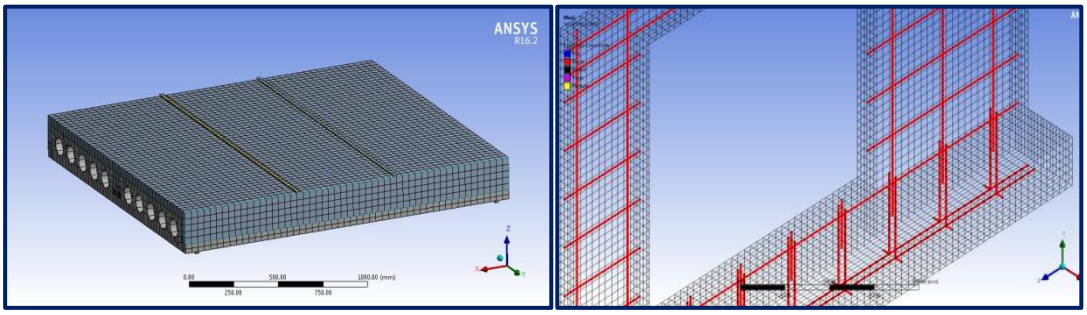


Fig. 97: Meshing of ICF slab and wall

3.5.3.8 Modeling and Meshing Technique of ICF Walls and Slabs

Square and rectangular meshing elements were implemented to obtain better results for solid 65 and solid185 elements.

The Nano-concrete ribbed slab part was divided into six regions to allow for separate meshing attributes for each region to accommodate the nodes of lattice girder to avoid meshing the whole model at very small mesh size due to the small concrete cover of 1cm for the lower bars of the lattice girder. The Blank Block "formwork" model was meshed according to the divisions of the Nano-concrete part. The members of the steel mesh, the longitudinal two steel bars, and ICF walls reinforcement, were meshed to match the meshing element size of the concrete meshing elements, and all the nodes along the members were merged with the Nano-concrete nodes, to allow bending. Unlike the lattice girder, which the truss members meshed as single meshing elements, so only the nodes at pivots were merged with the nodes of the Nano-concrete, to transmit axial load only. The regions of each part of the ICF slab model and the reinforcement were

combined to form a single entity through merging the nodes of connected surfaces Figure 98.

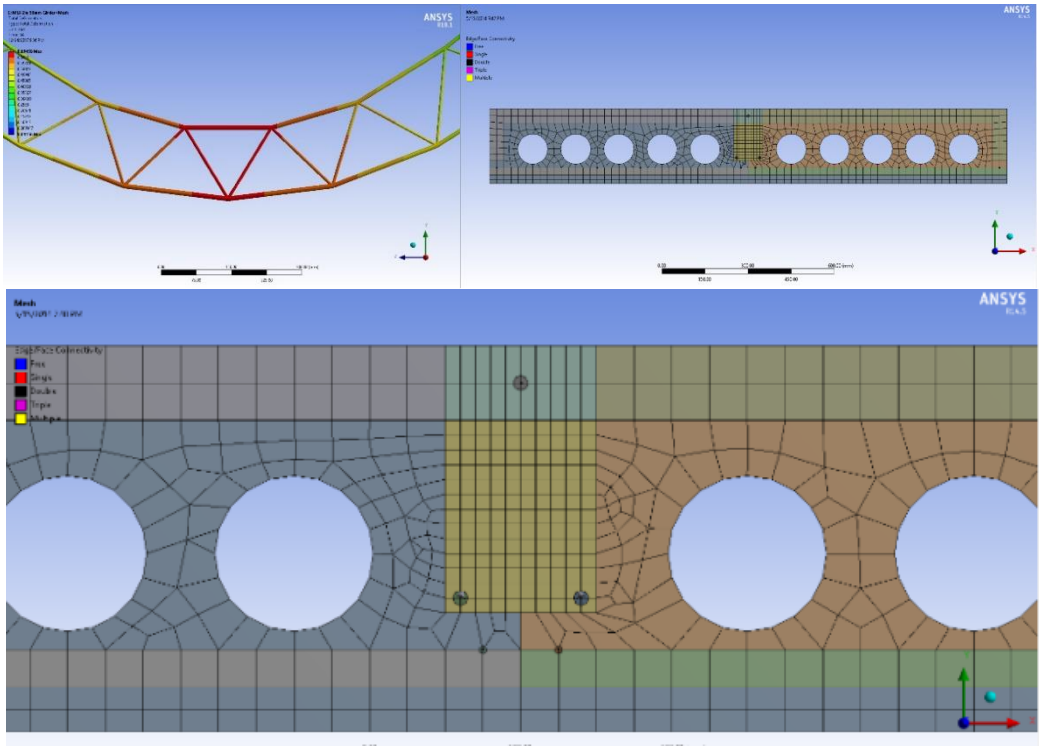


Fig. 98: Meshing methodology for the lattice girder and concrete

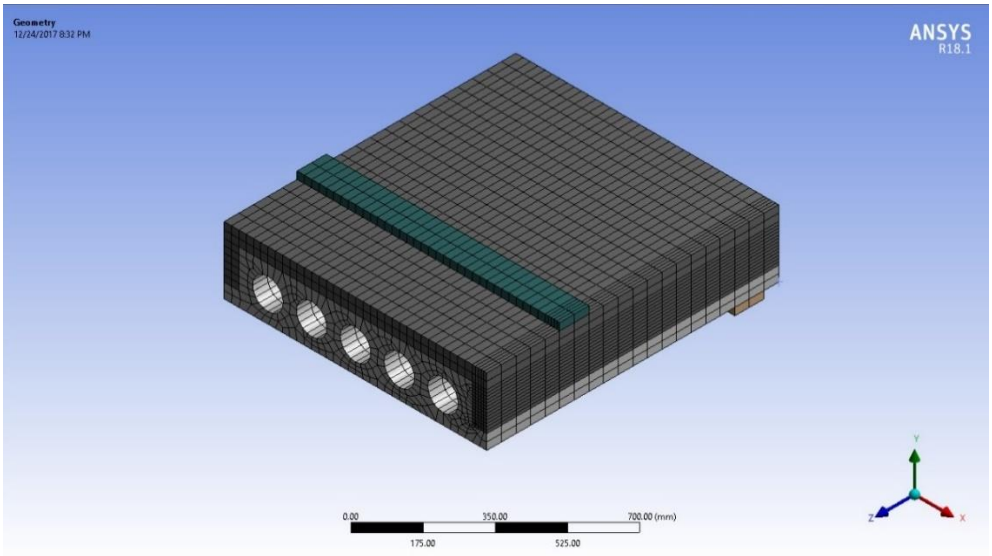


Fig. 99: Modeling and meshing of the quarter model of ICF slab

3.5.3.9 Using APDL Commands

Ansys workbench engineering data does not prompt the user for the material properties inputs of solid 65 and link180 FEM elements, except through APLD command, unlike Solid185 and Beam188 which are prompted by default. (Appendix F)

3.5.3.10 Loading and Boundary Conditions

For the FEA model to act the same way as the experimental ICF slab, boundary conditions are needed to constrain specific displacements in the model to get a positive solution. Therefore, boundary conditions must be imposed at points of symmetry, supports, and loadings.

The symmetry boundary conditions initially set for both planes of symmetry, shown in red Figure 100. The plane of symmetry was defined through the ICF slab cross-section centroid and across the nodes defining the vertical plane. Two planes of symmetry were selected through XY and ZX planes.

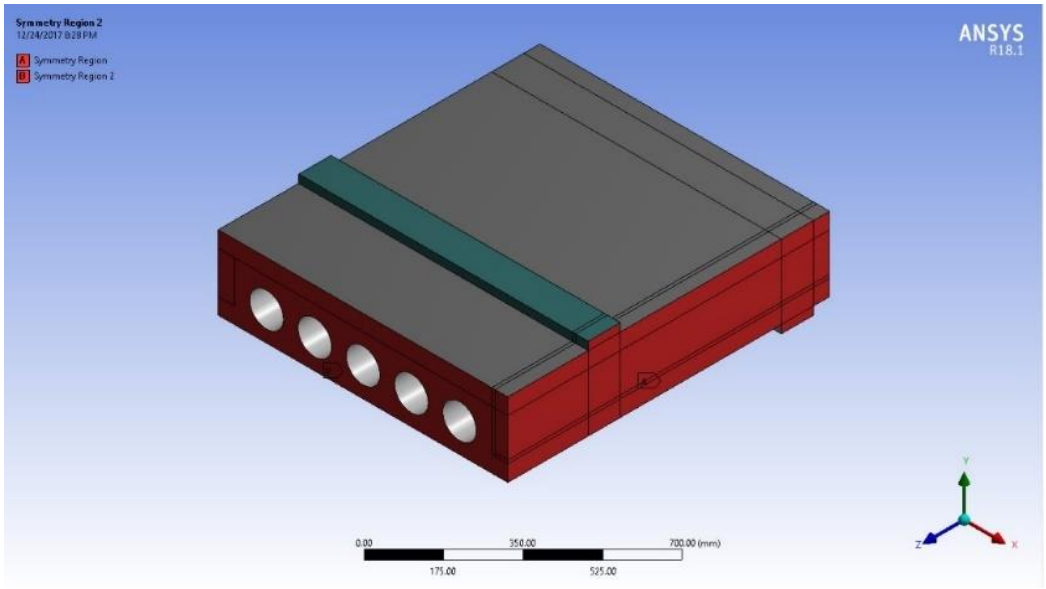


Fig. 100: Boundary conditions for planes of symmetry

The plate at the support was modeled to act as a roller. A single line of nodes on the plate was given constraint in the Y, and X directions applied as constant values of 0. Subsequently, the beam will be allowed to rotate at the support. The support conditions are shown in Figure 101.

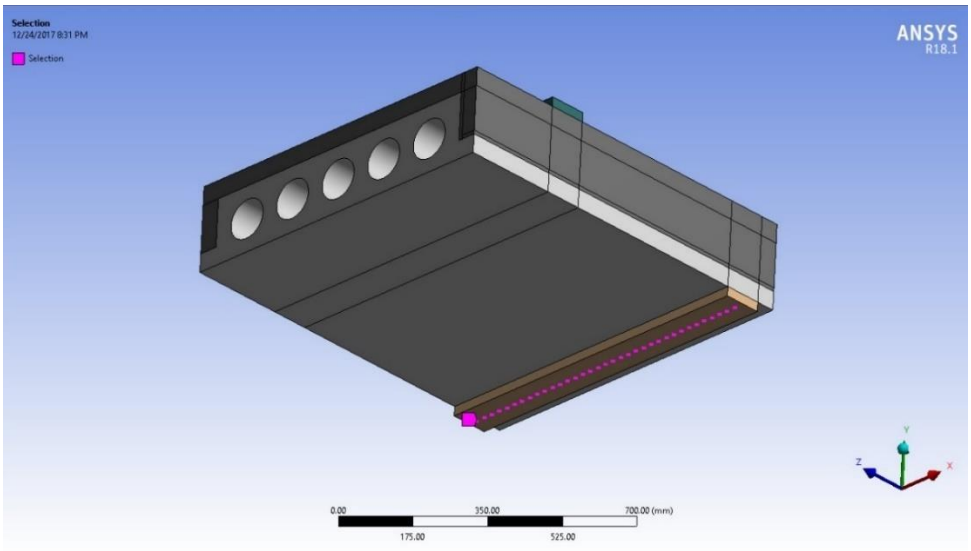


Fig. 101: Boundary condition for support

The force applied was divided on the number of nodes across the entire centerline of the plate0 the plate and the applied loading. Self-weight was imposed by applying standard earth gravity.

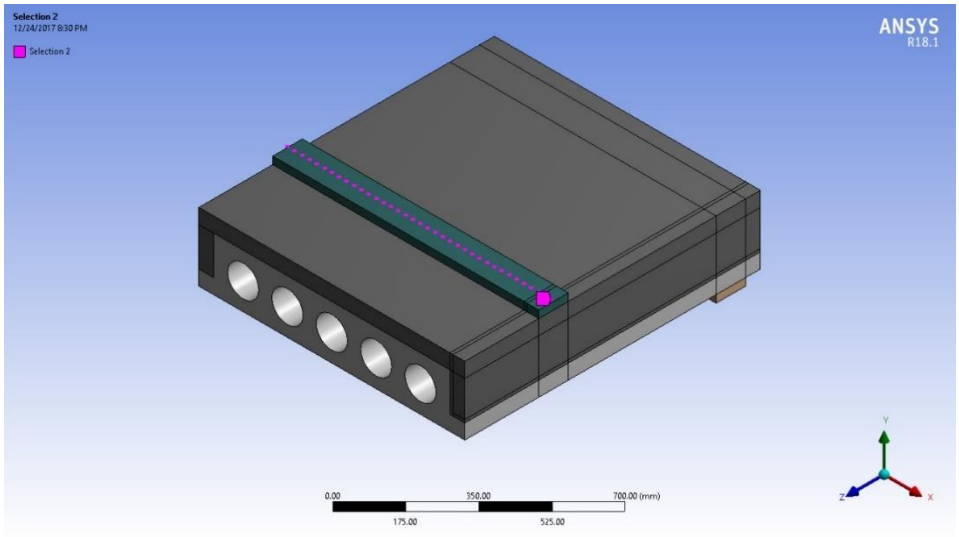


Fig. 102: Boundary Conditions at the Loading Plate

3.5.3.11 Solution Stage

Analysis Type: The static structural module was utilized to analyze the FEM models.

Step control: Loading Sub-steps control was used to match the experimental load increment of 6 kN, for an elastic-fully-plastic constitutive material model, applying such a small load increment resolves the convergence issue easily. Further ramped loading will result in easier convergence than suddenly applying step loads.

Non-linear controls: The nonlinear Newton-Raphson iteration processes were utilized to trace the equilibrium path during the load-deformation response. It was found that convergence of solutions for the model was not easy to achieve due to the composite materials and geometrical nonlinearity behaviors. The incremental stiffness matrix is found by $[K_T]$. Because the elastic plastic material matrix {Du} is used, the stiffness matrix is dependent on the state of deformation. A physical interpretation of the solution technique is that unbalanced forces due to incremental linearization are applied to the structure to obtain a new and improved set of displacements.

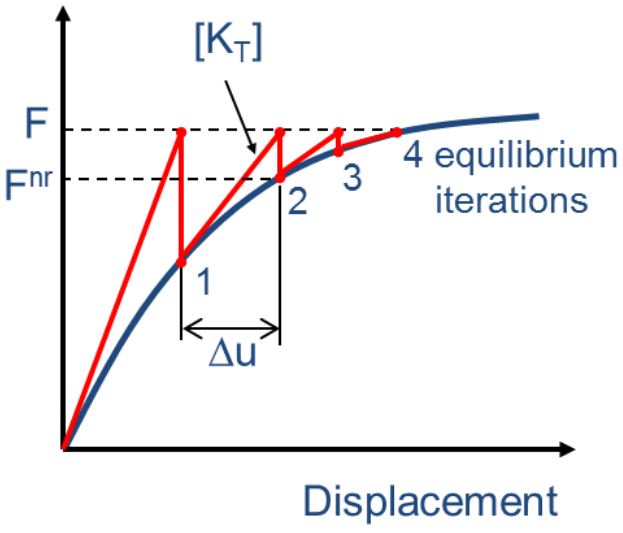


Fig. 103: Incremental and iterative solution

ANSYS uses the Newton-Raphson algorithm:

- Applies the load gradually, in increments.
- Also performs equilibrium iterations at each load increment to drive the incremental solution to equilibrium.
- Solves the equation $[K_T]\{Du\} = \{F\} - \{F^{nr}\}$

$[K_T]$ = tangent stiffness matrix

$\{\Delta u\}$ = displacement increment

$\{F\}$ = external load vector

$\{F^{nr}\}$ = internal force vector

- Iterations continue until $\{F\} - \{F^{nr}\}$ (difference between external and internal loads) is within a tolerance.

Convergence: Displacement convergence tolerance of 5% instead of the default 0.5% was used to avoid any difficulty in convergence, and a force convergence of 0.5% was used, which is Ansys workbench default value. Other nonlinear algorithm options were set to defaults.

Displacement Scaling: The magnitude of deflection can be controlled in Ansys workbench using either no scaling, true scale or auto scale which was selected to view an exaggerated deflection.

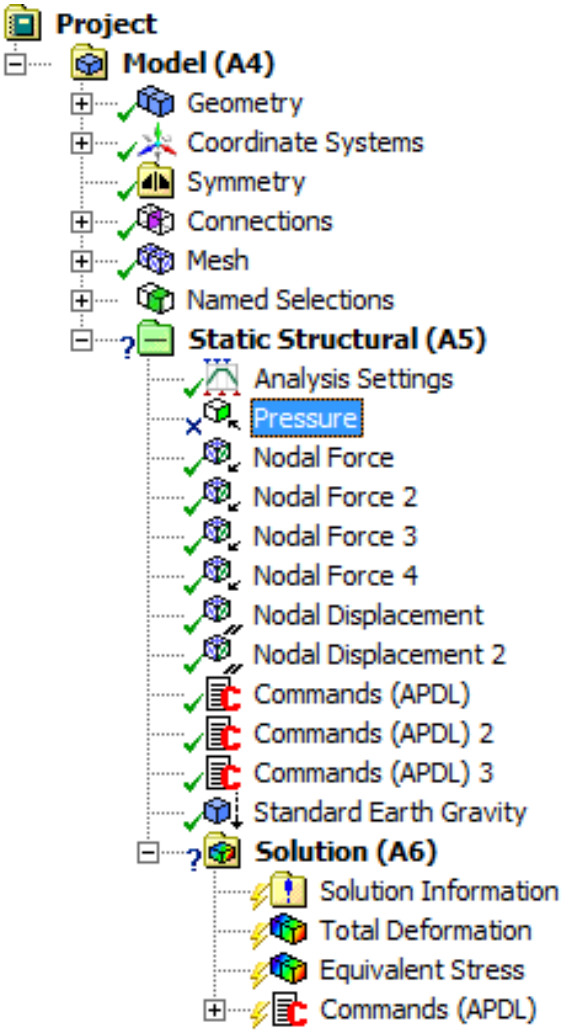


Fig. 104:Ansys workbench outline

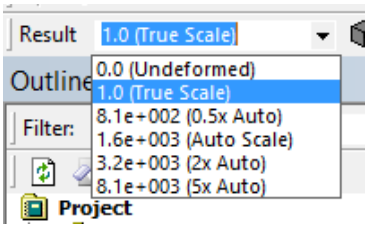


Fig. 105:Displacement scaling

3.5.4 Analytical modeling of ICF Slabs by ANSYS

In this part of the study, five categories of slabs and four categories of wall specimens are modeled using different FEM element types. The material properties considered for the modeling are exactly same as three types of materials namely polystyrene concrete, Nano-concrete, and steel used as reinforcement.

Simple support conditions are considered for ICF slab elements as is the case in experimental studies. Actual loading diagram is shown in

Figures 44 and 45. The same loading condition is produced in the ANSYS model. The load step applied in the finite element analysis was the same step size applied in the experimentation until the ultimate loading condition is reached. Meshing in the workbench is carried out automatically depending on the size and shape of the element. The last step in modeling is to select the parameters required to be analyzed like central deflection and stress development and then perform the analysis.

The FEM models of each category of the slabs namely B, S, MS, J and MSJ and walls namely ICF-04, ICF-06, ICF-09 and ICF-11are summarized in the following subsections.

3.5.4.1 Blank Block (Category B)

The Blank Block is the supporting formwork made from polystyrene concrete. The material properties of the polystyrene concrete are mentioned in Table 34. Wireframe model generated by the Blank Block which is named as category B is shown in Figure 106. Total 7 kN load was applied to the Blank Block with the load step of 1 kN.

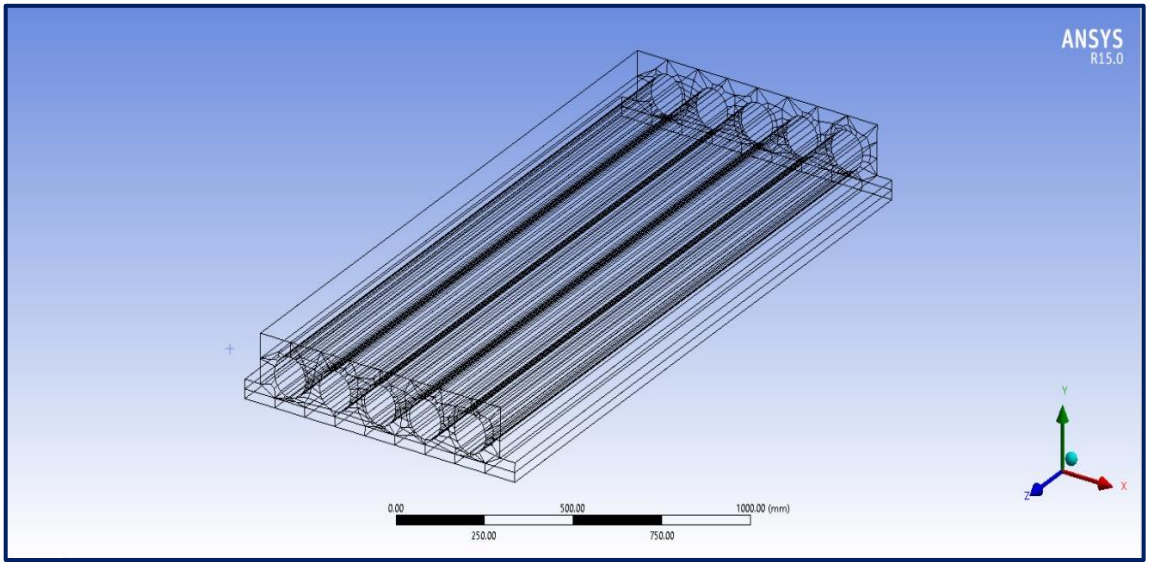


Fig. 106: Wireframe model of Blank Block B

3.5.4.2 ICF ribbed Slab with Two Bars Only (Category S)

The ICF ribbed slab with two bars is the combination of three materials namely polystyrene concrete, Nano-concrete, and steel reinforcement. The material properties of the polystyrene concrete, Nano-concrete, and steel reinforcement are mentioned in Table 35. Wireframe model generated of ICF slab with two bars which are named as category S is shown in Figure 107. The total 48kN load was applied to the Blank Block with the load step of 6kN.

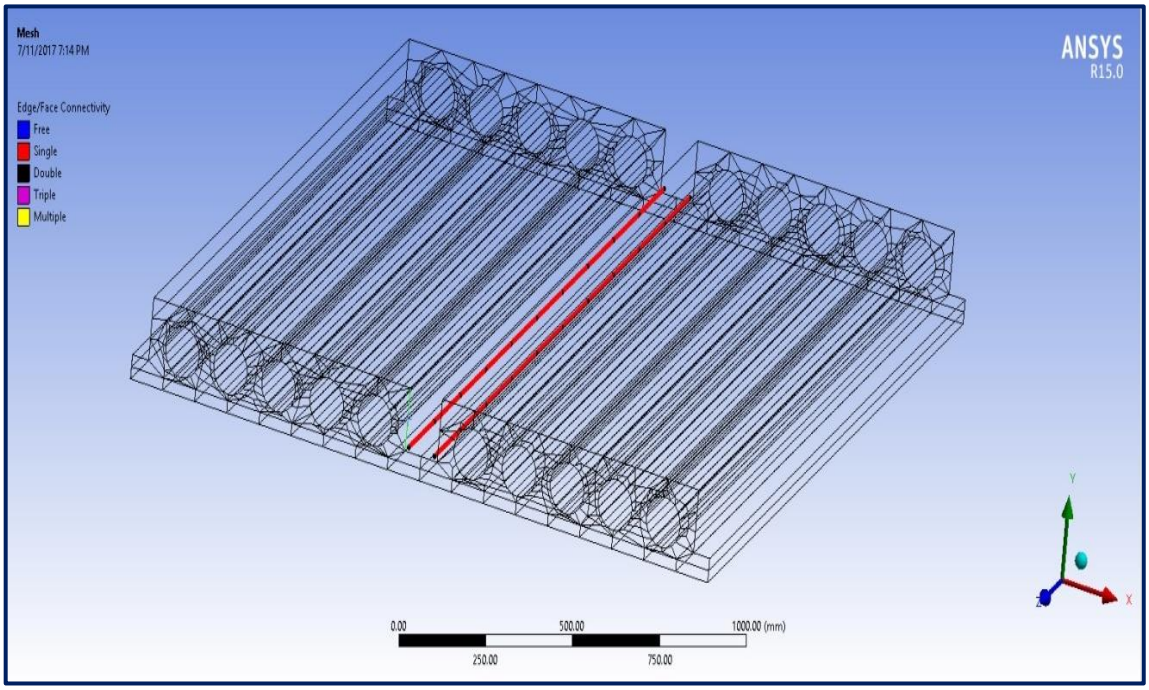


Fig. 107: Wireframe model ICF slab with two bars of category S

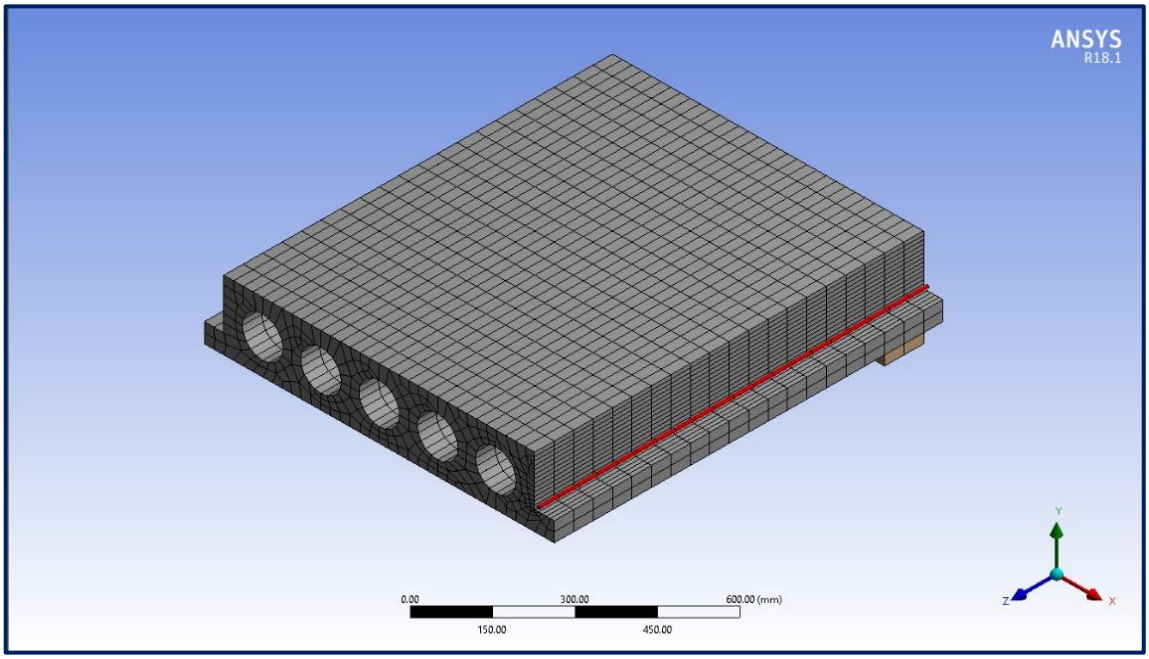


Fig. 108: Quarter symmetry model of ICF slab with two bars of category S

3.5.4.3 ICF Ribbed Slab with Two Bars and Mesh (Category MS)

The ICF ribbed slab with two bars and mesh is the combination of three materials namely polystyrene concrete, Nano-concrete, steel reinforcement, and mesh. The material properties of the polystyrene concrete, Nano-concrete, and steel reinforcement are mentioned in Table 35. Wireframe model generated of ICF slab with two bars which are named as category MS is shown in Figure 109. The total 60kN load was applied to the ICF slab with two bars and mesh with the load step of 6 kN.

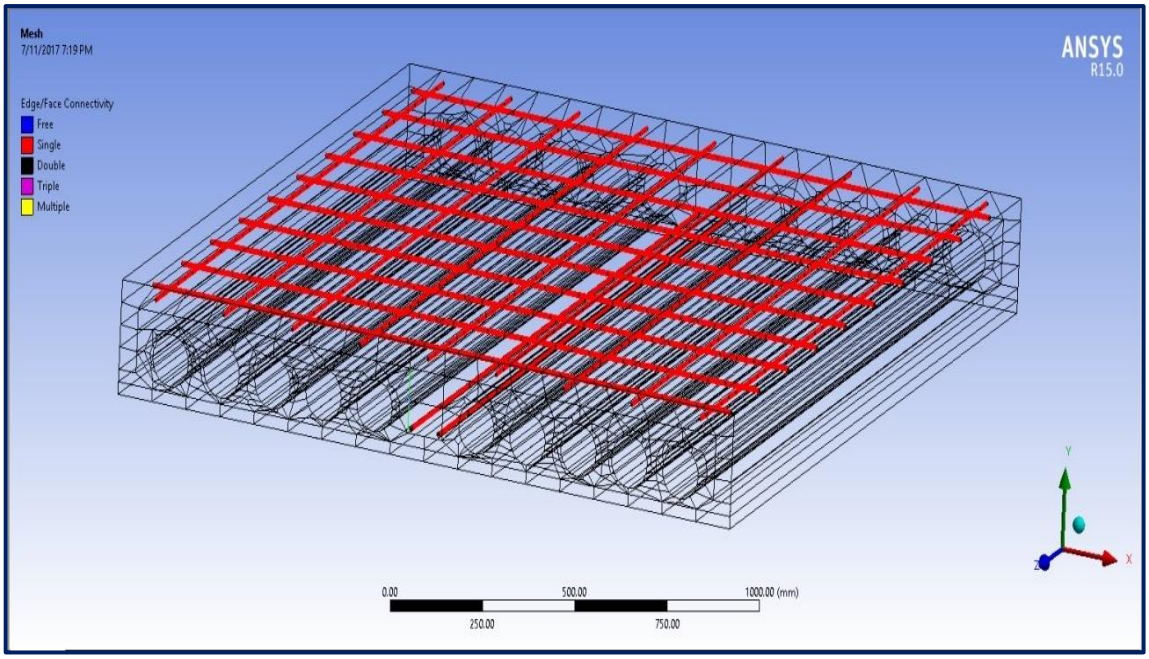


Fig. 109: Wireframe model ICF slab with two bars and mesh of category MS

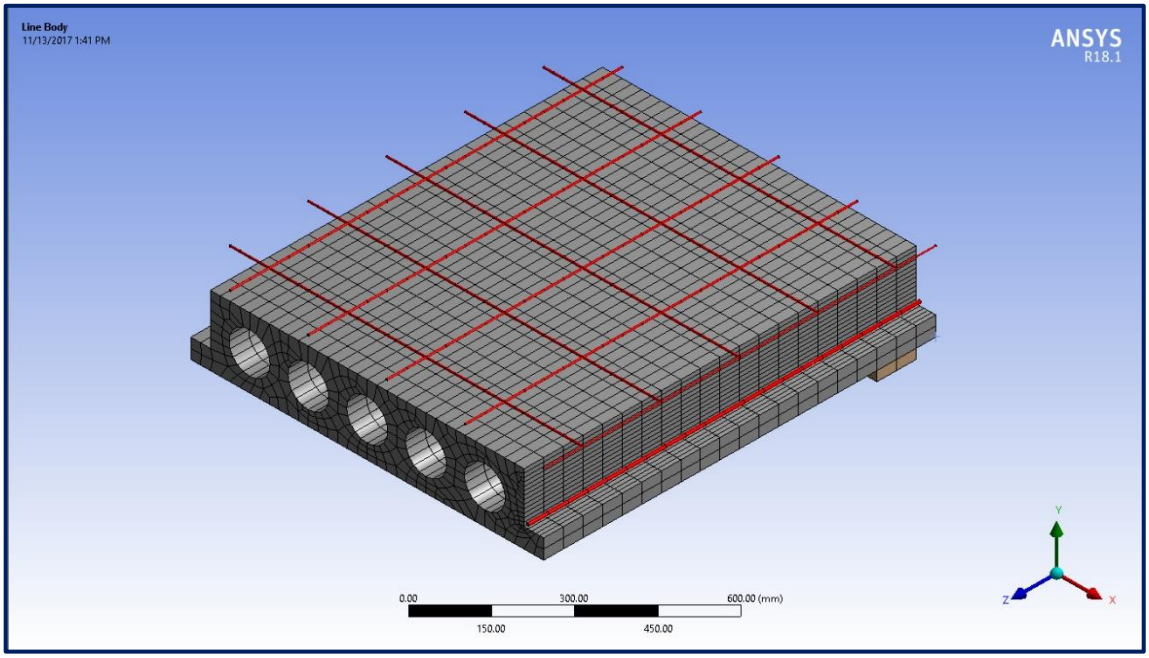


Fig. 110: Quarter symmetry model of ICF slab with two bars and mesh of category MS

3.5.4.4 ICF Ribbed Slab with Lattice Girder Only (Category J)

The ICF ribbed slab with lattice girder is the combination of three materials namely polystyrene concrete, Nano-concrete and steel reinforcement in lattice girder. The material properties of the polystyrene concrete, Nano-concrete, and steel reinforcement are mentioned in Table 35. Wireframe model generated of ICF slab with lattice girder which is named as category J is shown in Figure 111. The total 54kN load was applied to the ICF slab with lattice girder with the load step of 6kN.

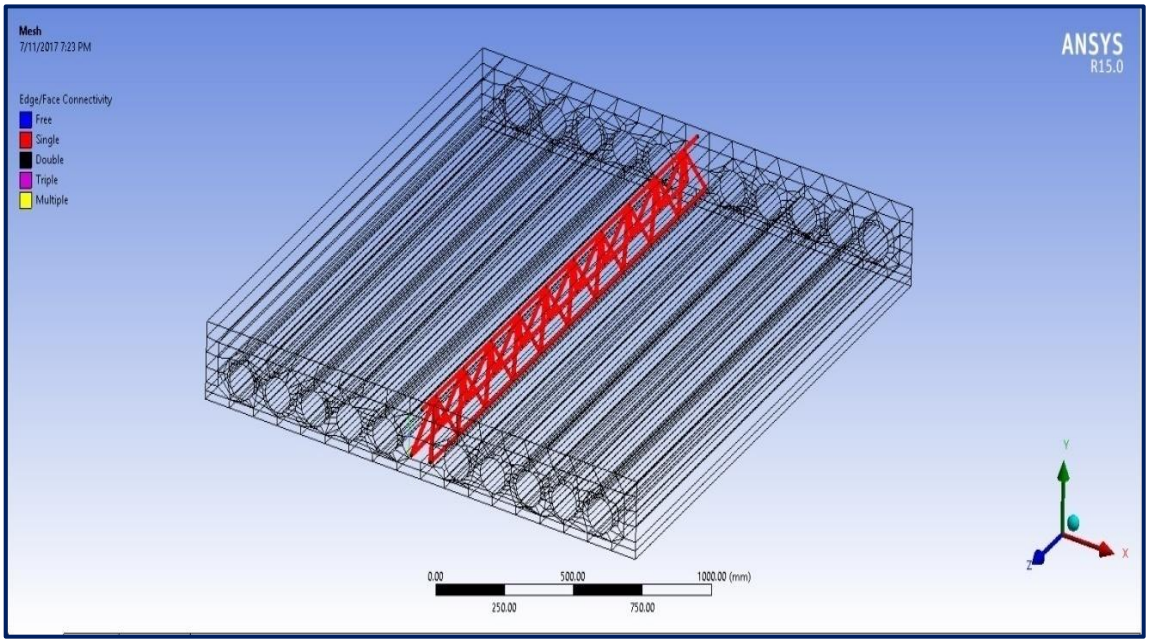


Fig. 111: Wireframe model ICF slab with lattice girder of category J

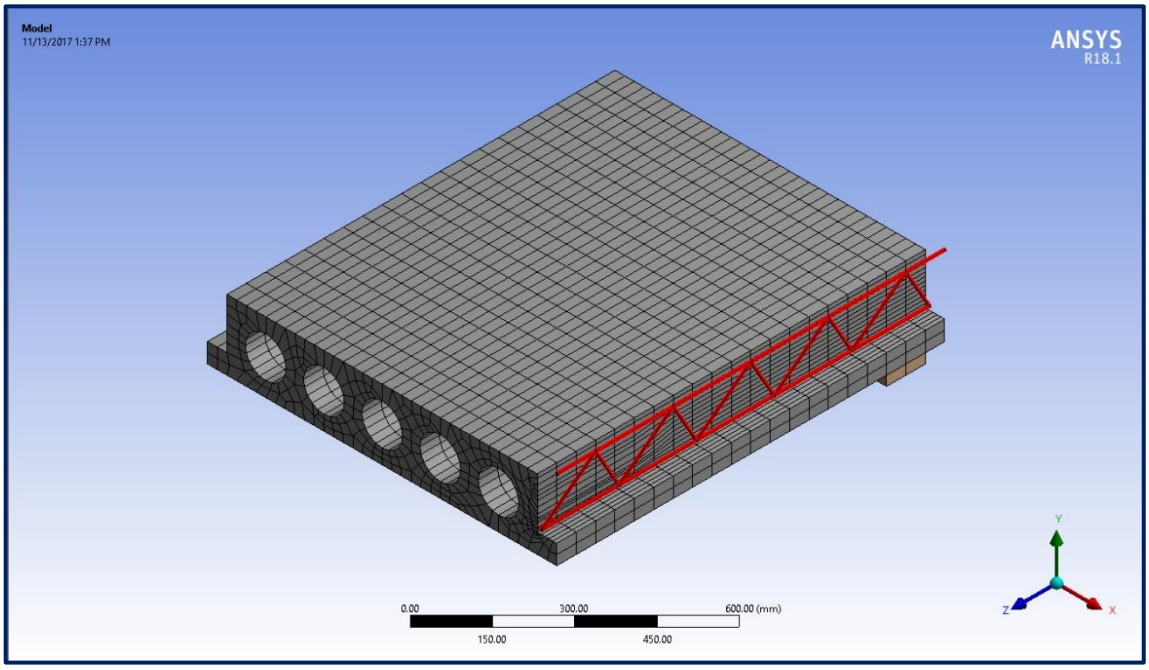


Fig. 112: Quarter symmetry model of ICF slab with lattice girder of category J

3.5.4.5 ICF ribbed slab with Lattice Girder and Mesh (Category MSJ)

The ICF ribbed slab with lattice girder with mesh is the combination of three materials namely polystyrene concrete, Nano-concrete, steel reinforcement in lattice girder and mesh at top. The material properties of the polystyrene concrete, Nano-concrete, and steel reinforcement are mentioned in Table 35. Wireframe model generated of ICF slab with lattice girder and mesh (for providing shear and flexural resistance to insure a flexural failure mechanism), which is named as category MSJ is shown in Figure 113. The total 90kN load was applied to the ICF slab with lattice girder and mesh with the load step of 6 kN.

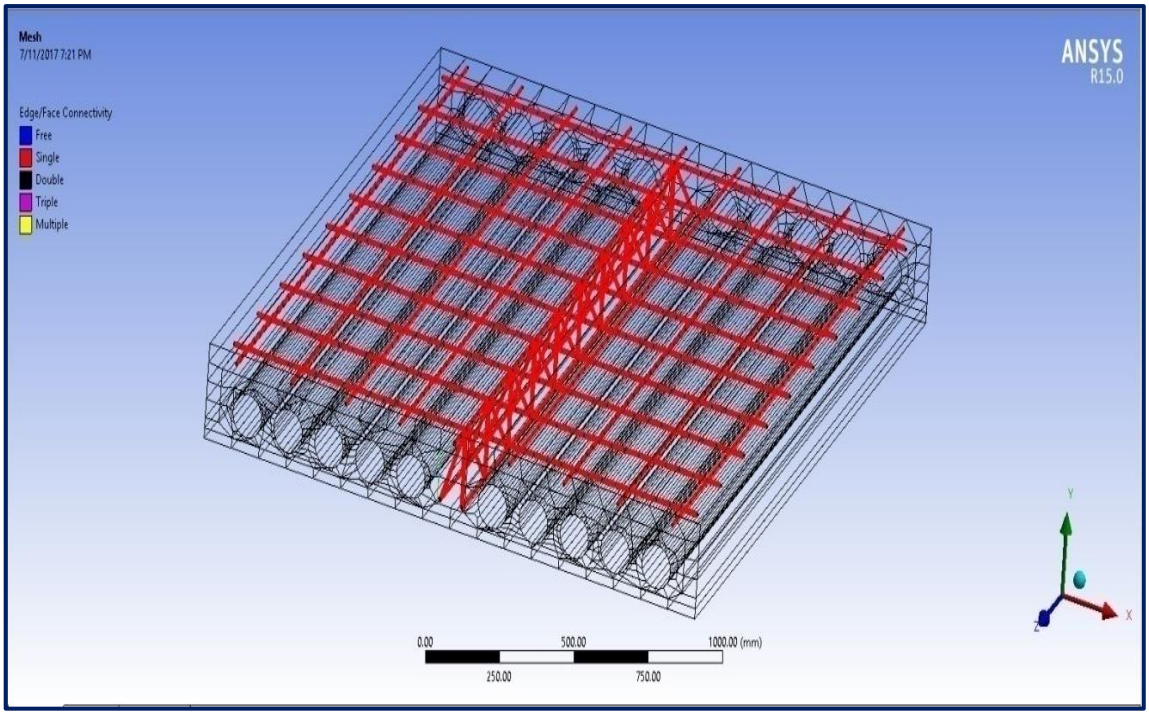


Fig. 113: Wireframe model ICF slab with lattice girder with mesh of category MSJ

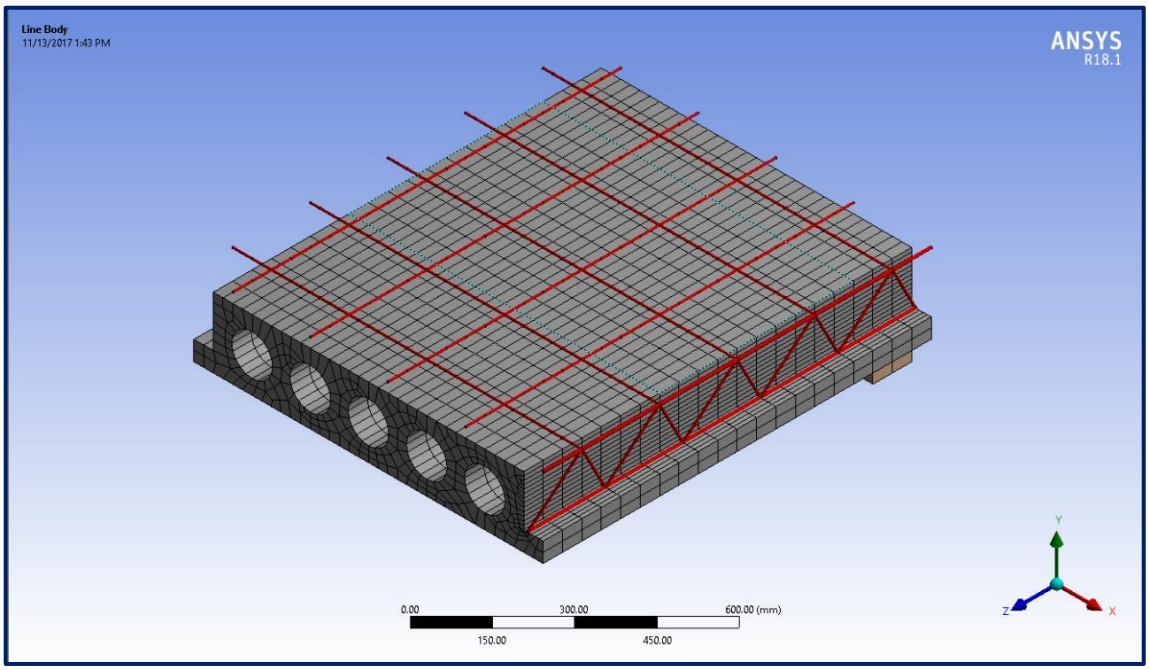


Fig. 114: Quarter symmetry model of ICF slab with lattice girder with mesh of category MSJ

3.5.5 Analytical Modeling of ICF Walls by ANSYS

The four types of wall specimens used in the experimental study were also modeled using the finite element package of ANSYS. Material properties have remained same as the materials used in the discrete modeling. Deformation and stress contour of all the wall elements are shown in the following subsections.

3.5.5.1 Wall ICF-04

Wall ICF-04 as per the details mentioned in Table 26 is modeled in ANSYS and subjected to the total load of 396 kN as per the loading condition similar to the experimental investigation.

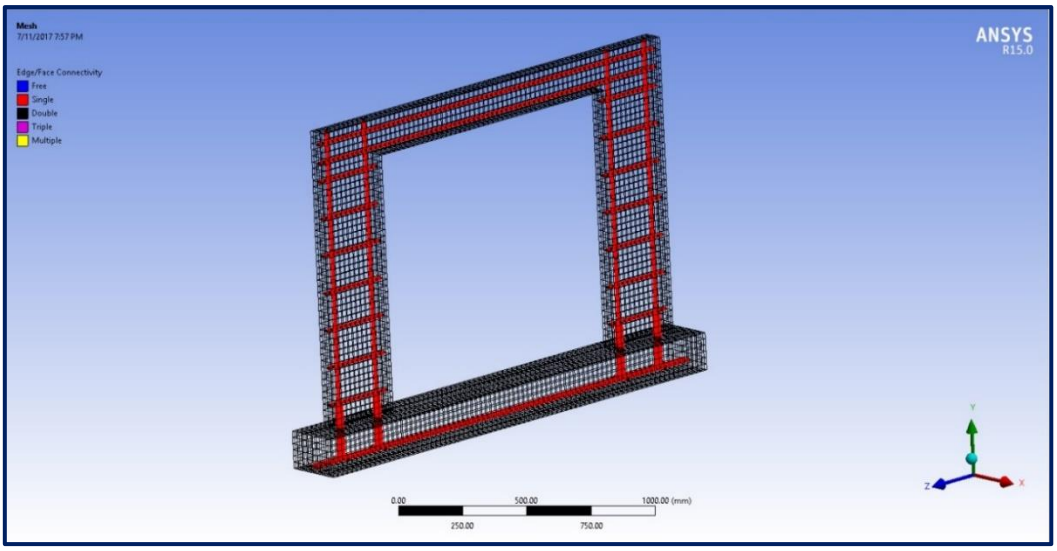


Fig. 115: Wireframe of wall model ICF-04

3.5.5.2 Wall ICF-06

Wall ICF-06 as per the details mentioned in Table 26 is prepared in ANSYS and given the total load of 400kN as per the loading condition similar to the experimental investigation. Figure 116 shows the reinforcement details within the wall.

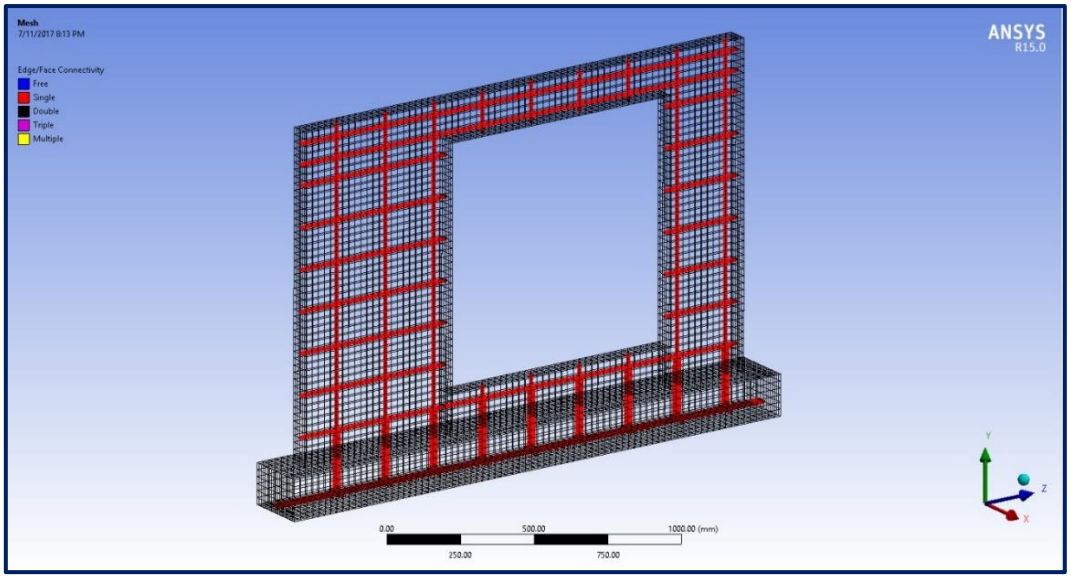


Fig. 116: Wireframe of wall model ICF-06

3.5.5.3 Wall ICF-09

Wall ICF-09 as per the details mentioned in Table 26 is prepared in ANSYS and given the total load of 300kN as per the loading condition similar to the experimental investigation. Figure 117 shows the reinforcement details within the wall.

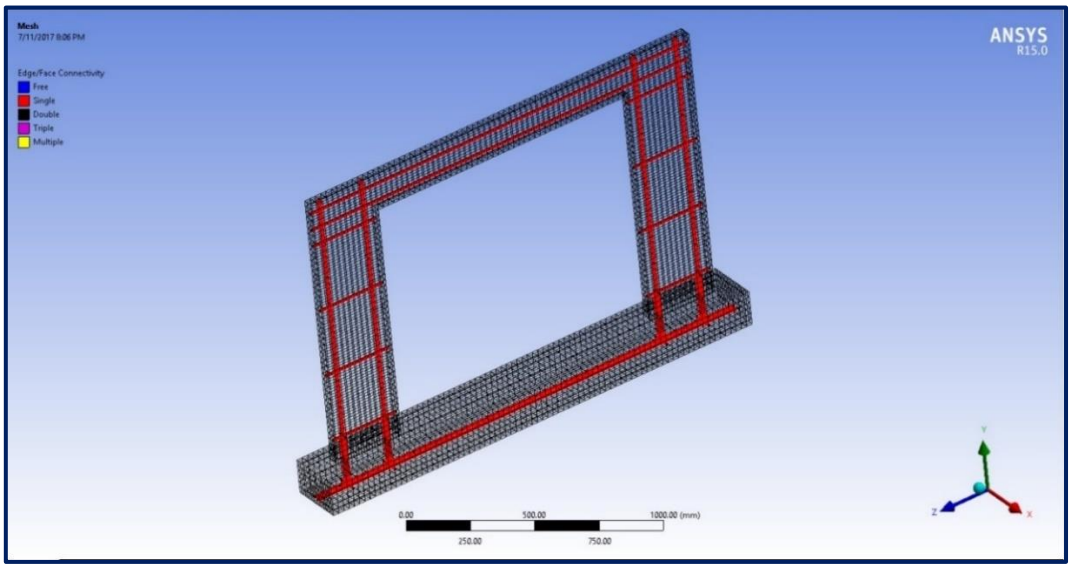


Fig. 117: Wireframe of wall model ICF-09

3.5.5.4 Wall ICF-11

Wall ICF-11 as per the details mentioned in Table 35 is prepared in ANSYS and given the total load of 400kN as per the loading condition similar to the experimental investigation. Figure 118 shows the reinforcement details within the wall.

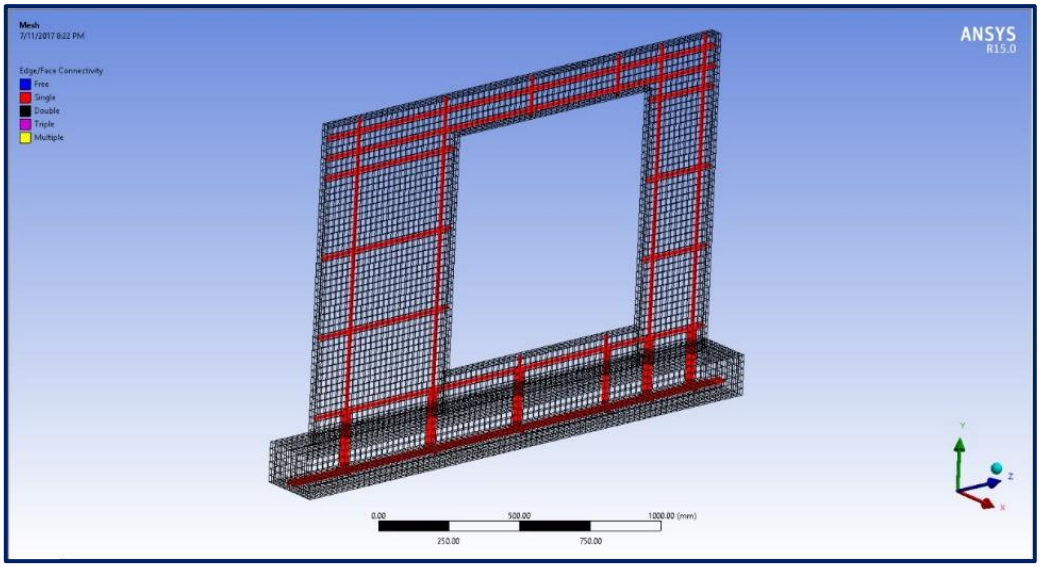


Fig. 118: Wireframe of wall model ICF-11

Chapter 4: RESULTS, CONCLUSIONS AND RECOMMENDATIONS

4.1Results and Discussions

8.1.1 Blank Block and ICF Slabs

8.1.1.1 Blank Block (CATEGORY B)

8.1.1.2 ICF ribbed slab with two bars only (Category S)

8.1.1.3 ICF ribbed slab with two bars and mesh (Category MS)

8.1.1.4 ICF Ribbed Slab with Lattice Girder Only (Category J)

8.1.1.5 ICF Slab with Lattice Girder and Mesh (Category MSJ)

8.1.1.6 ICF Slabs Experimental and FEM Results Comparison

8.1.1.7 Strength Limit State of ICF Slab (Category MSJ)

8.1.1.8 ICF Slab MSJ of Different Spans vs RCC Slabs

8.1.2 ICF Walls

8.1.2.1 Wall ICF-04

8.1.2.2 Wall ICF-06

8.1.2.3 Wall ICF-09

8.1.2.4 Wall ICF-11

8.1.2.5 ICF Walls Experimental and FEM results Comparison

8.1.3 3D ICF Building Design Example

8.1.4 Effect of Thermal Properties on Energy Saving

8.1.5 Cost Analysis

8.1.5.1 Cost Analysis in Various Forms

8.1.5.2 Cost Comparison of Conventional and Polyforms Construction

8.1.5.3 Discussion on Cost Analysis

4.2 Conclusions

4.3 Future Work

Chapter 4: RESULTS, CONCLUSIONS AND RECOMMENDATIONS

4.1 Results and Discussion

Comparisons were made between the results obtained by experimental and numerical analysis to verify the validity of the suggested models for the ICF slab and ICF wall specimens. The Comparison made for the ultimate carrying capacity, ultimate deflection, and overall behavior of the specimens. The following results are obtained from ANSYS:

- Deflection contours at failure load
- Failure load.
- Elastic and plastic stresses and strains in steel and concrete elements under the effects of ultimate loads.

The comparison of the overall behavior between the experimental and finite element analysis results for the ICF slab specimens show the behavioral stages. The comparison divided into three stages, pre-cracking (elastic stage), cracking stage (until yielding of steel) and yielding of steel and crushing of concrete.

The mid-span deflection values due to the application of two-line loads to the five tested ICF slab category is determined according to the formerly mentioned concept, fundamentals, and assumptions of ANSYS model.

Additionally, for the four types of ICF walls the deflection behaviors and strains were observed, simulated and compared.

4.1.1 Blank Block and ICF Slabs

All the analytical solutions of the slabs have shown conservative behavior in case of slabs, particularly for deflection. Deflections obtained

in analytical models are smaller compared to experimental results; however, the differences between both the values are very less. Notably, the deflection behavior in all the cases has remained very much similar to the experimental one.

In case of stress development and stress, zone has remained similar to the experimental behavior. This can be realized by observing tested samples and stress contour diagrams derived from ANSYS.

4.1.1.1 Blank Block (CATEGORY B)

Table 38 shows the deflections observed experimentally and analytically. It also shows the ratios between them. The obtained numerical failure load agrees well with the experimental ones of (7 kN). The mid-span deflection at failure has a highly matching agreement between the experimental value (1.87 mm) and that obtained numerically (1.73 mm). The average value of the obtained ratio between experimental and the numerical deflections of (0.89) shows a good average, and the standard deviation of (0.096) shows the data are consistent and measures very close to the mean. Image of contours for the deflection values derived from FE software ANSYS is shown in Figure 121. Stress developed in the Blank Block B due to applied load are shown regarding stress contours in Figure 120.

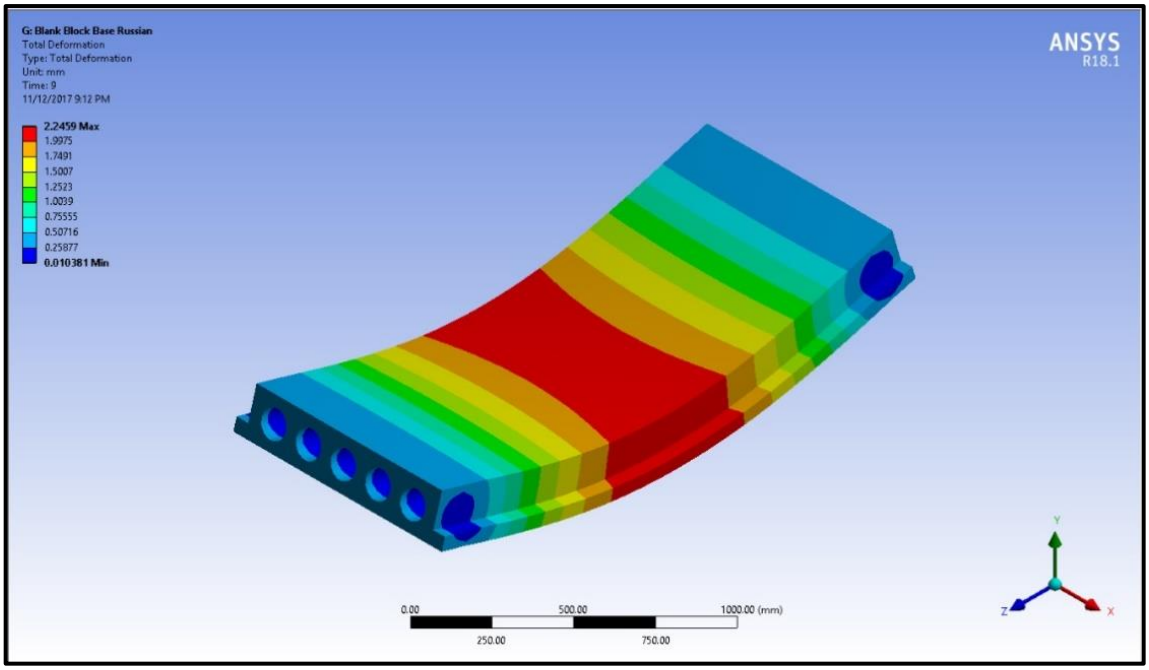


Fig. 119: Deflection contours derived from analytical model of Blank Block B

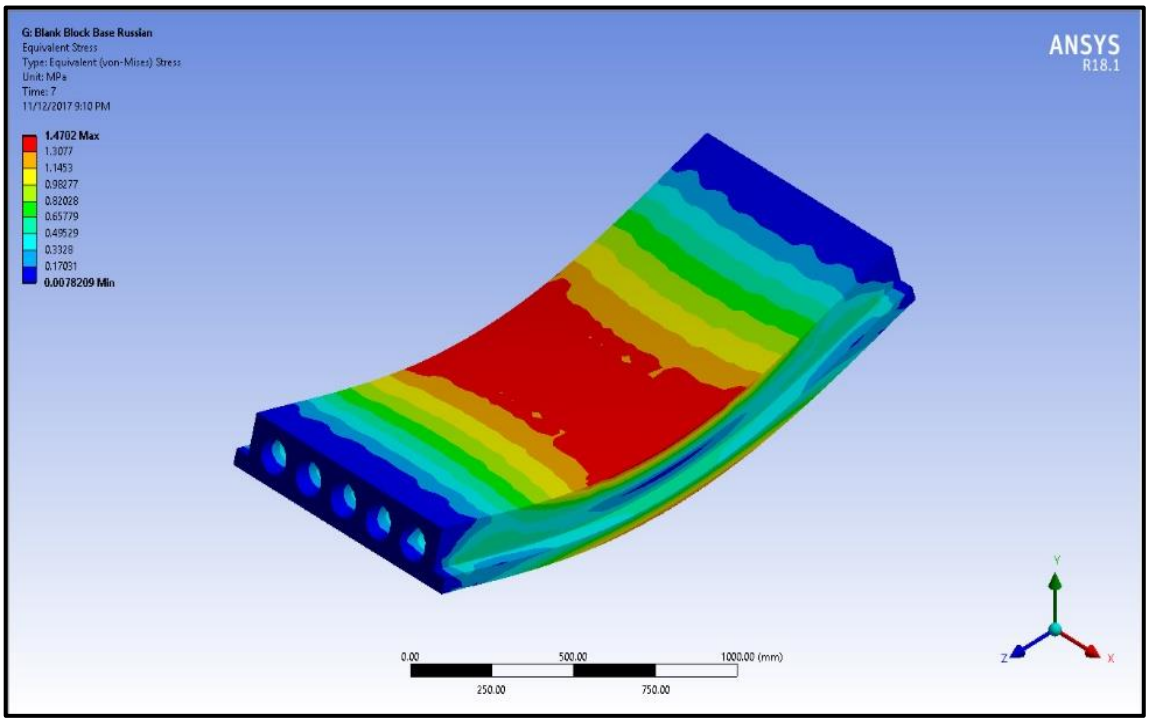


Fig. 120: Stress contours for Blank Block B

Table (38) Mid-span deflections of ICF slabs category B

Load (KN)	Deflection (mm)					
	Experimental				ANSYS (FEM)	Δ(EXP.)/ Δ(NUM.)
	B1	B2	B3	Average		
1	0.17959	0.239728	0.119444	0.17959	0.24	0.748275
2	0.42857	0.415529	0.441605	0.42857	0.49	0.874627
3	0.63128	0.623293	0.639275	0.63128	0.74	0.853086
4	0.93158	0.927791	0.935361	0.93158	0.99	0.940986
5	1.03504	1.01527	1.054806	1.03504	1.24	0.834708
6	1.32818	1.231446	1.424912	1.32818	1.48	0.897418
7	1.87198	1.567908	2.17606	1.87198	1.73	1.082072
					STD	0.095833
					Mean	0.890167

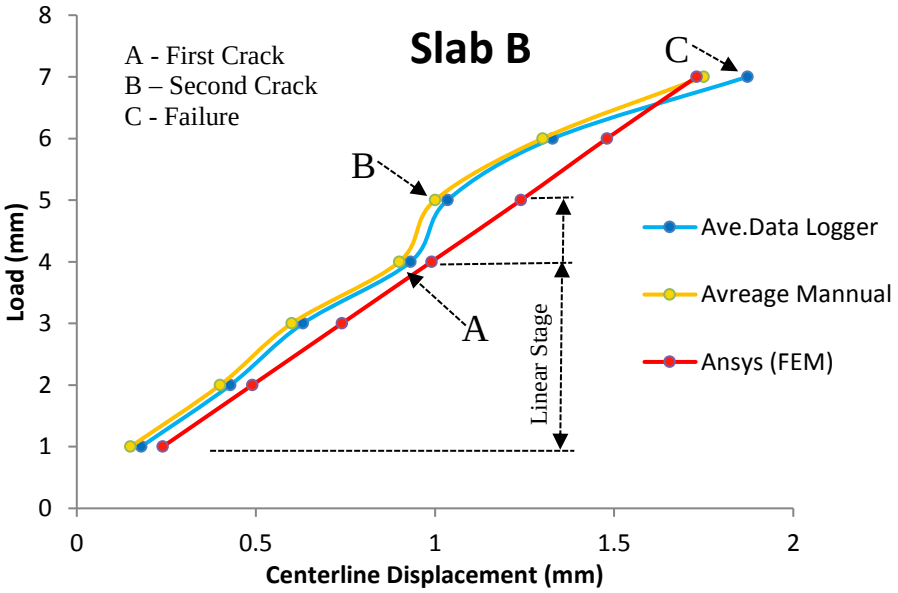


Fig. 121: Mid-span deflections of slab category B

Maximum stress observed is in the central portion (EPS concrete) of the slab is of (1.47 MPa) have also shown good agreement with the initially calculated one of (1.4 MPa) in Chapter 3.

However, sudden brittle failure without much deflection observed in the testing of all the three specimens of category B. When the first crack developed in the slab at around 4 kN at point A, immediately the slabs have collapsed at 7 kN at point C. The slab has failed precisely from the center as per the failure photos are shown in Figure 48, 50 and 52 in chapter 3.

In Figure 121, the numerical results are more linear and show a slight reduction in the stiffness compared to the experimental results. Also, the load-deflection curve shows a slight divergence between numerical and experimental results in the pre-cracking stage, in the cracking–elastic stage, there is moderate to significant divergence. At the third stage, there is an approximately close agreement between the experimental specimen curve and the finite element models curve. The primary reason for such behavior could have been associated with the presence of the Micro-cracks occurred due to drying shrinkage in the experimental specimens, unlike the numerical model.

4.1.1.2 ICF ribbed slab with two bars only (Category S)

In this category, two bars of 10 mm diameter provided in the rib beam to provide some interaction between adjacent Blank Block panels. The detail of the ICF slab panel given in Table 22 in chapter 3. Total of 54 kN load was applied with the load step of 6 kN in all the three specimens of the category S. Image of contours for the deflection values derived from FE software ANSYS is shown in Figure 122. Stresses developed in the ICF slab with two bars due to applied load are shown regarding stress contours in Figure 123.

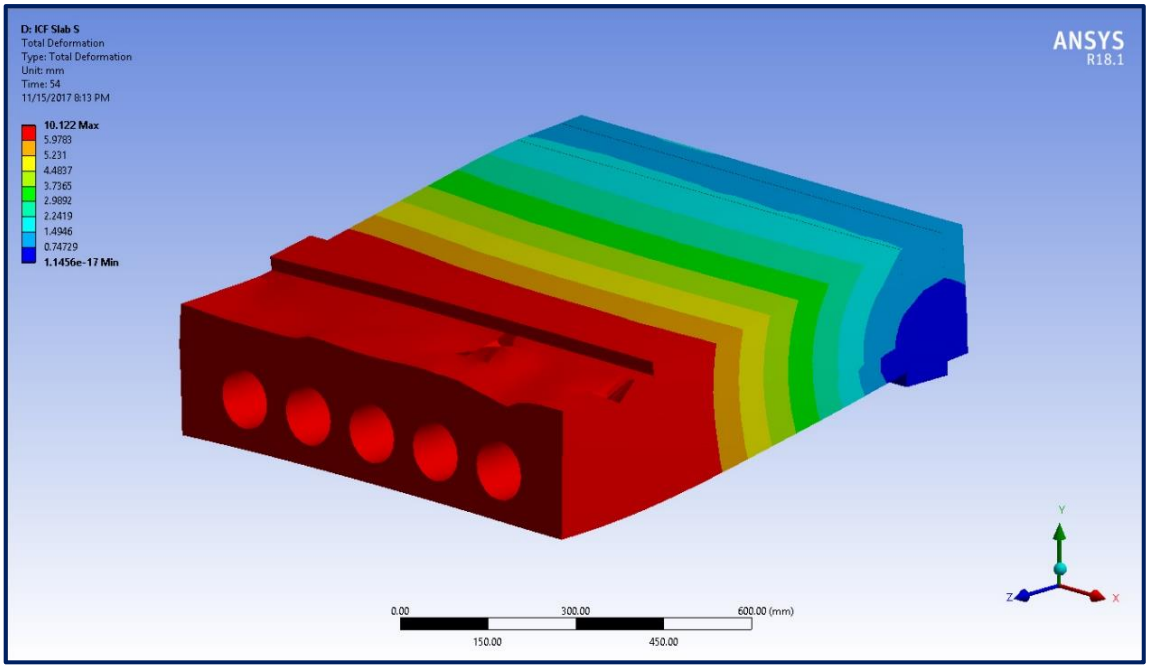


Fig. 122: Deflection contours derived from FEM of quarter symmetry model of ICF slab with two bars of category S

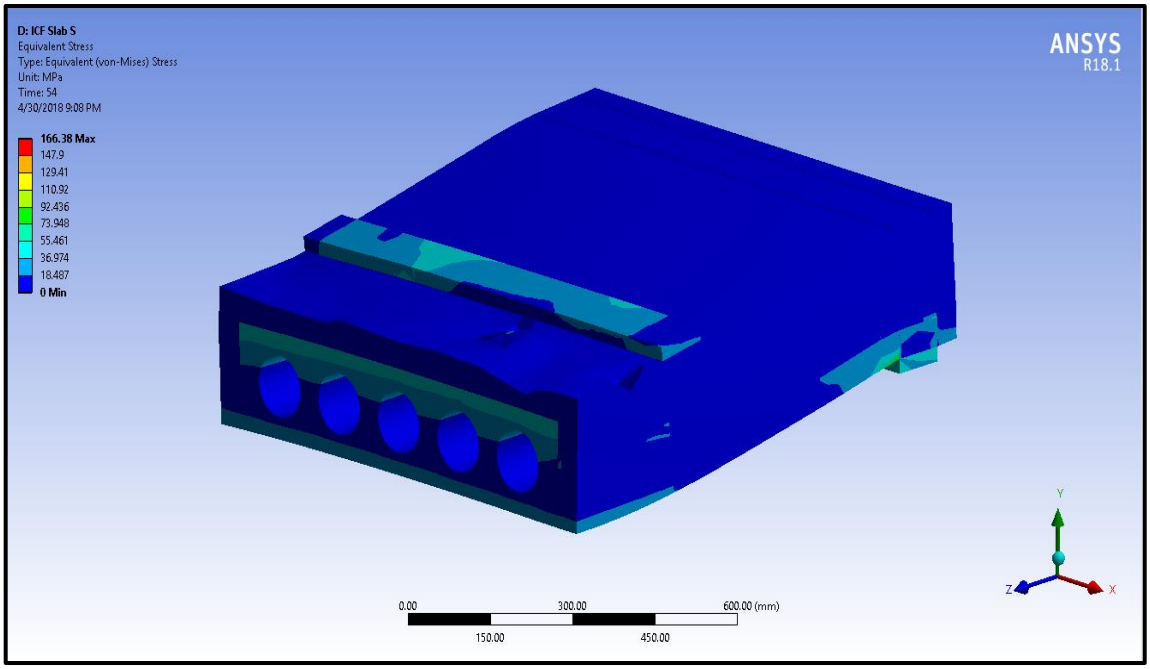


Fig. 123: Stress contours for quarter symmetry model of ICF slab with two bars of category S

Table (39) Mid-span deflections of slabs category S

Load (kN)	Deflection (mm)					
	Experimental				ANSYS (FEM)	Δ(EXP.)/ Δ(NUM.)
	S1	S2	S3	Average		
6	0.37179	0.121967	0.360013	0.28459	0.51259	0.555199
12	0.62077	0.322161	1.039662	0.660864	1.0605	0.623163
18	0.92443	0.719185	1.213784	0.952465	1.6282	0.58498
24	1.51828	1.02957	1.521646	1.356499	2.1897	0.619491
30	2.02886	1.41734	2.496538	1.980911	2.7558	0.718815
36	2.67739	1.936332	3.732192	2.78197	5.0497	0.550918
42	4.19146	2.864962	4.443806	3.833409	6.6246	0.578663
48	11.5145	11.48674	11.32	11.44043	7.9711	1.435238
54	12.34	0	0	12.34	10.122	1.219127
					STD	0.308
					Mean	0.77

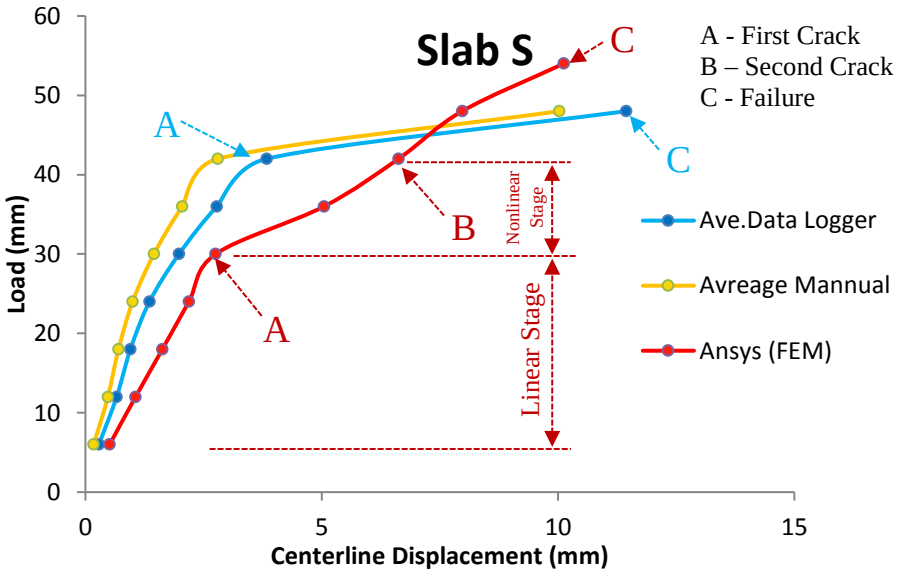


Fig. 124: Mid-span deflections of slabs category S

At the time of testing, the first crack observed are at 42 kN, 41 kN and 42 kN for the slabs S1, S2 and S3 respectively. Subsequently, all the slabs have failed at 48 kN. The slab has failed precisely from the center, and the vertical crack penetrated the compression concrete zone, as seen in Figures 55, 57 and 59 in chapter 3.

Table 39 shows the deflections observed experimentally and analytically. It also shows the ratios between them. Although the experimental results show a slight reduction in the failure load for most of the specimens, the obtained numerical failure of (54 kN) was close to the experimental one. The mid-span deflection at failure has slightly lower agreements between the experimental value of (12.34 mm) and that obtained numerically of (10.12 mm). The average value of the obtained ratio (0.77) between experimental and the numerical deflections showed an acceptable accuracy limit, and the standard deviation of (0.308) shows the data are consistent and measures very close and doesn't deviate or much from the mean.

The experimental load-deflection curve shown in Figure 124 is nonlinear and shows a sudden increase in the rate of deflections with the very slight divergence between numerical and experimental results in the pre-cracking stage, in the cracking–elastic stage, there is a significant divergence. At the third stage, there is not a good match between the experimental specimen curve and the finite element models curve. Many factors could be behind such behavior; the first could have been very much related to the presence of the micro-cracks which could be introduced by drying shrinkage in the experimental specimens, unlike the numerical model. The second assumption is that the bond between the concrete and steel in finite element model is assumed to be perfect, unlike the experimental model, this is why the numerical curve in the second stage

and the third stage, have a significant divergence from the experimental curve, because after point A (first crack) the steel and the concrete were coming apart in the experimental specimen. This phenomenon was noticed when the slabs remained self-supported after testing but entirely collapsed while removing from the loading frame. In other words, the parts are separating from each other in the experiment while in Ansys model they remained the same until the end.

4.1.1.3 ICF ribbed slab with two bars and mesh (Category MS)

In this category, two bars of 10 mm diameter provided in the rib beam along with the 5 mm diameter size square mesh at the top with the spacing of 200mm c/c both ways to provide some interaction between adjacent Blank Block panels. The details of the slab panel given in Table 23 in chapter 3. Total of 60 kN load is applied to the ICF slab with two bars and mesh with the load step of 6 kN in all the three specimens of this category of slab MS. Image of contours for the deflection values derived from FE software ANSYS is shown in Figure 125. Stress developed in the ICF ribbed slab with two bars and mesh due to applied load are shown regarding stress contours in Figure 126.

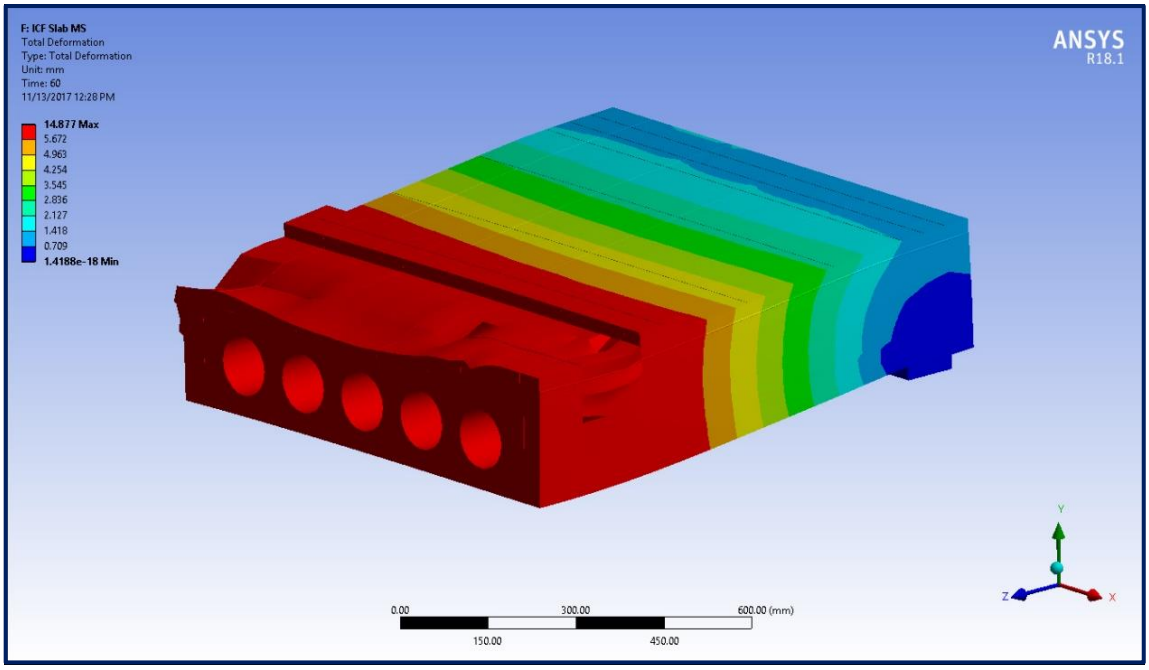


Fig. 125: Deflection contours derived from analytical model of quarter symmetry model of ICF slab with two bars of category MS

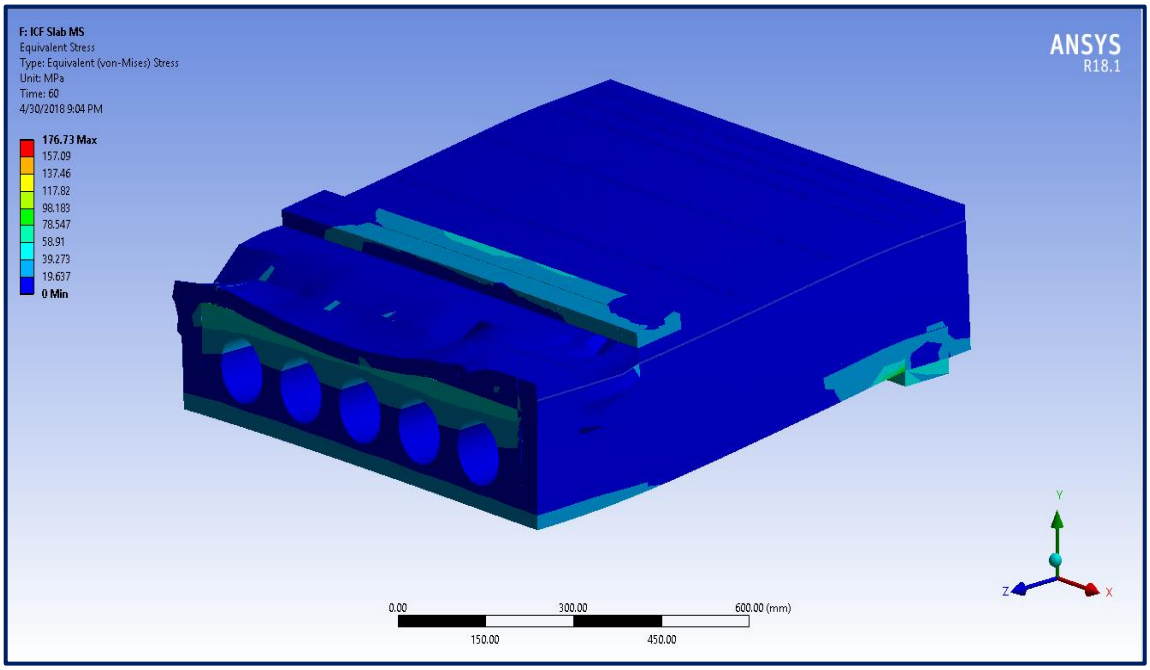


Fig. 126: Stress contours for quarter symmetry model of ICF slab with two bars and mesh of category MS

Table (40) Mid-span deflections of slabs category MS

Load (kN)	Deflection (mm)					
	Experimental				ANSYS (FEM)	Δ(EXP.)/ Δ(NUM.)
	MS1	MS2	MS3	Average		
6	0.1	0.220382	0.212812	0.177731	0.55759	0.318749
12	0.2	0.325526	0.365901	0.297142	1.1514	0.25807
18	0.5	0.418894	0.541702	0.486865	1.7823	0.273167
24	0.6	0.826852	1.045552	0.824135	2.4501	0.336368
30	1	2.207182	1.435004	1.547395	3.1128	0.497107
36	1.7	3.778454	2.335036	2.604497	3.822	0.681449
42	2.7	4.967	3.145908	3.604303	5.5367	0.650984
48	5		7.188486	6.094243	7.9391	0.767624
54			9.558008	9.558008	11.257	0.849072
60			16.59002	16.59002	14.877	1.115146
					STD	0.272269
					Mean	0.574774

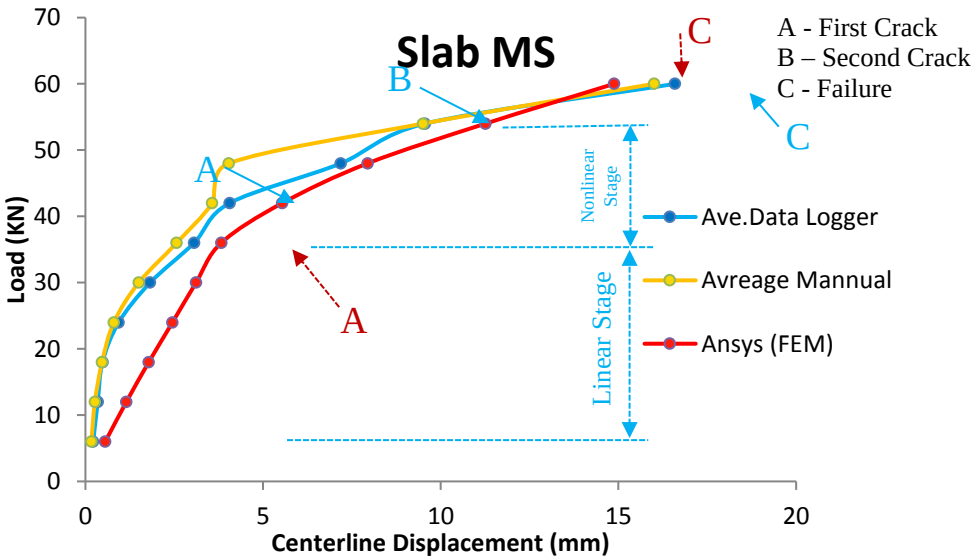


Fig. 127: Mid-span deflections of slabs category MS.

At the time of testing, first cracks observed are at 48 kN, 42 kN and 48 kN for the slabs MS1, MS2 and MS3 respectively. Subsequently, all the slabs have failed at about 60 kN, 48 kN, and 60 kN respectively. The slab has not precisely failed from the center, and the vertical crack developed on one side away from the load point and did not penetrate the compression concrete zone as per the failure photos are shown in Figure 62, 64 and 66 in chapter 3.

Table 40 shows the deflections observed experimentally and analytically. It also shows the ratios between them. The obtained numerical failure load agrees well with the experimental one of (60 kN). The mid-span deflection at failure has slightly lower agreements between the experimental value of (16.59 mm) and that obtained numerically of (14.88 mm). The average value of the obtained ratio (0.272) between experimental and the numerical deflections showed a good average, and the standard deviation of (0.575) shows the data are consistent and measures very close to the mean.

The load-deflection curve shown in Figure 127 is nonlinear and shows a sudden increase in the rate of deflections with the varying divergences between numerical and experimental results in the pre-cracking stage, in the cracking–elastic stage, there is also very slight divergence. At the third stage, there is almost complete agreement between the experimental specimen curve and the finite element models curve. The primary factor for such matching behavior is that the steel mesh has reduced the effect of the drying shrinkage micro-cracks and the concentrated stresses at the top of the experimental model. The slabs remained self-supported after testing and while removing from the loading frame, which complies very well with both experimental and numerical

curves, having the parts remained together until the end of the operation, in the experiment and Ansys models in this category.

4.1.1.4 ICF Ribbed Slab with Lattice Girder Only (Category J)

In this category, one lattice girder as per the details are given in Table 24 in chapter 3was provided for the improved behavior of the slab panel. Total 48 kN load was applied to the ICF slabs with lattice girder with the load step of 6 kN in all the three specimens of this category of slab J. Here, the contribution of lattice girder is observed clearly which holds the deflection up to its capacity of around 48 kN. The rate of deflection increased after this level. Image of contours for the deflection values derived from FE software ANSYS is shown in Figure 128. Stress developed in the ICF ribbed slab with lattice girder due to applied load are shown regarding stress contours in Figure 129.

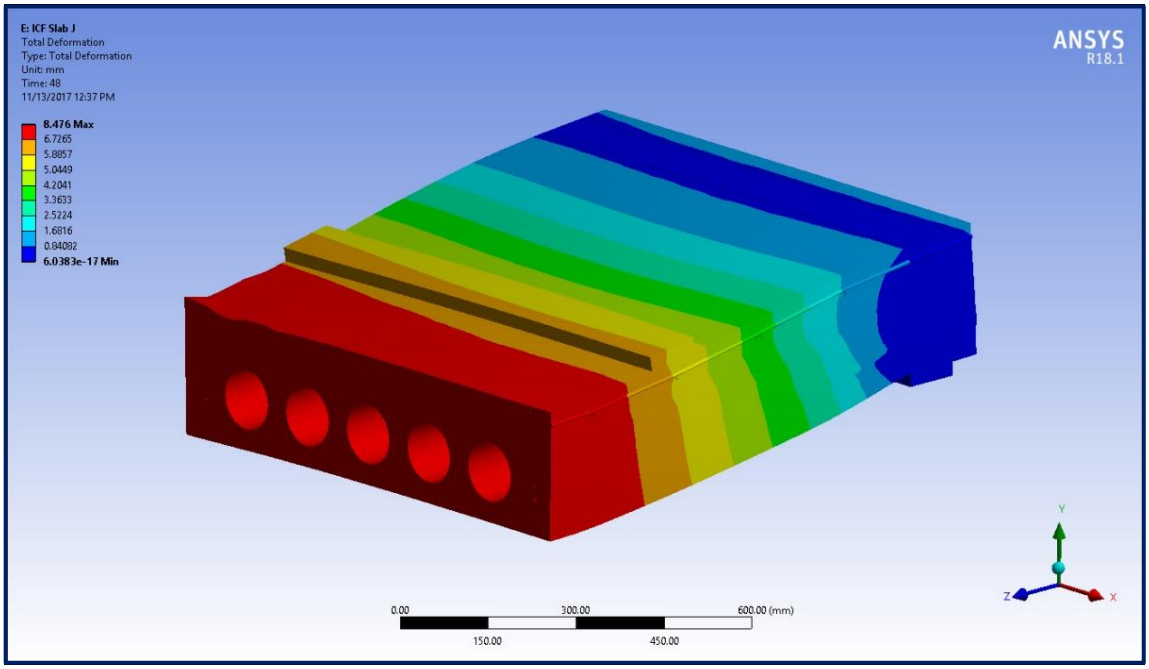


Fig. 128: Deflection contours derived from analytical model of quarter symmetry model of ICF slab with lattice girder of category J

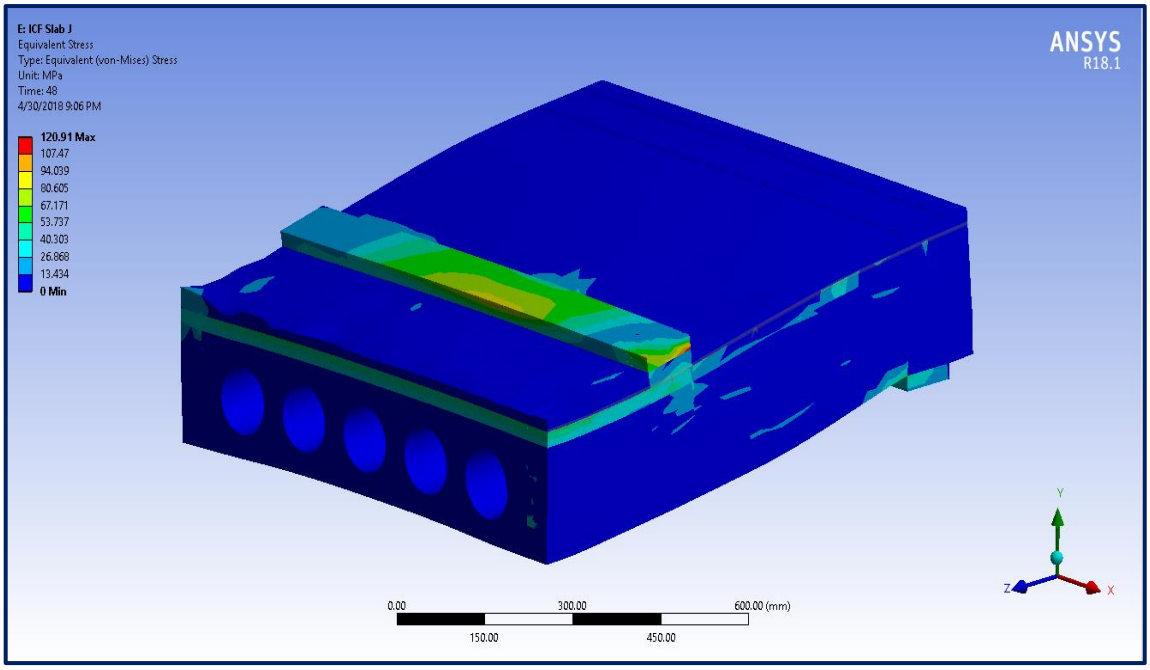


Fig. 129: Stress contours for quarter symmetry model of ICF slab with lattice girder of category J

Table (41) Deflection observed experimentally and analytically for category J.

Load (kN)	Deflection (mm)					
	Experimental				ANSYS (FEM)	Δ(EXP.)/ Δ(NUM.)
	J1	J2	J3	Average		
6	0.6275	0.406276	0.324685	0.45282	0.683	0.662987
12	0.91349	0.719185	0.75199	0.794889	1.404	0.56616
18	1.27939	0.808347	1.112844	1.066861	2.147	0.496908
24	1.76726	1.012748	1.326498	1.368835	2.897	0.472501
30	2.20887	1.250792	1.721836	1.727165	3.644	0.473975
36	2.93646	1.64277	2.264382	2.281204	4.663	0.489214
42	5.00401	2.3813	2.939826	3.441713	6.328	0.543886
48	7.79916	9.879326	9.657264	9.111917	8.476	1.075026
					STD	0.190034
					Mean	0.597582

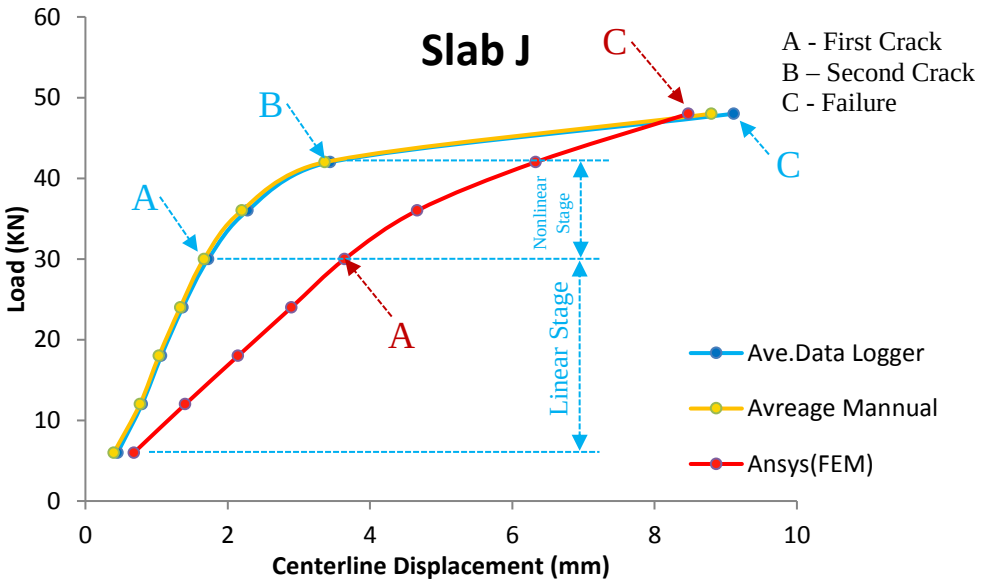


Fig. 130: Chart of load vs. deflection of experimental and analytical values for category J

At the time of testing, first cracks observed are at 41 kN, 42 kN and 42 kN for the slabs J1, J2 and J3 respectively. Subsequently, all the slabs have failed at about 47 kN, 48 kN, and 48 kN respectively. The slab has failed precisely from the center, and the vertical crack penetrated the compression concrete zone as per the failure photos are shown in Figure 69, 71 and 73 in chapter 4. The slabs remained self-supported after testing and while removing from the loading frame.

Table 41 shows the deflections observed experimentally and analytically. It also shows the ratios between them. The obtained numerical failure load agrees well with the experimental one of (48 kN). The mid-span deflection at failure shows good agreement between the experimental value of (9.11 mm) and that obtained numerically of (8.476 mm). The average value of the obtained ratio (0.19) between experimental and the numerical deflections showed a good average, and the standard deviation of (0.598) shows the data are consistent and measures very close to the mean.

The load-deflection curve shown in Figure 130 is nonlinear and shows a sudden increase in the rate of deflections with the significant divergence between numerical and experimental results in the pre-cracking stage and the cracking–elastic stage. At the failure stage, there is no agreement. In addition to the factors mentioned in (category S), behind the behavior being far not identical between the experimental and the finite element results is that the FEA solution influenced by the element type and mesh size.

4.1.1.5 ICF Slab with Lattice Girder and Mesh (Category MSJ)

In this category MSJ, lattice girder provided in the rib beam along with the 5 mm diameter size square mesh at the top with the spacing of 200mm c/c both ways to provide some interaction between adjacent Blank Block panels. The details of the slab panel given in, Table 25 in chapter 3. Total 90 kN load was applied to the ICF slab with lattice girder and mesh with the load step of 6 kN in all the three specimens of this category of slab MSJ. Image of contours for the deflection values derived from FE software ANSYS is shown in Figure 131. Stress developed in the ICF ribbed slab with lattice girder and mesh due to applied load are shown regarding stress contours in Figure 132.

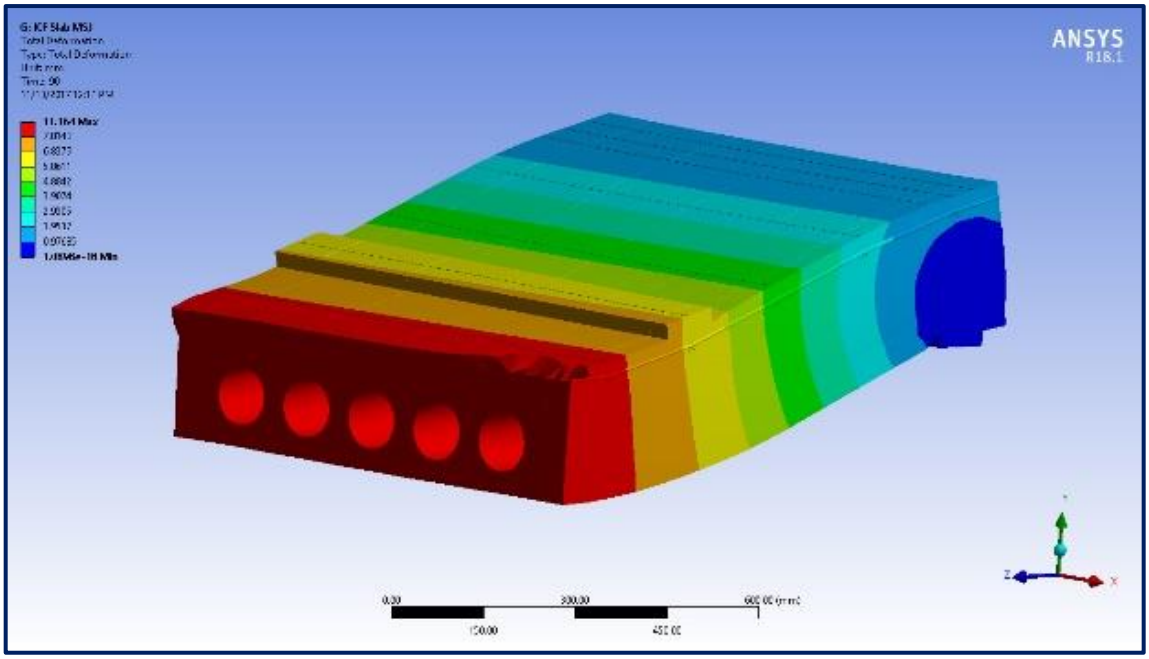


Fig. 131: Deflection contours derived from FEM model of quarter symmetry model of ICF slab with lattice girder with mesh of category MSJ

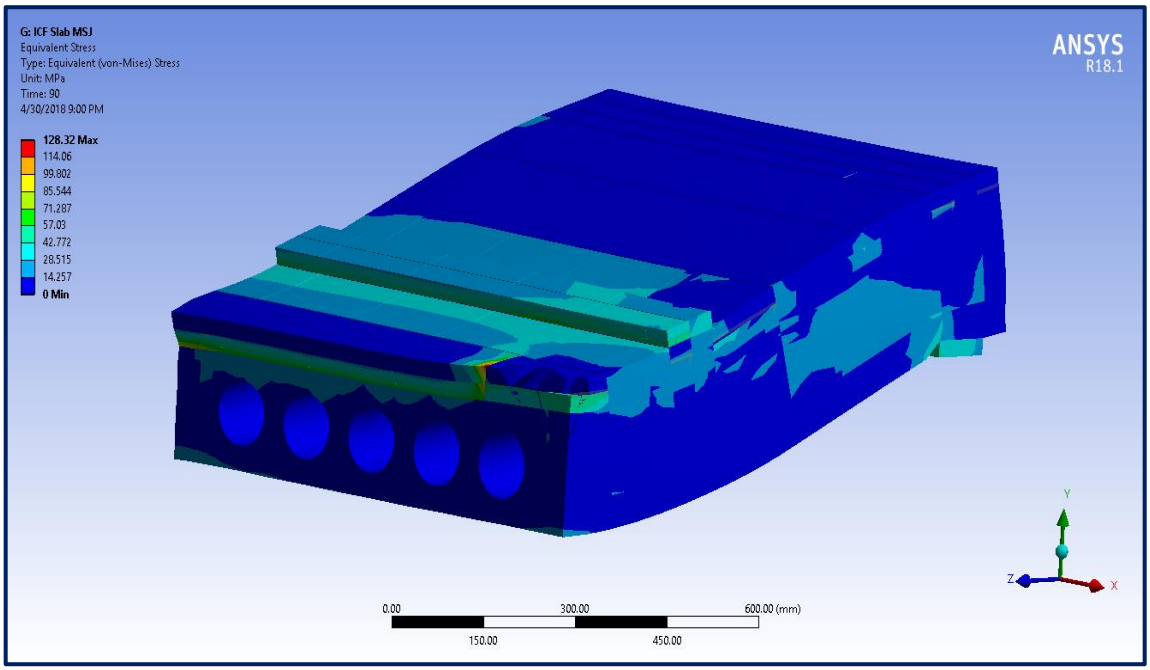


Fig. 132: Stress contours for quarter symmetry model of ICF slab with lattice girder with mesh of category MSJ

Table (42) Deflection observed experimentally and analytically for category MSJ

Load (KN)	Deflection (mm)					
	Experimental				ANSYS (FEM)	Δ(EXP.)/ Δ(NUM.)
	MSJ1	MSJ2	MSJ3	Average		
6	0.11566	0.008412	0.222905	0.115658	0.5270	0.219466
12	0.55011	0.736849	0.363377	0.550113	1.0700	0.514124
18	1.14691	1.619218	0.674604	1.146911	1.6800	0.682685
24	1.25037	1.755482	0.745261	1.250371	2.1500	0.581568
30	1.49515	2.08101	0.909285	1.495148	2.6900	0.555817
36	1.78955	2.323262	1.255838	1.78955	3.2330	0.553526
42	3.03151	2.742996	3.320024	3.03151	3.7990	0.797976
48	3.577	3.222452	3.931544	3.576998	4.3790	0.816853
54	4.08253	3.532838	4.632222	4.08253	5.0700	0.805233
60	4.81223	4.266322	5.358136	4.812229	5.7160	0.841888
66	5.58062	4.877842	6.283404	5.580623	6.5980	0.845805
72	6.49285	5.90741	7.078294	6.492852	7.5370	0.861464
78	7.80211	7.753736	7.850474	7.802105	8.5540	0.9121
84	9.72834	10.04335	9.41333	9.728341	9.8660	0.986047
90	12.6514	13.10432	12.1984	12.65136	11.2200	1.127572
					STD	0.13896
					Mean	0.854846

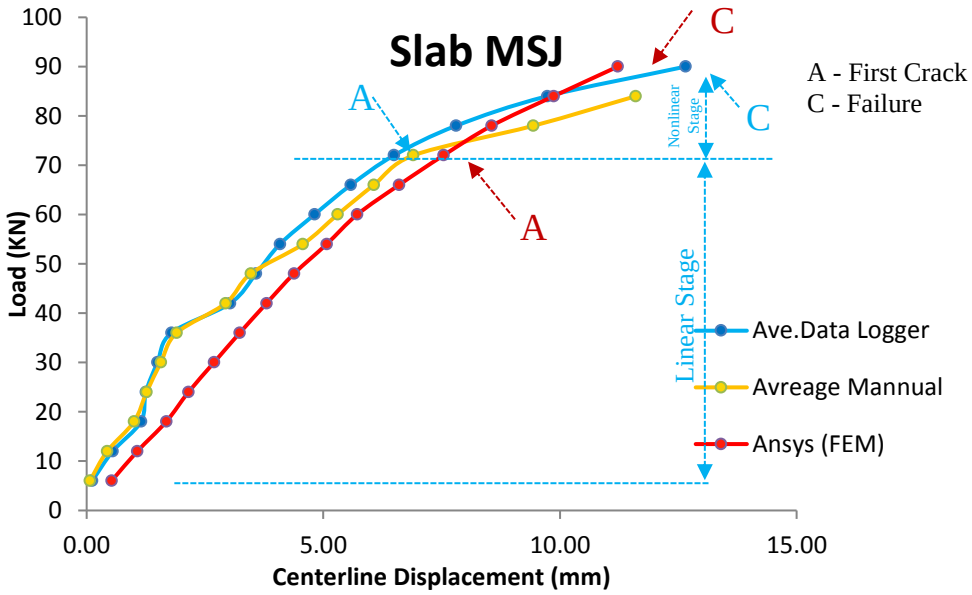


Fig. 133: Chart of load vs. deflection of experimental and FEM values for category MSJ

At the time of testing, first cracks observed are at 78 kN, 86 kN and 82 kN for the slabs MSJ1, MSJ2 and MSJ3 respectively. Subsequently, all the slabs have failed at about 88 kN, 90 kN, and 90 kN respectively. Tow vertical cracks developed near to the load point on both the side and did not penetrate the compression concrete zone. No cracks are developed near to the central part of the slab as per the failure photos are shown in Figure 76, 78 and 80 in chapter 3.

Table 42 shows the deflections observed experimentally and analytically. It also shows the ratios between them. The obtained numerical failure load agrees well with the experimental one of (90 kN). The mid-span deflections at failure have almost matching agreement between the experimental value of (12.65 mm) and that obtained numerically of (11.22 mm). The average value of the obtained ratio (0.139) between experimental and the numerical deflections showed a good average, and the standard deviation of (0.855) shows the data are consistent and measures very close to the mean.

The load-deflection curve in Figure 133 shows nonlinear behavior and reasonable correlation with experimental data, having very slight divergence between numerical and experimental results in the pre-cracking stage due to the the same reasons mentioned above, in the cracking–elastic stage and at the failure stage, there is almost complete agreement between the experimental specimen curve and the finite element models curve. The primary factor for such very well matching behavior is that the lattice girder and mesh stresses have distributed well along the concrete section and area of concentrated stresses reduced, for this reason, this category of ICF slabs has resisted more loads.

The slabs remained self-supported after testing and while removing from the loading frame, which complies very well with both experimental and

numerical curves, having the parts remained together until the end of the operation, in the experiment and Ansys models in this category.

4.1.1.6 ICF Slabs Experimental and FEM Results Comparison

The comparison in Figures 134 and 135, confirms that the lattice girder and the mesh steel reinforcements in the ICF slab systems were useful in exchanging the modes of failures, from shear failure to shear-ductile failure. The failure mode that controlled by a combination of shear-flexural behavior is one of the essential characteristics of the structural safety and stability. Figure 134 shows that results of the experimental curve of (categories MS&MSJ) are ductile. Because, following the elastic region, there is a rare section “necking, where a permanent deformation occurred. However, for (categories S&J) this phenomenon is not seen due to the low resistance of the reinforcement to the stresses which lead to the slippage of the steel.

MS&MSJ categories did not fail from the center because the effect of the zigzag lattice girder used in the ribs strengthened the shear resistance of the ribs. Also, The upper mesh reinforcement remained far more than the value of the yield stress with elastic behavior, and this contributed to the resistance of the development of the vertical cracks and prevented the penetration of the compression concrete zone. In turn, increased the ultimate strength capacity of the ICF slab specimens and improved the failure modes for these two categories.

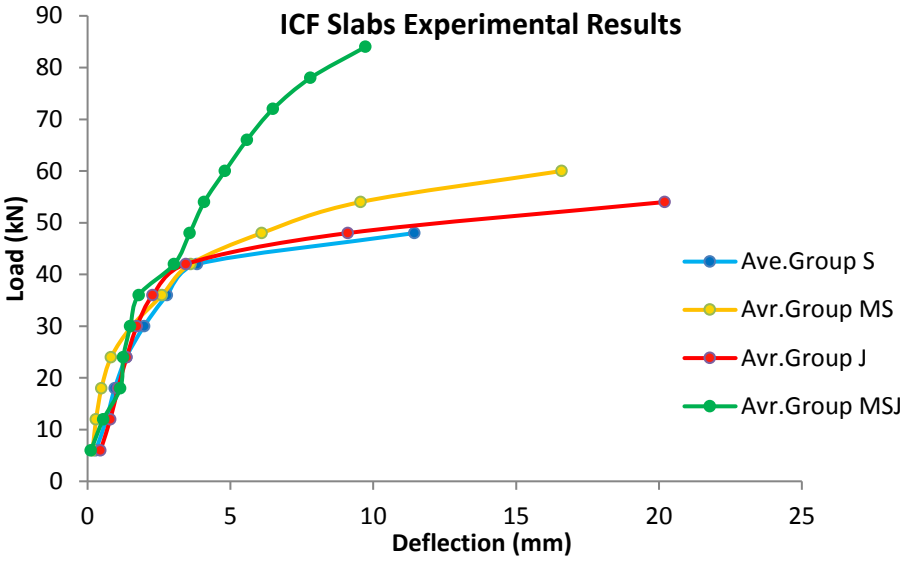


Fig. 134: Chart of load vs. deflection of experimental values for all categories.

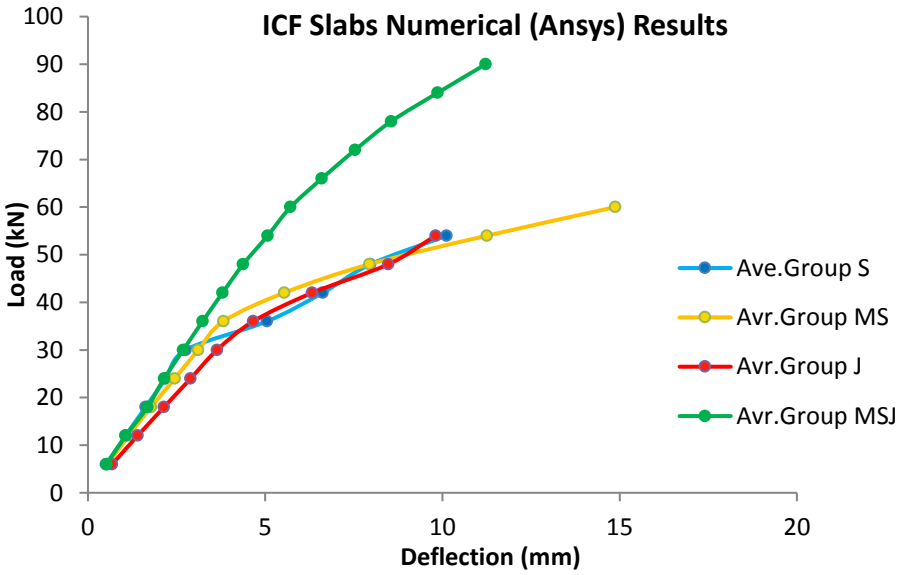


Fig. 135: Chart of load vs. deflection of FEM values for all categories.

The full FEM nonlinear load-deformation response can be seen in Figure 135. This response was calibrated by the step control setting and the nonlinear control tolerances so that the FEM load-deformation curve Figure 134 fits the experimental curves in Figure 135. The entire load-deformation responses of both models produced, compared well with each other and gave confidence in the use of the FEM models developed by

ANSYS. The approach than further utilized in this study to set appropriate parameters to work additional varying dimensional models under the finite element method.

Cook et al. (2002), Finally, some of the numerical models simulated the problems with high correctness. Nevertheless, the current errors between experimental and finite element results presented and influenced by the number of elements used, the number of nodes per element, the nature of element shape functions, integration rules used with isoparametric elements and other formulation details of particular elements.

It is essential to examine and evaluate the amount and type of stresses, whether it yields elastic or plastic strains, in the reinforcement and the mesh located at the top of the slab portion. The following Table 43 presents observations and points of the numerical analysis outputs of both concrete and reinforcement stresses in the ICF slabs at the ultimate loading stage.

Table (43) FEM stresses in the concrete and reinforcement of ICF slabs

Slab Categories	Ultimate Load (kN)	Deflection (mm)	Stress in Steel (N/mm^2)	Uniformly Distributed Load (kN/m)
S	54	12	75.82	27>5
MS	60	16	35.30	30>5
J	48	9	46.78	24>5
MSJ	90	12	38.42	45>5

Table 43 shows Von misses stress values of steel reinforcement in the four categories which are taken from Figures 136 to 139.

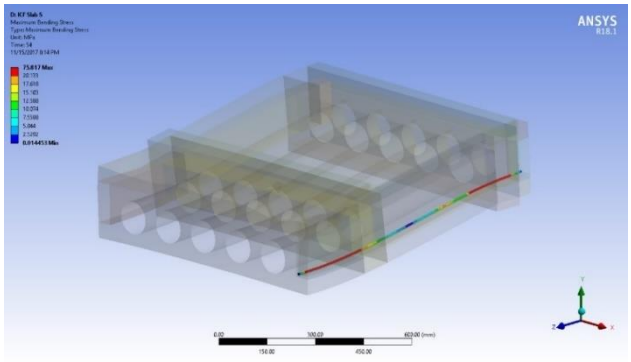


Fig. 138: FEM ultimate reinforcement stress of the quarter symmetry model of category S

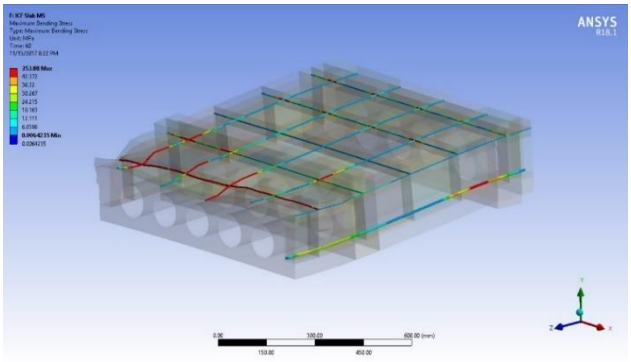


Fig. 139: FEM ultimate reinforcement stress of the quarter symmetry model of category J

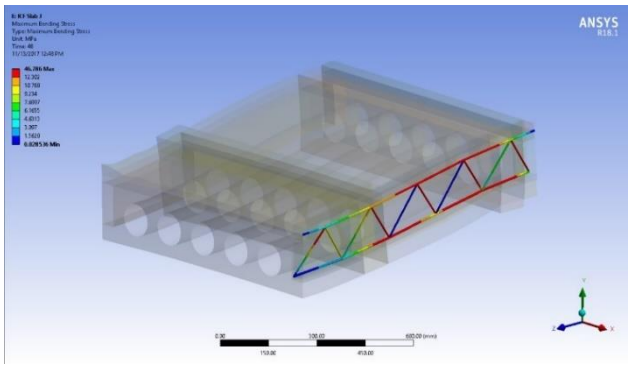


Fig. 136: FEM ultimate reinforcement stress of the quarter symmetry model of category J

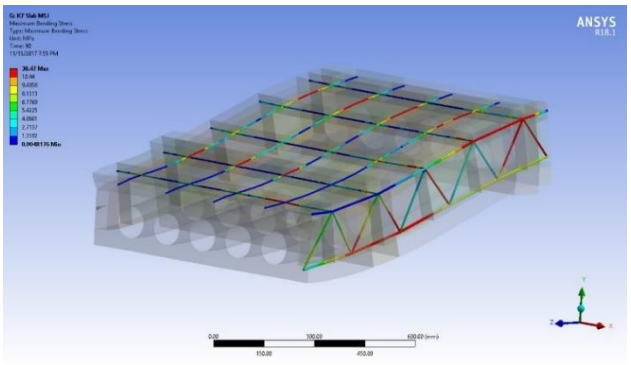


Fig. 137: FEM ultimate reinforcement stress of the quarter symmetry model of category

The maximum stresses in steel reinforcement were in (category S) (75.82MPa), which reduced to (46.78MPa) by introducing more steel, using lattice girder in (category J). However, the stresses in the reinforcement steel were significantly reduced in categories MS&MSJ, 35.3MPa and 38.42MPa respectively. As the mesh and the rib reinforcements shared the stress occurring in the ICF slabs sections, which provided more ductility and shear resistant, yielding identical results with the experimental specimens with perceiving that the steel reinforcements never yielded in all categories and yielded elastic strains. The deteriorated behavior of the ICF slabs beyond failure was due to the substantially diminished ability of the ICF slabs to distribute any more stresses throughout the cross-section, which primarily depends on the cracked

moment of inertia, yielding steel and nonlinear concrete material that define the flexural rigidity of the member. Therefore, higher deflections develop at failures.

The uniformly distributed loads of categories S, MS, J, MSJ is 27kN/m, 30kN/m, 24kN/m, and 45kN/m respectively, are all greater than the ultimate residential imposed design distributed load of (5kN/m) for total depth of 180mm of the ICF ribbed slabs.

4.1.1.7 Strength Limit State of ICF Slab (Category MSJ)

The ICF slabs of (Category MSJ) provided the safest and most stable failure mode, controlled by a combination of shear and flexural behaviors. At load 90kN, the ICF slabs of (Category MSJ) no longer can support the additional load as indicated by an overwhelming convergence failure. ANSYS displays circles at locations of various cracking patterns in concrete elements. Figure 140 shows the location of cracks and crushed integration points along the ICF slabs of (Category MSJ) plus ANSYS cracks signs explanations. A diverse cracking throughout the entire constant moment region occurs and off center of the ICF slab that is matching perfectly with the crack location in the picture of the experimental ICF slab.

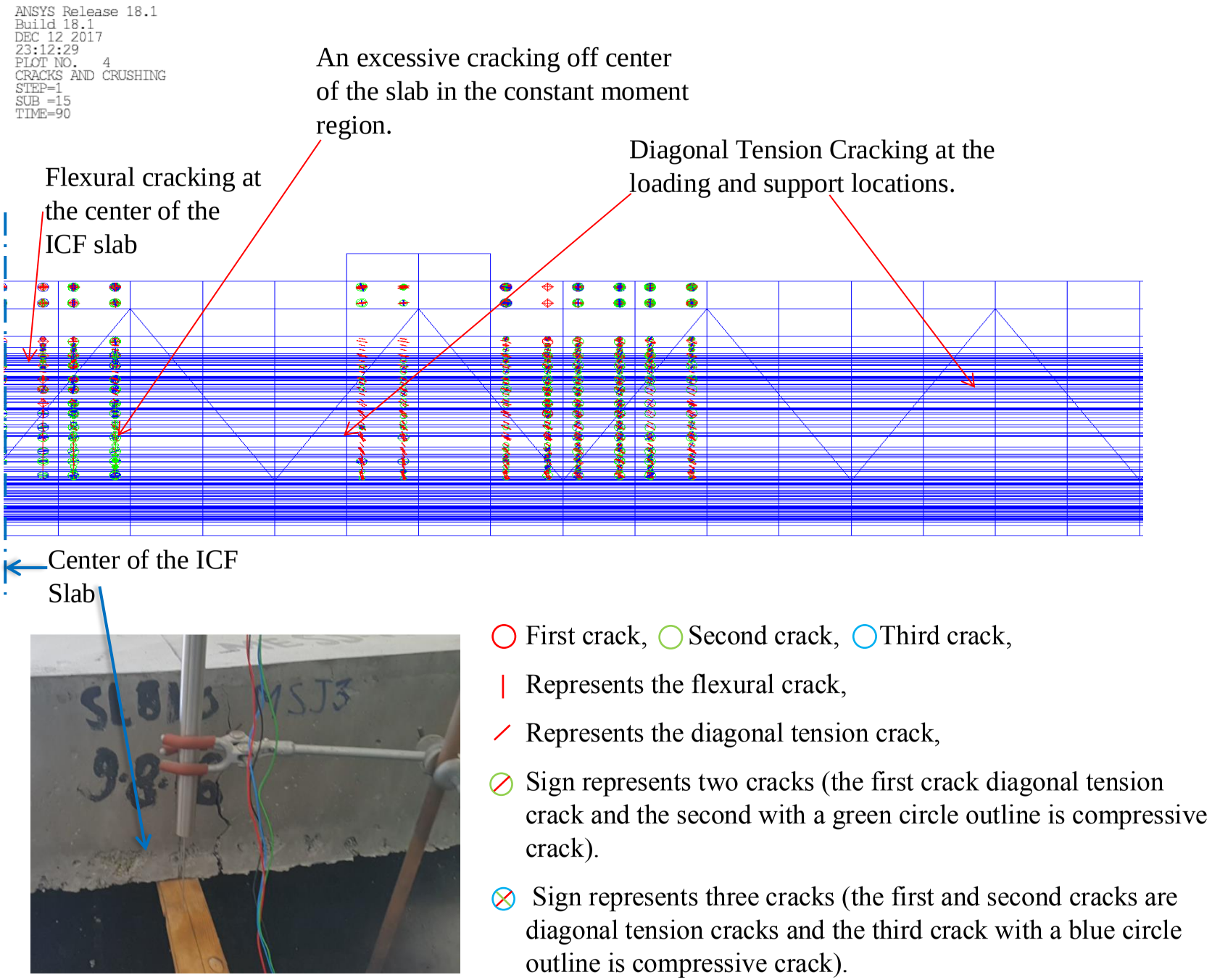


Fig. 140: Chart of cracks in the ICF slab category MSJ at failure.

4.1.1.8 ICF Slab MSJ of Different Spans vs RCC Slabs

The validation and acceptability of the results between experimental work and the finite element analysis by using ANSYS have proven the usability of the ICF slabs in practice. Hence it is decided to investigate the load carrying capacity of these slabs for different span lengths, and also to compare the results of the ICF slabs to the RCC slabs presented in the literature review (chapter 2) by Al- Azzwi, Adel A.

Table 44 demonstrates the UDL(kN/m) load and pressure capacities of the commonly used slab span lengths (2m, 4m, and 6m) in residential buildings with constant widths of 900mm of the ICF slabs (Category MSJ-B) see Figure 141, that were analyzed and validated by FEM. The ICF slabs with spans 2m and 4m, have uniformly distributed loads of 39 kN/m2 and 9 kN/m2, respectively, which are equal or exceed to the uniformly distributed imposed load of 5 kN/m. However, MSJ-B3 with 6m span and 230mm thickness, failed because the imposed UDL of 6.2 is graeter than the UDL capacity of the slab, therefore cross-section size and reinforcement need to be rectified.

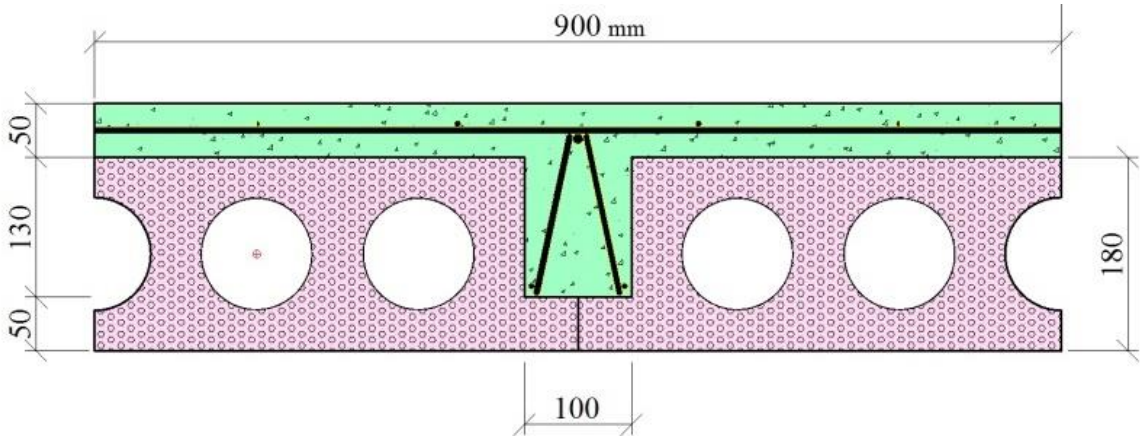
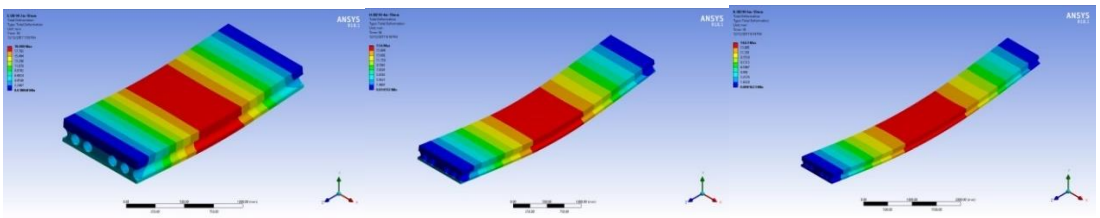


Fig. 141: Cross-section details of MSJ-B slabs

Table (44) Comparison between different spans of ICF Slabs (Category MSJ-B)

Specimens	Span (m)	Thickness (mm)	Residential Service Load (kN)	Imposed UDL (kN/m)	$P_{u\text{-}FEM}$ (kN)	UDL Slab Capacity (kN/m)
MSJ-B1	2	180	10	5	78	39
MSJ-B2	4	180	20	5	36	9
MSJ-B3	6	230	37.2	6.2	30	5

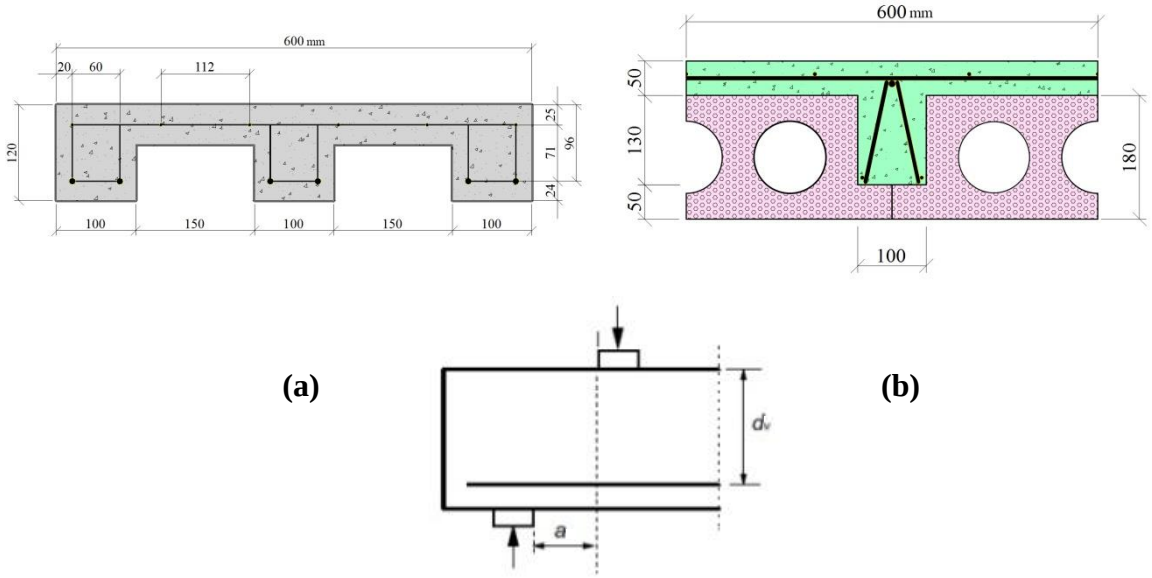


(a) **(b)** **(c)**

Fig. 142: Deflections curves of ICF slabs of category MSJ, (a) 2m span, (b) 4m span, (c) 6m span

Table 44 shows AI- Azzwi ribbed slabs models, HS6-A and HS14-A samples, which are having dimensions of length (L) = 1100 mm, width (B) = 600 mm and effective depth (d_v) = 96mm and shear span (a) = 300mm, also having three ribs and a weight reduction of 29.2%, in comparison with the RCC solid slab. The ICF slab (Category MSJ-A), have the same dimensions except for the effective depth (d_V) = 170mm, involving only one rib and a weight reduction of 40%, in comparison with the RCC solid slab. The ICF slab (Category MSJ-A), have a shear span/d_v ratio of 2.06 which makes it in a pure shear area and 100% resisted by Nano-concrete only, (as per ACI 318-02 for a/d_v =< 2.5 gives pure shear failure for short beams), the 1.1m short span and greater depth yields a shear failure mode, because there is almost zero deflection for high load. Moreover, the opposite, for Al Azawi RCC ribbed slab, which has a shear span/d_v ratio of 3.125 that makes it yields a Shear failure with the very small elastic region Figure 144 (a), (b). However, this small span lengths and section depths are not ideal for practical application and comparisons.

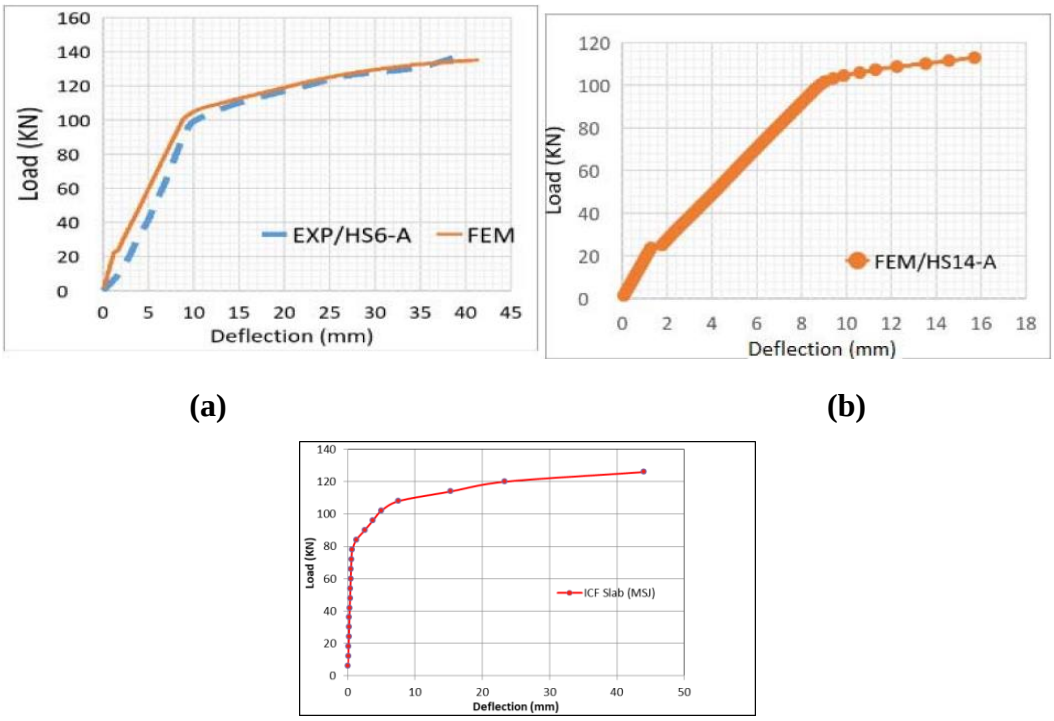
Therefore lager span lengths models with 2m spans were used for the same. However, AI- Azzwi RCC samples, HS6-A and HS14-A and the ICF slab (Category MSJ-A), have ultimate loads of 139.4kN, 112.9kN and 126kN, respectively, which are within the satisfactory range of AI- Azzwi.



(a) **(b)**

(c)

Fig. 143: Cross-section details of, (a) HS6-A, HS14-A, (b) MSJ-A slabs (c) shear span



(a) **(b)**

(c)

Fig. 144: Load-deflection curves of, (a) HS6-A, (b) HS14-A, (c) MSJ-A slabs

Table (45) Comparison of 1.1m spans of RCC ribbed slabs and ICF slabs MSJ-A

Specimens	a/d_v	R_w %	Comp. Strength (Mpa)	$P_{u\text{-}EXP.}$ (kN)	$P_{u\text{-}FEM.}$ (kN)	$\Delta_{u\text{-}EXP}$ (mm)	$\Delta_{u\text{-}FEM}$ (mm)	Failure mode
HS6-A	3.125	29.2	37	139.4	135.2	39.84	41.5	Shear failure
HS14-A	3.125	29.2	27	128.3	112.9	36.1	16.6	Shear failure
MSJ-A	2.06	49.8	23	x	126	x	44	Shear-ductile failure

Table (46) Comparison of 2m spans of RCC ribbed slabs and ICF slabs

Specimens	a/d	R_w %	Comp. Strength (Mpa)	$P_{u\text{-}FEM.}$ (kN)	$\Delta_{u\text{-}FEM}$ (mm)	Failure mode
HS6-A2	6.25	29.1	37	66	20	Shear failure
HS14-A2	6.25	29.1	27	54	25	Shear failure
MSJ-A2	3.53	49.8	23	84	35	Shear-ductile failure

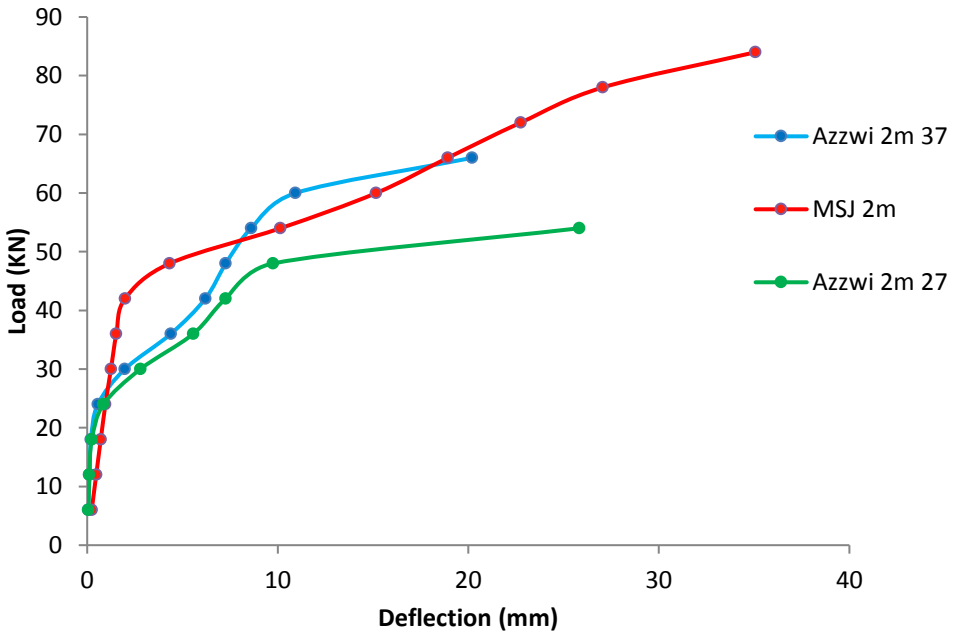


Fig. 145: Load-deflection curve of RCC ribbed & ICF slabs, (a) HS6-A2, (b) HS14-A2 and (c) MSJ-A2

The same set of AI- Azzwi ribbed slabs and the ICF slab (Category MSJ-A2) FEM model were analyzed, but with twice the span length of 2m, and a shear span of (a) = 600mm. Table 46 shows the results, the RCC ribbed slabs HS6-A2 and HS14-A2 yielded flexural-ductile failure mode, but again with the very small elastic region see Figure 145. Nevertheless, they lost about 51% to 52% of its ultimate load capacities, which reduced to 66kN and 54kN respectively. The MSJ-A2 model lost only 30% of its ultimate load capacity (84kN) with a very safe and stable failure mode (Shear-ductile failure, controlled by a combination of shear and flexural behaviors), having sizeable elastic region.

Moreover, the RCC ribbed slabs, HS6-A2 and HS14-A2, are even still less in the ultimate carrying capacities than the ICF slab (Category MSJ-B) ultimate carrying capacity of 78kN, that is having span length of 2m, and fascinatingly a total width of 900mm with one rib only. Also, laying and fixing the polystyrene shaping panels for the RCC ribbed slabs would be a challenging job, unlike the self-supported Blank Block.

The approach then further utilized to investigate the load carrying capacity of the ICF slabs for further longer span lengths with the same spacing of 600 mm between the ribs, having spans of 6, 7 and 8 meters. Table 48 shows the results for the ICF slabs MSJ-T1, MSJ-T1 and MSJ-T1 that yielded flexural-ductile failure mode, with reasonable elastic region Figure 147. The ICF slabs with spans 6m and 7m, have Ultimate UDL (Ansys) of 8.33 kN/m2 and 6.85 kN/m2 (Ansys results), respectively, which exceed to the imposed UDL (code, calculated) of 5.7 kN/m. the sections are valid for deflections see Table 47. However, MSJ-T3 with 8m span, worked with the rectified 230mm thickness, the imposed UDL of 6.5 is less than the Ultimate UDL of the ICF slab of 7.5 kN/m. (Section is valid).

Table (47) MSJ-T deformation check

Deformations Check			
SPAN (m)	DEFLECTION LIMIT (mm)	ANSYS \ SERVICE LOAD (Mpa)	Δ @ SERVICE LOAD (mm)
6	12	34.2	7.22
7	14	39.9	12.65
8	16	52	12.25

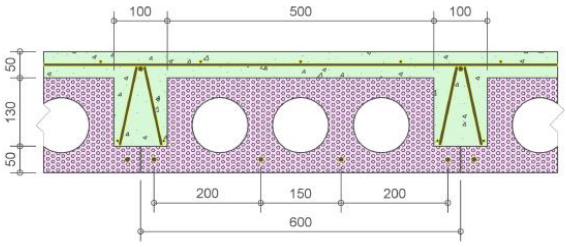
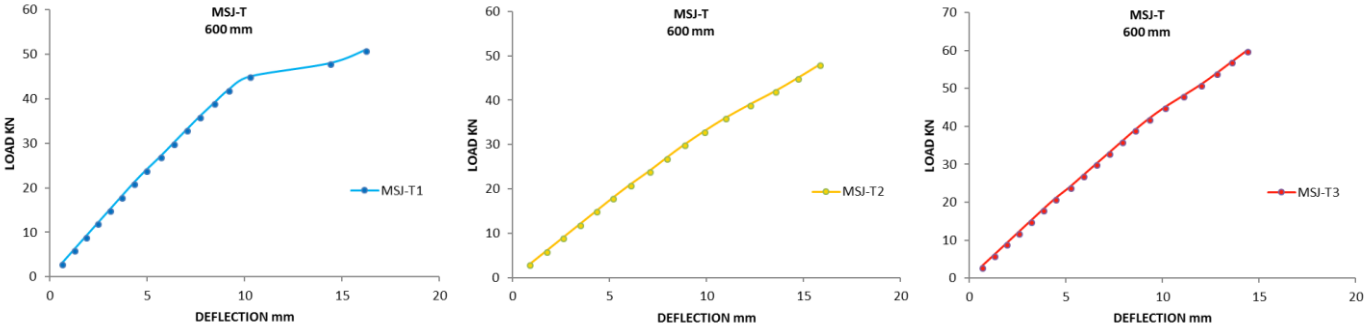


Fig. 146 MSJ-T group cross-section

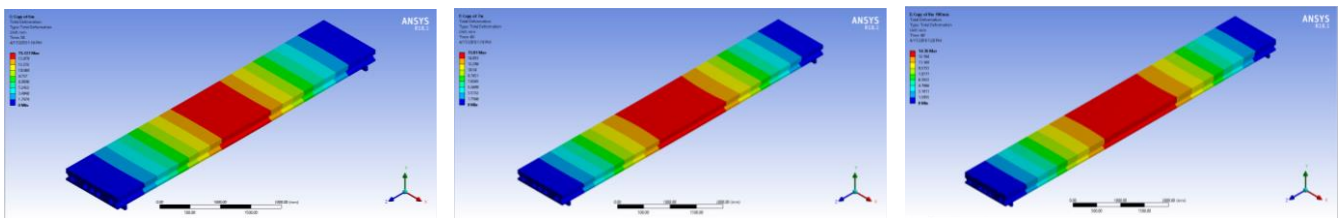
Table (48) MSJ-T span comparison

Specimens	Span (m)	Thickness (mm)	Residential Service Load (KN)	Imposed UDL (KN/m)	$P_{u\text{-}FEM}$ (KN)	Ultimate UDL (KN/m)
MSJ-T1	6	180	34.2	5.7	50	8.33 OK
MSJ-T2	7	180	39.9	5.7	48	6.85 OK
MSJ-T3	8	230	52	6.5	60	7.5 OK



(a) **(b)** **(c)**

Fig. 147: Load-deflection curve (a) MSJ-T1 (b) MSJ-T2 (c) MSJ-T3



(a) **(b)** **(c)**

Fig. 148: Deflection contours (a) MSJ-T1 (b) MSJ-T2 (c) MSJ-T3

4.1.2 ICF Walls

4.1.2.1 Wall ICF-04

The load of 398 kN with constant load step rate of 6 kN was applied on the ICF-04 wall. Horizontal and vertical cracks are observed at the top corner. Otherwise, the wall has remained intact. This happened because the capacity of the loading frame is achieved which was expected at the time of initial casting itself. The tested wall is shown in Figure 83. The deformation observed in FE model is shown in Figure 149.

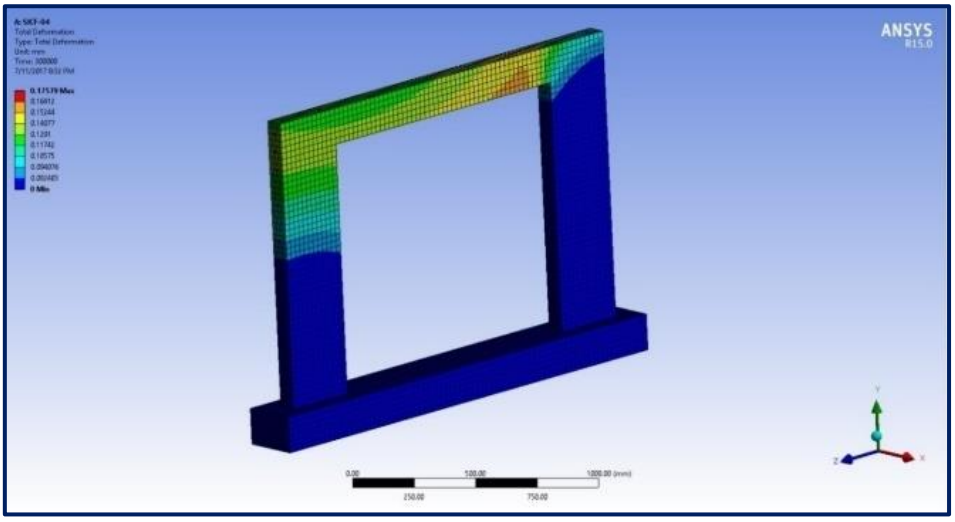


Fig. 149:Deflection contours of wall ICF-04

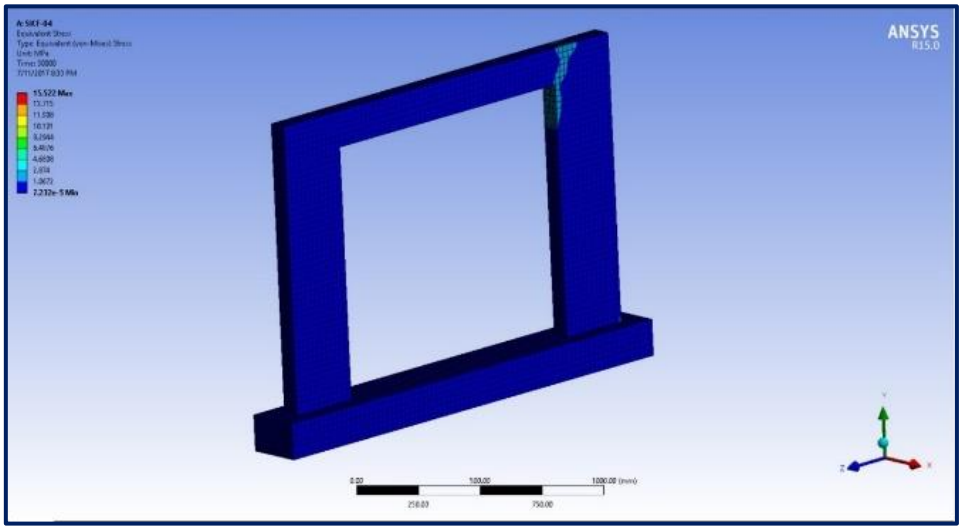


Fig. 150: Stress contours of wall ICF-04

Two strain gauges on the concrete surface are applied on the top corners of the wall. Table 49 shows the maximum strains for strain gauges (1) and (2) were (0.00017) and (0) respectively, whereas the same strains derived from FEM are (0.00045) and (0.000073) respectively. Moreover, the location of stress development has shown good agreement with the stress contours developed in the analytical model in ANSYS as per Figure 150.

4.1.2.2 Wall ICF-06

The load of 400 kN with constant rate was applied to the wall. Nothing has happened to the wall frame as the thickness is high and opening size is less in comparison. This happened because the capacity of the loading frame achieved which was expected at the time of initial casting itself. The tested wall is shown in Figure 85. The deformation observed in FE model is shown in Figure 151.

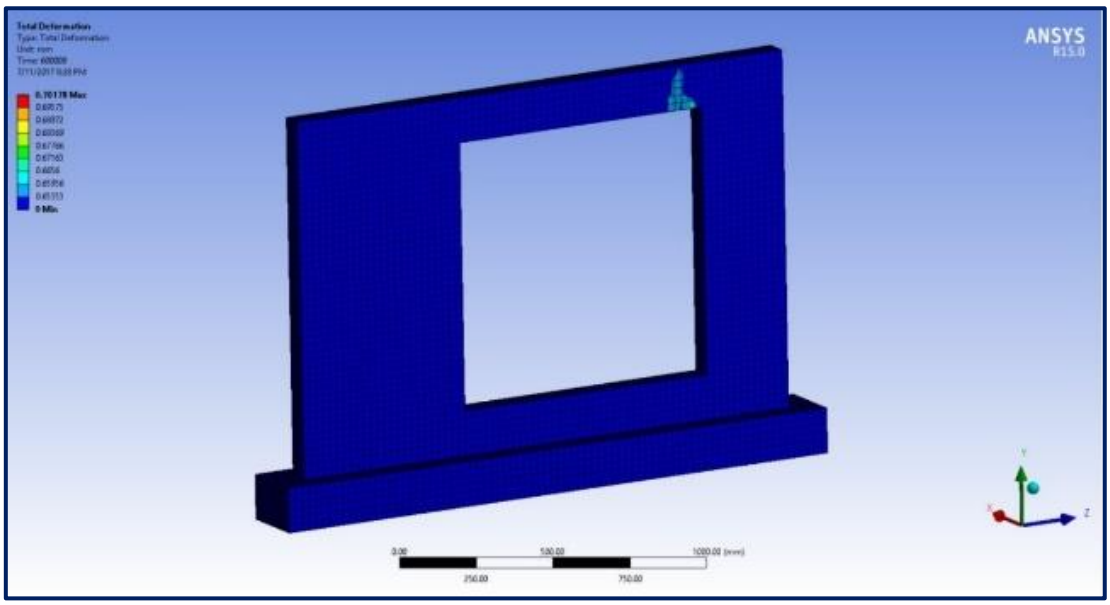


Fig. 151: Deflection contours of wall ICF-06

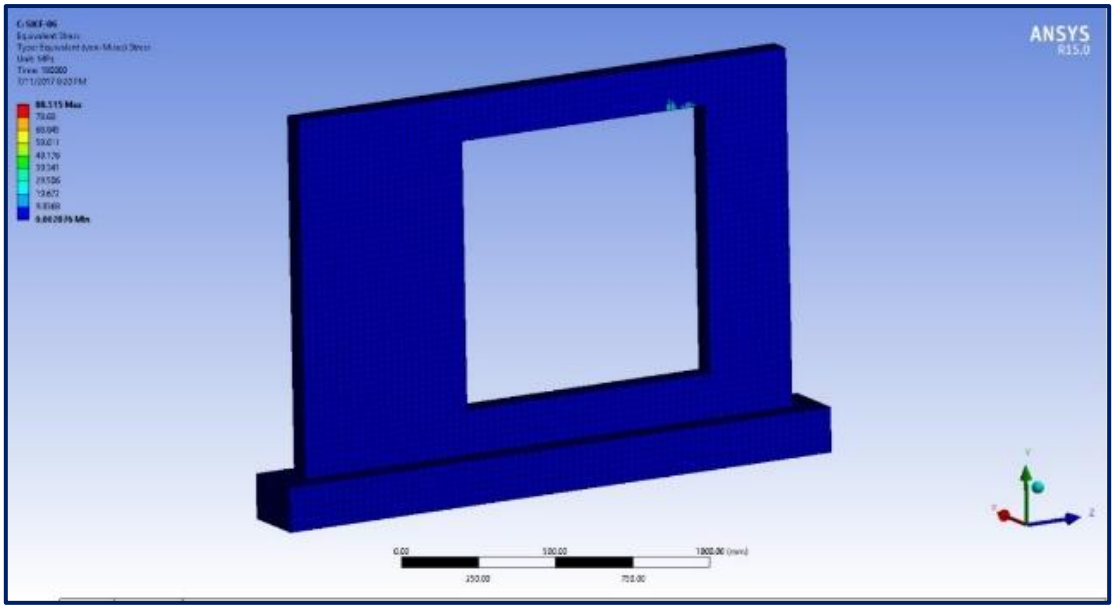


Fig. 152: Stress contours for wall ICF-06

Two strain gauges on the concrete surface are applied on the top corners of the wall. Table 49 shows the Maximum strains for strain gauges (1) and (2) were (0.00053) and (0) respectively, whereas the same strains derived from FEM are (0.0006) and (0.000068) respectively. Moreover, the minimum stress development (derived from strain data) has shown good agreement with the uniform stress contours developed in the analytical model in ANSYS as per Figure 152.

4.1.2.3 Wall ICF-09

The load of 300 kN with constant rate was applied to the ICF-09 wall. Because of the less thickness and large opening, it has failed from both of the top corners. The tested wall element is shown in Figure 87. The deformation observed in FE model is shown in Figure 153.

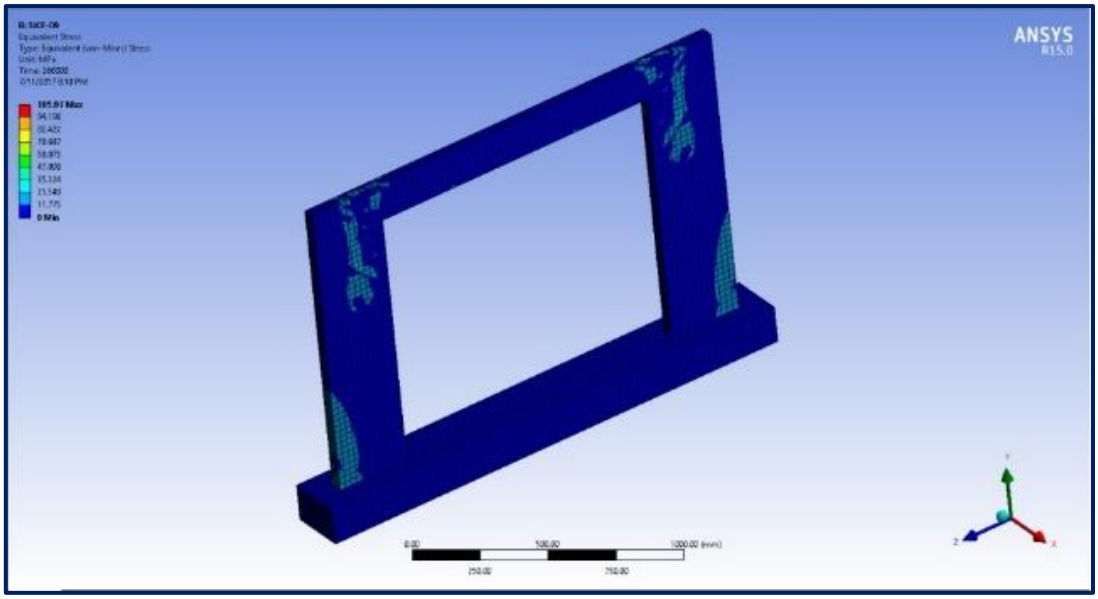


Fig. 153: Deflection contours of wall ICF-09

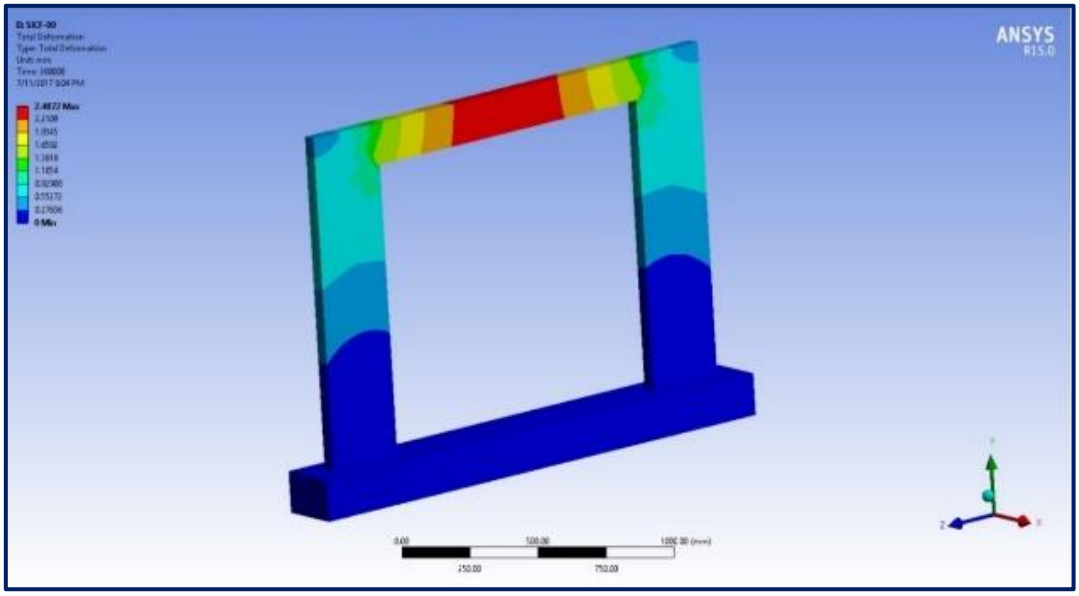


Fig. 154: Stress contours for wall ICF-09

Two strain gauges on the concrete surface are applied on the top corners of the wall. Table 49 shows the maximum strains for strain gauges (1) and (2) were (0.0054) and (0) respectively, whereas the same strains derived from FEM are (0.0081) and (0.018) respectively. Moreover, the maximum stress development (derived from strain data) have developed in

the top corners which have shown good agreement with the higher stress contours developed at the same location in the analytical model in ANSYS as per Figure 154.

4.1.2.4 Wall ICF-11

The load 400 kN with constant rate was applied to the ICF-11 wall. Because of the less opening in wall load distribution has taken place evenly and nothing has happened to the wall. The tested wall element is shown in Figure 89. The deformation observed in FE model is shown in Figure 155.

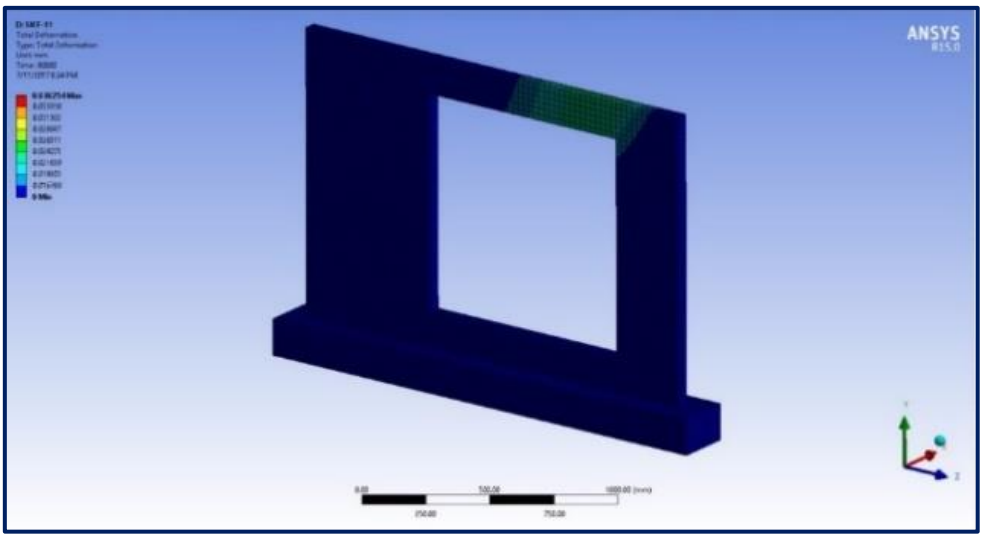


Fig. 155: Deflection contours of wall ICF-11

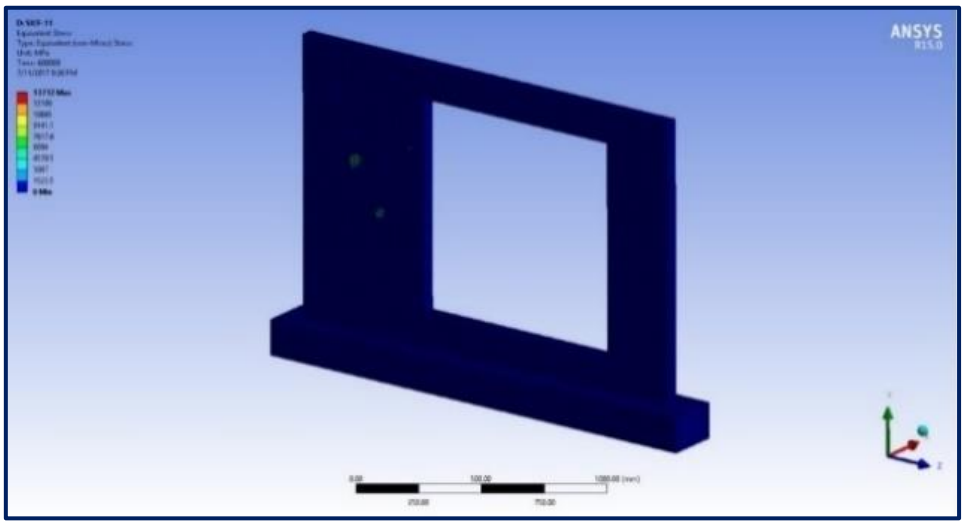


Fig. 156: Stress contours for wall ICF-11

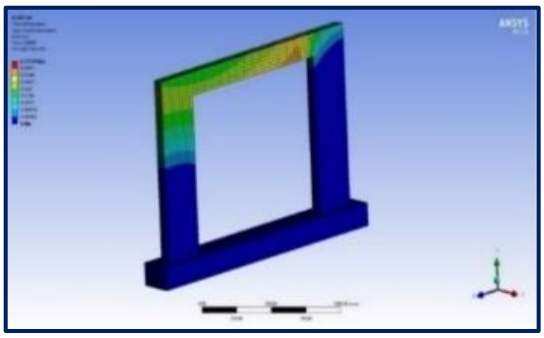
Two strain gauges on the concrete surface are applied on the top corners of the wall. Table 49 shows the maximum strains for strain gauges (1) and (2) were (0) and (0) respectively, whereas the same strains derived from FEM are (0.00027) and (0.0124) respectively. Moreover, the minimum stress development (derived from strain data) has shown good agreement with the uniform stress contours developed in the analytical model in ANSYS as per Figure 156.

4.1.2.5 ICF Walls Experimental and FEM results Comparison

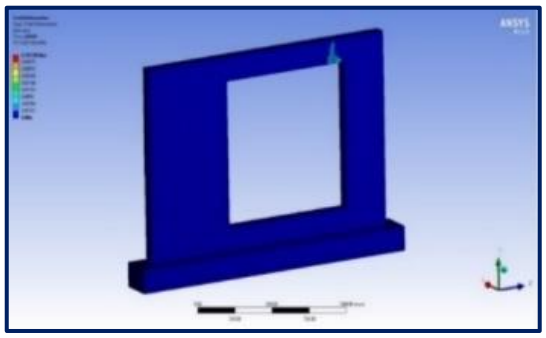
The experimental and the numerical results that are shown in Table 49 and Figures 157 are comparable and convincing results between all ICF walls, nevertheless many reasons could be behind such differences; the first could have been very much related to the presence of the micro-cracks and macro-cracks which introduced by drying shrinkage in the experimental specimens, and also happened during transporting the stand-alone slender ICF walls from the erection site to UOB structural laboratory, unlike the numerical model. The second assumption, even though, some of the numerical models simulated the problems with acceptable correctness, the diffrences between experimental and finite element results presented in Table 49 influenced same FEM factors mentioned above in the case of the ICF slabs. Finally, in all the ICF walls, the Universal testing frame capacity reached of 400 kN without any effect. For ICF wall 09, the strain gauges reading are reasonable. Nano-concrete max. strain exceeded of 0.0014, Therefore, failed.

Table (49) ICF walls experimental and numerical strain results

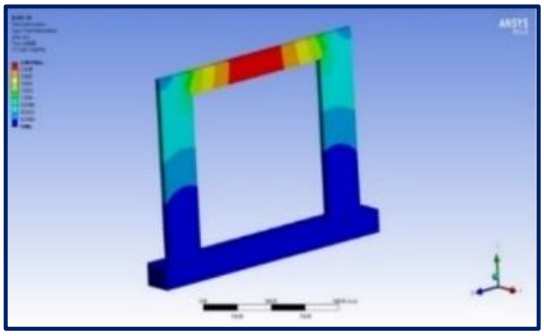
	Exp. Model Strain Results				Ansys Model Strain Results			
ICF Wall Specimen	Load 1 kN	Max. Strain 1	Load 2 kN	Max. Strain 2	Load 1 kN	Max. Strain 1	Load 2 kN	Max. Strain 2
ICF 04	312	0.000173	316	0	310	0.00045	316	0.000073
ICF 06	256.4	0.000532	335.4	0	240	0.0006	335.4	0.000068
ICF 09	310	0.00542	318.4	0	280	0.0081	318.4	0.018
ICF 11	382.6	0	382.6	0	382.63	0.00027	382.63	0.0124



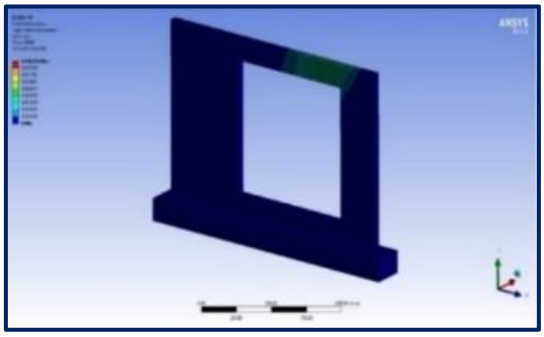
ICF-04 (75 mm TH.)



ICF-06 (75 mm TH.)



ICF-09 (50 mm TH.)



ICF-11 (50 mm TH.)

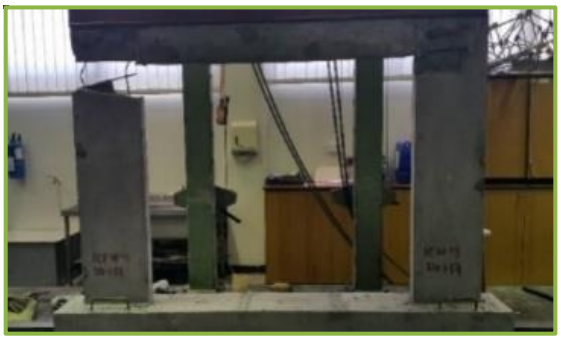
Fig. 157: Analytical model of wall deflections



ICF-04 (75 mm TH.)



ICF-06 (75 mm TH.)



ICF-09 (50 mm TH.)



ICF-11 (50 mm TH.)

Fig. 158: Experimental failure details of ICF walls

4.1.3 3D ICF Building Design Example

Finally, a three-dimensional ICF building design example of a residential five stories is analyzed by Ansys, modeled with ICF walls and ICF slabs(MSJ), A simple rectangular (4 by 8 m) house plan in this example. It has a ridge roof line parallel to the (8 m) dimension. Uniformly distributed service loads of 0.625 kN/m^2 applied on all the ICF slabs in the vertical direction, and a lateral wind load of 0.012 kN/m2 applied in the horizontal direction on each floor.

(Neal, 1963), formally expressed the so-called static and kinematic theorems, that underlying the plastic design approach to structural safety, require that any set of factored loads applied to a structure (any load case) satisfy two conditions:

- The external loads produce a distribution of internal forces that satisfies equilibrium.
- Moreover, any localized regions of contained plastic flow (yielding or cracking) are not sufficient to form a collapse mechanism for any part of the structure.

When these two conditions are satisfied for all parts of the structure, then the loading is and must be, less than the collapse (failure) load for the structure. In short, by the static theorem, a structure can demonstrate its safety (not in danger of collapse) and, subsequently, need only to satisfy serviceability requirements such as limitations on deflections, wind-borne projectile resistance, and the effect of load cycles or reversals to ensure an acceptable structural design.

The results in Figures 159 and 160 show the maximum deflection and maximum stress developed in the ICF 5 story building, are 0.00657mm and 0.2MPa respectively, Which was not sufficient to form a crack or collapse mechanism.

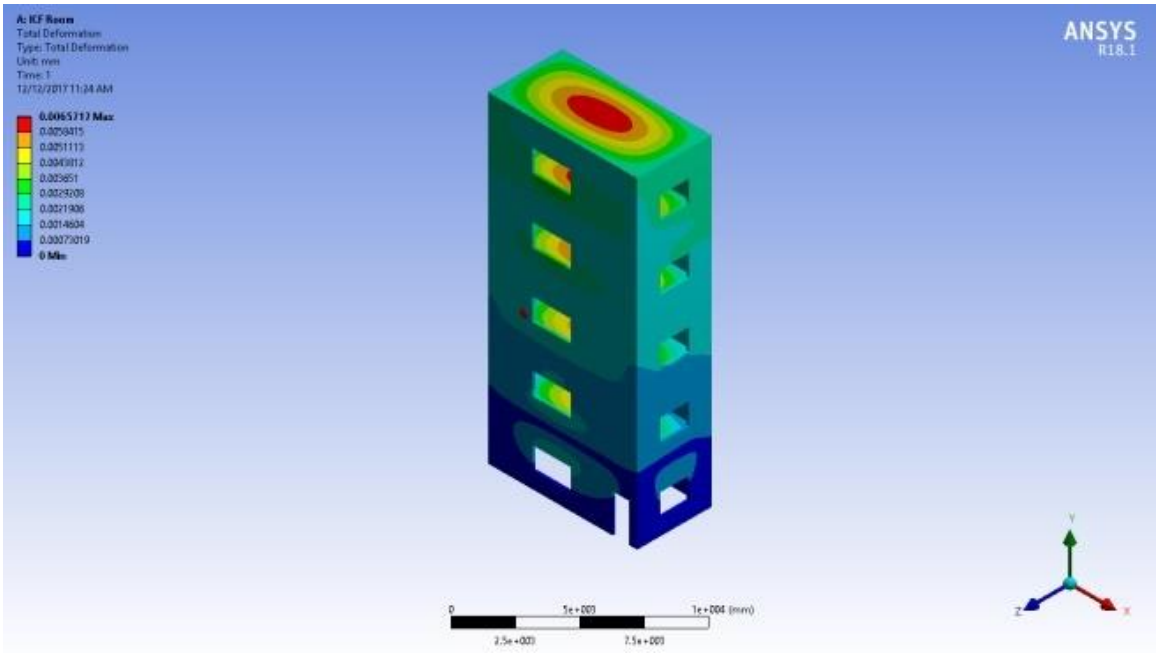


Fig. 159: Deflection contour of the ICF residential building

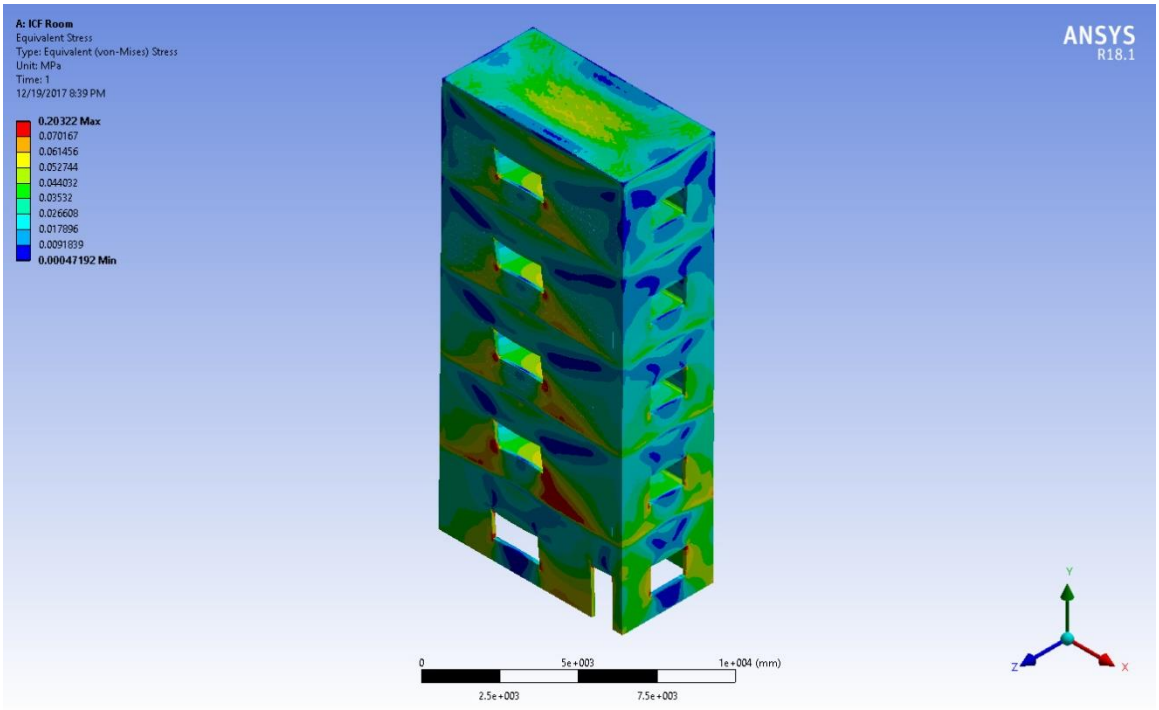


Fig. 160: Stress contour of the ICF residential building

4.1.4 Effect of Thermal Properties on Energy Saving

The most advantageous properties of ICF system is its thermal characteristics. The concept provides minimum heat and cold loss due to its less thermal conductivity. Thermal bridges are weaknesses within a building's structure where heat and cold are transferred at a substantially higher rate than through the surrounding envelope area.

It occurs when heat flow bypasses the insulated elements of the building enclosure. Bridging occurs through structural components such as the studs/plates, framing, and cladding supports as well as the larger columns, shear walls, and exposed floor slab edges and protruding balconies. While thermal bridging occurs through the roofs, floors, and below-grade assemblies, it is often most pronounced in above-grade wall assemblies. The heat flow through thermal bridges is significant and disproportionate to the overall enclosure area so that a seemingly well-insulated building can often fail to meet energy code requirements, designer intent, or occupant expectations.

Reducing thermal bridging saves on energy costs by minimizing the amount of heat transferred through the building envelope the floor, walls, roof, doors, and windows separating the interior and exterior environments. Here, ICF system proves to be the best thermal bridge to minimize the heat and cold loss.

In an analytical investigation at the University of Bahrain, three types of building systems have been considered for the comparison namely T3M House Unit (Appendix I), EIFS (Exterior Insulating Finishing System) and Gulf Polyforms System (ICF System). The results of the comparative study are shown in Table 50. It can be observed that the overall electrical consumption and its costing are lowest in case of Gulf Polyforms Systems. CO_2 emission also has remained lowest in comparison

of all the three systems. Hence, it can be concluded that the ICF systems are most economical, from the life cycle cost analysis point of view as well as environmentally friendly.

Table (50) Electrical consumptions for different building systems

Energy Consumption by Target	T3M House	EIFS system	Gulf Polyforms
Solar Gain (KWh/a)	8869.7	6613.4	2361.6
Cooling (KWh/a)	46168.3	37128.2	24536.6
Electricity (KWh/a)	43327	24588	19918
Total Energy Consumption (KWh/a)	85919	55691	40554
CO_2 Emission (KWh/a)	10294	5842	4732
Cost (BD/a)	1299	737	597

Figure 161, 162 and 163 shows the thermal view obtained from the above-mentioned investigation, of all the three systems T3M House Unit, EIFS System, and Gulf Polyforms System respectively. It can be observed from the figures that Gulf Polyforms Systems seems to be the best system from thermal conductivity point of view.

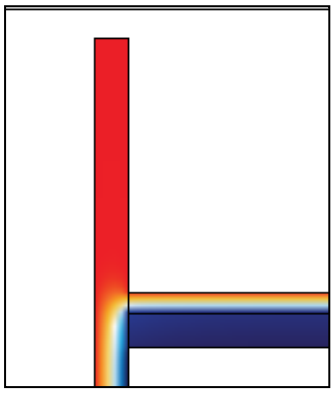


Fig. 161: Thermal analysis of T3M house system

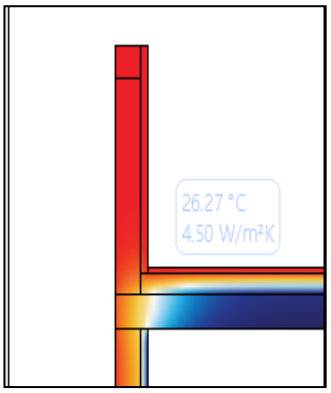


Fig. 162: Thermal analysis of EIFS system

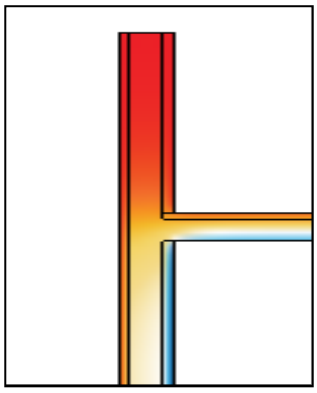


Fig. 163: Thermal analysis of Polyforms system

In another study, three different systems concrete walls and insulated core slab, masonry blocks and insulated core slab and Polyforms system

have been compared. K values of the different materials used are shown in Table 51. Figure 164 are showing the FEM thermal view of concrete walls and insulated core slab, masonry blocks and insulated core slab and Polyforms system respectively. It is apparent from the figures that the polyforms system has slowed the passage of the conducted heat and reduced the defamations compared to the traditional constructions. Hence, the thermal bridging eliminated, and the thermal insulation preserved throughout the building.

Table (51) K values of different materials used in building systems

	K value (W/mK)	Concrete walls and insulated Core Slab	Polyforms System	Masonry Block and insulated Core Slab
Plater	1.065	✓	✓	✓
PU Foam	0.024	✓		✓
Masonry Block	1			✓
Polystyrene panels	0.032		✓	
Normal Concrete	2.25	✓	✓	✓
Lightweight Concrete	1.45	✓		✓
Nano Concrete Wall (CSC1-13)	1.065		✓	
Nano Concrete Slab (CSC1-13)	1.065		✓	
Poly. Concrete BB forms	0.325		✓	
Core Slab	0.83	✓		✓

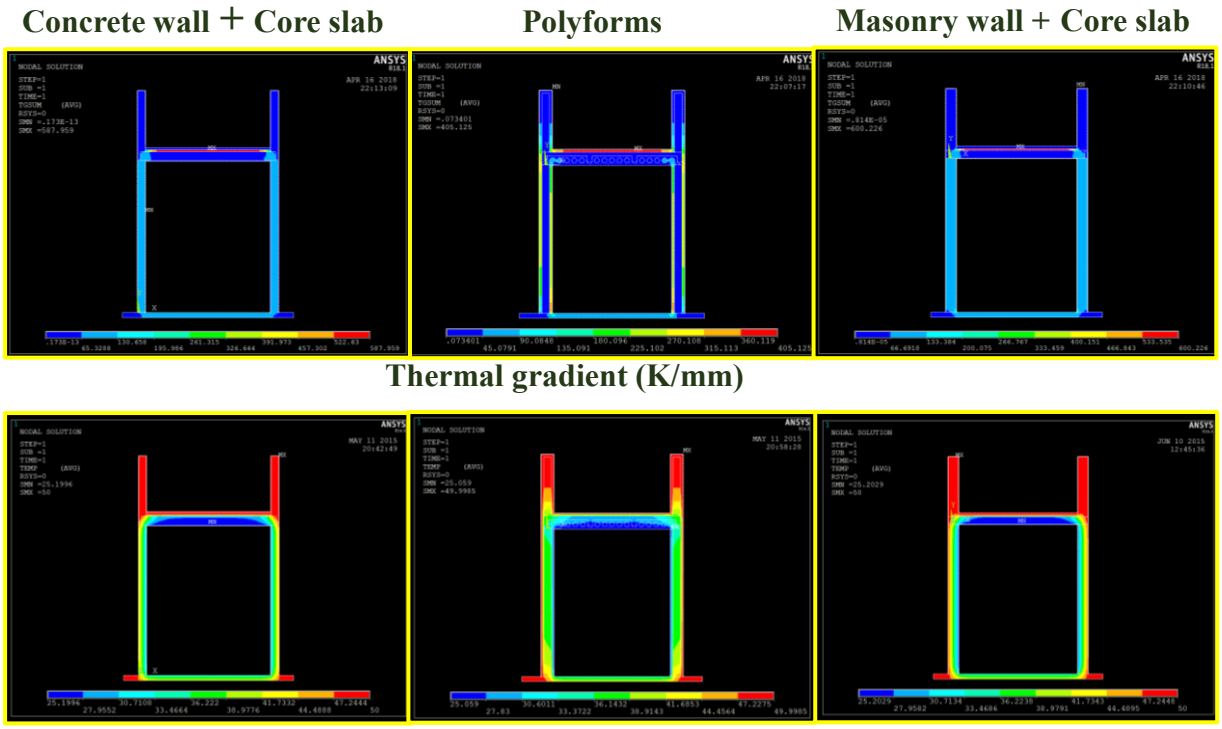


Fig. 164: Thermal deformation (mm)

Table (52) R & U values of different types of walls

Wall Type	Concrete	Masonry	EIFS	Polyforms ICF Wall	Insulation Properties
R-value (M^2.K/W)	0.09	0.23	1.79	3.29	higher numbers better insulation
U-value (W/M2.K)	11.11	4.44	0.56	0.30	Lower numbers better insulation

Table (53) R & U values of different types of slabs

Slab Type	Precast core slab		Polyforms ICF Slab		Insulation Properties
Insulation Type	PU	ESP	PU	ESP	
R-value (M^2.K/W)	3.39	1.69	4.82	2.21	higher numbers better insulation
U-value (W/M2.K)	0.30	0.59	0.21	0.45	Lower numbers better insulation

The R-value measures the tendency of a material to slow the passage of conducted heat, and the U-value determines the heat flow through a given component in the building.

(MEW, 2006), the Ministerial Order No. 8/1999 makes it compulsory to provide thermal insulation in all buildings in Kingdom of Bahrain. The Order stipulates the U value limitations for the thermal insulation materials that are used in roofs and walls of all buildings that require air-conditioning:

1. The overall U-value for the roof should not be more than 0.6 W/m2Co
2. The U-value for external walls should not be more than 0.75 W/m2Co"

Here also the U values of 0.3 for the ICF walls in Tables and U between (0.2-0.44), for the ICF slabs in Tables 52 and 53. Hence, Polyforms system is the best option from thermal conductivity point of view. With these insulation values, the Polyforms system overcomes building location and directions difficulties, such as solar orientation.

4.1.5 Cost Analysis

Cost-effectiveness of ICF system developed in this study is very important because it should be able to compete with existing green building options available in the market. Its construction should be easy and should not need too many labors, and furthermore, it should be profitable. These features of the proposed system are examined in this section.

Industrial data are used to observe the cost-effectiveness specifically in two categories for materials and labor to obtain average cost data for precast ICF wall systems.

4.1.5.1 Cost Analysis in Various Forms

Primary functions of any new system like safety, functional aspects and durability are to comply initially. Then, to have long-term involvement

in the process, it is very much important to compare the cost of any new system with the existing system. Hence, this new ICF system is compared to total constructions cost is compared as mentioned below. A MOH (Type T3M) house model was considered in this study; (Appendix I) for the floor plans.

- ✓ Conventional construction with EIFS
- ✓ Polyforms ICF construction system

4.1.5.2 Cost Comparison of Conventional and Polyforms Construction

Considering all the construction procedures and primary differences of construction activities in conventional and Polyforms construction cost per house is listed in Tables 54 and 55 respectively.

Table (54) Estimated cost of job build EIFS wall

Conventional Construction			
Description	Quantity	Rate BD	Cost BD
Foundation			
Foundation	100 m2	40	4000
Total			4000
Block Work			
External Insulated Block Work	236 m2	9	2600
Internal ordinary Block work	80 m2	7.5	600
Internal Block work 150mm	62 m2	6.5	403
Filled Block work Main walls	51 m2	10.5	535
Filled Block work for Parapet	10 m2	10.5	105
Total			4243
RCC work			
Lentils Cills and Beams	8 m3	120	960
Stair Case	5 m3	160	800
RCC Sunken Slabs	1.5 m3	140	210
Total			1970
Main Slabs			
Core Slabs	220 m2	8.5	1870
Total			1870
Finishing Items			
Exterior Iinsulation Finishing System (EIFS)	460 m2	17.5	8050
Internal Plastering	600 m2	2.4	1440
External Wall Painting	460 m2	2	920
Internal Paintring	600 m2	2.2	1320
Ceialing Painting	150 m2	1.8	270
Floor Screed	180 m2	3.5	630
Wall Tiling	115 m2	4.5	517.5
Floor Tiling	32 m2	4.5	144
Wall Skirting	14.5 m2	4	58
Weatherproof Ceiling Tile	32 m2	6	192
Door + Shatters + Iron Mangory			2000
Aluminum Windows			1200
Kitchen + Kitchen Top			500
Staircase Hand Rail	12 m	120	1440
Plumbing Work			1500
Electrical Work			1500
Water Pumps + Tanks			250
Mescilenius			500
Total			22431.5
Water Proofing			
PU Foam	95 m2	6	570
PVC membrane	95 m2	2	190
Screed	95 m2	3	285
Total			1045
Grand Total			35559.5

Table (55) Estimated cost of industrial build ICF wall

Polyforms Construction					
Description	Quantity		Area	Rate BD	Cost BD
Foundation					
Foundation			100 m2	40	4000
Total					4000
Wall Element					
Polystyrene panles m2	439.0	0.3	2926.7	0.6	1837.9
Lightweight Concrete m3	70.4			30.5	2146.9
Fasteners	4.0		1463.3	0.1	585.3
Horizontal Reinforcement kg/m2	2.2		439.0	0.2	183.2
Vertical Reinforcement	1.8		439.0	0.2	146.9
EPS Plaster			878.0	2.2	1931.6
Total					6831.9
RCC work					
Lentils Cills and Beams			8 m3	120	960
Stair Case			5 m3	160	800
RCC Sunken Slabs			1.5 m3	140	210
Total					1970
Main Slabs					
Core Slabs			220m2	7	1540
Total					1540
Finishing Items					
External Wall Painting			460 m2	2	920
Internal Paintring			600 m2	2.2	1320
Ceialing Painting			150 m2	1.8	270
Floor Screed			180 m2	3.5	630
Wall Tiling			115 m2	4.5	517.5
Floor Tiling			32 m2	4.5	144
Wall Skirting			14.5 m2	4	58
Weatherproof Ceiling Tile			32 m2	6	192
Door + Shatters + Iron Mangory					2000
Aluminum Windows					1200
Kitchen + Kitchen Top					500
Staircase Hand Rail			12 m	120	1440
Plumbing Work					1500
Electrical Work					1500
Water Pumps + Tanks					250
Mescilenius					500
Total					12941.5
Water Proofing					
PVC membrane			95 m2	2	190
Total					760
Grand Total					27473.403

It can be observed from the Tables 45 and 55 that difference of construction cost between conventional and a Polyforms construction is BHD 8086.097 (22.73 %) per house Unit in Bahrain (Type T3M). Which is a considerable saving in the initial investment of the housing projects Although this is not yet the final savings; Polyforms construction also reduces the operation cost by consuming less energy throughout the day. Details of the thermal analysis are mentioned in subsequent sections.

4.1.5.3 Discussion on Cost Analysis

The results of the cost analysis show that Polyforms construction system is 22.73% less at of initial cost compared to conventional job built EIFS construction system. It is worthy to mention that Polyforms construction system is cost efficient regarding material, formwork, and labor, and environmental friendly as well. When one would think about life cycle cost analysis then due to higher thermal insulating properties, such construction system will be highly profitable.

The results also showed that implementing innovative sustainability concepts in residential construction process did not affect its cost competitiveness.

The proposed system was shown to be sustainable, cost-competitive, environmentally friendly and structurally safe.

4.2 Conclusions

In this research work, the experimental and analytical investigation has been carried out on the ICF slabs and walls. Total five types of slabs specifically one Blank Block and four slabs, as well as four types of the ICF wall with different configurations, have been cast at Bardex Industries, Bahrain. Three elements in each category of slabs and one element of the

wall have been tested at Structures Laboratory of the University of Bahrain. Conclusions derived from the study have been listed below.

- Nano-concrete can be identified as a suitable material to replace the ordinary concrete.
- The ICF MSJ slabs and ICF walls systems passed the serviceability as well as strength tests.
- The assumption for the 4M pre-stressed Blank Block to carry the wet concrete and labors without supports was not fulfilled, however, the primary function of the "Blank Block", of acting as formwork during construction over which essential structural slab layer of Nano-concrete shall be applied, thus a prop at every (1 m) is required, with an alternative further "Blank Block" design is proposed.
- It opens the doors for the civil engineering field to implement and adopt this novel methodology for similar experimental and analytical studies in exploring and developing new composite materials and adding green values to the building constructions industry.
- To the best of my knowledge, and based on the extensive literature review carried out in this study, it can be concluded that there is no such study exist, that integrates a green construction system and satisfies the main criteria of LEED-like environmental, economic, health and safety aspects as such.
- The primary function of this polystyrene concrete blank Block is to act as formwork during construction over which essential structural slab layer of Nano-concrete shall be applied. This blank Block has taken a total load of 7 kN at ultimate which is almost equal to the service load of (6.68 kN) imposed by the fresh Nano-concrete and labor weights.
- ICF slab system contributed to the weight reduction by 40.8% to 68.69% (Appendix G) for RCC ribbed slabs and solid slabs

respectively, which could lead to the same reductions in the overall initial construction cost of slabs, especially in large projects.

- The Nano-concrete contributed to the resistance of shear, due to its linear nature of its stress-strain relationship that was dominated by shear only. Moreover, Nano-concrete can be identified as a suitable material to replace the ordinary concrete.
- Hollow core provided can be used as conduits for various functional services at the same time it increases the moment of inertia of the section which helps in reducing the overall deflection of the section.
- Slabs with lattice girder of category J performed better, compared to slabs with two bars of category S in the rib.
- In the slab system with a mesh of category MS & MSJ and without mesh of category S & J in the top Nano-concrete layer, a stable behavior observed in the slabs with mesh that is in MS and MSJ.
- Out of four systems developed for the comparative study, the provision of the lattice girder and the mesh in the ICF slabs category MSJ (the best performer), improved the strength, failure mode as well as serviceability, especially over regular RCC ribbed slabs.
- Single crack at the centerline drawn up in the categories S, MS and J where two cracks are developed near to the load points in category MSJ. This happened due to combined contribution of lattice girder and mesh provided at the top. Because of this only category, MSJ could bear more loads, due to the even distribution of the loads across the section.
- The behavior of category MS and J have remained almost similar regarding first crack load, ultimate load, and maximum deflection. However, category MS can be considered superior compared to J, because the upper mesh reinforcement provided, remains close to the value of the yield stress with elastic behavior, and this contributes in restricting the development of the vertical cracks and its penetration to

the compression concrete zone. Subsequently, the upper mesh increases the ultimate strength capacity of the ICF slab and improves the failure modes.

- Category MSJ has remained top performer with an average first crack load of 82 kN, ultimate load of 90 kN and ultimate deflection of 12.64 mm.
- Sudden failure with minor deflection observed in case of Blank Block. Where all other types of slabs, have shown ductile failure and deflection as a warning of collapse.
- Slabs of category S have suddenly failed after crack development in the loading frame itself. Where in other cases all have remained self-supported after failure.
- Nothing has happened to the walls ICF-06 and ICF-11 during loading, despite the fact, that the capacity of the loading frame of 400 kN was reached.
- ICF-09 failed during testing at the load of about 300 kN. The wall specimen has failed from the top corners. Here also two-point load system was applied to the walls at the center. The wall had failed due to stress concentrations at the corners due to loading conditions.
- ICF-04 has observed cracks at the top cornered at the total load of 398 kN. Moreover, complete failure did not happen as compared to ICF-09, Which was due to the higher thickness of the wall in this category.
- Analytical models of slabs have shown good behaviors and results compared to experimental behavior in most of the cases.
- Stress contours developed in the models have shown similar behavior compared to experimental observations.
- The initial cost of Polyforms ICF system construction is 22.73 % less compared to conventional construction system.

- Carbon emission of ICF systems is almost 54.03 % and 19.00 % less compared to D11 house system and EIFS system respectively.
- Total electrical consumption is 54.02 % and 18.99 % less compared to D11 house system and EIFS system respectively.
- ICF system is proved to be environmentally friendly and economical solution compared to any other conventional system.
- The innovative designs of the Polyforms ICF system regarding geometry, dimensions and the lightweight materials used, contributed in construction time and cost reductions, structural strength, stability, and safety.

4.3 Future Work

Following are the future recommendations to improve the applicability of ICF systems in civil engineering.

- Various durability tests should be done on polystyrene concrete.
- Strain gauges should also be used for measuring the steel reinforcement strains.
- The structural effects of the steel fasteners in the ICF wall should be investigated.
- ICF Slabs shall be tested experimentally for the different span to meet field requirements.
- Development of design interaction diagrams for plain and structural ICF walls with Nano-concrete.
- Testing of seismic behavior and wind loads of a complete room should be done with ICF walls and slabs in shaking table.
- The fitting of the ICF slabs onto the ICF walls or beams, and the behavior of the connection, in term of displacements and its interaction with each other, are aspects that deserve a more in-depth study.

- Parametric studies on the behavior of ICF wall panels using the developed analytical models.
- Evaluation of the construction methods to frame openings and the reinforcement required at corners and lintels prescribed by the manufacturer and residential codes would be of importance to insurance and loss with environmental damage in residential construction.
- The hypothesis that the pre-stressed Blank Block act as formwork during construction and carry the weight of the wet structural Nano-concrete and labors, tending to eliminate the underneath supports, can be investigated with the prestressed ICF slab section.

References

Abrams Daniel, P. (2002). *State Farm Report on the Experimental Study of Insulated Concrete Forms.* USA: Mid America Earthquake Center, University of Illinois.

ACI 2008b. (2008). *Acceptance criteria for special un-bonded post-tensioned precast structural walls based on validation testing and commentary.* Skokie, IL: American Concrete Institute (ACI).

ACI 318-02. (2002). *Building Code Requirements for Structural Concrete.* Farmington Hills,MI: American Concrete Institute.

ACI 318-08. (2008). *Building Code Requirements for Structural Concrete and Commentary.* Farmington Hills,MI: American Concrete Institute.

ACI 318-11. (2011). *Building Code Requirements for Structural Concrete* . Farmington Hills: American Concrete Institute.

ACI 318-99. (1999). *Building Code Requirements for Structural Concrete and Commentary.* Farmington Hills, MI: American Concrete Institute.

ACI 544.5R-10. (2010). *Report on the Physical Properties and Durability of Fiber- Reinforced Concrete,.* American Concrete Institute .

ACI C213. (1999). *Guide for Structural Lightweight Aggregate Concrete.* Farmington Hills: American Concrete Institut.

ACI ITG-5.1. (2008). *Acceptance criteria for special un-bonded post-tensioned precast structural walls based on validation testing and commentary.* Skokie, IL: American Concrete Institute (ACI). Retrieved from http://www.constructionspecifier.com/enhancing-energy-performance-with-balcony-thermal-breaks/.

Ahmed, R. (2013). *Promoting Sustainable and Green Construction.* Bahrain: Bahrain Society of Engineers, Issue 57.

Aldea, C. M., Rapoport, J., P., S. S., & and Karr, A. (2001). *Combined Effect of Cracking and Water Permeability of Fiber-Reinforced Concrete: Concrete Under Severe Conditions.* Canada: Proceedings of the Third International.

Ali, A. a. (1990). *Reinforced Structural Walls with Staggered Opening Configurations Under Reversed Cyclic Loading.* Ann Arbor: Department of Civil Engineering, University of Michigan.

Andreea Mircea, R. C. (2000). *Analysis of an ICF Technology Shear Walls System.* Latest Trends on Engineering Mechanics, Structures, Engineering Geology.

Arsène M-A, S. J. (2003). *Cementitious composites reinforced with vegetable fibers.* Joao-Pessoa Brazil: Proceedings of the First Interamerican conference on non-conventional materials and technologies in the Eco-construction and Infrastructure.

Ashok, G. (2004). *Mix Design And Testing Of Self- Consolidating Concrete Using Florida Materials.* FL , USA: Embry-Riddle Aeronautical University Daytona Beach.

ASTM C 295. (1994). *trographic examination of aggregates for concrete.* ASTM Publication.

ASTM C143/C143M-15a. (2000). *Standard Test Method for Slump of Hydraulic-Cement Concrete.* West Conshohocken, PA.: ASTM.

ASTM C348-14. (2014). *Standard test method for flexural strength of hydraulic-cement mortars.* West Conshohocken, PA: ASTM international.

ASTM C39. (2017). *Standard Test Method for Compressive Strength of Cylindrical Concrete Specimens.* West Conshohocken, PA: ASTM International.

ASTM C78. (2016). *Test Method for Flexural Strength of Concrete (Using Simple Beam with Third-Point Loading).* ASTM C 78Standard.

ASTM E564. (2012). *Standard Practice for Static Load Test for Shear Resistance of Framed Walls for Building* (Vol. 04.11). ASTM Standards.

ASTM E72-15. (2015). *Standard Test Methods of Conducting Strength Tests of Panels for Building Construction.* West Conshohocken, PA: ASTM.

ASTM E72-95. (1995). *Construction Strength Tests of Panels for Building Construction.* West Conshohocken: American Society of Testing and Materials (ASTM).

ASTM E72-98. (1998). *Standard Test Methods of Conducting Strength Tests of Panels for Building Construction.* West Conshohocken, PA: ASTM.

Ayşin Sev, M. E. (2014). *Nanotechnology Innovations for the Sustainable Buildings of the Future* (Vols. 8, No:8). World Academy of Science, Engineering and TechnologyInternational Journal of Civil, Environmental, Structural, Construction and Architectural Engineering.

Banthia N, M. A. (1994). *Micro-fiber reinforced cement composites. I. Uniaxial tensile response.* Can J Civil Eng.

Bilba K, A. M.-A. (2003). *Sugar cane bagasse fibre reinforced cement composites. Part I. Influence of the botanical components of bagasse on the setting of bagasse/cement composite.* Cem Concr Compos.

Bin Shamsuri, K. (2011). *Development Of Lightweight Concrete By Using Polystyrene Beads.* Universiti Teknologi Malaysia.

Bledzki, J. G. (196). *Einfluß von haftvermittlern auf das feuchteverhalten naturfaserverst¨arkter kunststoffe* (Vol. 236). Die Angewandte Makromolekulare Chemie.

Bookers, R. B. (2005). *Nanotechnology for the Dummies, The hitchhiker's guide to Nanotechnology.* Hobkon, New Jersey: Wiley Publishing Inc.

Brandon, D. P. (2009). *Flexural Strength Capacity for Hobbs Building Systems (Hobbs Wall).* Iowa, USA: Iowa State University Ames.

Brown, H. J. (2010). *Applications of Alkaline-Resistant Cellulose Polymer Fiber in Ready Mixed Concrete* (Vol. 268). ACI journal.

Cain, R. (2004). *Aggregate Sensor Suite for Bridge Deck Measurements – phase 1.* Johns Hopkins University applied physics labororatory.

Camacho, M. d. (2014). *Mechanical Properties and Durability of CNT Cement Composites.* Spain: Civil Engineering Department, Universidad de Alicante.

Cao, Y. (2016). *The influence of cellulose nanocrystals on the microstructure of cement paste.* West Lafayette, USA: SSCI, Albany Molecular Research Inc.

Cao, Y. (2016). *The relationship between cellulose nanocrystal dispersion and strength.* West Lafayette, USA: Purdue University. Retrieved from www.elsevier.com/locate/cemconcomp

Cement and Concrete Industry. (2006). *Concrete Buildings Scheme Design Manual.* Surrey : The Concrete Centre.

Christian, S. (2009). *Mechanical Characterization And Structural Assessment Of Biocomposites For Construction.* Department of Civil and Environmental Engineering, Stanford University.

Christian, S. (2009). *Sustainable Biocomposites for Construction.* Tampa, FL USA: COMPOSITES & OLYCON.

Collepardi, M. (2003). *A Holisne Approach to Concrete Damage Induced, by Delayed Ettringite Formation.*

Cook, R. D. (n.d.). *Concepts and Applications of the Finite Element Applications* (4th ed.). United States: John Wiley & Sons, Inc.

Crystal Research Associates, LLC. (2012). *Nanotechnology and the built environment: investing in green infrastructure* (Second ed.).

Davies G, O. R. (1987). *Use of the NBRI accelerated test to evaluate the effectiveness of mineral admixtures in preventing the alkali–silica reaction* (Vol. 17). Cem Concr Res.

DCC. (2015). *WalKel Methylcellulose for Cement Render: Robust Performance in a Range of Cement Qualities.* Dow Construction Chemicals. Retrieved from http://www.dowconstructionchemicals.com/eu/en/pdf/840-02201.pdf

Design - Net Connections. (n.d.). Retrieved from http://www.netconnections.name/123/vincent/green.html

Dhir, R. K. (2005). *Introduction.* Scotland: Proceedings of the International Conference – Application of Technology in Concrete Design.

donatz.info. (n.d.). Retrieved from http://donatz.info/precast-floor-panels/precast-floor-panels-stylish-on-regarding-precast-construction-3/

Dowell, J. G. (2003). *Concrete Consolidation and the Potential for Voids in ICF Walls.* Skokie, IL: Portland Cement Association.

Elvin, G. (2007). *Nanotechnology for Green Building.* Green Technology Forum. Retrieved from http://esonn.fr/esonn2010/xlectures/mangematin/Nano_Green_Building55ex.pdf

EN 1992-1-1 . (1992). *Eurocode 2: Design of concrete Structures-Part 1: General Rules for buidings.*

F. Sanchez, K. S. (2010). *Nanotechnology in Concrete – A Review.* Construction and Materials.

F.F., F. (2012). *NanoArchitecture and Sustainability (M. Thesis).* University of Alexandria, Arch. Dpt.

Farhad, A. (2015). *Nanoparticles in self-compacting concrete – a review.* Sydney,: University of New South Wales.

Feynmann, P. R. (1960). *There's plenty of room at the bottom (reprint from the speech given at the annual meeting of the West Coast section of the American Physical Society).* Engineering Science.

Florence, S. K. (2010). *Nanotechnology in concrete – A review* (Vol. 24). Construction and Building Materials. Retrieved from www.elsevier.com/locate/conbuildmat

Garboczi EJ, B. D. (1996). *Modelling of the microstructure and transport properties of concrete.* Construct Build Mater.

Garboczi EJ, B. D. (1998). *Multiscale analytical/numerical theory of the diffusivity of concrete.* Adv Cem Based Mater.

Garth, J. S. (2014). *Experimental Investigation of Lateral Cyclic Behavior of Wood-Based Screen-Grid Insulated Concrete Form Walls.* USA: Portland State University.

Gheitasi, A. (2014). *What is the best suitable element type for material non linearity problem for 3D geometry in ANSYS APDL?* Retrieved from https://www.researchgate.net/post/What_is_the_best_suitable_element_type_for_material_non_linearity_problem_for_3D_geometry_in_ANSYS_APDL2

Gindl W, K. J. (2004). *Tensile properties of cellulose acetate butyrate composites reinforced with bacterial cellulose.* Compos Sci Technol.

Going Green. (n.d.). Retrieved from http://www.miamibeachfl.gov/green/default.aspx?id=19072

Gopalakrishnan, K. B.-O. (2011). *Nanotechnology in Civil Infrastructure Paradigm Shift.* he Springer Book Archives (SBA).

Green/leed. (n.d.). Retrieved from http://www.parex.com/green.shtml.

Hasdemir, S. (n.d.). *Evaluation of alkali reactivity of natural sands.* Istanbul University. Retrieved from www.elsevier.com/locate/conbuildmat

Hatem S., A. H. (n.d.). *EVALUATION OF BOND CHARACTERISTICS OF MMFX STEEL.* North Carolina State University. Retrieved from http://mmfx.com/dK2/Evaluation_Bond_Characteristics_Seliem.pdf

Hooton RD, R. C. (1992). *Development of the NBRI rapid mortar bar test leading to its use in North America.* London: Proceedings ninth international conference on AAR in concrete.

Housing, U. (2001). *Inplane Shear resistance of Insulating Concrete Form Walls.* PATH.

ICC. (2000). *International Residential Code* . Reston,VA: International Code Council.

ICC. (2014). *International Residential Code for One- and Two-Family Dwellings.* Falls Church, VA: International Code Council.

ICC Evaluation Service. (2012). *ICC-ES Evaluation Report ESR-1770.* APEX Block Interlocking System.

ICC-ES ESR 1770. (2012). *The International Building Code Council Evaluation Service* .

inhabitat.com. (n.d.). *Scientists Use Lightning Blasts To Recycle Old Concrete*. Retrieved from https://inhabitat.com/scientists-use-lightning-blasts- to-recycle- concrete-debris

Insulating Concrete Forms. (n.d.). Retrieved from http://www.cement.org/cement-concrete-

integralbook.com. (n.d.). Retrieved from https://integralbook.com/CONCRETE-CEILING-DETAIL

João Paulo Saraiva Moraisa, M. d. (2013). *Extraction and characterization of nanocellulose structures from raw cotton linter* (Vol. 91). Carbohydrate Polymers.

John, G. (2003). *Concrete Consolidation and the Potential for Voids in ICF Walls.* USA: Research and Development Bulletin, Portland Cement Association, Illinois.

John, M. J. (2009). *HYBRID COMPOSITES.* Port Elizabeth 6000, South Africa: CSIR Materials Science and Manufacturing.

K. Bilba, M.-A. A. (2008). *Silane treatment of bagasse fiber for reinforcement of cementitious composites.* Guadeloupe: Université des Antilles et de la Guyane.

K. E. Drexler, C. P. (1991). *Unbounding the Future: The Nanotechnology Revolution.* New York: William Morrow.

K. Oksman, A. P. (2006). *Manufacturing process of cellulose whiskers/polylactic acid,nanocomposites* (Vol. 66). Composites Science and Technology.

Kibert, C. (2008). *Sustainable Consttruction: Green Building Design and Delivery.* New York: Wiley Inc.

Lee, K.-Y. (2014). *On the use of nanocellulose as reinforcement in polymer matrix composites.* Composites Science and Technology. Retrieved from www.elsevier.com/locate/compscitech

Lizzi, F. (1981). *The static restoration of monuments.* Genoa: SAGEP.

Lobo, C. (1998). *Challenging ASR predictive testing.* The Aberdeen Group.

M.Z.Rong, M. Q. (2001). *The effect of fiber treatment on themechanical properties of unidirectional sisal-reinforced epoxy composites* (Vol. 61). Composites Science and Technology.

M-A. Arsène, H. S. (n.d.). *CEMENTITIOUS COMPOSITES REINFORCED WITH.* Rio de Janeiro, Brazil.

Maj Munch Andersen, B. A. (2010). *Green Nanotechnology in Nordic Construction Eco-innovation Strategies and Dynamics in Nordic Window Value Chains.* Technical University of Denmark, Chalmers University of Technology and Advansis Ltd.

Manolia, A. (2012). *The Possibility of Produce Self Compacted Polystyrene Concrete.* Iraq: Al- Mustansiriya University College of Engineering.

Maura, G. (1978). *Lightweight concrete made with expanded polystyrene.* IL. Cement.

McDonald, L. W. (2016). *A Review on Grafting of Biofibers for Biocomposites.* Moscow: Department of Forest, Rangeland and Fire Sciences, University of Idaho.

McKee, S. C. (2001). *In-Plane Shear Resistance of Insulating Concrete Form Walls.* Upper Marlboro, MD: National Association of Home Builders Research Center, Inc.

Mehrabi, A. B. (2000). *In-Plane Lateral Load Resistance of Wall Panels In Residential Building.* Portland Cement Association.

Mehta, P. K. (2002). Greening of the concrete industry for sustainable development.

Mehta, P. K. (2006). *Concrete: Microstructure, Properties and Materials.* New York: McGraw-Hill.

MENA. (2014). *United Kingdom: Private sector vital to creating a sustainable Wales.*

MEW. (2006). *Thermal Insulation in Buildings* (First ed.). Ministry of Electricity & Water, Kingdom of Bahrain.

Michael, T. (2013). *Production and Applications of Cellulose Nanomaterials.* Bilodeau University of Maine, Process Development Center.

Microfibers, Z. S. (n.d.). *Mechanical Properties and Nanostructure of Cement-Based Materials Reinforced with Carbon Nanofibers and Polyvinyl Alcohol.*

Miled, K. (2003). *Compressive behavior of an idealized EPS lightweight concrete: size effects and failure mode.* France,: LAMI (ENPC/LCPC, Institut Navier). Retrieved from www.elsevier.com/locate/mechmat

Mircea, A. a. (2010). *Research Contributions to the Seismic Performance of ICF Technology Wall Systems.* Romania: Wseas Transactions on Information Science and Applications.

Mitra, B. B. (2014). *Nanomaterials for Construction Engineering-A Review.*

Mohamed, A. P. (2015). *Nano-Innovation in Construction.* Pattaya (Thailand): International Conference on Environment And Civil Engineering April 24-25, 2015.

Mohr, B. J., El-Ashkar, N. H., & Kurtis, K. E. (2004). *Fiber-Cement Composites for Housing Construction: State-of-the-Art.* Orlando, USA: in Proceedings of the NSF Housing Research Agenda Workshop.

Mondal, P. M. (2007). *Reliable Technique to Determine the Local Mechanical Properties at the Nanoscale for Cementitious Materials* (Vol. 37). Cement and Concrete Research.

Nagaraj, T. S. (1993). *Re-proportioning concrete mixes.* ACI Mater, 90(1), 50-58.

nano.org.uk. (2014). *What's nanotechnology*. Retrieved from http://www.nano.org.uk/whatis.htm

nanoforum.org. (2006). *Nanoforum report: Nanotechnology and Construction*. Retrieved from http://nanotech.law.asu.edu/Documents/2009/10/Nanotech%20and% 20Construction%20Nanoforum%20report_259_9089.pdf

Neal, B. G. (1963). *The Plastic Methods of Structural Analysis.* London: Chapman and Hall, Ltd.

Ning Lin, A. D. (2014). *Nanocellulose in biomedicine Current status and future prospect.* France: Elsevier. Retrieved from https://www.deepdyve.com/lp/elsevier/nanocellulose-in-biomedicine-current-status

Ning Lin, A. D. (2014). *Nanocellulose in biomedicine: Current status and future prospect.* European Polymer Journal.

Nutcher, P. (2015). *Enhancing Energy Performance with Balcony Thermal Breaks.* The Construction Specifier Magazine. Retrieved from http://www.constructionspecifier.com/enhancing-energy-performance-with-balcony-thermal-breaks/.

Obinna Onuaguluchi, D. K. (2014). *Properties of nanofibre reinforced cement composites.* Toronto,Canada: University of Toronto. Retrieved from www.elsevier.com/locate/cemconcomp

Paper, C. F. (2001). *What is nanotechnology? What are its implications for construction?* Foresight/CRISP workshop on Nano technology.

Patel Abhiyan, S. (2013). *International Journal of Innovative Research in Science, Engineering and Technology* (Vol. 2).

PATH. (1998). *Prescriptive Method for Insulating Concrete Forms in Residential Construction.* Upper Marlboro: National Association of Home Builders Research Center, Inc.

Pauline L. Nasatto, M. (2015). *A Cellulose Derivative with Original Physical Properties and Extended Applications.* Brazil: Federal University of Paraná. Retrieved from www.mdpi.com/journal/polymers

Peter Dusicka, a. T. (2011). *In-Plane Lateral Cyclic Behavior of Insulated Concrete Form Grid Walls.* Journal Structural Engineering.

Peters, S. J. (2010). *Nanocellulose and Microcellulose Fibers for Concrete.* Transportation Research Record Journal of the Transportation Research Board.

Pickering, K. (2015). *A review of recent developments in natural fibre composites and their mechanical performance.* New Zealand: University of Waikato.

R. J.-M. Pellenq, A. K. (2009). *realistic molecular model of cement hydrates* (Vol. 106). Proceedings of the National Academy of Sciences of the United States of America.

Radovic, M. (2012). *In-Plane Shear Resistance of Sustainable Structural Walls with Large Openings.* Lincoln: University of Nebraska.

Raki, L. (2010). *Cement and Concrete Nanoscience and Nanotechnology.* Ontario, Canada: National Research Council Canada, Institute for Research in Construction.

Rao, D. B. (2016). *A Study on Steel Fiber Reinforced Normal Compacting Concrete* (Vol. 6). Andhra Pradesh, India: Int. Journal of Engineering Research and Application.

Raoa, N. V. (2014). *The Future of Civil Engineering with the Influence and Impact of Nanotechnology on Properties of Materials.* CNT: 2nd International onference on Nanomaterials and Technologies.

Ravindrarajah, R. S. (1994). *Properties of Hardened Concrete Containing Treated Expanded Polystyrene Beads.* Sydney: University of Technology.

Roller, J. (1996). *esign Criteria for Insulating Concrete Form Wall Systems (RP116).* Skokie: Portland Cement Association.

Rudison, M. &., & Ning, Z. (2014). *Mitigating Elevated Co2 By Urban Trees.* NAAAS Conference Proceedings.

S. Anitei, ". D. (2014). *Product of Nanotechnology.* Retrieved from http://news.softpedia.com/news/Damascus-Swords-Product-of Nanotechnology-40503.shtml

S. Kalia, B. S. (2009). *Pretreatments of natural fibers and their application as reinforcing material in polymer composites-a review* (Vol. 49). Polymer Engineering and Science.

S.F. Santo, G. T. (2015). *Non-conventional cement-based composites reinforced with vegetable fibers: A review of strategies to improve durability.* Sao Paulo, Brazil: State University of Sao Paulo (UNESP).

Sabaa, B. (1998). *Engineering Properties of Polystyrene Aggregate Concrete.* Sydney: Faculty of Engineering University of Technology.

Sain, B. W. (2007). *Dispersion of soybean stock-based nanofiber in a lastic matrix* (Vol. 56). Polymer International.

Sains, G. M. (1983). *Structural Modeling and Exprimental Techniques.* Prentice Hall Inc.

Sanchez F, B. A. (2010). *Multi-scale performance of carbon microfiber reinforced cement-based composites exposed to a decalcifying environment.* Mater Sci Eng.

Sanchez F, Z. L. (2009). *Multi-scale performance and durability of carbon nanofiber/cement composites.* Prague, Czech Republic: 3rd international symposium on nanotechnology in construction.

Sasmal, S. (2013). *an Carbon Nanotubes Make Wonders in Civil/Structural Engineering?* Taramani,India: CSIR-Structural Engineering Research Centre, CSIR Complex.

Savastano Jr H, W. P. (2000). *Brazilian waste fibres as reinforcement for cement-based composites* (Vol. 22). Cem Concr Co.

Sciencedaily.com. (2012). *Could Lightning Strikes Be Used To Break.* Retrieved from https://www.sciencedaily.com/releases/2012/10/121005123732.htm

Setiawan, A. (2013). *Experimental Study On Epoxy Polystyrene As A Partial Substitution Of Fine Aggregate Of Concrete Mixture.* Indonesia : Pembangunan Jaya University.

Shama Parveen, S. R. (2013). *A Review on Nanomaterial Dispersion, Microstructure,and Mechanical Properties of Carbon Nanotube and Nanofiber Reinforced Cementitious omposites.* University of Minho.

Sideris, K. (2003). *Estimation of ultimate modulus of elasticity and Poisson ratio of normal concrete.* Xanthi, Greece: Democritus University of Thrace.

Sinem Korkmaz, & Duygu Erten. (2009). *A Review of Green Building Movement Timelines in Developed and Developing Countries to Build an International Adoption Framework.* Istanbul: Fifth International Conference on Construction in the 21st Century (CITC-V) "Collaboration and Integration in Engineering, Management and Technology".

Sobolev, K. a. (2014). *How Nanotechnology can Change the Concrete World* (Vol. 8). American Ceramic Society Bulletin. Retrieved from https://pantherfile.uwm.edu/sobolev/www/SobolevP2.pdf

Steve, M. (2005). U. T. Dallas-Led Research Team Produces Strong, Transparent Carbon Nanotube Sheets,‖ UT Dallas News Release. Retrieved from http://www.utdallas.edu/news/archive/2005/carbon-nanotube-sheets.html

T. H. Wegner, J. E. (2005). *Nanotechnolgy opportunities in residential and non-residential construction.* Bilbao: 2nd International Symposium on Nanotechnolgy in Construction.

T. W. Odom, J.-L. H. (2000). *Structure and electronic properties of carbon nanotubes* (Vol. 104). Journal of Physical Chemistry B.

Tonoli, G. (2009). *Cellulose modified fibres in cement based composites.* Brazil: Elsevier.

UniMeasure . (2012). *STD Series General Page.* Retrieved from http://www.unimeasure.com/webpages/stda.htm

V.R.Rathi, C. (2014). *An overview on the Influence of NanoMaterials on Properties of Concrete* (Vol. 3). Gujarat, India: International Journal of Innovative Research in Science, Engineering and Technology. Retrieved from http://www.ijirset.com/upload/2014/february/20_Anoverview.pdf

VanderWerf, P. A. (1997). *Insulated Concrete Forms for residential design and construction.*

Vranka, A. (1998). *Structural Design of Insulating Concrete Form Walls in Residential construction.* NAHB Research Center under sponsorship of the Portland Cement Association (PCA).

W. Zhu, P. B. (2004). *Application of nanotechnology in construction.* Materials and Structures.

Werner, C. S. (2010). *Cyclic Behavior of Screen Grid Insulated Concrete Form Components.* USA: Portland State University.

Whatmore, R. a. (1995). *Nanotechnology in the Marketplace,‖* (Vol. 6). Computing & Control Engineering Journal.

wikipedia.org. (n.d.). *Alkali–silica reaction*. Retrieved from https://en.wikipedia.org/wiki/Alkali%E2%80%93silica_reaction

wikipedia.org. (n.d.). *Concrete*. Retrieved from https://en.wikipedia.org/wiki/Concrete

Wikipedia.org. (n.d.). *Insulating concrete form*. Retrieved from https://en.wikipedia.org/wiki/Insulating_concrete_form#Development

wikipedia.org. (n.d.). *Thermal mass*. Retrieved from https://en.wikipedia.org/wiki/Thermal_mass

wiktionary.org. (2016). *Methylcellulose*. Retrieved from https://en.wiktionary.org/wiki/methylcellulose

Wolanski, A. J. (2004). *Flexural Behavior of Reinforced and Prestressed Concrete Beams Using Finite Element Analysis.* Milwaukee, Wisconsin, USA: Marquette University.

X. Li, W. C. (2004). *Nanoscale structural and mechanical characterization of a natural nanocomposite material: the shell of red abalone.* Nano Letters.

Xuli, F. D. (1996). *Effect of methylcellulose admixture on the mechanical properties of cement* (Vol. 26). Original Research Article Cement and Concrete Research.

Yatzer. (n.d.). *Off the Grid*. Retrieved from http://www.yatzer.com/1095_off_the_gridsustainable_habitat_2020

Yizheng Cao, W. J. (2013). *Performance-Enhanced Cementitious Materials by Cellulose Nanocrystal Additions.* Production and Applications of Cellulose Nanoma terials.

Yizheng Cao, W. J. (2013). *Performance-Enhanced Cementitious Materials by Cellulose Nanocrystal Additions.* Production and Applications of Cellulose Nanomaterials.

Yland, C. V. (2000). *Experimental and Analytical Studies of the Structural Performance of Innovative Structural Grid Walls.* Irvine: University of California.

Z. S. Metaxa, M. S.-G. (2010). *Mechanical Properties and Nanostructure of Cement-Based Materials Reinforced.* USA: Northwestern University.

Zaocka, Z. (1989). *Effects of high-range water reducers on the properties of fresh and hardened concrete.* Austin.: University of Texas.

Zhao, J. (2016). *Smart Aggregate-Piezoceramic Patch Combination for Health Monitoring of Concrete Structures.* Journal of Sensors. Retrieved from http://dx.doi.org/10.1155/2016/3270916

Zhi Ge, Z. G. (2008). *Applications of Nanotechnology and Nanomaterials in Constr.* Karachi: First International Conference on Construction In Developing Countries (ICCIDC–I)"Advancing and Integrating Construction Education, Research & Practice.

Zollinger, D. G. (2001). *Use of High Fines Concrete (HFC) in Insulated Concrete Form (ICF) Construction.* Texas A&M University SystemCollege Station.

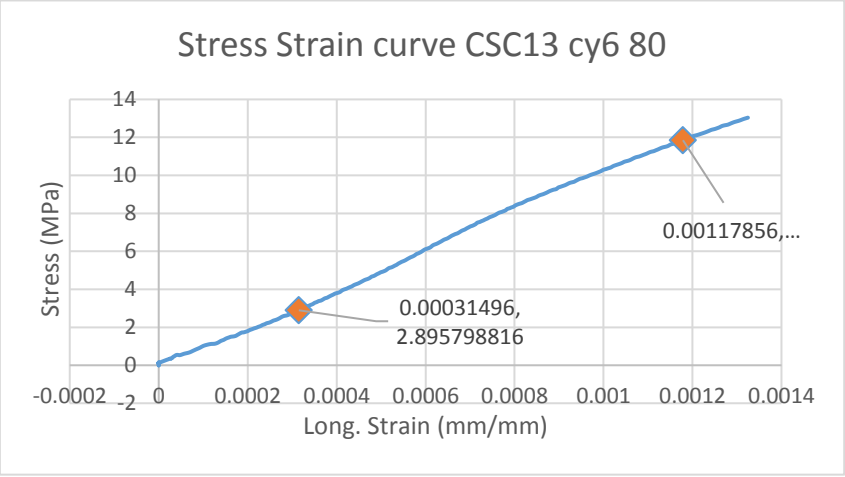
Zollo, R. F. (2003). *Fiber-Reinforced Concrete Walls Using Insulated Formwork.* Skokie: ACI T1-1R-01.

APPENDICES

Appendix A

SAMPLE CALCULATION OF MODULUS OF ELASTICITY

Time (sec)	Load (Lb)	Stress (psi)	Lon.Disp (in)	Lateral Disp (in)	Time (sec)	Load (KN)	Stress (MPa)	Axil Lon. Disp (mm)	Transv. Lateral Disp. (mm)	Long. Strain (mm/mm)	Lateral Strain (mm/mm)	Poisson Ratio
4.8	769	28	0.00006	0.00001	4.8	3.420682	0.193053	0.001524	0.000254	7.62E-06	1.693E-06	0.222222
5	1350	49	0.00019	0.00003	5	6.005099	0.337843	0.004826	0.000762	2.413E-05	5.08E-06	0.210526
5.2	1375	50	0.00021	0.00002	5.2	6.116305	0.344738	0.005334	0.000508	2.667E-05	3.387E-06	0.126984
5.4	1425	52	0.00021	0.00002	5.4	6.338716	0.358527	0.005334	0.000508	2.667E-05	3.387E-06	0.126984
5.6	1438	52	0.00022	0.00003	5.6	6.396543	0.358527	0.005588	0.000762	2.794E-05	5.08E-06	0.181818
5.8	1545	56	0.00024	0.00003	5.8	6.872502	0.386107	0.006096	0.000762	3.048E-05	5.08E-06	0.166667
6	1697	62	0.00025	0.00003	6	7.548632	0.427475	0.00635	0.000762	3.175E-05	5.08E-06	0.16
6.2	1930	70	0.00028	0.00002	6.2	8.585068	0.482633	0.007112	0.000508	3.556E-05	3.387E-06	0.095238
6.4	2132	78	0.00031	0.000039	6.4	9.483608	0.537791	0.007874	0.000991	3.937E-05	6.604E-06	0.167742
6.6	2163	79	0.00034	0.000039	6.6	9.621503	0.544686	0.008636	0.000991	4.318E-05	6.604E-06	0.152941
6.8	2113	77	0.00037	0.000039	6.8	9.399092	0.530896	0.009398	0.000991	4.699E-05	6.604E-06	0.140541
7	2252	82	0.00041	0.00003	7	10.0174	0.56537	0.010414	0.000762	5.207E-05	5.08E-06	0.097561
7.2	2403	88	0.00045	0.000039	7.2	10.68908	0.606739	0.01143	0.000991	5.715E-05	6.604E-06	0.115556
7.4	2542	93	0.0005	0.000059	7.4	11.30738	0.641213	0.0127	0.001499	0.0000635	9.991E-06	0.157333
7.6	2725	99	0.00055	0.000059	7.6	12.1214	0.682581	0.01397	0.001499	6.985E-05	9.991E-06	0.14303
7.8	2990	109	0.0006	0.000049	7.8	13.30018	0.751529	0.01524	0.001245	0.0000762	8.297E-06	0.108889
8	3312	121	0.00066	0.000049	8	14.73251	0.834266	0.016764	0.001245	8.382E-05	8.297E-06	0.09899
8.2	3684	134	0.00073	0.000069	8.2	16.38725	0.923898	0.018542	0.001753	9.271E-05	1.168E-05	0.126027
8.4	4050	148	0.00079	0.000069	8.4	18.0153	1.020424	0.020066	0.001753	0.0001003	1.168E-05	0.116456
8.6	4302	157	0.00086	0.000079	8.6	19.13625	1.082477	0.021844	0.002007	0.0001092	1.338E-05	0.122481
8.8	4466	163	0.00093	0.000089	8.8	19.86576	1.123846	0.023622	0.002261	0.0001181	1.507E-05	0.127599
9	4504	164	0.00099	0.000089	9	20.03479	1.13074	0.025146	0.002261	0.0001257	1.507E-05	0.119865

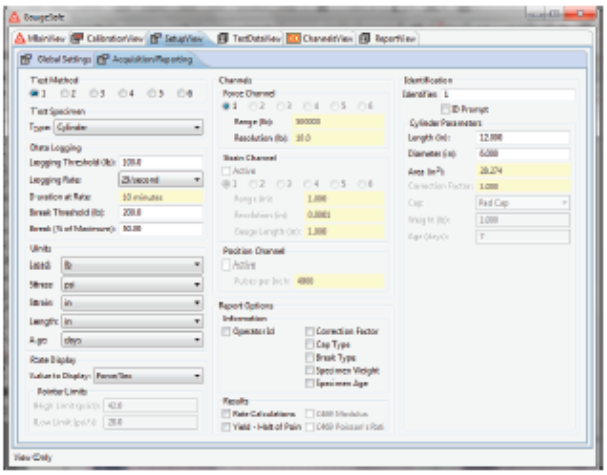


S1	2.8958	ST1	0.000315
S2	11.8521	ST2	0.001179

E	10370.89

GaugeSafe for GB2
Operators Manual

Acquisition / Reporting



Test Method

Select the desired test method 1-6.

Test Specimen

Select basic specimen geometry to define the dimensional parameters needed for calculations.

Data Logging

Logging threshold - Define when data collection for the test begins based on current load reading (setting this value to 0 turns off the threshold).

Logging Rate - Select the data collection rate of testing. Rate is selectable for 1-100 samples per second. The time till the buffer fills is based on current data collection settings is shown in Duration at Rate. The buffer size on the indicator is 15000 points.

Break - Break Threshold defines when the program starts looking for the break condition. Break defines the break condition as a percent drop of peak load, i.e. 20% Break of 100lbs max load would be 80 lbs registered by the loadcell.

Units

Set the units displayed for test method.

Rate Display

Set the rate of change to be displayed on the indicator during the test run. The upper and lower bounds for the pointer rate option are set here.

Channels

Select the desired transducer channels to active and select the calibration to be used. Range and resolution currently set are displayed but can only be changed under the calibration tab.

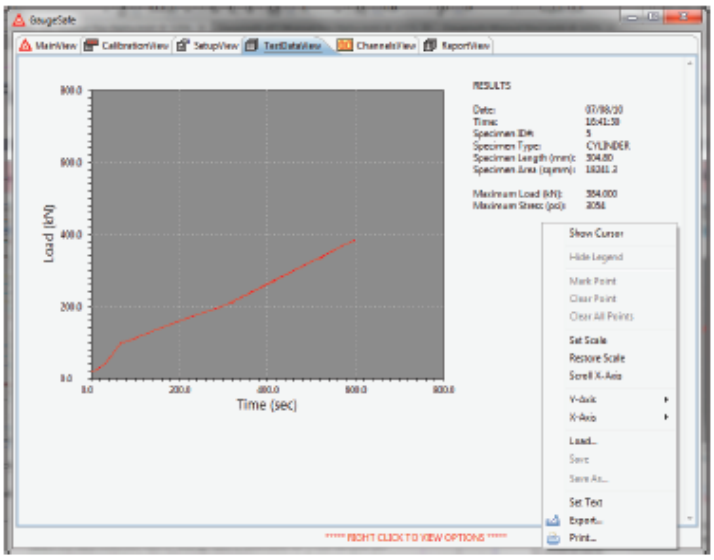
Report Options / Results

Select optional information and calculations to be included in Results Report.

Identification

Set sample ID and geometric properties.

Test Data View



Right Click in the TestDataView Tab to see XY graph options.

Results
This section displays the selected test information.

Graph
This section displays the live and saved tests respectively.

Show/Hide Cursor
Use the cursor on the graph to highlight specific points along the curve and to select points to be reported in the Legend by clicking or using the Mark Point feature. With cursor hidden click and drag over a section of the graph to zoom in on it.

Show/Hide Legend
Shows and hides the XY Legend at the top left of the plot.

Mark Point
Marks current cursor location and adds the values to the XY Legend.

Clear Point
Clears the highlighted point from the Graph and XY Legend. Mouse over a point to highlight it.

Clear All Points
Clears all points from the Graph and XY Legend.

Set Scale
Allows the user to manually select the scale of the X and Y axis as well as the number of divisions.

Restore Scale
Restores the scale to default scale based on current data or user defined values.

Table A1

	Ultimate Compressive Strength/Sress (2ed Trial) CSC Mix group Sandseived one time																							
	SPECIEMEN	CSC-11		Casting Date	Testing Date	CSC-12		Casting Date	Testing Date	CSC-12.5		Casting Date	Testing Date	CSC-13		Casting Date	Testing Date	CSC-14		Casting Date	Testing Date	CSC-15		Casting Date	Testing Date
	LOAD/Stress	KN	Mpa			KN	Mpa			KN	Mpa			KN	Mpa			KN	Mpa			KN	Mpa		
Only comressive Test	Clineder # 1	916.5	51.86287603	04.03.14	09.08.15	492	27.84	05.03.14	09.08.15	493.8	27.94	20.04.14	09.08.15	302.60	17.12	07.03.14	09.08.15	167.20	9.46	15.08.15	21.09.15	149.60	8.47	18.08.15	21.09.15
	Clineder # 2	752.7	42.59376627	04.03.14	09.08.15	535.70	30.31	05.03.14	09.08.15	544.3	30.80	20.04.14	09.08.15	320.1	18.11	07.03.14	09.08.15	185.3	10.49	15.08.15	21.09.15	146.5	8.29	18.08.15	21.09.15
	Clineder # 3	750	42.44097875	04.03.14	09.08.15	400.7	22.67	15.04.14	09.08.15	445.7	25.22	20.04.14	09.08.15	363.1	20.55	25.04.14	09.08.15	189.4	10.72	15.08.15	21.09.15	160.6	9.09	18.08.15	21.09.15
	Clineder # 4	612.3	34.64881505	28.03.14	11.08.15	393.5	22.27	15.04.14	09.08.15	510	28.86	20.04.14	17.08.15	600.4	33.98	25.04.14	09.08.15	218.7	12.38	15.08.15	21.09.15	166.9	9.44	18.08.15	21.09.15
	Clineder # 5			28.03.14		375.1	21.23	15.04.14	09.08.15	Al-hoty	31.92	20.04.14	22.08.15	628.7	35.58	25.04.14	09.08.15	226.9	12.84	15.08.15	05.10.15	192	10.86	18.08.15	06.10.15
compressive Test + Modulus and Ratio	Clineder # 6	688.1	38.9381833	28.03.14	11.08.15	363	20.54	15.04.14	13.08.15	Al-hoty	28.89	20.04.14	22.08.15	377.7	21.37	26.06.14	13.08.15	199	11.26	15.08.15	05.10.15	198	11.2	18.08.15	06.10.15
	Clineder # 7	702	39.72475611	15.04.14	11.08.15	414	23.43	15.04.14	13.08.15	382.00	21.62	19.08.15	07.10.15	582.2	32.95	26.06.14	13.08.15	215	12.17	16.08.15	05.10.15	202	11.43	17.08.15	06.10.15
	Clineder # 8	723.2	40.92442111	15.04.14	11.08.15	378.1	21.40	12.08.15	13.08.15	393.00	22.24	19.08.15	07.10.15	301	17.03	26.06.14	13.08.15	179	10.13	16.08.15	05.10.15	188	10.64	17.08.15	06.10.15
	Clineder # 9	774.6	43.83304285	15.04.14	12.08.15	417	23.60	12.08.15	13.08.15	383.00	21.67	19.08.15	07.10.15	360.5	20.40	30.12.14	13.08.15	183.3	10.37	16.08.15	05.10.15	208	11.77	17.08.15	06.10.15
	Clineder # 10	558	31.57608819	25.06.15	12.08.15	477.3	27.01	12.08.15	16.08.15	337.00	19.07	19.08.15	07.10.15	329	18.62	30.12.14	16.08.15	203	11.49	16.08.15	05.10.15	215	12.17	17.08.15	06.10.15
	Clineder # 11	666.8	37.7328595	25.06.15	12.08.15	475.2	26.89	26.06.15	16.08.15	333.00	18.84	19.08.15	07.10.15	Missing		30.12.14			10.41	15.10.15	13.01.16		8.57	15.10.15	13.01.16
	Clineder # 12	683.3	38.66656104	25.06.15	12.08.15	544.4	30.81	26.06.15	04.10.15	362.00	20.48	19.08.15	07.10.15	361.00	20.43	12.08.15	04.10.15		10.2	15.10.15	13.01.16		8.85	15.10.15	13.01.16
	Clineder # 13	807	45.66649313	12.08.15	04.10.15	557.6	31.55	26.06.15	04.10.15	376.00	21.28			348.30	19.71	12.08.15	04.10.15								
	Clineder # 14	798	45.15720139	12.08.15	04.10.15		29.05	11.10.15	13.01.16	373.00	21.11				16.01	14.10.15	13.01.16								
	Clineder # 15		36.51	11.10.15	13.01.16		25.41	11.10.15	13.01.16	387.00	21.90				17.04	14.10.15	13.01.16								
	Clineder # 16 ICFW2		39.81	11.10.15	13.01016						21.29	13.10.15	13.01.16	493.3	27.91	30.11.15	02.05.16								
	Clineder # 17 ICFW4										20.53	13.10.15	13.01.16	493.9	27.95	09.12.15	02.05.16								
	Clineder # 18 ICFW2										20.57	13.10.15	13.01.16	479.9	27.16	30.11.15	02.05.16								
	Clineder # 19 ICFW3													422	23.88	05.12.15	02.05.16								
	Clineder # 20 ICFW4													498.3	28.20	09.12.15	02.05.16								
	Clineder # 21 ICFW1													265	15.00	25.11.15	02.05.16								
	Clineder # 22 ICFW3													306	17.32	05.12.15	02.05.16								
	Clineder # 23 ICFW1													273	15.45	25.11.15	02.05.16								
	Clineder # 24 ICFW1													322	18.22	25.11.15	03.05.16								
	Clineder # 25 ICFS 1J													237	13.41	06.04.16	03.05.16								
	Clineder # 26 ICFS 2J													270	15.28	07.04.16	03.05.16								
	Clineder # 27 ICFS 1J													261.9	14.82	06.04.16	03.05.16								
	Clineder # 28 ICFS 2J													326.7	18.49	07.04.16	03.05.16								
	Clineder # 29 ICFS 1J													317.6	17.97	06.04.16	03.05.16								
	Clineder # 30 ICFS 2J													311.7	17.64	.07.04.16	03.05.16								
	Clineder # 31 S2													329.7	18.66	11.04.16	17.05.16								
	Clineder # 32 J3													312.9	17.71	09.04.16	17.05.16								
	Clineder # 33 S1													347	19.64	10.04.16	17.05.16								
	Clineder # 34 J3													305.2	17.27	09.04.16	17.05.16								
	Clineder # 35 S1													283.8	16.06	10.04.16	17.05.16								
	Clineder # 36 S3													382.3	21.63	11.04.16	17.05.16								
	Clineder # 37 S3													320.1	18.11	11.04.16	17.05.16								
	Clineder # 38 S3													399.2	22.59	11.04.16	23.05.16								
	Clineder # 39 S2													411.3	23.27	11.04.16	23.05.16								
	Clineder # 40 S2													406.6	23.01	11.04.16	23.05.16								
	Clineder # 41 S1													293	16.58	10.04.16	23.05.16								
	Clineder # 42 J3													350	19.81	10.04.16	23.05.16								
	Clineder # 43 MSJ3															09.08.16	26.09.16								
	AVERAGE	725.5769231	41.05892636			447.9692308	25.61			498.45	24.12			416.53	23.6			196.68	10.99			182.66	10.07		

Table A2

Ultimate Compressive Strength/Sress (2ed Trial) SNBR Mix group												
SPECIEMEN	SBNBR-2		Casting Date	Testing Date	SBNBR-7		Casting Date	Testing Date	BBNN-1		Casting Date	Testing Date
LOAD/Stress	KN	Mpa			KN	Mpa			KN	Mpa		
Clineder # 1	76.4	4.32	18.04.14	11.08.15	49.1	2.78	20.04.14	11.08.15	39	2.21	31.08.15	05.10.15
Clineder # 2	81.6	4.62	18.04.14	11.08.15	60	3.40	20.04.14	11.08.15	38.7	2.19	31.08.15	05.10.15
Clineder # 3	43	2.43	18.04.14	16.08.15	78	4.41	20.04.14	16.08.15	40	2.26	31.08.15	05.10.15
Clineder # 4	43	2.43	18.04.14	16.08.15	55	3.11	20.04.14	16.08.15	38	2.15	31.08.15	05.10.15
Clineder # 5	45	2.55	18.04.14	16.08.15	49.9	2.82	20.04.14	17.08.15	31.8	1.799497	31.08.15	05.10.15
Clineder # 6	73.9	4.18	23.08.15	17.08.15	64.8	3.666900564	20.04.14	17.08.15			31.08.15	
Clineder # 7	69.9	3.96	23.08.15	17.08.15	Al-hoty	3.48	19.11.14	22.08.15			31.08.15	
Clineder # 8	Al-hoty	4.76	18.04.14	22.08.15	Al-hoty	2.62	19.11.14	22.08.15			04.09.15	
Clineder # 9	Al-hoty	4.20	18.04.14	22.08.15	35.6	2.014531791	21.08.15	05.10.15			04.09.15	
Clineder # 10	63.1	3.57	23.08.15	05.10.15	41.2	2.331424432	21.08.15	05.10.15			04.09.15	
Clineder # 11	71.3	4.03	23.08.15	05.10.15	50	2.829398583	21.08.15	05.10.15			04.09.15	
Clineder # 12	58.1	3.29	23.08.15	05.10.15	50	2.829398583	21.08.15	05.10.15			04.09.15	
Clineder # 13	59.9	3.39	23.08.15	05.10.15	59	3.338690328	21.08.15	05.10.15			04.09.15	
Clineder # 14	59.5	3.37	23.08.15	05.10.15	46	2.603046696	21.08.15	05.10.15			04.09.15	
Clineder # 15 3J			03.03.16	04.05.16								
Clineder # 16 2 BLK	50	2.83	28.02.16	04.05.16								
Clineder # 17 S1	32.4	1.83	05.03.16	04.05.16								
Clineder # 18 S3	27.9	1.58	19.03.16	04.05.16								
Clineder # 19 S1	29.2	1.65	15.03.16	04.05.16								
Clineder # 20 S2	44.7	2.53	16.03.16	04.05.16								
Clineder # 21 S2	27.7	1.57	16.03.16	04.05.16								
Clineder # 22 2 BLK	70.3	3.98	28.02.16	04.05.16								
Clineder # 23 1 BLK	43.9	2.48	27.2.16	04.05.16								
Clineder # 24 3 BLK	79.4	4.49	29.02.16	04.05.16								
Clineder # 25 3 J	22.3	1.26	03.03.16	04.05.16								
Clineder # 26 1J	36.2	2.05	22.02.16	19.06.16								
Clineder # 27 1J	45.4	2.57	20.02.16	19.06.16								
Clineder # 28 1 BLK	36.7	2.08	27.02.16	19.06.16								
Clineder # 29 1 BLK	51.9	2.94	27.02.16	19.06.16								
Clineder # 30 1J	45.4	2.57	20.02.16	19.06.16								
Clineder # 31 1J	64.2	3.63	22.02.16	19.06.16								
Clineder # 32 S3	45.3	2.56	18.03.16	19.06.16								
Clineder # 33 S1	29.5	1.67	15.03.16	19.06.16								
Clineder # 34 3 BLK	96.2	5.44	29.02.16	19.06.16								
Clineder # 35 3 BLK	87	4.92	29.02.16	19.06.16								
Clineder # 36 3 S	40.2	2.27	18.03.16	19.06.16								
Clineder # 37 2 S	22.4	1.27	16.03.16	19.06.16								
Clineder # 38 1 BLK	72.6	4.11	27.02.16	19.06.16								
Clineder # 39 2 J	41.9	2.37	24.02.16	19.06.16								
Clineder # 40 2 S	45	2.55	17.03.16	19.06.16								
Clineder # 41 2 J	50	2.83	24.02.16	19.06.16								
Clineder # 42 2 J	29.2	1.65	23.02.16	20.06.16								
Clineder # 43 3 S	35.2	1.99	18.03.16	20.06.16								
Clineder # 44 3 S	36.8	2.08	18.03.16	20.06.16								
Clineder # 45 S1	39.6	2.24	15.03.16	20.06.16								
Clineder # 46 3 S	32.2	1.82	19.03.16	20.06.16								
Clineder # 47 1J	50.9	2.88	22.02.16	20.06.16								
Clineder # 48 1 BLK	47.5	2.69	27.02.16	20.06.16								
Clineder # 49 3 S	38.5	2.18	19.03.16	20.06.16								
Clineder # 50 2 BLK	65.9	3.73	28.02 .16	20.06.16								
Clineder # 51 3 S	42.2	2.39	19.03.16	20.06.16								
Clineder # 52 2 J	33.3	1.88	24.02.16	20.06.16								
Clineder # 53 2 J	31	1.75	23.02.16	20.06.16								
Clineder # 54 1J	51.1	2.89	22.02.16	20.06.16								
Clineder # 55 MS	43.4	2.46	16.02.16	20.06.16								
Clineder # 56 MS	28.6	1.62	14.03 16	20.06.16								
Clineder # 57 MS	42	2.38	06.03.16	20.06.16								
Clineder # 58 MS	34.3	1.94	14.03 16	20.06.16								
AVERAGE	61.83	3.65			58.40	3.02						

Appendix B

REINFORCEMENTS TEST REPORTS

AL HOTY ANALYTICAL SERVICES	MR. ADEL JASIM SANAD	DATE: 28.12.2014
		REF NO.:
	TEST REPORT ON STRAND TEST / BREAKLOAD	SAMPLE NO. : 146670-1
		TWO NO. : 146670
	METHOD : BS 5896 ; 1980	REPORT NO.:R163725/14

PROJECT : Bahrain University
SAMPLE ID : Cold Drawn Wire (5.00mm Dia.)
DATE SUBMITTED : 24.12.2014
DATE TESTED : 27.12.2014

RESULTS:

TEST	UNIT	RESULTS
Length	(m)	0.695
Weight	(kg)	0.107
Weight / Length	(kg/m)	19.612
Area	(mm^2)	19.612
Nominal Diameter	(mm)	5.00
Tensile Load	(kN)	19.100
Tensile Stress	(N/mm^2)	974
Elongation	(%)	4.0
Load @ 1 % Elongation	(kN)	17.150

مملكة البحرين
س.ت : ١٢٣٩٢
Kingdom of Bahrain
CR. No: 12392
AL HOTY ANALYTICAL SERVICES

NITIL K. SHRIVASTAVA
Material Laboratory Manager

Checked by:

/MDLC

DISCLAIMER
The test reports / certificates issued by AAS are records of the actual test conducted on sample and the details submitted to us for testing and the results thereof.
The results are applicable only to those sample/s, which have been tested and do not apply to other sample/s even though declared to be identical.
Test report / certificate if reproduced, for any purpose commercial or otherwise, should be reproduced in full.
AAS shall not be liable for any changes in reported factual data due to any cause related to sample tested after the report / certificate, in respect of it, has been issued.
The results reported in the test report / certificates are valid only at the time of and under the stated conditions of the testing.
Measurements are traceable to National/International Standard.

AL HOTY ANALYTICAL SERVICES	MR. ADEL JASIM SANAD	DATE : 28.12.2014
		REF. :
	TEST REPORT ON TENSILE STRENGTH OF PLAIN COLD DRAWN ROUND BAR	SAMPLE NO. : 146670-3
		TWO NO. : 146670
	METHOD : BS 4482 : 1985	REPORT NO. : R163725/14

PROJECT : Bahrain University
SAMPLE ID : Plain Cold Drawn Round Bar
DATE SUBMITTED : 24.12.2014
DATE TESTED : 28.12.2014

RESULT			SAMPLE ID	BS 4482 : 1985
			Plain Cold Drawn Round Bar	Specification Requirements
Condition of the Sample upon Receipt			Satisfactory	
Length		(m)	0.597	
Weight		(kg)	0.125	
Weight / Length		(kg/m)	0.209	
Area		(mm^2)	26.7	
Yield Stress	Re	(N/mm^2)	516	Min. 460
Tensile Stress	Rm	(N/mm^2)	536	Min. 510
Stress Ratio	Rm/Re		1.04	
Initial Gauge Length		(mm)	100.00	
Final Gauge Length		(mm)	108.89	
% Elongation at Max. Force		(%)	8.89	Min. 12

مملكة البحرين
س.ت : ١٢٣٩٢
Kingdom of Bahrain
CR. No: 12392
AL HOTY ANALYTICAL SERVICES

NITIL K. SHRIVASTAVA
Material Laboratory Manager

Checked by : _____
/MDLC

DISCLAIMER
The test reports / certificates issued by AAS are records of the actual test conducted on sample and the details submitted to us for testing and the results thereof. The results are applicable only to those sample/s, which have been tested and do not apply to other sample/s even though declared to be identical.
Test report / certificate if reproduced," for any purpose commercial or otherwise, should be reproduced in full. AAS shall not be liable for any changes in reported factual data due to any cause related to sample tested after the report / certificate, in respect of it, h as been issued . The results reported in the test report/ certificates are valid only at the time of and under the stated conditions of the testing. Measurements are traceable to National/International Standards.

Test Certificate

Name of Company : AL HOTY ANALYTICAL SERVICES
Address : P.O.BOX 26577

To : ADEL JASIM SANAD
Address : BAHRAIN UNIVERSITY

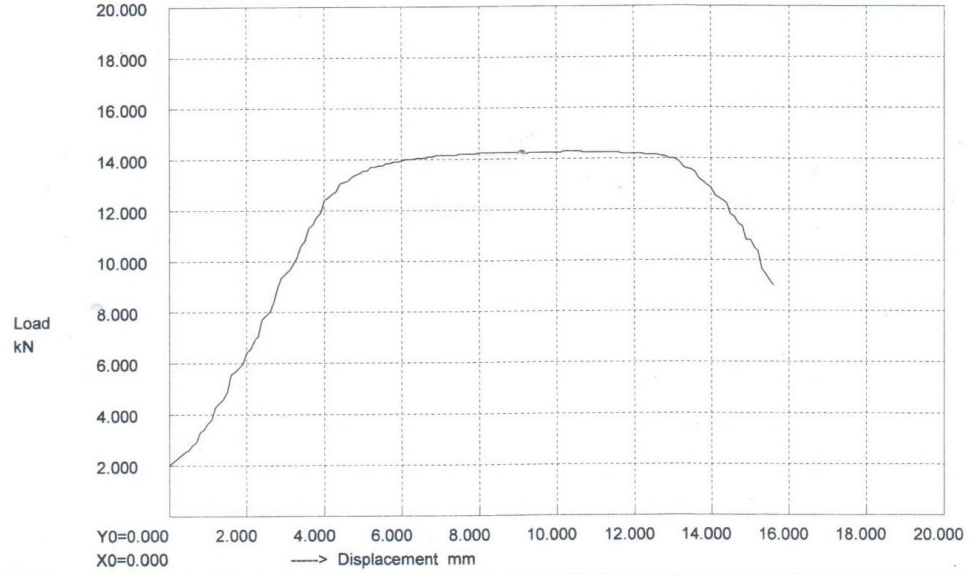
Sample Identification : REBARS 5.00mm dia./PLAIN ROUND BAR

Machine : Universal Testing Machine, 1000 kN

Input Data : File Name : ADEL JASIM 14122718 , Record No. : 1 , Date : 27/09/2014
: Sample Type : TMT , Area : 26.673 mm ²
: Length = 597.0 mm , Weight = 0.125 kg
: Gauge Length : 100 mm Final Gauge Length: 108.89 mm

Results of : Tension Test
Ult./Break Load : 14.300 kN
Ult. Stress : 0.536 kN/mm ²
Elongation : 10.200 %
Yield Load : 13.750 kN
Yield Stress : 0.516 kN/mm ²

Graph : Load Vs Displacement



For AL HOTY ANALYTICAL SERVICES

Test Certificate

Name of Company : AL HOTY ANALYTICAL SERVICES
Address : P.O.BOX 26577

To : ADEL JASIM SANAD
Address : BAHRAIN UNIVERSITY

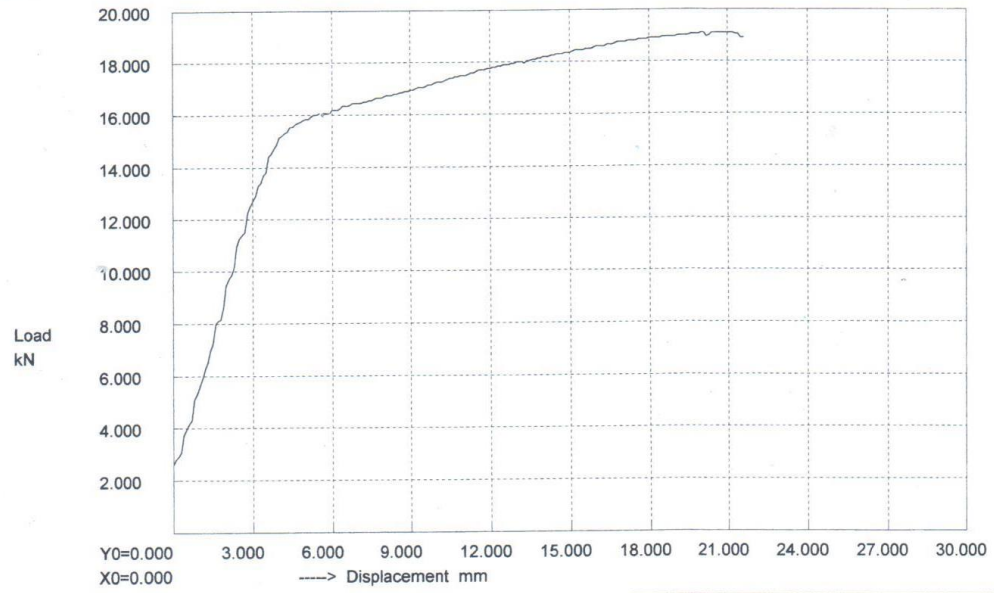
Sample Identification : COLD DRAWN WIRE(5.00 mm DIA.)

Machine : Universal Testing Machine, 1000 kN

Input Data : File Name : ADEL JASIM 14122705 , Record No. : 1 , Date : 27/09/2014
: Sample Type : Other Area : 19.612 mm ²
: Sample Area = 19.612 mm ²
: Gauge Length : 500 mm

Results of : Tension Test
Ult./Break Load : 19.100 kN
Ult. Stress : 0.974 kN/mm ²
Elongation : 4.000 %
Load at 1% Elong. : 17.150 kN
Yield Load : 16.100 kN
Yield Stress : 0.821 kN/mm ²
* Note : Yield Calculated from graph

Graph : Load Vs Displacement



For AL HOTY ANALYTICAL SERVICES

AL HOTY ANALYTICAL SERVICES	MR. ADEL JASIM SANAD	DATE : 28.12.2014
		REF. :
	TEST REPORT ON TENSILE STRENGTH BEND & REBEND OF 8 mm REBAR	SAMPLE NO. : 146670-1
	METHOD : BS 4449 : 2005 / BS EN ISO 15630-1:2000	TWO NO. : 146670
		REPORT NO. : R163725/14

PROJECT : Bahrain University
SAMPLE ID : 8mm Ø Rebar
STEEL MANUFACTURER : Qatar Steel
GRADE : 500B
DATE SUBMITTED : 24.12.2014
DATE TESTED : 27.12.2014

RESULT			SAMPLE ID	BS 4449 – 2005
			8 mm	Spec. Requirements of 8 mm
Condition of the Sample upon Receipt			Satisfactory	
Length		(m)	0.597	
Weight		(kg)	0.231	
Weight / Length		(kg/m)	0.387	0.395 ± 6.0%
Area		(mm^2)	49.3	50.3 ± 8%
Nominal Diameter		(mm)	8.0	
Yield Stress	Re	(N/mm^2)	685	485 – 650
Tensile Stress	Rm	(N/mm^2)	728	
Stress Ratio	Rm/Re		1.06	Min. 1.06
Initial Gauge Length		(mm)	100.00	
Final Gauge Length		(mm)	114.90	
Elongation at fracture		(%)	14.90	Min. 14
Total Elongation, Agt		(%)	5.00	Min. 4
Bend			No Sign of fracture	No Sign of fracture
Rebend			No Sign of fracture	No Sign of fracture

الحوطي للخدمات التحليلية
مملكة البحرين
س.ت : ١٢٣٩٢
Kingdom of Bahrain
CR. No: 12392
AL HOTY ANALYTICAL SERVICES

NITIL K. SHRIVASTAVA
Material Laboratory Manager

Checked by : /MDLC

DISCLAIMER
The test reports / certificates issued by AAS are records of the actual test conducted on sample and the details submitted to us for testing and the results thereof. The results are applicable only to those sample/s, which have been tested and do not apply to other sample/s even though declared to be identical.
Test report / certificate if reproduced, for any purpose commercial or otherwise, should be reproduced in full. AAS shall not be liable for any changes in reported factual data due to any cause related to sample tested after the report / certificate, in respect of it, h as been issued . The results reported in the test report/ certificates are valid only at the time of and under the stated conditions of the testing. Measurements are traceable to National/International Standards.

AL HOTY ANALYTICAL SERVICES	MR. ADEL JASIM SANAD	DATE : 28.12.2014
		REF. :
	TEST REPORT ON TENSILE STRENGTH, BEND & REBEND OF 10 mm REBAR	SAMPLE NO. : 146670-2
	METHOD : BS 4449 : 2005 / BS EN ISO 15630-1:2000	TWO NO. : 146670
		REPORT NO. : R163725/14

PROJECT : Bahrain University
SAMPLE ID : 10mm Ø Rebar
STEEL MANUFACTURER : Qatar Steel
GRADE : 500B
DATE SUBMITTED : 24.12.2014
DATE TESTED : 27.12.2014

RESULT			SAMPLE ID	BS 4449 – 2005
			10 mm	Spec. Requirements of 10 mm
Condition of the Sample upon Receipt			Satisfactory	
Length		(m)	0.597	
Weight		(kg)	0.372	
Weight / Length		(kg/m)	0.623	0.617 ± 4.5%
Area		(mm^2)	79.4	78.5 ± 8%
Nominal Diameter		(mm)	10.0	
Yield Stress	Re	(N/mm^2)	244	485 – 650
Tensile Stress	Rm	(N/mm^2)	326	
Stress Ratio	Rm/Re		1.34	Min. 1.06
Initial Gauge Length		(mm)	100.00	
Final Gauge Length		(mm)	120.23	
Elongation at fracture		(%)	20.23	Min. 14
Total Elongation, Agt		(%)	7.00	Min. 4
Bend			No Sign of fracture	No Sign of fracture
Rebend			No Sign of fracture	No Sign of fracture

الحوطي للخدمات التحليلية
مملكة البحرين
س.ت : ١٢٣٩٢
Kingdom of Bahrain
CR. No: 12392
AL HOTY ANALYTICAL SERVICES

NITIL K. SHRIVASTAVA
Material Laboratory Manager

Checked by : /MDLC

DISCLAIMER
The test reports / certificates issued by AAS are records of the actual test conducted on sample and the details submitted to us for testing and the results thereof. The results are applicable only to those sample/s, which have been tested and do not apply to other sample/s even though declared to be identical.
Test report / certificate if reproduced,,for any purpose commercial or otherwise, should be reproduced in full. AAS shall not be liable for any changes in reported factual data due to any cause related to sample tested after the report / certificate, in respect of it, h as been issued . The results reported in the test report/ certificates are valid only at the time of and under the stated conditions of the testing. Measurements are traceable to National/International Standards.

Test Certificate

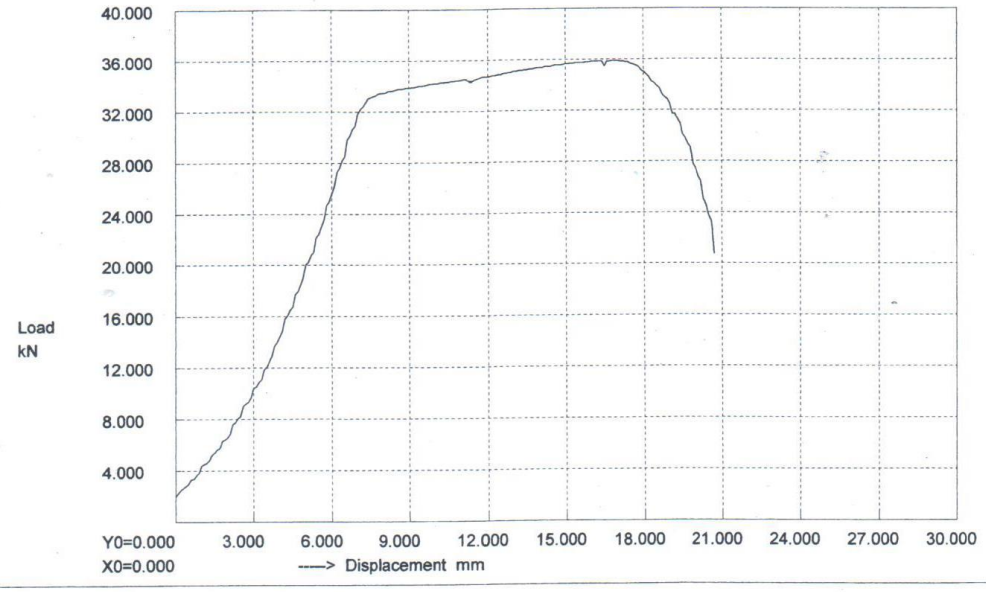
Name of Company : AL HOTY ANALYTICAL SERVICES
Address : P.O.BOX 26577

To : ADEL JASIM SANAD
Address : BAHRAIN UNIVERSITY
Sample Identification : REBARS 8.00mm dia.
Machine : Universal Testing Machine, 1000 kN

Input Data : File Name : ADEL JASIM 14122712 , Record No. : 1 , Date : 27/09/2014
: Sample Type : TMT , Area : 49.291 mm ²
: Length = 597.0 mm , Weight = 0.231 kg
: Gauge Length : 100 mm Final Gauge Length: 114.9 mm

Results of : Tension Test
Ult./Break Load : 35.900 kN
Ult. Stress : 0.728 kN/mm ²
Elongation : 14.900 %
Yield Load : 33.750 kN
Yield Stress : 0.685 kN/mm ²
* Note : Yield Calculated By Offset method as per ASTM E8 at .3 % Strain offset

Graph : Load Vs Displacement



For AL HOTY ANALYTICAL SERVICES

Test Certificate

Name of Company : AL HOTY ANALYTICAL SERVICES
Address : P.O.BOX 26577

To : ADEL JASIM SANAD
Address BAHRAIN UNIVERSITY

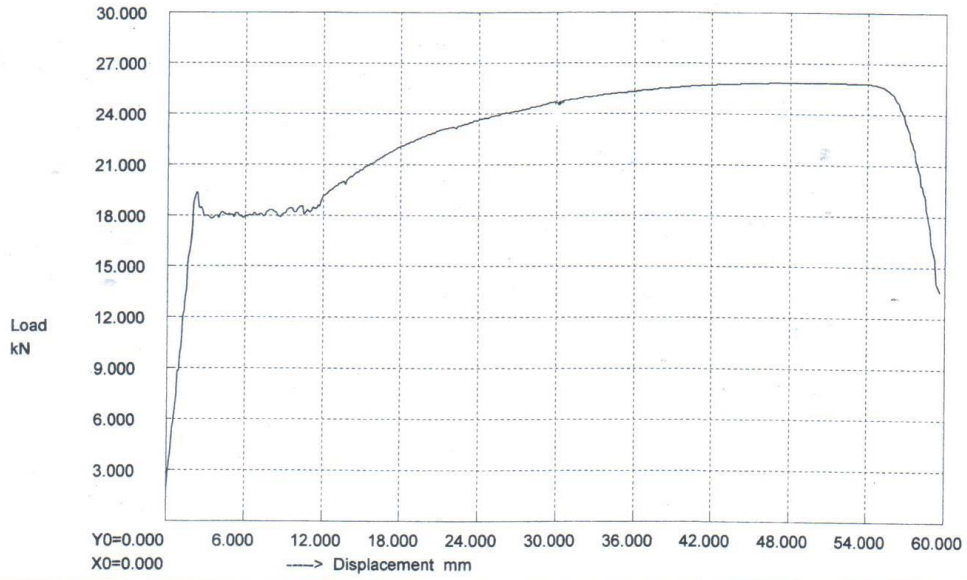
Sample Identification : REBARS 10.00mm dia./QATAR STEEL

Machine : Universal Testing Machine, 1000 kN

Input Data : File Name : ADEL JASIM 14122714 , Record No. : 1 , Date : 27/09/2014
: Sample Type : TMT , Area : 79.378 mm ²
: Length = 597.0 mm , Weight = 0.372 kg
: Gauge Length : 100 mm Final Gauge Length: 120.23 mm

Results of : Tension Test
Ult./Break Load : 25.850 kN
Ult. Stress : 0.326 kN/mm ²
Elongation : 20.230 %
Yield Load : 19.350 kN
Yield Stress : 0.244 kN/mm ²
* Note : Yield Calculated from graph

Graph : Load Vs Displacement



For AL HOTY ANALYTICAL SERVICES

AL HOTY ANALYTICAL SERVICES W.L.L.

Mina Salman Industrial Area, P.O.Box 26577, Manama, Kingdom of Bahrain

TENSILE TEST REPORT

Machine Model	: TUF-C-1200	Test File Name	: ADEL 16030200.Utm
Machine Serial No	: 2013 / 10	Date & Time	: 02/03/2016 11:14 AM
Customer Name	: ADEL JASIM BIN SANAD		
Lot No.	:		
Order No.	:		
Item	:		
Test Method	:		

Input Data

SpecimenType	: TMT Bar	
Specimen Description	: QATAR STEEL /10MM	
Specimen Mass	: 0.377	kg
Specimen Density	: 7.85E-06	kg/mm3
Guage Length	: 100	mm
Total Length	: 600	mm
Pre Load Value	: 0	kN
Max. Load	: 1200	kN
Max. Elongation	: 250	mm
Specimen Cross Section Area	: 80.04	mm2
Nominal Diameter	: 10	mm
Final Gauge Length	: 119.6	mm

Output Data

Load At Yield	: 49.59	kN
Elongation At Yield	: 7.760	mm
Yield Stress	: 619.546	N/mm2
Ultimate Load	: 57.600	kN
Elongation at Peak	: 40.250	mm
Ultimate Stress	: 719.618	N/mm2
Load At Break	: 38.370	kN
% Elongation	: 19.60	%
weight/meter	: 0.6283	kg/meter
weight/meter	: 0.6283	kg/meter

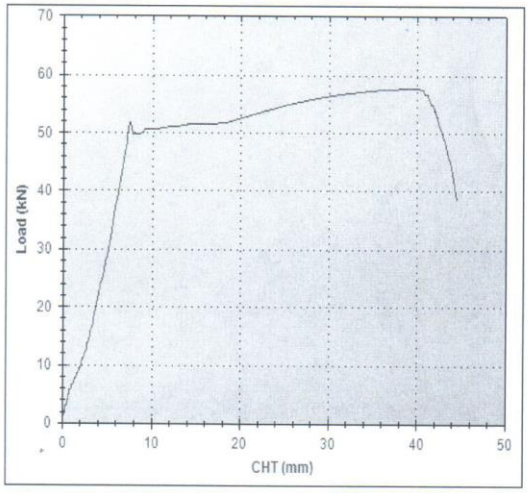
Load Rate

Load Rate(kN/sec)	Target Load(kN)	Hold Time(sec)
5	1200	100

Strain Rate

CHT Rate	Target C.H.T.	Hold Time (sec)
10	250	1

Load Vs. Cross Head Travel



Completion Reason	Test Terminated due to Specimen Break	Remark
Tested By	admin	

Appendix C

MARINE SAND AND SRC CEMENT TEST REPORTS

MAGNUM INDUSTRIAL LABORATORIES
A Member of Al Khalidia Group

مختبرات ماغنوم الصناعية
عضو مجموعة الخالدية

P.O.Box: 28778 - Kingdom of Bahrain - C.R : 20707-06

ص.ب :٢٨٧٧٨ - مملكة البحرين - س.ت :٢٠٧٠٧-٠٦

DECEMBER 07, 2005

SIEVE ANALYSIS
METHOD BS: 812

LAB REF. No. :MIL/RPT/4378/LP/12/05
CLIENT :NATIONAL WASHED SAND & AGGREGATE CO.
SAMPLE DESCRIPTION :DOUBLE WASHED SAND FOR MORTAR & PLASTER

Following are the test results of the sample delivered to our Laboratory by your representative on 05.12.05.

SIEVE SIZE (mm)	% PASSING
5.0	100
2.36	100
1.18	97.1
0.6	78.9
0.3	52.0
0.15	19.4
0.075	1.2

Note: 1. The grading of the Sand for Plaster sample comply with BS 1199 -Table 1 Type "B" specification limits.
2. The grading of the Sand for Mortar sample comply with BS 1200-Table 1 Type "G" specification limits.

for MANAGER
MAGNUM INDUSTRIAL LABORATORIES

مختبرات ماغنوم الصناعية P.O.BOX : 28778 BAHRAIN MAGNUM INDUSTRIAL LABORATORIES

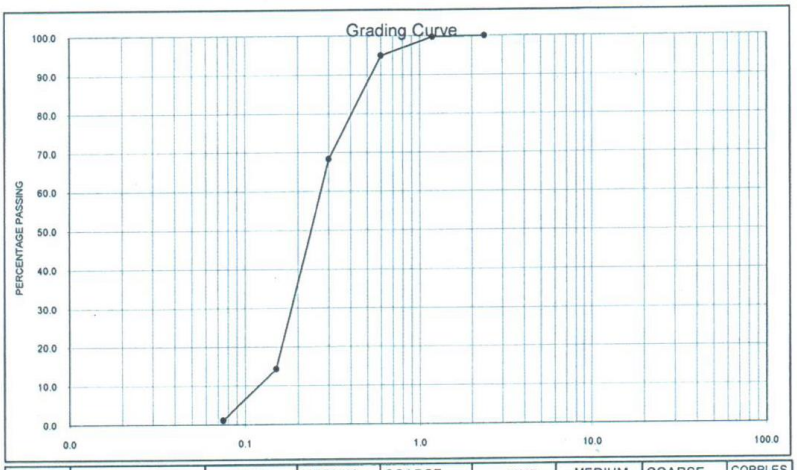
AL HOTY ANALYTICAL SERVICES	NATIONAL CONCRETE COMPANY W.L.L. P.O.Box 15561, Manama, Kingdom of Bahrain	DATE: 13.01.2015
		REF.: RN 002
	TEST REPORT ON SIEVE ANALYSIS	TWO: 146982
		SAMPLE No.: 146982-4
	METHOD: BS 812: Part 103.1 - '85	REPORT NO.: R164002/15

SAMPLE ID: Double Washed Sand

Method of test to be used : Wet Sieving

Condition of the sample upon receipt: Satisfactory Date Submitted to our lab.: 10.01.2015

Original Weight of the sample: (g) 1097.0 Date Tested : 11.01.2015



	CLAY/SILT	FINE	MEDIUM	COARSE	FINE	MEDIUM	COARSE	COBBLES
		SAND			GRAVEL			

Sieve Size mm.	% Passing
2.36	100.0
1.18	99.7
0.600	95.0
0.300	68.3
0.150	14.1
0.075	1.1

الحوطي للخدمات التحليلية
مملكة البحرين
س.ت: ١٢٣٩٢
Kingdom of Bahrain
CR. No: 12392
AL HOTY ANALYTICAL SERVICES

NITAI K. SHRIVASTAVA
Material Laboratory Manager

DISCLAIMER
The test reports / certificates issued by AAS are records of the actual test conducted on sample and the details submitted to us for testing and the results thereof.
The results are applicable only to those sample/s, which have been tested and do not apply to other sample/s even though declared to be identical.
Test report / certificate if reproduced, for any purpose commercial or otherwise, should be reproduced in full.
AAS shall not be liable for any changes in reported factual data due to any cause related to sample tested after the report / certificate, in respect of it, has been issued.
The results reported in the test report / certificates are valid only at the time of and under the stated conditions of the testing.
Measurements are traceable to National/International Standards.

/minerva
Checked by :

AL HOTY ANALYTICAL SERVICES	THE NATIONAL CONCRETE COMPANY W.L.L. Manama, Kingdom of Bahrain	DATE: 12.01.2015
		REF.:
	TEST REPORT ON AGGREGATE ANALYSIS	TWO No.: 146982
		SAMPLE No.:146982/1
		REPORT No.: R164002/15

SAMPLE ID : Double Washed Sand

DATE SUBMITTED : 10.01.2015

DATE TESTED : 11.01.2015 – 12.01.2015

TEST	TEST METHOD	UNIT	RESULT
Total Sulphate Content (Acid Soluble) of the sample expressed as SO_3% by mass of dry Aggregate	BS 812 Part 118:1988 Clause 6	%	0.01
Acid Soluble Chloride Content of the sample expressed as Cl^- ions % by mass of dry Aggregate	BS 812 Part 117:1988 APPENDIX C	%	0.04

SAPPANI MUTHIAH
Chemistry Laboratory Manager

Checked by:

/mae

DISCLAIMER
The test reports / certificates issued by AAS are records of the actual test conducted on sample and the details submitted to us for testing, and the results thereof.
The results are applicable only to those samples which have been tested and do not apply to other sample/s even though declared to be identical.
Test report / certificate if reproduced, for any purpose commercial or otherwise, should be reproduced in full.
AAS shall not be liable for any changes in reported factual data due to any cause related to sample tested after the report / certificate, in respect of it, has been issued.
The results reported in the test report / certificates are valid only at the time of and under the stated conditions of the testing.
Measurements are traceable to National/International Standards.

AL HOTY ANALYTICAL SERVICES	ADEL JASSIM BIN SANAD	DATE: 27.07.2016
		REF:
	TEST REPORT ON PHYSICAL PROPERTIES OF CEMENT (AUTOCLAVE EXPANSION)	REQ.NO.: CMQ-160727/097
		SAMPLE NO.: CMS-160727/097
	Method : ASTM C 1260	REPORT NO.: CMR-160727/167

Project : General
Sample Description : SRC (M_2S_2)
Casting Date : 10.07.2016
Date Submitted : 10.07.2016
Date Tested : 24.07.2016

Sample No.	Type of Cement	Test Age	Autoclave Expansion %
2	SRC	14 Days	0.10

NITIL K. SHRIVASTAVA
Material Laboratory Manager

Checked by:

/MDLC

DISCLAIMER
The test reports / certificates issued by AAS are records of the actual test conducted on sample and the details submitted to us for testing and the results thereof.
The results are applicable only to those sample/s, which have been tested and do not apply to other sample/s even though declared to be identical.
Test report / certificate if reproduced, for any purpose commercial or otherwise, should be reproduced in full.
AAS shall not be liable for any changes in reported factual data due to any cause related to sample tested after the report / certificate, in respect of it, has been issued.
The results reported in the test report / certificates are valid only at the time of and under the stated conditions of the testing.
Measurements are traceable to National/International Standard.

AL HOTY ANALYTICAL SERVICES W.L.L.	ADEL JASSIM BIN SANAD	DATE: 24.08.2016
		REF:
	TEST REPORT ON PHYSICAL PROPERTIES OF CEMENT (AUTOCLAVE EXPANSION)	REQ.NO.: CMQ-160802/100
		SAMPLE NO.: CMS-160802/100
	Method : ASTM C 1260	REPORT NO.: CMR-160802/171

Project : General
Sample Description : SRC (M_2S_2)
Casting Date : 04.08.2016
Date Submitted : 02.08.2016
Date Tested : 18.08.2016

Sample No.	Type of Cement	Test Age	Autoclave Expansion %
2	SRC	14 Days	0.20

for NITIL K. SHRIVASTAVA
Material Laboratory Manager

Checked by: Q

/MDLC

DISCLAIMER
The test reports / certificates issued by AAS are records of the actual test conducted on sample and the details submitted to us for testing and the results thereof.
The results are applicable only to those sample/s, which have been tested and do not apply to other sample/s even though declared to be identical.
Test report / certificate if reproduced, for any purpose commercial or otherwise, should be reproduced in full.
AAS shall not be liable for any changes in reported factual data due to any cause related to sample tested after the report / certificate, in respect of it, has been issued.
The results reported in the test report / certificates are valid only at the time of and under the stated conditions of the testing.
Measurements are traceable to National/International Standard.

AL HOTY ANALYTICAL SERVICES W.L.L.	ADEL JASSIM BIN SANAD	DATE: 24.08.2016
		REF:
	TEST REPORT ON PHYSICAL PROPERTIES OF CEMENT (AUTOCLAVE EXPANSION)	REQ.NO.: CMQ-160802/100
		SAMPLE NO.: CMS-160802/100
	Method : ASTM C 1260	REPORT NO.: CMR-160802/171

Project : General
Sample Description : SRC (M_1S_1)
Casting Date : 04.08.2016
Date Submitted : 02.08.2016
Date Tested : 18.08.2016

Sample No.	Type of Cement	Test Age	Autoclave Expansion %
1	SRC	14 Days	0.11

for NITIL K. SHRIVASTAVA
Material Laboratory Manager

Checked by: _____

/MDLC

DISCLAIMER
The test reports / certificates issued by AAS are records of the actual test conducted on sample and the details submitted to us for testing and the results thereof.
The results are applicable only to those sample/s, which have been tested and do not apply to other sample/s even though declared to be identical.
Test report / certificate if reproduced, for any purpose commercial or otherwise, should be reproduced in full.
AAS shall not be liable for any changes in reported factual data due to any cause related to sample tested after the report / certificate, in respect of it, has been issued.
The results reported in the test report / certificates are valid only at the time of and under the stated conditions of the testing.
Measurements are traceable to National/International Standard.

AL HOTY ANALYTICAL SERVICES	ADEL JASSIM BIN SANAD	DATE: 27.07.2016
		REF:
	TEST REPORT ON PHYSICAL PROPERTIES OF CEMENT (AUTOCLAVE EXPANSION)	REQ.NO.: CMQ-160727/097
		SAMPLE NO.: CMS-160727/097
	Method : ASTM C 1260	REPORT NO.: CMR-160727/167

Project : General

Sample Description : SRC (M_1S_1)

Casting Date : 10.07.2016

Date Submitted : 10.07.2016

Date Tested : 24.07.2016

Sample No.	Type of Cement	Test Age	Autoclave Expansion %
1	SRC	14 Days	0.12

مملكة البحرين
س.ت : ١٢٣٩٢
Kingdom of Bahrain
CR. No: 12392
الحوطي للخدمات التحليلية
AL-HOTY ANALYTICAL SERVICES

NITIL K. SHRIVASTAVA
Material Laboratory Manager

Checked by: _____

/MDLC

DISCLAIMER
The test reports / certificates issued by AAS are records of the actual test conducted on sample and the details submitted to us for testing and the results thereof.
The results are applicable only to those sample/s, which have been tested and do not apply to other sample/s even though declared to be identical.
Test report / certificate if reproduced, for any purpose commercial or otherwise, should be reproduced in full.
AAS shall not be liable for any changes in reported factual data due to any cause related to sample tested after the report / certificate, in respect of it, has been issued.
The results reported in the test report / certificates are valid only at the time of and under the stated conditions of the testing.
Measurements are traceable to National/International Standard.

AL HOTY ANALYTICAL SERVICES	BARDEX Manama, Kingdom of Bahrain	DATE : 06.03.2016
		REF. NO. :
	TEST REPORT ON AGGREGATE ANALYSIS	TWO NO. : 09723
		SAMPLE NO.: 09723/1
		REPORT NO.: CR100673/16

SAMPLE DESCRIPTION : Sand
DATE RECEIVED : 24.02.2016
DATE TESTED 29.02.2016 – 05.03.2016

PARAMETERS	TEST METHOD	UNIT	RESULTS
Silicon Dioxide (SiO_2)	Gravimetry	%	59.6
Sulphur Trioxide (SO_3)			0.03
Aluminum Oxide (Al_2O_3)	ICP - AES		4.7
Iron Oxide (Fe_2O_3)			1.0
Calcium Oxide (CaO)			16.8
Magnesium Oxide (MgO)			3.0
Sodium Oxide (Na_2O)			0.12
Potassium Oxide (K_2O)			0.06
Loss on Ignition @ 950°C	Ignition		13.8
Chloride (Cl^-)	Volhard		0.07
Equivalent Alkalies (Na_2O + 0.658 K_2O)	By Calculation		0.16
Density	BS 812 Part 2	Mg/m^3	1.81
Moisture Content	BS 812 Part 109	%	0.16

SAPPANI MUTHIAH
ChemistryLaboratory Manager

Checked by: MM
/Ali

DISCLAIMER
The test reports / certificates issued by AAS are records of the actual test conducted on sample and the details submitted to us for testing and the results thereof.
The results are applicable only to those sample/s, which have been tested and do not apply to other sample/s even though declared to be identical.
Test report / certificate if reproduced, for any purpose commercial or otherwise, should be reproduced in full.
AAS shall not be liable for any changes in reported factual data due to any cause related to sample tested after the report / certificate, in respect of it, has been issued.
The results reported in the test report / certificates are valid only at the time of and under the stated conditions of the testing.
Measurements are traceable to National/International Standards.

ADITYA BIRLA

UltraTech

QUALITY TEST CERTIFICATE

SULPHATE RESISTING PORTLAND CEMENT (PORTLAND CEMENT TYPE V)

IN ACCORDANCE WITH BS-4027:1996, Strength Class 42.5 N

Week No - 45	Date of Issue : 10/12/16
Dispatched Period : 05/11/16 - 11/11/16	Date Tested : 12/11/16

SI	Description	Unit	Specification	Results
	Chemical Analysis			
1	Silicon Dioxide (SiO_2)	%		20.61
2	Aluminium Oxide (Al_2O_3)	%		4.11
3	Ferric Oxide (Fe_2O_3)	%		4.97
4	Calcium Oxide (CaO)	%		63.75
5	Magnesium Oxide (MgO)	%		1.83
6	Sulfur Trioxide (SO_3)	%	Max 2.50	2.21
7	Loss on Ignition (L.O.I)	%	Max 3.00	1.91
8	Insoluble Residue (I.R)	%	Max 1.50	0.38
9	Alkalies ($Na_2O + 0.658 \times K_2O$)	%		0.56
10	Chloride (Cl)	%	Max 0.10	0.02
11	Lime saturation factor (L.S.F)	%		94.43
12	Tricalcium Silicate (C_3S)	%		61.87
13	Dicalcium Silicate (C_2S)	%		12.41
14	Tricalcium Aluminate (C_3A)	%		2.48
15	Tetracalcium Aluminoferrite (C_4AF)	%		15.12
	Physical Analysis			
16	Fineness, Air permeability Test	Cm^2/gm		3076
17	Soundness, Le Chatelier	mm	Max 10	0.10
18	Compressive strength, Mortar Prism	N/mm^2		
	2 - Days		Min 10	22.42
	7 - Days			34.22
	28 - Days		Min 42.5	49.53
19	Setting Time, Vicat Test	min		
	Initial		Min 60	208
	Final			312
20	Normal Consistency	%		27.80

Quality Control Head

Plant Head

Arabian Gulf Cement Co. W.L.L.
P.O. Box : 50605
Hidd, Kingdom of Bahrain
Tel. Board +973 17 671011, Sales: +973 17 672424
Fax: +973 17 671698
E-mail: star-bahrain.sales@star.adityabirla.com

UltraTech CEMENT
The Engineer's Choice

شركة أسمنت الخليج العربي ذ.م.م.
ص.ب ٥٠٦٠٥
الحد، مملكة البحرين
هـاتـف: ٦٧١٠١١ ١٧ ٩٧٣+، مبيعات: ٦٧٢٤٢٤ ١٧ ٩٧٣+
فـاكـس: ٦٧١٦٩٨ ١٧ ٩٧٣+
بريد إلكتروني: star-bahrain.sales@star.adityabirla.com

Appendix D

THERMAL CONDUCTIVITY REPORT

RWTH RHEINISCH-WESTFÄLISCHE TECHNISCHE HOCHSCHULE AACHEN

Institut für Gesteinshüttenkunde
Lehrstuhl für Keramik und feuerfeste Werkstoffe
Professor Dr. Rainer Telle

Institute of Mineral Engineering

RWTH Aachen, Germany

TEST REPORT

GA-Nr. 3637

Client:	University of Bahrain Civil Engineering Department P. O. Box 32038 Bahrain
Order:	Determination of thermal conductivity at 20 and 50°C according to DIN EN 993-14/15 of samples type "SBNBR 2", "CSC1-11", "CSC1-12", "Plaster" and "P24"
Date of test report:	10.03.2015

2 Pages

1. Data of test specimen

No. and type of the samples: Samples type "SBNBR 2", "CSC1-11", "CSC1-12", "Plaster" and "P24"

Sample description:	Sample-No.:
SBNBR 2 230 mm x 114 mm x 64 mm	7957/1-3
CSC1-11 230 mm x 114 mm x 64 mm	7958/1-3
CSC1-12 230 mm x 114 mm x 64 mm	7959/1-3
Plaster 230 mm x 114 mm x 64 mm	7960/1-3
P24 230 mm x 114 mm x 64 mm	7961/1-3

Received on: 04.02.2015 (7956, 7958, 7959, 7961)
09.02.2015 (7960)

Order placed: Purchase order, 04.02.2015 (Adel Bin Sanad)

Note: Sampling was performed by the client.

2. Test report

In compliance with the order the following tests were performed on samples type "SBNBR 2", "CSC1-11", "CSC1-12", "Plaster" and "P24", sample no. 7957-7961

1. Determination of thermal conductivity at 20 and 50°C according to DIN EN 993-14/15, hot wire method

3. Results

3.1 Determination of thermal conductivity at 20 and 50°C according to DIN EN 993-14/15, hot wire method

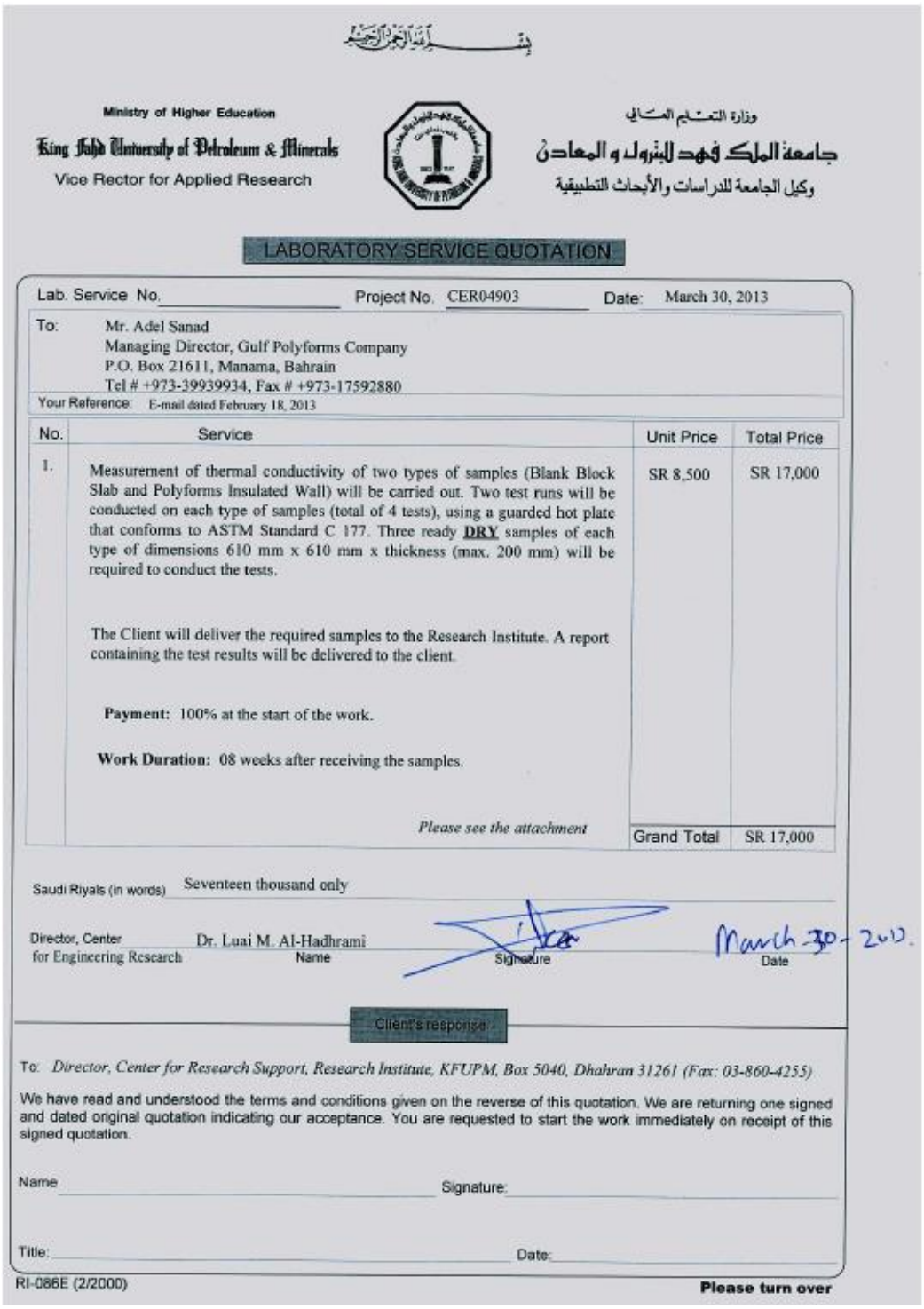
Thermal conductivity was performed with the hot wire method according to DIN EN 993-14/15 at 20 and 50°C. The samples of the size 230x114x64 mm³ have been dried at 50°C immediately before testing. The mean values of single measurements are given in table 1.

Table 1: Thermal conductivity at 20 and 50°C according to DIN EN 993-14/15 of samples type "SBNBR 2", "CSC1-11", "CSC1-12", "Plaster" and "P24" (Sample-No. 7957-7961)

Sample No.	Type	Temperature [°C]	Thermal conductivity Mean value / standard deviation [W/mK]	Bulk density Mean value / standard deviation [kg/m³] Before test	After test
7957	SBNBR 2	22	0,31 / < 0,01	887 / 63	875 / 64
		50	0,34 / 0,01		
7958	CSC1-11	20	1,33 / 0,03	1908 / 71	1880 / 85
		50	1,37 / 0,07		
7959	CSC1-12	20	1,29 / 0,05	1919 / 17	1905 / 21
		50	1,23 / 0,02		
7960	Plaster	20	1,05 / 0,02	1864 / 23	1850 / 28
		50	1,08 / 0,05		
7961	P24	20	0,032 / 0,001	22 / 1	22 / 1
		50	-		

Prof. Dr. R. Telle Dr.-Ing. Th. Tonnesen

Institut für Gesteinshüttenkunde
der Rhein. Westf. Techn. Hochschule
A A C H E N



بسم الله الرحمن الرحيم

Ministry of Higher Education
King Fahd University of Petroleum & Minerals
Vice Rector for Applied Research

وزارة التعليم العالي
جامعة الملك فهد للبترول و المعادن
وكيل الجامعة للدراسات والأبحاث التطبيقية

LABORATORY SERVICE QUOTATION

Lab. Service No. _____ Project No. CER04903 Date: March 30, 2013

To: Mr. Adel Sanad
Managing Director, Gulf Polyforms Company
P.O. Box 21611, Manama, Bahrain
Tel # +973-39939934, Fax # +973-17592880

Your Reference: E-mail dated February 18, 2013

No.	Service	Unit Price	Total Price
1.	Measurement of thermal conductivity of two types of samples (Blank Block Slab and Polyforms Insulated Wall) will be carried out. Two test runs will be conducted on each type of samples (total of 4 tests), using a guarded hot plate that conforms to ASTM Standard C 177. Three ready **DRY** samples of each type of dimensions 610 mm x 610 mm x thickness (max. 200 mm) will be required to conduct the tests. The Client will deliver the required samples to the Research Institute. A report containing the test results will be delivered to the client. **Payment:** 100% at the start of the work. **Work Duration:** 08 weeks after receiving the samples. *Please see the attachment*	SR 8,500	SR 17,000
		Grand Total	SR 17,000

Saudi Riyals (in words) Seventeen thousand only

Director, Center for Engineering Research — Dr. Luai M. Al-Hadhrami (Name) — (Signature) — March 30, 2013 (Date)

Client's response

To: *Director, Center for Research Support, Research Institute, KFUPM, Box 5040, Dhahran 31261 (Fax: 03-860-4255)*

We have read and understood the terms and conditions given on the reverse of this quotation. We are returning one signed and dated original quotation indicating our acceptance. You are requested to start the work immediately on receipt of this signed quotation.

Name _____ Signature: _____

Title: _____ Date: _____

RI-086E (2/2000)

Please turn over

UPM Research Institute Laboratory service quotation

Appendix E

STRAIN GAUGE DATA

Table (G1)
Concrete Surface Strain on Wall ICF-04

Sr. No.	Shear Force (kN)	Concrete Strain (μStrain)	
		CH-1	CH-2
1	10	-3.34	-0.027
2	20	0.386	-0.031
3	30	3.09	-0.021
4	40	5.66	-0.019
5	50	7.46	-0.021
6	60	10.68	-0.028
7	70	13.39	-0.031
8	80	15.45	-0.031
9	90	18.28	-0.022
10	100	19.44	-0.018
11	110	22.28	0.0061
12	120	27.94	0.0037
13	130	39.53	0.0190
14	140	45.33	0.0274
15	150	55.37	0.0427
16	160	62.46	0.0519
17	170	65.03	0.0571
18	180	82.16	0.0778
19	190	86.67	0.0820
20	200	88.73	0.0851
21	210	97.23	0.0949
22	220	108.31	0.0973
23	230	111.40	0.0994
24	240	114.36	0.0997
25	250	122.73	0.1068
26	260	134.84	0.1068
27	270	144.50	0.1065
28	280	156.86	0.0955
29	290	165.36	0.0906
30	300	167.42	0.0833
31	312	173.00	0.0842

Table (G2)
Concrete Surface Strain on Wall ICF-06

Sr. No.	Shear Force (kN)	Concrete Strain (μStrain)	
		CH-1	CH-2
1	10	-9.53035	0
2	20	-18.6743	0
3	30	-20.4774	0
4	40	-27.6895	0
5	50	-29.235	0
6	60	-29.3638	0
7	70	-27.6895	0
8	80	-25.6289	0
9	90	-22.7956	0
10	100	-21.7653	0
11	110	-21.5077	0
12	120	-20.091	0
13	130	-19.0607	0
14	140	-14.5531	0
15	150	-14.1667	0
16	160	-14.5531	0
17	170	-11.8485	0
18	180	-10.3031	0
19	190	-239.933	0
20	200	-308.577	0
21	210	-409.934	0
22	220	-487.722	0
23	230	-506.783	0
24	240	-525.843	0
25	250	-533.056	0
26	256.40	-551.472	0

Table (G3)
Concrete Surface Strain on Wall ICF-09

Sr. No.	Shear Force (kN)	Concrete Strain (μStrain)	
		CH-1	CH-2
1	10	1.287	-0.004
2	20	3.090	-0.038
3	30	2.31	-0.059
4	40	2.45	-0.050
5	50	13.39	0.070
6	60	-3.48	0.730
7	70	-10.82	0.943
8	80	-17.00	1.15
9	90	-19.83	1.30
10	100	-20.73	1.47
11	110	-23.44	1.62
12	120	-24.60	1.78
13	130	-25.24	1.90
14	140	-26.53	2.05
15	150	-29.75	2.21
16	160	-37.48	2.62
17	170	-45.98	3.29
18	180	-55.25	4.09
19	190	-60.9	5.43
20	200	-101.74	6.84
21	210	-247.66	8.30
22	220	-306.00	9.31
23	230	-315.79	9.31
24	240	-314.63	9.31
25	250	-326.99	9.31
٢٦	260	-330.21	9.31
٢٧	270	-327.12	9.31
٢٨	280	-2783.51	9.31
٢٩	290	-223.19	9.31
٣٠	300	-307.93	9.31
٣١	٣١٠	-5416.60	9.31

Table (G4)
Concrete Surface Strain on Wall ICF-11

Sr. No.	Shear Force (kN)	Concrete Strain (μStrain)	
		CH-1	CH-2
1	10	0	0.0168
2	20	0	0.0009
3	30	0	-0.0055
4	40	0	-0.011
5	50	0	-0.0200
6	60	0	-0.0360
7	70	0	-0.0537
8	80	0	-0.0647
9	90	0	-0.0824
10	100	0	-0.0961
11	110	0	-0.1172
12	120	0	-0.1853
13	130	0	-0.2402
14	140	0	-0.2634
15	150	0	-0.2887
16	160	0	-0.3168
17	170	0	-0.3699
18	180	0	-0.4883
19	190	0	-0.5325
20	200	0	-0.5683
21	220	0	-0.6458
22	230	0	-0.8087
23	260	0	-0.9900
24	270	0	-1.0123
25	280	0	-0.5298
26	290	0	-0.4877
27	300	0	-0.4862
28	310	0	-0.4868
28	320	0	-0.4795
29	330	0	-0.47245
30	340	0	-0.47825
31	350	0	-0.48190
32	382.6	0	9.5300

Appendix F

APDL COMMANDS

EPS Concrete: SBNBR-2

```
ET,matid,solid65


MPTEMP,,,,,,,,
MPTEMP,1,0
MPDATA,DENS,matid,,887

MPDATA,EX,matid,,3239
MPDATA,PRXY,matid,,0.24
TB,CONC,matid,1,9,
TBTEMP,0
TBDATA,,0.8,1,1.69,5,,
TBDATA,,,,,,,


R,matid, , , , , , ,
RMORE, , , , , , ,
RMORE, ,
```

Nano Concrete: CSC-13

```
ET,matid,solid65

MPTEMP,,,,,,,,
MPTEMP,1,0
MPDATA,DENS,matid,,1864

MPDATA,EX,matid,,10000
MPDATA,PRXY,matid,,0.198
TB,CONC,matid,1,9,
TBTEMP,0
TBDATA,,0.3,1,1.52,23.57,,
TBDATA,,,,,,,

R,matid, , , , , , ,
RMORE, , , , , , ,
RMORE, ,
```

Steel Reinforcement:

```
ET,matid,Beam188
```

```
MPDATA,EX,matid,,2e11
MPDATA,PRXY,matid,,0.3
R,matid,78.5,
```

Nodal Merge:

```
ESEL,S,ENAME,,65
ESEL,A,ENAME,,8
ESEL,A,ENAME,,180
ESEL,A,ENAME,,188
ALLSEL,BELOW,ELEM

NSLE,S

CPINTF,ALL,0.000001,
ALLSEL,ALL

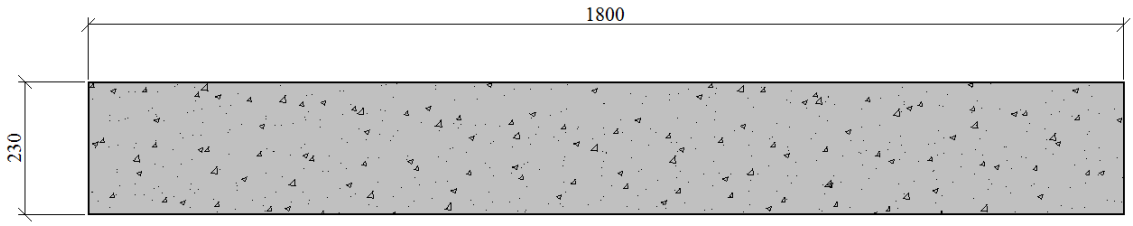
/SOLU
```

Crack Plot:

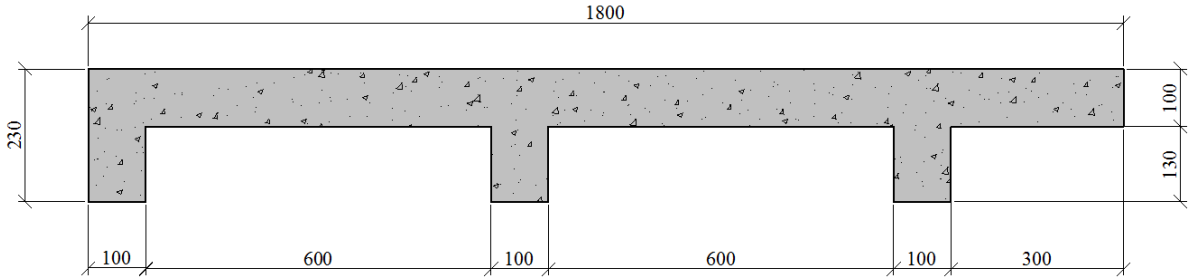
```
set,second
/show,png
!
/VIEW, 1 0,90,0
/ANG, 1,0
/SHOW,WIN32
/DEVICE,VECTOR,1
/DEVICE,BBOX,1
/DEVICE,DITHER,1
/DEVICE,ANIM,BMP
!
Plcrack,0,1
Plcrack,0,2
Plcrack,0,3
Plcrack,0,0
```

Appendix G

WEIGHT REDUCTION CALCULATIONS



Solid Concrete Slab



Ribbed Concrete Slab

ICF Ribbed Slab

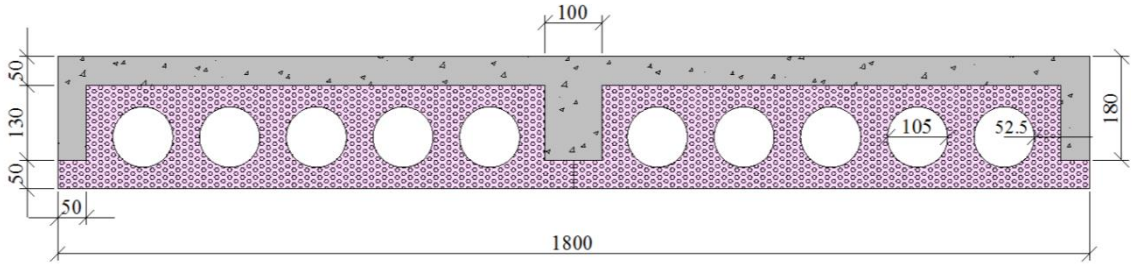


Table (G1)

Solid Slab 230mm						
Normal Concrete	Height m	Width m	Length m	Volume m3	Density Kg/m3	Weight Kg
Total	0.23	1.8	2	0.828	2400	1987.2

Ribbed Slab 230mm						
Normal Concrete	Height m	Width m	Length m	Volume m3	Density Kg/m3	Weight Kg
Full Rectangular Section	0.23	1.8	2	0.828		
Subtraction	0.13	1.5	2	0.39		
			Total	0.438	2400	1051.2

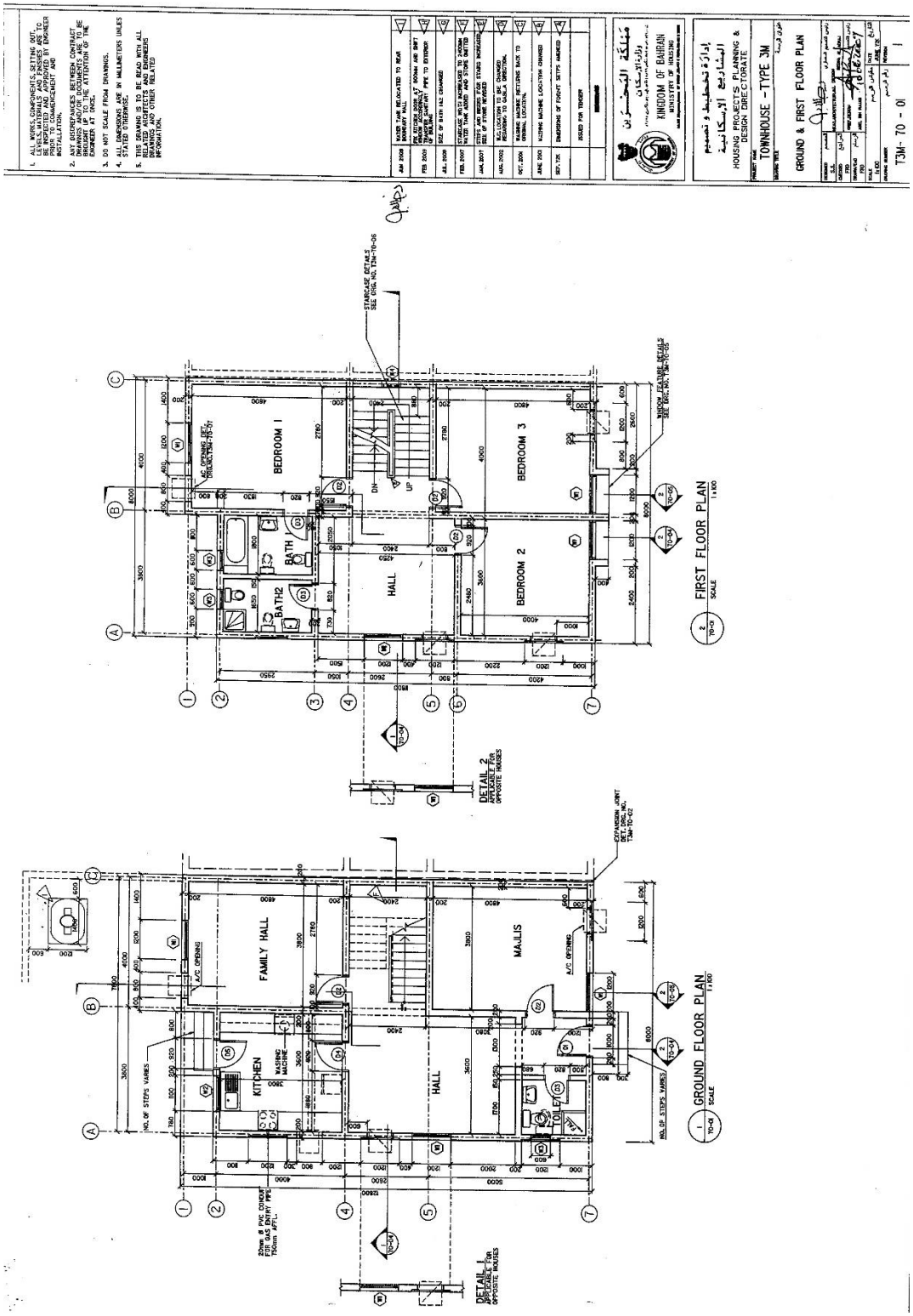
ICF Ribbed Slab 230mm						
Nano Concrete	Height m	Width m	Length m	Volume m3	Density Kg/m3	Weight Kg
Full Rectangular Section	0.18	1.8	2	0.648		
Subtraction	0.13	1.6	2	0.416		
			Total	0.232	1864	432.448
EPS Conc	Count	Section Area m2	Length m	Volume m3	Density Kg/m3	Weight Kg
	2	0.1057	2	0.4228	449	189.8372
				ICF Slab Total		622.2852

ICF Slab to Solid Slab		
	Weight Ratio	0.313147
	Weight Reduction	68.69%

ICF Slab to Ribbed Slab		
	Weight Ratio	0.591976
	Weight Reduction	40.80%

Appendix I

House Type T3M FLOOR PLANS

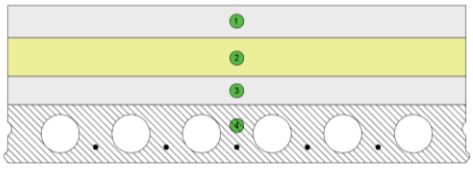


Appendix J

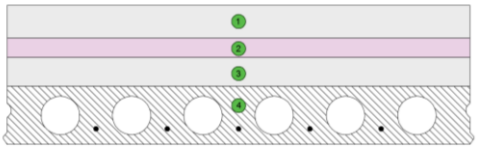
R & U Values Calculation

Type of Slab

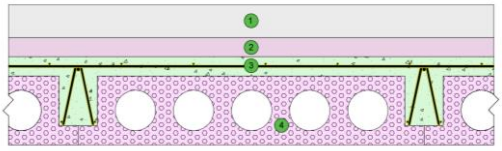
	Pecast Hollow Core Slab				
		Thickness (M)	K-alue (W/M.K)	R-value (M^2.K/W)	U-value (W/M^2.K)
1	L.W. Concrete	0.085	0.66	0.128788	0.30
2	PU	0.1	0.032	3.125	
3	Screed	0.075	2.25	0.033333	
4	Core Slab	0	0	0.1	
			R-total	3.39	



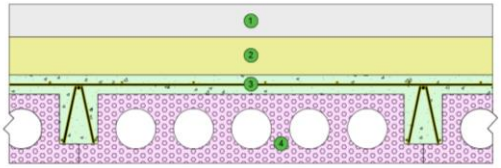
	Pecast Hollow Core Slab				
		Thickness (M)	K-alue (W/M.K)	R-value (M^2.K/W)	U-value (W/M^2.K)
1	L.W. Concrete	0.085	0.66	0.128788	0.59
2	EPS	0.05	0.035	1.428571	
3	Screed	0.075	2.25	0.033333	
4	Core Slab	0	0	0.1	
			R-total	1.69	



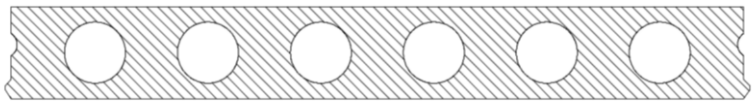
	ICF Slab				
		Thickness (M)	K-alue (W/M.K)	R-value (M^2.K/W)	U-value (W/M^2.K)
1	L.W. Concrete	0.085	0.66	0.128788	0.45
2	EPS	0.05	0.032	1.5625	
3	Nano	0.075	1.065	0.070423	
4	Blank Block	0	0	0.45	
			R-total	2.21	



	ICF Slab				
		Thickness (M)	K-alue (W/M.K)	R-value (M^2.K/W)	U-value (W/M^2.K)
1	L.W. Concrete	0.085	0.66	0.128788	0.21
2	PU	0.1	0.024	4.166667	
3	Nano	0.075	1.065	0.070423	
4	Blank Block	0	0	0.45	
			R-total	4.82	



*Sample Calculation for Hollow Core Slab



Hollow core slab overall thermal transmittance calculations for R&U values without including the external and internal surface resistance as per (MEW, 2006):

Given (k) for the concrete material used for the Hollow core slab as= 2.25 W/m.K.

- Calculations of the thermal resistance of the heat flow through concrete:

$$R_{HC} = 0.15/2.25 = 0.07 \text{ K./W.}$$

- Calculations of the thermal resistance of the heat flow through heat concrete and cavity:

$R_c/air = (0.325/2.25+0.18+0.325/2.25) = 0.21$ m^2.K./W.

- Calculations of areas:

1. Fraction of the concrete area compared to the total cross-sectional area of the hollow core slab:

$$Fc = (0.085*5+0.88+0.88) *(0.15/0.17986) = 0.5$$

2. Fraction of the cavity area compared to the total cross-sectional area of the hollow core slab:

$$A_{HC/air} = 1-0.5 = 0.5$$

Assuming that the heat flow is parallel:

$1/R_{Total} = (1/ R_{HC*} Fc) + (1/ R_c/air * A_{HC/air}) = 9.91$

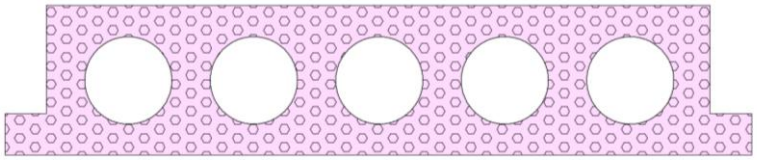
$R_{Total} = 0.1$ m^2.K./W.

Therefore, the overall transmittance of the hollow core is:

$U_{Hollowcore} = 1/ R_{Total} = 9.91 W/m^2 K$

Precast U&R	
$R_{HC.}$	0.07
Rc/air	0.21
Fc	0.50
A_{HC}/air	0.50
$1/R_{total}$	9.91
Rtotal	0.10
U_{PC}	9.91

Sample Calculation for Blank Block



Blank Block overall thermal transmittance calculations for R&U values without including the external and internal surface resistance as per (MEW, 2006):

Given (k) for the concrete material used for the Blank Block as= 0.325 W/m.K.

- Calculations of the thermal resistance of the heat flow through EPS concrete:

$$R_{BB} = 0.18/0.325 = 0.55 \text{ K./W.}$$

- Calculations of the thermal resistance of the heat flow through heat EPS concrete and cavity:

$$R_c/air = (0.0375/0.325+0.18+0.0375/0.325) = 0.41 \text{ m}^2\text{.K./W.}$$

- Calculations of areas:

3. Fraction of the EPS concrete area compared to the total cross-sectional area of the Blank Block slab:

$$Fc = (0.04625*6) *0.18/0.149 = 0.34$$

4. Fraction of the cavity area compared to the total cross-sectional area of the hollow core slab:

$$A_{BB/air} = 1-0.34 = 0.66$$

Assuming that the heat flow is parallel:

$$1/R_{Total} = (1/ R_{BB*} Fc) + (1/ R_c/air * A_{BB/air}) = 2.22$$

$$R_{Total} = 0.45 \text{ m}^2\text{.K./W.}$$

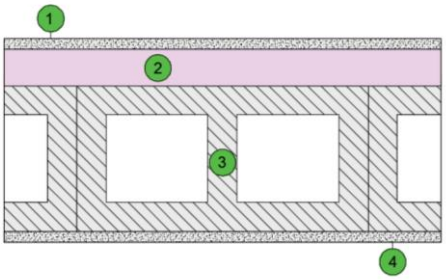
Therefore, the overall transmittance of the Blank Block is:

$$U_{BB} = 1/ R_{Total} = 2.22 \text{ W/m}^2\text{ K}$$

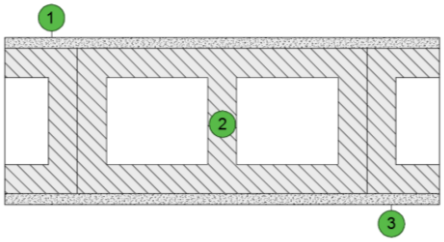
BB U&R Values	
R_{BB}	0.55
Rc/air	0.41
Fc	0.34
A_{BB}/air	0.66
$1/R_{total}$	2.22
Rtotal	0.45
U_{BB}	2.22

Type of Wall

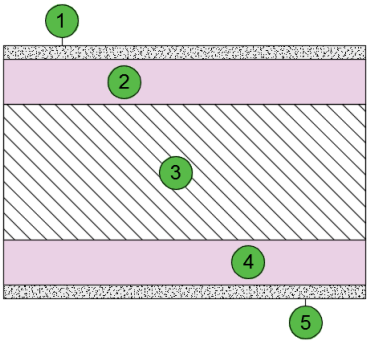
	EIFS Wall				
		Thickness (M)	K-alue (W/M.K)	R-value (M^2.K/W)	U-value (W/M^2.K)
1	Plaster	0.012	0.75	0.016	0.56
2	EPS	0.05	0.032	1.5625	
3	M. Block	0	0	0.2	
4	Plaster	0.012	0.75	0.016	
			R-total	1.79	



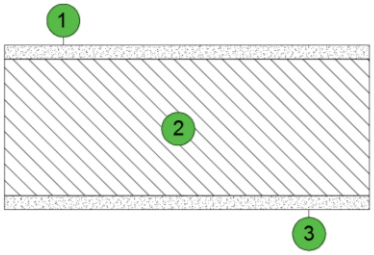
	Masonary Wall				
		Thickness (M)	K-alue (W/M.K)	R-value (M^2.K/W)	U-value (W/M^2.K)
1	Plaster	0.012	0.75	0.016	4.24
2	Block	0	0	0.2	
3	Plaster	0.015	0.75	0.02	
			R-total	0.24	



	Plolforms System Wall				
		Thickness (M)	K-alue (W/M.K)	R-value (M^2.K/W)	U-value (W/M^2.K)
1	Plaster	0.015	0.75	0.02	0.30
2	EPS	0.05	0.032	1.5625	
3	Nano	0.15	1.065	0.140845	
4	EPS	0.05	0.032	1.5625	
5	Plaster	0.015	0.75	0.02	
			R-total	3.31	



	Concrete Wall				
		Thickness (M)	K-alue (W/M.K)	R-value (M^2.K/W)	U-value (W/M^2.K)
1	Plaster	0.015	0.75	0.02	9.38
2	Concrete	0.15	2.25	0.066667	
3	Plaster	0.015	0.75	0.02	
			R-total	0.11	



Appendix K

AWARDS and RECOGNITIONS

This wall and slab systems are a Green Construction Technology registered at GCC patent office and for industrial design in the Kingdom of Bahrain and the Kingdom of Saudi Arabia under the name of "Polyforms System".

1. Golden medal awarded from the 5th international invention fair in the middle east in Zahra, Kuwait in November 2012 plus the Golden Astrolabe from the executive manager of the first gulf campaign for invention pioneers' industry.







GOLD MEDAL CERTIFICATE

FME

Kuwait Foundation for the Advancement of Sciences

The Organizing Committee of
The 5th International Invention Fair in the Middle East
hosted by **The Kuwait Science Club**
from the 19th - 22nd of November 2012 under the patronage of

His Highness the Amir
Sheikh Sabah Al-Ahmed Al-Jaber Al-Sabah

hereby awards to

Adel Jasim Sanad With Complements of the Jury

for the display of

Gulf Polyforms wall system

Eyad Jassim Al-Kharafi
Head of Higher Organizing Committee

2. The inventor of Bahrain medal awarded in Riyadh, Kingdom of Saudi Arabia, from the first gulf campaign for invention pioneers' industry (Gulf Inventors 2012) in February 2013.



3. Silver medal awarded from the 41st International Exhibition of Inventions of Geneva for the category of building and construction and the DIPLÔME of invention in Geneva, Switzerland in April 2013.



DIPLÔME

inventions Geneva

SALON INTERNATIONAL DES INVENTIONS

GENÈVE

Après examen, le Jury International a décidé

de remettre à: Adel Sanad & Ehsan Abdul Qudocs

pour l'invention: Blocs neutres auto-porteurs pour fabriquer des dalles légères sans coffrage

MÉDAILLE D'ARGENT
SILVER MEDAL
SILBERNE MEDAILLE

Genève, le 12 avril 2013

Le Président du jury: David Taj

Le Président du Salon: Jean-Luc Vincent



ملخص

تتناول هذه الرسالة تطبيق تكنولوجيا الابتكار في تقنيات النانو المتعلقة بالبناء لمواجهة التحديات التي يواجهها مجال البناء، بدءا من أداء مواد البناء إلى قضايا البيئة والسلامة وتكلفتها واستهلاكها وقابليتها للاستدامة. ان الترشيد في استخدام الكميات الكبيرة من الأسمنت المستورد والركام (الكنكري) المستورد والرمال البحرية في مملكة البحرين من المؤكد انه سوف يساهم في تحسين الجودة والأداء الاقتصادي والبيئي لصناعة الخرسانة.

ينبغي للمرء أن يراهن على جوانب الاستدامة والمتانة للخرسانة التي يمكنها تحسين الكفاءة والقوة والعزل الحراري والوزن والدمج الذاتي وتكلفة الإنتاج والتخفيف من آثار المناخ مثل التآكل والشقوق الناتجة عن التفاعل القلوية للسيليكا (ASR). ان هذه الدراسة تقدم نهج بناء للمباني الخضراء "نظام البوليفورمز" المبنية على علم الميكانيكا وهندسة المواد، المدعومة بواسطة تصاميم خرسانة النانو المبتكرة وقوالب البوليستيرين العازلة (ICF). والتي تظهر كيفية الحد من استخدام المواد ودمج الكفاءة البيئية وتقنيات الحوسبة المتقدمة والتجارب المختبرية ولتطوير فئات جديدة من مواد البناء وتوصيف سلوكياتها الهيكلية والحرارية، والتي غالباً ما تعتبر بديلاً للتكنولوجيات التقليدية، مما يتيح نهج تصميم جديد للمباني الخضراء.

تتكون المنهجية المستخدمة في هذه الدراسة من ثلاثة أجزاء ، الجزء الأول يحتوي على الاختبارات المعملية لتطوير خرسانة النانو و هي خرسانة للهياكل الانشائية ذاتية الانضغاط، مدمجة مع جسيمات متناهية الصغر (CNCs) التي توفر وتعزز الخصائص الميكانيكية والكيميائية والحرارية والانضغاط الذاتي وسهولة الصب بكثافة خفيفة تبلغ ١٨٦٤ كجم/ م^{٣}. حيث تشكل خرسانة البوليسترين قوالب ال (Blank Block)، بكثافة خفيفة تصل إلى ٤٤٩ كجم/ م^{٣}، والتي توفر خواص ميكانيكية أقوى وعزل حراري وثبات صفري لسهولة التصنيع بالبثق. كلا النوعين من هذه الخرسانات النانوية لا تحتاج الي تسوية مستوى سطح الخرسانة بالاهتزاز، وهو ما يتمثل في المحافظة على الاستدامة لأنه ينطوي على خفض كبير في الطاقة اللازمة لبناء الهياكل الخرسانية. تضمن الجزء الثاني اختبارات معملية على نماذج اسقف ال(ICF) الكاملة بتشكيلات التسليح المتنوعة المكونة من (١٢) عينة، وبقياسات هندسية متنوعة مع تشكيلات تسليح مختلفة لأنواع جدران (ICF) المكونة من (٤) عينات ، بالإضافة إلى ثلاث عينات لـ (Blank Block). في حين أن الجزء الثالث هو تقييم للسلوك الهيكلي لل(Blank Block) و اسقف ال(ICF) و جدران (ICF) باستخدام برنامج (ANSYS) والتي تم التحقق منها بواسطة البيانات التي تم الحصول عليها تجريبيا.

في الختام ، يمكن تحديد الخرسانة النانوية على أنها مادة مناسبة لتحل محل الخرسانة العادية من الناحية الهيكلية. اسقف ال(ICF) فئة (MSJ) وأنظمة الجدران (ICF) اجتازت اختبارات الاداء وكذلك اختبارات القوة. علماً، إن الوظيفة الأساسية لل (Blank Block) هي العمل كقالب صب لخرسانة النانو، الطبقة الهيكلية الأساسية، فلذالك يجب أن يكون هناك سقلة دعامة بعد كل متر واحد. نظام Plyforms يوافق معايير (LEED) الرئيسية، حيث انه يقلل من وزن المبنى بنسبة تصل إلى ٥٠٪ و استهلاك الكهرباء بنسبة ٥٠٪ ، والتكلفة بنسبة ٢٢,٧٣٪ و تقلل من انبعاث ثاني اكسيد الكربون بنسبة ٥٤,٠٣٪. هذه الدراسة تفتح المجال امام الهندسة المدنية لتنفيذ وتبني هذه المنهجية الجديدة للدراسات المختبرية والتحليلية المماثلة لاستكشاف وتطوير المواد المركبة الجديدة وإضافة قيم خضراء لصناعة إنشاءات المباني.

جامعة البحرين

كلية الهندسة **قسم الهندسة المدنية**

تصميم مبتكر للمباني الخضراء للبيئة ذات الطبيعة القاسية

أطروحة مقدمة لاستكمال متطلبات الحصول على درجة الدكتوراه في الهندسة المدنية

اعـــداد

عادل جاسم محمد بن سند

الرقم الجامعي: 19840018

اشراف

محمد بولات ساكا

(أستاذ)

جامعة البحرين

مملكة البحرين

مارس 2018